

AD-A110 231

LOCKHEED-GEORGIA CO MARIETTA

F/S 1/3

NUMERICAL AIRCRAFT DESIGN USING 3-D TRANSONIC ANALYSIS WITH OPT--ETC(U)

AUG 81 A J SROKOWSKI, M E LORES, R A WEED

F33615-78-C-3014

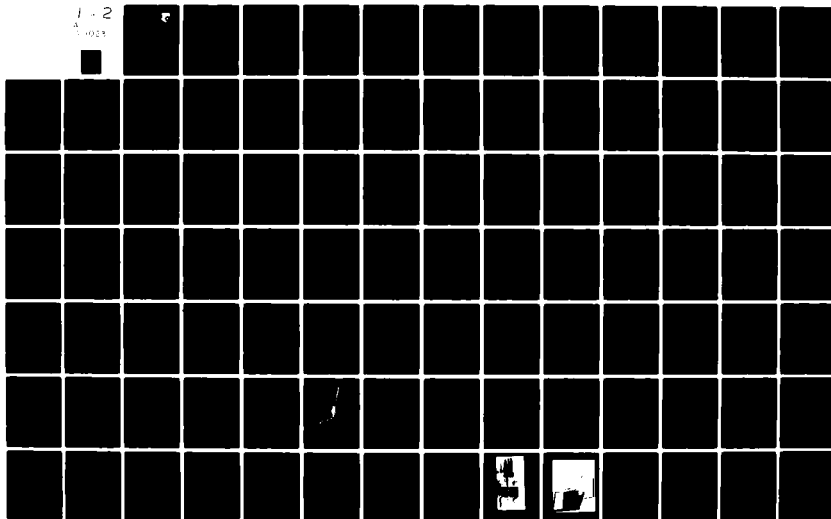
UNCLASSIFIED

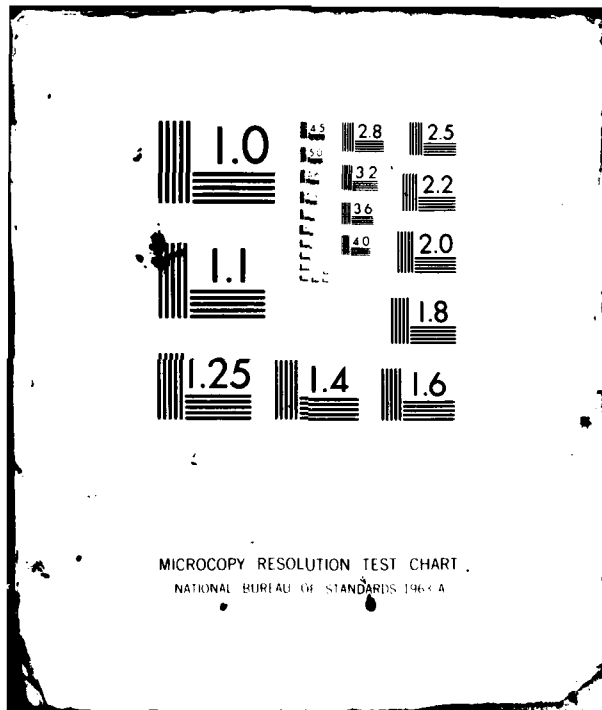
LG81ER0107-VOL-2-PT-1

AFWAL-TR-81-3091-VOL-2-PT- NL

1 - 2

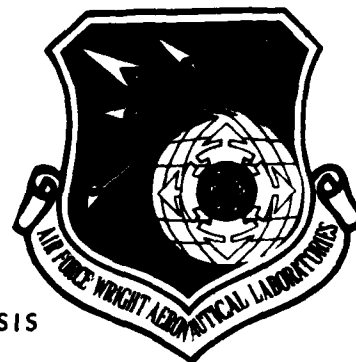
A 1013





DA110231

AFWAL-TR-81-3091-VOL-2-PT-3
VOLUME II, PART I



NUMERICAL AIRCRAFT DESIGN USING 3-D TRANSONIC ANALYSIS
WITH OPTIMIZATION
VOLUME II
PART I: TRANSPORT DESIGN

LOCKHEED-GEORGIA COMPANY
86 SOUTH COBB DRIVE
MARIETTA, GEORGIA 30063

GRUMMAN AEROSPACE CORPORATION
BETHPAGE, NEW YORK 11714

AUGUST 1981
Final Report May 1978 to September 1980

Approved for public release; distribution unlimited

FLIGHT DYNAMICS LABORATORY
AIR FORCE WRIGHT AERONAUTICAL LABORATORIES
AIR FORCE SYSTEMS COMMAND
WRIGHT-PATTERSON AIR FORCE BASE, OHIO 45433

DTIC FILE COPY

210065

DTIC
SELECTE
FEB 2 1982

A
0125 82044

NOTICE

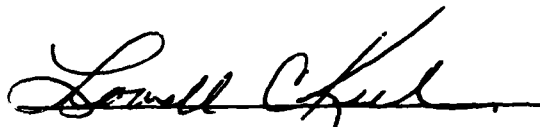
When Government drawings, specifications, or other data are used for any purpose other than in connection with a definitely related Government procurement operation, the United States Government thereby incurs no responsibility nor any obligation whatsoever; and the fact that the government may have formulated, furnished, or in any way supplied the said drawings, specifications, or other data, is not to be regarded by implication or otherwise as in any manner licensing the holder or any other person or corporation, or conveying any rights or permission to manufacture use, or sell any patented invention that may in any way be related thereto.

This report has been reviewed by the Office of Public Affairs (ASD/PA) and is releasable to the National Technical Information Service (NTIS). At NTIS, it will be available to the general public, including foreign nations.

This technical report has been reviewed and is approved for publication.



ROBERT A. LARGE, Capt, USAF
Project Engineer



LOWELL C. KEEL, Maj, USAF
Chief, Aerodynamics & Airframe Branch
Aeromechanics Division

FOR THE COMMANDER



JOHN R. CHEVALIER, Colonel, USAF
Chief, Aeromechanics Division

"If your address has changed, if you wish to be removed from our mailing list, or if the addressee is no longer employed by your organization please notify AFWAL/FIMM, W-PAFB, OH 45433 to help us maintain a current mailing list".

Copies of this report should not be returned unless return is required by security considerations, contractual obligations, or notice on a specific document.

Unclassified

SECURITY CLASSIFICATION OF THIS PAGE (When Data Entered)

REPORT DOCUMENTATION PAGE		READ INSTRUCTIONS BEFORE COMPLETING FORM
1. REPORT NUMBER AFWAL-TR-81-3094, VOLUME II, PART I	2. GOVT ACCESSION NO. AD-A110231	3. RECIPIENT'S CATALOG NUMBER
4. TITLE (and Subtitle) NUMERICAL AIRCRAFT DESIGN USING 3-D TRANSONIC ANALYSIS WITH OPTIMIZATION VOLUME II, PART I, TRANSPORT DESIGN	5. TYPE OF REPORT & PERIOD COVERED Final Report May 1978 - September 1980	
7. AUTHOR(s) A. J. Srokowski, M. E. Lores, R. A. Weed, P. R. Smith	6. PERFORMING ORG. REPORT NUMBER LG81ER0107-VOL 2-P11	
9. PERFORMING ORGANIZATION NAME AND ADDRESS Lockheed-Georgia Company ✓ 86 South Cobb Drive Marietta, Georgia 30063	8. CONTRACT OR GRANT NUMBER(s) F33615-78-C-3014 ✓ OK	
11. CONTROLLING OFFICE NAME AND ADDRESS Flight Dynamics Laboratory (AFWAL/FIMM) Air Force Wright Aeronautical Laboratories Wright-Patterson Air Force Base, Ohio 45433	10. PROGRAM ELEMENT, PROJECT, TASK AREA & WORK UNIT NUMBERS 62201F 24041026	
14. MONITORING AGENCY NAME & ADDRESS (if different from Controlling Office)	12. REPORT DATE August 1981	
	13. NUMBER OF PAGES 185	
	15. SECURITY CLASS. (of this report) Unclassified	
16. DISTRIBUTION STATEMENT (of this Report) Approved for public release; distribution unlimited		
17. DISTRIBUTION STATEMENT (of the abstract entered in Block 20, if different from Report)		
18. SUPPLEMENTARY NOTES		
19. KEY WORDS (Continue on reverse side if necessary and identify by block number) Aircraft Wing Design Numerical Optimization Aerodynamics Computational Aerodynamics Transonic Flow Transport Aircraft Design Optimization Transonic Flow Analysis		
20. ABSTRACT (Continue on reverse side if necessary and identify by block number) This volume details results obtained by the Lockheed-Georgia Co. and Grumman Aerospace Corp. under AFWAL Contract #F33615-78-C-3014. The purpose of the contract was to develop and validate a new transonic wing design procedure using the numerical optimization technique. The new procedure was used to design both a transport and a fighter configuration. Because the missions and design requirements of a fighter and transport are so different, the design procedure was developed along parallel lines. Lockheed-Georgia Co.		

DD FORM 1 JAN 73 1473 EDITION OF 1 NOV 65 IS OBSOLETE

Unclassified

SECURITY CLASSIFICATION OF THIS PAGE (When Data Entered)

Unclassified

SECURITY CLASSIFICATION OF THIS PAGE(When Data Entered)

car developed the transport design procedure, and Grumman Aerospace Corp. developed the fighter design procedure.

This is Part 1 of a two-part volume: Part 1 details the transport development, and Part 2 describes the fighter development. There are two other volumes which make up the final report. Volume 1 is an executive summary. It highlights the information that has been presented in detail here. Volume 1 is also divided into two parts with Part 1 dealing with transport design and Part 2 concerned with the fighter design. Volume 3 is a detailed user's guide to the computer programs produced under this contract. Volume 3 is similarly divided into two parts.

The results of a transport design case study performed to evaluate the transonic aircraft design procedure developed as part of the Advanced Transonic Technology (ATT) program are presented. A derivative of the C141B aircraft was selected as the design configuration. The design procedure was applied to the baseline configuration and the performance of resulting configuration was then compared to the C141 aircraft. Extensive wind tunnel testing of the design configuration was performed to validate the design procedure. The results of the wind tunnel tests are correlated with computational results generated in the design process. In addition, the evolution of the design procedure and its application in the transport design case study is discussed.

Unclassified

SECURITY CLASSIFICATION OF THIS PAGE(When Data Entered)

PREFACE

This volume details results obtained by the Lockheed-Georgia Co. and Grumman Aerospace Corp. under AFWAL Contract # F33615-78-C-3014. The purpose of the contract was to develop and validate a new transonic wing design procedure using the numerical optimization technique. The new procedure was used to design both a transport and a fighter configuration. Because the missions and design requirements of a fighter and transport are so different, separate design procedures were developed along parallel lines. Lockheed-Georgia Co. developed the transport design procedure, and Grumman Aerospace Corp. developed the fighter design procedure.

This is Part 1 of Volume 2: Part 1 details the transport development, and Part 2 describes the fighter development. There are two other volumes which make up the final report. Volume 1 is an executive summary. It highlights the information that has been presented in detail here. Volume 3 is a detailed user's guide to the computer programs produced under this contract. Volumes 1 and 3 are also divided into two parts with Part 1 dealing with transport design and Part 2 concerned with the fighter design.

Personnel who contributed to this contract effort are: Lockheed-Georgia Company, A. J. Srokowski, M. E. Lores, R. A. Weed and P. R. Smith; Grumman Aerospace Corp., P. Aidala.

The authors wish to acknowledge the assistance given by Capt. R. A. Large who was the AFWAL contract monitor.



A

TABLE OF CONTENTS

<u>SECTION</u>		<u>Page</u>
I	INTRODUCTION	1
II	DISCUSSION	1
	1. TASK 1 - CONFIGURATION SELECTION	1
	a. Transport Configuration	2
	2. TASK 2 - SELECTION AND DEVELOPMENT OF METHODS	4
	a. Correlations with Transport Test Data	5
	b. Code Modifications	6
	c. Design Procedure	7
	3. TASK 3 - CONFIGURATION DESIGN AND WIND TUNNEL TEST - TRANSPORT	9
	a. Starting Wing Selection.	10
	b. Interference Pressures	10
	c. Design Pressures	10
	d. Numerical Optimization	10
	e. Wind Tunnel Test	11
	(1) Apparatus	11
	(2) Tests and Methods	13
	(3) Test Techniques	14
	(4) Test Results.	15
	4. TASK 4 - AERODATA EVALUATIONS	16
	a. Force Data	16
	b. Correlations	17
	c. Effect of Wind Tunnel Walls.	18
	d. Evaluation of Pressure and Force Balance Data.	19
	5. TASK 5 - EVALUATION OF DESIGNS	20
	a. Performance Improvements	20
	b. ATT Cost Benefit Analysis.	20
	c. Critique of Design Procedure	23
	6. TASK 6 - FINAL DESIGN PROCEDURE	25
	a. Starting Wing.	25
	b. Inviscid Solution	25
	c. Boundary Layer Analysis.	26
	d. Link Up.	26

TABLE OF CONTENTS (CONT'D)

	<u>Page</u>
e. Design Pressures	26
f. Design	26
g. Inviscid Analysis	27
h. Boundary Layer Analysis	27
i. Link-Down.	27
j. Viscous Analysis	27
k. A Final Note	27
III CONCLUDING COMMENTS	28
REFERENCES.	29

LIST OF TABLES

Table No.	Title	Page
1	Transport Wing Design Variables	8
2	C-141 Pressure Tap Locations	31
3	C-141/AC2 Pressure Tap Location	32
4	C-141B/AC2 Measured Model Ordinates & Estimated Twists ZU = Upper Surface ZL = Lower Surface	33
5	Test Matrix	35
6	Run Summary Test CFWT053 C-141B/AC2 Configuration	36
7	Run Summary Test CFWT-52 C-141B Configuration	42

LIST OF ILLUSTRATIONS

Figure No.	Title	Page
1	Program Plan	43
2(a)	C-141B Configuration	44
2(b)	C-141B/AC2 Configuration	45
3	Effect of Wing Loading and Aspect Ratio on C-141B/AC2 Fuel and Weight	46
4	Effect of Initial Cruise Altitude and Wing Sweep on C-141B/AC2 Fuel and Weight	47
5	C-141B/AC2 Configuration Data and Target Performance . .	48
6	Payload/Range Comparison	51
7	Impact of Advanced Technologies on the C-141B/AC2 . . .	52
8	Inviscid Pressure Correlations for C-141 Mach = .77, $\alpha_F = 1.2^\circ$	53
9	Pressure Correlations for C-141 with Weak Viscous Interaction, Mach = .77, $\alpha_F = 1.2^\circ$	57
10	Transport Wing Design Procedure	61
11	Starting Wing Selection	62
12	C-141B/AC2 Paneling	63
13	Interference Pressures	64
14	Wing Design Stations	65
15	Comparison of ESD Design Pressures	66
16	ESD and FPE Fluid Wing Analysis	69
17	Calculated Pressures for Final Wing	72
18	C-141 Fuselage	76
19	C-141 Planform	77
20	C-141B/AC2 Wing Planform	78
21	Comparison of C-141B and C-141B/AC2 Planforms	79
22	Lockheed-Georgia Compressible Flow Wind-Tunnel	80
23	Photograph of Test Apparatus	81
24	Far-Field Rail Locations - cm (Inches)	82
25	Calibration of Floor Static Pressure Orifices and Far-Field Rails	83
26(a)	C_L vs α C-141 Baseline Configuration	85
26(b)	C_L vs C_M C-141 Baseline Configuration	86
26(c)	C_L vs C_D C-141 Baseline Configuration	87

Figure No.	Title	Page
27(a)	C_L vs α C-141B/AC2 Wing Alone	88
27(b)	C_L vs C_M C-141B/AC2 Wing Alone	89
27(c)	C_L vs C_D C-141B/AC2 Wing Alone	90
28(a)	C_L vs α C-141B/AC2 Wing + Pylon/Nacelle	91
28(b)	C_L vs C_M C-141B/AC2 Wing + Pylon/Nacelle	92
28(c)	C_L vs C_D C-141B/AC2 Wing + Pylon/Nacelle.	93
29(a)	C_L vs α C-141B/AC2 Wing + Fuselage + Gearpod	94
29(b)	C_L vs C_M C-141B/AC2 Wing + Fuselage + Gearpod	95
29(c)	C_L vs C_D C-141B/AC2 Wing + Fuselage + Gearpod.	96
30(a)	C_L vs α C-141B/AC2 Wing + Fuselage + Gearpod + Pylon/ Nacelle	97
30(b)	C_L vs C_M C-141B/AC2 Wing + Fuselage + Gearpod + Pylon/Nacelle	98
30(c)	C_L vs C_D C-141B/AC2 Wing + Fuselage + Gearpod + Pylon/Nacelle	99
31(a)	C_L vs α C-141B/AC2 Wing + Fuselage + Pylon/Nacelle	100
31(b)	C_L vs C_M C-141B/AC2 Wing + Fuselage + Pylon/Nacelle	101
31(c)	C_L vs C_D C-141B/AC2 Wing + Fuselage + Pylon/Nacelle	102
32(a)	C_L vs α C-141B/AC2 Wing + Fuselage	103
32(b)	C_L vs C_M C-141B/AC2 Wing + Fuselage	104
32(c)	C_L vs C_D C-141B/AC2 Wing + Fuselage	105
33	C-141B/AC2 Gearpod Effects ($M = 0.8$, $\alpha = 2^\circ$)	106
34	C-141B/AC2 Wing Alone, Isometric Pressure Plots $Mach = 0.80$ ($\alpha = -1^\circ$)	111
35	Measured Drag Rise Characteristics	118
36	Measured Drag Divergence Mach Numbers	119
37	C-141B/AC2 Measured and Computed Lift	120
38	Full Potential Correlation: $M = 0.78$, $C_L = .33$	122
39	Full Potential Correlation: $M = 0.78$, $C_L = .43$	127
40	Full Potential Correlation: $M = 0.78$, $C_L = 0.60$	132
41	Full Potential Correlation: $M = 0.80$, $C_L = 0.330$	137
42	Full Potential Correlation: $M = 0.80$, $C_L = 0.445$	142
43	Full Potential Correlation: $M = 0.80$, $C_L = 0.60$	147
44	Extended Small Disturbance Correlation, $M = 0.80$, $C_L = 0.32$	152
45	Extended Small Disturbance Correlation, $M = 0.80$, $C_L = .49$	157

Figure No.	Title	Page
46	Correlation of Pylon/Nacelle Interference Effects. M = 0.80, (Wing Alone $C_L = .445$)	162
47	Effect of Wind Tunnel Wall Boundary Conditions; M = 0.80, $\alpha = 0.7^\circ$	166
48	Pressure Integration vs. Force Balance Comparisons . . .	171
49	Comparison of Measured Model Drag with Estimates	172
50	Payload - Range Performance.	173
51	Summary of Aircraft Parameters	174
52	Airfoil Ordinate and Curvature Change	175
53	Design Procedure	176

SECTION I

INTRODUCTION

Computational aerodynamic methods that are significantly better than existing techniques are needed to design advanced aircraft configurations in a timely and cost-effective manner. The need for better methods is due in part to the demand for computational accuracy brought about by the increased aerodynamic sensitivity at transonic speeds of advanced technology concepts such as supercritical wings, active controls, variable camber wings, and laminar flow control. Also, improved aerodynamic tools are required to handle new configurational concepts such as (1) high aspect ratio wings, spanloader designs with thick wings, and winglets for transport-category aircraft; and, (2) swept forward wings, variable camber wings with direct lift control, canards, and blended-wing concepts for fighters. Because efficient transonic performance continues to be an important design requirement for military and commercial aircraft, there is also a particular need for improved transonic aerodynamic computational tools to accurately calculate the performance for each of these new technology and configurational concepts.

Significant strides have been made in the development of 3-D transonic aerodynamic design and analysis codes over the past few years. Although many of the methods are still in the evolutionary stage, a few have matured to the point where application to the solution of aircraft design problems is practical.

The primary objective of the Advanced Transonic Technology (ATT) program was to demonstrate that performance improvements and/or reduced development time and costs can be achieved by incorporating 3-D transonic methods into aircraft design procedures. The attainment of the objective would result not only in very efficient advanced technology configurations which meet future Air Force mission requirements, but also would produce an experimentally verified, efficient, and documented transonic configuration design method.

The overall program approach and the individual tasks are summarized in Figure 1. As shown in that figure, the program was conducted by performing six technical tasks which were grouped into three time phases.

During Phase I, a fighter and a transport configuration employing advanced technology were selected. Also, during Phase I, the 3-D transonic analysis codes were evaluated, and necessary modifications for design procedure use were made.

Following Air Force approval of the selected configurations, computer codes, and the design procedure, the detailed configuration aerodynamic designs and wing tunnel tests were performed in Phase II. During the third and final phase: (1) wind tunnel data were used to determine mission performance; (2) theoretical predictions and experimental results were compared; and (3) a final production design procedure was developed.

SECTION II

DISCUSSION

1. TASK 1 - CONFIGURATION SELECTION

During Task 1, a transport configuration was selected as the baseline aircraft for the detailed aerodynamic design of Task 3, using the advanced

transonic methods developed under Task 2. The choice of the baseline configuration was dictated by the requirements that the resulting aircraft design incorporate advanced technologies and/or unique configuration concepts. Additional requirements were that the selected configuration offer significant performance improvements for an existing or projected Air Force mission. A further criterion was that the chosen configuration should be amenable to design using the new 3-D transonic methods.

a. Transport Configuration

There were two possible approaches in the choice of the transport configuration. A completely new design, based on advanced transport studies being conducted at Lockheed-Georgia, could be selected; alternatively, the selected configuration could be based on a refinement of an existing aircraft design. The political and economic environment relative to military transport aircraft at the time of the initiation of the contract made the development of a modified or derivative configuration a more realistic prospect than the development of a completely new transport aircraft, where design requirements were ill-defined. Thus, the selected transport configuration has been based on the redesign of an existing transport configuration with increased aerodynamic and propulsive efficiencies. The derivative aircraft exhibits significantly improved performance for its original design mission, and increased ability to perform alternate missions.

Mission Definition

The selected configuration is a derivative of the C-141B transport aircraft designated as the C-141B/AC2. Figure 2a shows the C-141B configuration and Figure 2b shows the C-141B/AC2 configuration. The new design is intended to satisfy long-range cargo transport, tanker, and missile launcher missions. The selected configuration is designed for a cruise Mach number of 0.80 with a payload of 75,000 pounds over a range of 3,500 nautical miles. Performance constraints include a field length of 7,500 feet, and an initial cruise altitude of 35,000 feet.

Configuration Development

The primary design goal in the development of the C-141/AC2 design is to minimize the fuel required to perform the design mission. The C-141B/AC2 configuration was sized using the Lockheed-Georgia General Aircraft Sizing Program (GASP), a proprietary computer program presently used for all company preliminary design studies. The program accounts for the interaction of the various design constraints and technical disciplines involved in the aircraft design process. Drag coefficients and weights are calculated on a component basis and integrated into complete aircraft drag and weight. The propulsion system is sized by matching cruise thrust requirements within the constraints of specified takeoff field length.

Technology levels for the various disciplines are controlled by the use of input adjusting factors. The C-141B/AC2 aircraft was sized using advanced technology levels which are appropriate to an initial operational capability date in the mid-1980's. The technologies incorporated into the design are as follows:

Aerodynamics - The transonic aerodynamic technology level is based on a method of Dr. Whitcomb of NASA-Langley for the estimation of wing thickness to chord ratio. Thickness is calculated as a function of lift coefficient, cruise Mach number, aspect ratio and compressibility drag level at cruise. Airfoil technology level is selected by a M_{DD} (drag divergence Mach number) adjustment which has been assumed to be zero for the C-141B/AC2 1985 IOC date. Thus, aerodynamic estimates used in GASP for this study are conservative.

Flight Controls - The C-141B/AC2 configuration includes automatic load alleviation of wing bending loads, relaxed static stability and a stability augmentation system. The wing load alleviation system employs active aileron and elevator controls to reduce bending loads at frequencies up to the first wing bending mode. This load alleviation permits incorporation of a higher aspect ratio wing for enhanced fuel efficiency. The relaxed static stability system consists of automatic flight control functions which provide artificial static/dynamic aircraft stability thereby allowing a substantial reduction in tail size. Stability augmentation is employed in the lateral-directional axes to improve flying qualities.

Structures - Composite materials are used for the secondary structure, and for selected reinforcement of the primary structure.

Propulsion - The C-141B/AC2 was sized using current technology engine performance represented by a rubberized version of the CFM 56 engine.

A matrix of configuration variables was input to the sizing program to determine the minimum fuel aircraft which met the design mission. The range of variables considered was:

Wing loading	100 to 140 lb/ft ²
Aspect ratio	8 to 12
Wing Sweep	10 to 25 deg
Initial cruise altitude	31,000 to 35,000 ft.
Cruise power setting	0.7 to 1.0

The constraints imposed on the parametric designs were:

Fuel volume ratio	≥ 1.0
<i>(Fuel volume available/fuel required for 3500 NM)</i>	
Field length	$\leq 7,500$ ft.
Aspect ratio	≤ 12
<i>(To avoid excessive wing weights or the necessity for strut-braced wings)</i>	
Cruise altitude	$\geq 31,000$ ft.

A typical sizing plot from which the wing planform geometry was selected is shown in Figure 3. The choice of wing loading and sweep is established by the combined requirements of minimum mission fuel, and the fuel volume ratio required to meet the design range ($FVR = 1.0$). The selected wing loading of 130 lb/ft^2 and wing quarter chord sweep of 25 degrees satisfies the minimum mission fuel objective, and also minimizes the aircraft ramp weight. The selected cruise altitude of 35,000 ft and a wing sweep of 25 degrees result from the parametric variations shown in Figure 4. While an increase in initial cruise altitude above 35,000 ft. would save more fuel, the engine thrust requirement and empty weight would rise significantly.

Configuration Characteristics and Performance

The resulting C-141B/AC2 configuration is shown in the general arrangement drawing of Figure 2b. A complete summary of the aircraft characteristics as computed by the GASP Program is given in Figure 5. The major features of the design are:

T.O. gross weight	261,100 lbs
O.W.E.	118,300 lbs
Block fuel	61,500 lbs
Cruise lift	.58
Start cruise wing load	130 lb/sq ft
Wing area	1960 sq ft
Quarter chord sweep	25°
Aspect ratio	12
Taper ratio	.4
Average thickness	10.9%
Start cruise power setting	80%
Installed thrust	38,800 lbs

The payload/range capability of C-141B/AC2 aircraft is compared to the C-141A and C-141B in Figure 6. The C-141B/AC2 OWE is about 80% that of the C-141B, and the former aircraft requires approximately 64% of the fuel used by the latter airplane. Figure 7 shows in bar chart form, the impact of advanced technologies on the C-141B/AC2 configuration relative to the baseline aircraft (C-141B).

2. TASK 2 - SELECTION AND DEVELOPMENT OF METHODS

The objectives of this task were to evaluate existing three-dimensional transonic methods, improve selected methods, and develop a preliminary version of the desired transonic design method.

The improvement of 3-D transonic codes capable of treating the sophisticated configurations developed in Task 1 was critical to the success of the design method. Numerous 3-D codes (e.g. Refs. 1 through 5) were available. These codes differ from one another in both problem formulations and solution techniques, and each could be expected to excel in certain

applications and to be less successful in others. Consequently, more than one method would possibly be needed in the design procedure.

We emphasized evaluation of the NASA-Ames 3-D transonic small disturbance code because this code is more easily modified to provide increased configuration flexibility and requires less computation time than full potential techniques.

a. Correlations with Transport Test Data

Code evaluation for transport design centered on correlations of computations using the Ames 3-D transonic code with C-141 data from a recent AEDC 16T test (Ref. 6). A Lockheed version (ATWP) of the Ames code was used in those calculations. The distinguishing features of this code are simplified input, automatic smooth grid generation, a revised solution loop coding, and control stream linking with boundary layer codes.

The first solutions were computed for an isolated basic C-141 wing (pylon and nacelles off) using theoretical model ordinates. Inviscid results computed using nonconservative relaxation (NCR) and fully conservative relaxation (FCR) are summarized in Figure 8. The following observations can be made:

1. As expected, NCR inviscid results are in better (fairly good) agreement with experiment than FCR solutions.
2. The gear pods (which are large on the C-141) have a significant influence on the lower surface flow as evidenced by the $n \approx .19$ results. This disturbance propagates outboard spreading over the entire wing.
3. Leading edge pressures are not well predicted, possibly in part due to inaccuracies in the wind tunnel model leading edge contours.
4. Although NCR results are in fair agreement with experiment, inviscid results are not adequate for wing design.
5. Fuselage effects (other than gear pod) are not of critical importance for high wing transports at cruise lift coefficients, provided the fillet is well designed.

The effects of viscosity were examined using the Lockheed control stream linking of the 3-D inviscid transonic code with a strip boundary layer routine. This flexible procedure permits the use of any boundary layer routine and user adjustment of fluid wing ordinates. The latter feature proves to be extremely useful in modeling the trailing edge separation predicted on the C-141 wing.

The effects of viscosity were accounted for by first computing NCR inviscid potential flow solutions because such solutions are a better approximation to the real viscous flow than FCR results, and use of NCR inviscid pressures in the subsequent boundary layer analysis should yield a fairly good approximation of the viscous flow. Strip boundary layer analyses were

done at the four wing defining stations (not the code output stations shown in Figure 8). Trailing edge separation was predicted at each control station. Four heuristic models were used in the separated regions: $\delta^* = \text{constant}$, $z_{\text{fluid airfoil}} = \text{constant}$, $d\delta^*/dx = \text{constant}$, and $dz_{\text{fluid airfoil}}/dx = \text{constant}$. The last model produced the best agreement with experiment. The modified δ^* 's were added to the wing ordinates at the defining stations to account for boundary layer displacement effects, and linear lofting was used between the defining stations to produce the "fluid" wing. The inviscid 3-D transonic code was then used in the FCR mode to calculate the potential flow about the "fluid" wing.

The results of this non-iterative weak interaction viscous analysis are summarized in Figure 9. Good agreement with experiment, especially shock strength and location, is evident in these results.

The results shown in Figure 9 were generated using measured model ordinates. Comparing the inviscid NCR solutions with those of Figure 8 (which were computed using theoretical ordinates) show little difference between the theoretical results in the leading edge region (where differences are known to exist between the two sets of ordinates), and generally poor agreement with experiment. This disagreement is probably a shortcoming of small disturbance theory. Consequently, a full potential equation code would probably be needed when accurate leading edge solutions are required.

b. Code Modifications

Critical code modifications to permit the detailed aerodynamic design of the Task 1 configurations were the addition of pylon/nacelle modeling for transport design.

The ability to treat pylon/nacelles was added to the ATWP 3-D transonic code. This was done in two phases. In the first phase, the objective was to produce a procedure for determining the effect of pylon/nacelle geometry on the wing flow field, and not for computing accurate installed pylon/nacelle aerodynamics. In this case, the approach selected involves first the calculation of the isolated nacelle flow field. This was done using a modified version of a full potential equation code written by Caughey (Ref. 7) for axisymmetric nacelles.

Once the nacelle solution is calculated, nacelle boundary conditions are computed on the surfaces of a rectangular prism. The prism surfaces correspond to horizontal and vertical grid planes in the 3-D transonic code. Nacelle boundary conditions are imposed on these grid planes. Small disturbance pylon boundary conditions are incorporated in a standard manner by modifying the difference equations to include the pylon surface slopes, dy_{pylon}/dx , in the spanwise difference terms.

In the second phase, an extended small disturbance flow through nacelle code was written and linked to the ATWP 3-D wing code. This combined code (TALA) can treat mildly non-axisymmetric nacelles at small angles of attack and yaw. It also cycles back and forth between nacelle solutions and wing solutions to obtain the mutual interference effects between nacelle and wing.

c. Design Procedure

The transport wing design procedure is shown schematically in Figure 10. The procedure is based upon the use of an isolated wing code for the transonic design. Interference pressures are obtained from a transonic wing-pylon-nacelle code, and also from a more economical subsonic panel method (for lower surface gear pod interference).

The key element in the procedure is the use of numerical optimization in the wing design. The wing design code was developed by linking Vanderplaats constrained function minimization program (CONMIN, Ref. 8) with the ATWP 3-D wing code. As part of this task, a design objective and appropriate constraints were selected, and the permissible geometric perturbations (i.e. design variables) were specified. The entire process is described in detail in the following paragraphs.

Design Objective and Constraints

To avoid using inaccurately calculated quantities such as drag in the optimization procedure, the program was developed to permit the design of wings with specified chordwise pressure distributions. The capability of examining two pressure design objectives was provided. One design objective was the minimization of the RMS deviation between the target and actual pressures:

$$OBJ_1 = \left[\sum (C_p - C_{pD})^2 / N \right]^{1/2}$$

where N is the number of pressure coefficients, and C_{pD} is the target pressure coefficient. The second objective considered was

$$OBJ_2 = (C_p - C_{pD}); \quad \text{Constraint} = C_{pD} < C_p.$$

Notice the constraint required to make the second objective meaningful.

Both objectives were tried in the design study, and the first objective proved to be superior. Consequently, OBJ_1 was used in the transport wing design.

Design Variables

Consistent with established wing geometry definition procedures, the wing geometry is determined by specifying the airfoil sections at various geometric control span stations and connecting these sections by linear loft elements. At each control station, the permissible surface perturbations are listed in Table 1. The magnitude of each of these 14 surface perturbation functions plus the section twist angle are the fifteen design variables available for each surface at each geometric control span station. Thus, for a four control station wing, if all the surface perturbations were used, and if all the sections were designed simultaneously, a total of 15 variables per surface per station x 2 surfaces x 4 stations = 120 design variables, would be required.

Implementation

The simultaneous use of 120 design variables would result in an inordinately long computer run (greater than 10 hours on a CDC 7600). Job turn-around time on such a run would be very long, and a mistake would waste a lot of computer time. Consequently, wing design was accomplished in a series of steps. First, the upper surface was designed one section at a time proceeding from the root to tip. Next, the lower surface was designed, again proceeding from root to tip. The optimization is done using ATWP in the fully conservative relaxation (FCR) mode, and the desired viscous pressure distribution is specified. Consequently, the design procedure produces the "fluid" wing geometry (that is, the desired solid wing geometry plus the boundary layer displacement thickness). The fluid wing is then analyzed using FCR and the entire process, or parts thereof, are repeated as required to produce the desired pressures.

Extraction of Solid Wing Geometry

The wing contours produced by the optimization include the boundary layer displacement thickness, δ^* . The solid wing geometry is found by subtracting δ^* from the computed wing contours at each of the design stations.

TABLE 1 TRANSPORT WING DESIGN VARIABLES

$$V(1) = 3.89 (X/C)^{.25} (1 - X/C)e^{-20 (X/C)}$$

$$V(2) = 10.68 (X/C)^{.5} (1 - X/C)e^{-20 (X/C)}$$

$$V(j) = \sin^3 (\pi(X/C)^{r_j}), \quad j = 3, 12$$

$$V(13) = (X/C)^8$$

$$V(14) = (X/C)^{20} e^a \sqrt{1 - (X/C)}$$

$$a = .5/(1 - (X/C)_M) - 20/(X/C)_M$$

$$(X/C)_M \equiv (X/C) \text{ for max camber}$$

$$V(15) = \theta_{\text{TWIST}}$$

TABLE 1 TRANSPORT WING DESIGN VARIABLES (continued)

Sine deformations

<u>j</u>	<u>r_j</u>	<u>(X/C) Max deflection</u>
3	.231	.05
4	.301	.10
5	.431	.30
6	.576	.30
7	.756	.40
8	1.000	.50
9	1.357	.60
10	1.943	.70
11	3.106	.80
12	6.579	.90

A conventional (Ref. 9) 2-D integral boundary layer code is used to compute δ^* .

Analysis of Optimized Wing

The performance of the optimized solid wing is then investigated using both the full potential and extended small disturbance transonic codes. This analysis should use the viscous linking technique of the design method, and a coupled viscous analysis technique.

Second Iteration Wing Optimization

If analyses show that the wing does not perform as expected, a second pass is made through the design process. All or part of the procedure may be repeated as dictated by the cause of the unacceptable performance.

3. TASK 3 - CONFIGURATION DESIGN AND WIND TUNNEL TEST - TRANSPORT

The design procedure developed in Task 2 was used to design a new wing for the C-141B/AC2 configuration selected during Phase I. The goal of this study was to improve the wing aerodynamics and at the same time increase the wing thickness for the Mach = .80, $C_L = .60$ design condition. Increased wing thickness was sought to increase the fuel volume, and to reduce wing weight. The new wing was built and tested in the Lockheed-Georgia Company's compressible flow transonic wind tunnel (CFWT).

a. Starting Wing Selection

Two starting wings were considered. One wing used airfoil sections developed at NASA-Langley as part of the Energy Efficient Transport Program (Ref. 10). The second wing used airfoils designed at Lockheed-Georgia in support of in-house configuration Advanced Transonic Aircraft (ATA) design studies (Ref. 11). Two wings were analyzed using ATWP; results are summarized in Figure 11. These results show that both wings have well-behaved design point pressures. Thus, either wing is satisfactory for starting the design process.

The wing with the Lockheed airfoils was selected as the starting wing because the airfoils were systematically developed using state-of-the-art airfoil inverse (Ref. 12) and analysis (Ref. 13) transonic methods. Consequently, this initial wing design lends itself well for inclusion in a formal design procedure.

b. Interference Pressures

Using an isolated wing code during numerical optimization is a key feature of the design method because this minimizes computer resource requirements. During Phase I the isolated wing version of ATWP was shown to yield good predictions of upper surface pressures for high-wing configurations. The interference pressure perturbations are confined to the lower surface and are primarily due to the gear pod. Since the flow is subcritical on the lower surface, and since the interference pressures are small, they can be calculated using any subsonic panel method which provides very good geometric resolution in the wing-body-gear pod area as shown in Figure 12.

The calculated isolated wing and wing-body-gear pod pressures are compared in Figure 13 where the lower surface interference pressures are apparent. These interference pressures are taken into account in the specification of the target isolated wing design pressures. The interference effects of the pylon-nacelle were determined by including pylon-nacelle analysis capability in the ATWP 3-D transonic analysis code.

c. Design Pressures

Target wing pressures were originally specified near the wing root, break and tip. The upper surface pressures were selected to provide a weak shock wave on the outer panel near the 60% chord station. The root pressures were selected to minimize isobar unsweeping and to avoid large trailing edge pressure gradients which might result in the formation of a strong trailing edge shock wave.

d. Numerical Optimization

The numerical optimization procedure described in Subsection 2-C was used to determine the wing geometry which produces the desired wing pressures. The wing geometry was determined by designing the four wing control stations shown in Figure 14 and using linear lofting to generate intermediate ordinates. Early numerical experiments showed that the additional $\eta = .6$ design station was needed because perturbations of the wing tip section were inadequate to control mid-semispan and tip pressures simultaneously. A constant normalized section wing carry-through was used.

Of note also in Figure 14 is the specification of tip pressures near the $\eta = .85$ station. This choice was made because of the inaccuracy of computed results near the wing tip.

Extended Small Disturbance Design - The ATWP extended small disturbance program was used in the initial wing design. The final wing pressures are compared with the target pressures in Figure 15. Also shown here is the agreement between target and computed pressures (labeled as upper) after the upper surface design of each span station. The agreement between target and computed pressures is good. The computed pressures do produce a slightly stronger than desired shock wave.

The solid wing geometry was then analyzed using both full potential (FL022, Ref. 14) and extended small disturbance (ATWP) codes with weak interaction viscous linking. The results of these calculations are shown in Figure 16. On the premise that the FPE results are correct, these data show that the ESD code entirely mispredicts the wing leading edge flow field, and this error causes complete disagreement between ESD and FPE results.

Full Potential Design - The failure of the ESD optimization to accurately design the wing leading edge made a second pass through the design procedure using a full potential equation analysis code necessary. The optimization code was modified for this purpose, and the FPE optimization was done using the same design variables and objectives used in the ESD optimization. However, the target pressures for the FPE design were modified to produce a slightly weaker shock wave.

The span load distribution of the resulting wing was not satisfactory because the outboard section of the wing was too highly loaded, while the root section was unloaded. The lower surface of the root was modified using a simple Lockheed linear design method to increase the section loading at a small sacrifice in wing root thickness. The wing twist was also adjusted using a very efficient panel method to decrease the tip loading.

The resulting wing was analyzed using both the FPE and ESD codes with viscous linking (as described in Subsection 2-a). The results are summarized in Figure 17. The codes produce results in good agreement with one another, indicating that ESD methods yield accurate results if the leading edge is properly designed. The wing pressures are quite satisfactory. There is no tendency for isobars to coalesce near the root trailing edge, nor is there a tendency for a leading edge shock wave to form. The desired mid-chord shock is weak (normal Mach number less than 1.16). Consequently, this FPE-designed wing was selected as the final C-141B/AC2 wing design.

e. Wind Tunnel Test

(1) Apparatus

Models

An existing .0188 scale C-141A semi-span model, was used to obtain baseline data for comparison with the C-141B/AC2 configuration. The wing on this model is instrumented with 126 surface static pressure taps located at three span stations. The new, .0188 scale C-141B/AC2 wing, was machined from a solid billet of 17-4PH stainless steel by a numerically controlled milling machine. The model was hand finished to a tolerance of $\pm .002$ in.

Actual model coordinates were measured at several stations by a precision measuring machine, and compared to lofted coordinates used to define the wing. The C-141B/AC2 wing had a total of 140 static pressure taps located in chordwise rows at 5 span stations. The upper surface pressure orifices were installed by drilling completely through the wing so that all pressure tube routing is on the wing lower surface. This installation technique makes the upper surface completely free of tube routing channels which can cause possible discontinuities in curvature that may affect the supersonic flow on the upper surface.

The fuselage used in these tests was a C-141A model fuselage originally built for the C-141 semi-span wing. Using the A model fuselage would make little difference aerodynamically and would save the cost of fabricating a new B model fuselage. A sketch of the fuselage is shown in Fig. 18. The C-141 wing planform is shown in Fig. 19. Table 2 lists the C-141 wing pressure tap locations. Fig. 20 shows the C-141B/AC2 wing planform. Table 3 lists the AC2 pressure tap locations. Table 4 lists the AC2 wing ordinates as measured by a numerical measuring machine. Fig. 21 shows a direct comparison of the C-141 and C-141B/AC2 wing planforms.

Test Facility

The general arrangement of the Lockheed Compressible Flow Wind Tunnel (CFWT) is shown in Fig. 22. The tunnel is of the blow-down type, exhausting directly to the atmosphere. The air storage capability is 13,000 ft³ at 600 PSIA. A sleeve type control valve accurately maintains the settling chamber stagnation pressure at selected pressure less than or equal to the 250 psia maximum at a mass flow rate less than 2400 lb/sec. The test section is 20.0 in. wide by 28.0 in. high by 72.0 in. long and is enclosed in a 12.0 ft. diameter plenum chamber. The top and side walls of the three-dimensional test section have variable porosity capability (from 0 to 10 percent), obtained by sliding two parallel plates with .250 in. diameter holes slanted 60 degrees from the vertical. The bottom wall, where the model is mounted, is not porous. The model is mounted on a five-component balance located in the floor. The balance and model rotate together on a turntable to vary angle of attack. A bleed duct is located 21 in. ahead of the balance centerline to remove the wind tunnel boundary layer. The boundary layer bleed system has an independent control valve and exhausts to atmosphere through a separate pipe system. The main features of the test apparatus are illustrated in Fig. 23. A more detailed description of the facility may be found in Reference 15.

Instrumentation

Instrumentation for this test program consists of a five-component strain gauge balance to measure model aerodynamic forces. Six far-field pressure rails, each containing 31 static pressure taps, were mounted on the tunnel walls as shown in Fig. 23 and detailed in Fig. 24. The far-field measurements were extended to the symmetry plane by a row of fourteen stream-wise pressure taps along the tunnel floor on each side of the model. These pressure orifices were displaced 2.0 in. inward from the tunnel sidewalls.

Measurements of the static pressures on the wing surface and the wall rails were made using electronically actuated pressure scanning valves. The full-scale range of the quarter percent accuracy Statham pressure transducers in the scanning valves were selected to provide maximum accuracy for the wind tunnel conditions tested (wall rails ± 12.5 psi and airfoil pressures ± 50 psi). CEC force balance pressure transducers were used in conjunction with CEC servo amplifiers to provide a precise measurement of the atmospheric pressure, stagnation pressure, and test section static pressure to 0.05% of the 250 psi capacity. These transducers allow determination of the test section Mach number to an accuracy of ± 0.002 at the highest stagnation pressure.

Angle of attack was measured with a calibrated potentiometer operated by the angle-of-attack drive mechanism.

The balance used to measure forces on the model was designed and built by Lockheed-California Co. It is a strain gauge five-component temperature compensated balance designed to the following load capacities:

Normal force	± 750 lbs.
Axial force	± 75 lbs.
Pitching moment	± 1800 in. lb.
Rolling moment	± 6000 in. lb.
Yawing moment	± 600 in. lb.

Design accuracy of the balance is 1/4% of design load and 1/2% of applied load. Raw pressure and balance data were recorded on magnetic tape utilizing the CFWT high speed data acquisition system. The data acquisition system consists of a Lockheed Electronics Company MAC-16 computer and associated peripheral equipment. The raw data was reduced to coefficient form with a TI-990 computer. Machine plots were made on a Calcomp 765 plotter.

Data Reduction

Balance data - The force balance data were acquired by taking one hundred samples over a one second time span. The average of the 100 samples was reduced to pounds of force and inch pounds of moment by multiplying the five measured values by the calibration matrix. The resulting measurements were converted to conventional coefficient form using the tunnel conditions at the time the force measurements were made.

Pressure data - All static pressure measurements from the wing and far-field rails were reduced to standard coefficient form using instantaneous tunnel conditions at the time each pressure was measured. Pressure coefficients for each spanwise station were numerically integrated to determine a local lift coefficient.

(2) Tests and Methods

Test Conditions

The configurations were tested over a wide range of conditions to provide data at off-design as well as design conditions. The test Reynolds number based on mean aerodynamic chord was nominally 5 million. Although the wind tunnel was capable of much higher unit Reynolds numbers, the actual test values were limited by the capacity of the wind tunnel force-balance.

The angle of attack and tunnel Mach number were varied over a wide range: from zero-lift to above design values and subcritical speeds through drag-rise, respectively. A complete summary of the test matrix is given in Table 5. Table 6 gives a detailed breakdown of the run numbers corresponding to each test condition for the C-141B/AC2 wing. Table 7 gives the run numbers for the C-141B wing.

Most of the wind tunnel testing was conducted at a fixed wall porosity of 4% because previous tests in the CFWT had indicated this value would provide minimum wall interference effects.

Transition

For the unit Reynolds numbers of these tests, experience with the CFWT facility indicates that significant regions of laminar flow would exist on a smooth model. Therefore, to fix transition and to eliminate the uncertainties of the transition location, a transition strip was applied to each model. The transition strips were applied to both the upper and lower surface and were located and sized according to the guidelines of reference 16. The strips were thus located a fixed distance from the leading edge equal to 5% of the mean aerodynamic chord. The grit consisted of .0023 in. diameter glass beads, set in a lacquer fixative. The width of the strips was constant at .05 in. Strips were also placed on the fuselage.

(3) Test Techniques

Boundary Layer Removal System

One unique aspect of the test facility used in this test program was the bleed system used to remove the wind tunnel boundary layer ahead of the model (Fig. 23). The operational procedure used in all of the testing was to set the bleed rate so that the static pressures measured at the leading edge of the flat plate which formed the top of the bleed duct did not indicate any angle-of-attack loading.

Tunnel Calibration

Fig. 25 shows that the CFWT Tunnel Mach number distribution is uniform. The force balance used for these tests was calibrated prior to the conduct of the tests.

Fuselage/Wing Seal

The wing/fuselage configurations were tested with the fuselage non-metric. The fuselage was cut out so that the wing could fit through the fuselage with a nominal gap of .040 in. This gap was filled with a foam seal. Any possible tare effects of the foam seal on the balance reading

were accounted for by applying loads to the clean wing, and then to the wing + seal + fuselage to obtain corrections to the balance readings. In any case, required corrections turned out to be small.

(4) Test Results

We will show plots of all of the force data obtained, and selected samples of the pressure data. All of the data from this test can be obtained on magnetic tape.

Force Data

All of the force data obtained during the wind tunnel test is shown in Figures 26 through 32. The data is grouped by configuration, and three figures are shown for each configuration (C_L vs. α , C_L vs. C_M , and C_L vs. C_D).

These force data plots will be discussed in Subsection 4. The force data for the baseline C-141B wing-body-gearpod configuration and the C-141B/AC2 wing-body-gearpod configuration were used to determine performance improvements. These performance comparisons will be discussed in detail in section Subsection 5.

Pressure Data

Much of the pressure data obtained for the C-141B/AC2 wing along configuration is given in the discussion of code correlations later in this report. Here, we will show only some sample data.

Fig. 33 is presented to show the effects of the gearpod, on lower surface pressures. These effects are apparent, especially near the inward part of the wing.

Fig. 34 is a set of isometric plots of the pressure data for the C-141B/AC2 wing alone configuration at Mach 0.8. At the lower angles of attack, the outboard wing section shows negative lift in the first 20 to 30 percent chord. The shock wave at approximately 60% chord is apparent. This shock wave was specified in the design.

4. TASK 4 - AERODATA EVALUATIONS

The purpose of Task IV was to evaluate the wind tunnel data and compare this data with computed results.

a. Force Data

All of the force data obtained during the wind tunnel test is shown in Figures 26 through 32. In this section we will discuss that part of the force data which is relevant to a) configuration performance comparisons, and b) code correlations.

Figures 27a to 27c are plots of C_L vs. α , C_L vs. C_M , and C_L vs. C_D , respectively, for the C-141B/AC2 wing alone configuration. For the C_L vs. α curves in Figure 27a, as Mach number increases, the slope becomes steeper in the mid C_L range. At higher values of lift and Mach number, the slope decreases, and the data become non-linear, reflecting the effect of super-critical flow on the wing. The pitching moment curves in Figure 27b are generally non-linear. Additionally, the pitching moments are generally positive, whereas, for most transport type wings, the pitching moments would be expected to be negative. This can be explained by the fact that for this wing, the break occurs on the leading instead of the trailing edge. As a result, the inboard part of the wing makes a large positive contribution to the total moment about the quarter chord point of the mean aerodynamic chord (MAC). The drag polars (Figure 27c) vary as expected, with drag increasing for a fixed lift coefficient, as the Mach number increases.

Figures 29a through 29c give the C_L vs. α , C_L vs. C_M , and C_L vs. C_D variations for the C-141B/AC2 wing + fuselage + gearpod configuration. Comparing Figure 29a with Figure 27a, we see that the effect of the fuselage and gearpod is to reduce the lift somewhat (remember that the fuselage was non-metric). The reduction in lift is slightly higher at higher angles of attack. The pitching moment data (Figure 29b) is generally non-linear, except at lower values of lift, where for a given Mach number, there is little variation in C_M . The drag polars of Figure 29c exhibit the same sort of variation as the wing alone configuration, except for somewhat lower lifts due to the effects of the fuselage.

Figures 26a through 26c summarize the force data obtained for the C-141B baseline wing + fuselage + gearpod configuration. The lift and pitching moment data do not exhibit any unexpected variations. The drag polars from Figures 26c and 29c will be used as the basis for evaluating the C-141B/AC2 against the baseline C-141.

Drag Rise Characteristics

Figure 35 gives the drag rise characteristics for the baseline C-141B and the C-141B/AC2 wing + fuselage + gearpod configurations. The drag divergence Mach number curves which were derived from Figure 35, are given in Figure 36. The original C-141B/AC2 design point is indicated in Figure 36. The target drag divergence Mach number at $C_L = .6$ was not achieved in the wind tunnel test, mainly because of aeroelastic deformation of the model wing, and viscous uncambering in the cove region. However, it will be shown later that a very satisfactory, high performance configuration was obtained at $C_L = .56$ and $M_D = .78$.

b. Correlations

Correlations of the computer codes with the wind tunnel results were made for the C-141B/AC2 wing alone, and wing + pylon-nacelle configurations. The correlations were done by trying to match the measured wind tunnel lift by adjusting the angle of attack used in the computer codes. The correlations were made at nominal Mach numbers of .78 and .80. No Mach number corrections were attempted because it would have required many more computer runs to match lift, and because the uncertainties in predicting aeroelastic model deformation would overshadow any small Mach number correction.

The effects of model deformation under aerodynamic loading can be seen in Figure 37, where measured lift is compared to computed lift. The computed lift was obtained from a full potential equation code with iterated boundary layer (FLO22NM). Notice that when measured ordinates along with twist values which have been corrected for aerodynamic loading are used, the predicted C_L vs. α is much closer to the data.

Full Potential Equation Correlations -- Wing Alone

The code correlations shown in Figures 38 through 43 were made for the C-141B/AC2 wing alone configuration, using a full potential equation code with iterated boundary layer. The angles of attack used in the computations were chosen so as to match experimental lift values obtained from the force balance. The correlations were done for two Mach numbers (.78, .80) and three values of lift ($C_L = .33, .43, .60$). For each of these combinations of Mach number and lift, we made two calculations. The first calculation was made using the final design ordinates, and the design twist distribution. The second calculation used measured model ordinates and estimated twist.

After fabrication, the model was measured by a special measuring machine, to obtain the "as built" geometry. Initial correlations using measured ordinates and design twist showed that the twist distribution was wrong. The reason for this was that the model, having an aspect ratio of 12, was long and thin. This tended to make the model susceptible to aeroelastic deformation. An additional factor was the routing of 140 pressure tubes. Routing these tubes necessitated cutting a large channel in the lower surface of the wing which further weakened the structure.

To estimate what the aeroelastic deformation might actually be when the wing is in the tunnel and under load, we applied known loads to the wing to obtain its structural influence coefficients. These influence coefficients together with measured tunnel pressures were used to estimate corrections to the design twist distribution. The measured ordinates and estimated twists were then used for a second set of correlations.

Examining Figures 38 through 43, we see that by using measured ordinates and a twist distribution adjusted for aeroelastic deformation, we have improved the correlations. In general, the best correlations are obtained at the $\eta = .403$ station. Most of the correlations show discrepancies in the leading edge upper surface, and in the lower surface cove region. The discrepancy in the cove pressures is characteristic of flow separation (which was not modeled).

There are several possible reasons for the discrepancy near the leading edge, and we were not able to isolate any one reason in particular. The leading edge discrepancy is probably due to several factors acting together. The possibilities are: (1) Correlations were made to match total lift and not leading edge pressures, (2) Existence of a short separated region near the leading edge, (3) Transition strips which affect the readings of some of the leading edge pressure taps, (4) An actual twist distribution due to aerodynamic loading that is different from the predicted twist distribution, and (5) The small physical scale of the model which is conducive to leading edge irregularities.

Of particular note in the pressure distributions is the presence of a shock wave with an approximately constant angle. This weak swept shock wave was specified in the target pressures used to design the wing.

Extended Small Disturbance Equation Correlations - - Wing Alone

The code correlations shown in Figures 44 and 45 were made for the C-141B/AC2 wing alone configuration using the extended small disturbance code ATWP. Boundary layer effects were included by using viscous linking process of the design procedure. Angles of attack used in the computations were chosen so as to match the experimental lift values of the force balance. Correlations were done for one Mach number (.80) and two values of lift ($C_L = .32, .49$). The small disturbance computations used design ordinates and twist.

Examining Figures 44 and 45 we see that discrepancies in the correlations occur in the vicinity of the upper surface leading edge and in the lower surface cove region. The reasons for these discrepancies are as discussed in the section on the full potential equation correlations.

Correlations for Wing-Pylon-Nacelle Configuration

Figure 46 shows computations made using the Lockheed small disturbance wing-pylon-nacelle code. Because of restrictions on the way the nacelle computational grid is distributed, the computed and experimental results shown in Figure 46 are not exactly at the same spanwise location. But they are close enough to make a meaningful comparison, and thus, only the pressure row n station is given in the figure.

The pylon/nacelle was positioned at $\eta = .309$. Although the small disturbance code mispredicts the wing leading edge upper surface, the pylon/nacelle interference predictions are excellent. At locations inboard of the nacelle the interference effects are strong. Outboard of the nacelle the interference is minor. The predictions follow the experimental trends closely.

c. Effect of Wind Tunnel Walls

Figure 47 shows the effect on computed wing pressures of including measured wind tunnel wall pressures as boundary conditions. Two computed sets of pressures are shown. The first is a small disturbance solution at $M = .8$ and angle of attack = $.7^\circ$ with free air boundary conditions. The second is a small disturbance solution where measured wind tunnel wall static pressures were imposed as boundary conditions. The biggest effect of the wind tunnel walls is to move the upper surface shock forward. The effects on the lower surface pressures are not large, except at the two inboard stations.

d. Evaluation of Pressure and Force Balance Data

We took the measured pressures on the C-141B/AC2 model, integrated them to obtain section lifts, and then integrated the section lifts to obtain total lift. We then compared the total lift obtained from the pressure integration with lift obtained from the force balance. In general, the force balance lift was higher than the pressure lift. A difference between the two lifts is to be generally expected and would normally not exceed 5 or 6 percent. In our case, however, differences of the order of 10 or 12 percent were obtained for some runs. Figure 48 illustrates the problem.

The question then is what would account for such a discrepancy. Either the force balance readings were incorrect, or there was something wrong with the results from the pressure integration. We checked the force balance electronics and data acquisition system, and found them to be operating properly. As a further check on the force balance we installed a Lockheed ATA-V wing model in the wind tunnel, tested it, and compared these results with those obtained from a previous tunnel entry; the lift and drag data from the two entries were consistent. We then integrated ATA-V surface pressures and compared them to the force data. These comparisons showed differences that were in the acceptable range. It can, therefore, be concluded that neither the force balance readings nor the pressure integration methodology are responsible for the observed C-141B/AC2 lift discrepancies.

We then carefully checked the pressure data, eliminating or fairing through suspicious pressure readings, such as those in the vicinity of the transition strips. By integrating these new curves, we could eliminate about half of the excessive discrepancy. Although we could not pinpoint the exact cause of the remaining portion of the discrepancy, we have identified a number of possible contributing factors. These include a) the existence of a small region of separated flow on the upper surface leading edge, b) the aeroelastic twist and deflection due to the flexible wing structure, and c) the viscous lag in the smaller-than-normal (.020") tubing used because of the relatively small size of the wing. The latter (lag) effects were re-checked experimentally, and were found to account for a pressure error of less than one percent under even the most adverse sampling conditions.

In summary, then, our investigations indicate that the force balance readings of lift are correct. Because of a combination of factors which adversely affect the precision of our surface pressure readings, however, pressure-integrated lift values cannot be expected to produce an exact match for comparable force measurements.

5. TASK 5 - EVALUATION OF DESIGNS

There were two subtasks associated with Task V. The first subtask was to use the results of the wind tunnel tests to quantify the performance improvements of the new C-141B/AC2 configuration over the baseline C-141B, and in addition, to determine the cost savings attributable to the new design procedure. The second subtask was to evaluate the design procedure.

a. Performance Improvements

The C-141B/AC2 design conditions and wing geometry are substantially different from the C-141. Consequently, a comparison of wing aerodynamics does not by itself provide a true measure of the effectiveness of the new wing. For example, a comparison of drag polars at the C-141B/AC2 design Mach number would not be meaningful because the C-141 was designed to cruise at .77 Mach, and its wing is well into drag rise at .80 Mach. Consequently, the efficiency of the design procedure is evaluated by comparison of complete airplane performance capabilities rather than by reference to incremental aerodynamic characteristics. To make these comparisons, flight aerodynamics for the C-141B/AC2 are extrapolated from wind tunnel data using the known C-141 flight characteristics as a calibration.

In the Compressible Flow Wind Tunnel, the tunnel top and bottom walls are relatively close - approximately $3\frac{1}{2}$ mean chords - to the wing. Although a procedure for taking wall effects into account is under development, it is not at the point where it can be used with confidence. Accordingly, the analysis method we used is based on a comparison of uncorrected measured and estimated drag differences for the two wing-fuselage-gear pod configurations. The drag estimation technique is known to agree well with C-141 flight experience.

A drag estimation at $M = 0.70$ was made for each configuration at the wind tunnel Reynolds number and then compared with the measured model drag. The resulting drag differences are shown in Figure 49. The variation with lift coefficient is identical for the two designs, and the C-141B/AC2 drag is 10 counts less than the C-141B drag. The actual drag of the C-141B full-scale aircraft is known from flight tests and is reproduced by the drag estimation method employed. Assuming that the drag increment is insensitive to Reynolds numbers, the full-scale drag of the C-141B/AC2 aircraft at $M = 0.70$ can be obtained by subtracting 10 counts from the full-scale estimation drag polar for the C-141B.

The next step in the drag analysis procedure was the determination of the drag rise Mach number and the compressibility drag increment. A direct comparison of the measured drag rise characteristics of the wing-fuselage-gear pod configurations at constant C_L is presented in Figure 35. The corresponding drag divergence Mach numbers, M_D , are shown as a function of lift coefficient in Figure 36. The target M_D value for the C-141B/AC2 design of $M = 0.80$ at $C_L = 0.60$ was not achieved. This results partly from the viscous uncambering of the cove region at the relatively low tunnel Reynolds number, and partly from the aeroelastic deformation of the model wing at the high dynamic pressures of the Compressible Flow Wind Tunnel.

Reducing the full-scale design Mach number and lift coefficient to $M = 0.78$ and $C_L = 0.56$ in accordance with the measured data of Figure 36, nevertheless results in a highly satisfactory advanced technology C-141B/AC2 aircraft design. Figure 50 gives comparisons of payload-range performance. These comparisons show the actual payload-range performance of the C-141B, the C-141B/AC2 target performance which was based on what performance improvements we would expect to obtain by applying the new design method, and the predicted (based on wind tunnel test results) C-141B/AC2 performance which we actually did obtain. Of note is the better than targeted ferry range of the C-141B/AC2 made possible by the thick wing resulting from the application of the new wing design method.

The reduction in aircraft weights and fuel made possible by advanced technology are shown in Figure 51. The predicted gross weight reduction is 21%. This is 1% better than the target value of 20%. The predicted empty weight reduction is 24%, which is 4% better than the target value of 20%. The predicted block fuel decrease is 36% which is equal to the target value of 36%. Thus, with the exception of the .80 cruise Mach number, the study design objectives have been achieved.

b. ATT Cost Benefit Analysis

The question is always asked: "Can you quantify the benefits of new computational methods"? In this section we will do that for the ATT design procedure.

Previous Method

During 1977 and the early part of 1978, a transonic wing was designed at Lockheed-Georgia for the Advanced Transport Aircraft (ATA) configuration. The ATA configuration was a company-funded design exercise to produce an Advanced Transport Cargo Aircraft. The wing was designated ATA - V.

The design process for the ATA - V wing involved a total of 7 different computer programs and 7 engineers. The computer programs used were:

- (1) Carlson Transonic inverse 2-D code
- (2) TAP - 2-D analysis code
- (3) WPRESS - 2-D analysis code
- (4) WPRESS2 - improved 2-D analysis code
- (5) L-7 3-D lifting surface analysis code
- (6) ATWP - 3-D Transonic analysis code
- (7) AFSMOOTH - interpolation code

COMPUTER COSTS

The following runs were made for the ATA - V Design:

	CODE	NO. OF RUNS	COST
(1)	CARLSON	20	\$ 600
(2)	TAP	35	875
(3)	WPRESS & WPRESS2	30	150
(4)	L-7	20	300
		21	

(5)	ATWP	24	6,000
(6)	AFSMOOTH	Charges not significant	

TOTAL DOLLARS	\$7,925
---------------	---------

<u>LABOR</u>	<u>COST</u>
2,196 Manhours	\$73,675
TOTAL ATA-V DESIGN COST	= \$81,600

Present Method

The numerical optimization design procedure developed under the ATT contract was used in the high speed wing design of the projected new military transport currently known as the C-X. This gives us a cost figure for a wing design exclusive of any design procedure development costs, which is what we need. The C-X wing design involved 3 engineers over a span of 16 days. Here's the cost breakdown:

<u>COMPUTER RUNS</u>	<u>COST</u>
32	\$35,000
 <u>LABOR</u>	 <u>COST</u>
420 manhours	\$14,091
 TOTAL COSTS:	 \$49,091

In looking at the relative costs, we can see that the ATT procedure required \$27,075 more dollars in computer charges, but \$49,584 less in labor, thus resulting in a net savings of \$32,509. This amounts to a 40% reduction of total wing design costs.

Such savings are significant in terms of dollars. What is even more significant is that the calendar time required to do the design is substantially less. The ATA-V design was spread over a period of 14 months. If a concentrated effort was made, the ATA-V design could have been done in six months under the old procedure. This means that using the new design procedure would, in a case like this, decrease transonic wing design from six months to just over two weeks.

The potential for even further reduction in design cost is inherent in the ATT design procedure. Under Lockheed-Georgia internal funding we have carried out proof of concept studies where 2-D airfoil optimization computer time has been decreased by a factor of 5. For 3-D wing design using numerical optimization the factor of 5 is probably a bit conservative. Nevertheless, with improvement by a factor of 5 in a design such as the C-X the computer charge would then be \$7,000 for a total including labor of \$21,091. This is 26% of the ATA-V design cost.

c. Critique of Design Procedure

We have shown that using numerical optimization is a successful way to design wings which produce desired cruise pressure distributions and that the method can be incorporated within the framework of current aircraft design procedures. However, we have identified several areas where the current design procedure may be improved. These areas are:

1. Design variables
2. User expertise
3. Computation time

Design Variables

Sine deformation shape functions of the form $\sin^n(\pi x)$ provide the primary means of modifying the wing geometry to produce the desired pressures. The intent of these functions is to provide local geometric control. For example, the shape function $\sin^3 \pi x$ produces maximum geometric change at the 50% chord station as shown in Figure 52.. Also shown in that figure is the change in curvature produced by the shape function. Although the maximum curvature change occurs at 50% chord, there are two other locations of significant curvature change. Since curvature plays a dominant role in the development of the flow field, the non-localized curvature changes produced by the sine shape functions can cause undesired changes in the flow field and that introduces ambiguity in the optimization process.

A remedy for this is to use design variables based on the second derivative of the airfoil surface. Such shape functions not only localize the curvature variations, but also produce very smooth airfoils. Research is presently underway at Lockheed-Georgia and at the Ames Research Center, NASA, to develop efficient curvature-based design variables.

User Expertise

Engineers who are skilled aerodynamicists and who are familiar with numerical optimization are needed to successfully use optimization in aircraft design. This need exists because of (1) the requirement to accurately specify desirable pressure distributions which produce realistic wing geometries, and (2) difficulties encountered in selecting design shape functions which will produce the desired flow field modifications. The latter difficulty can be ameliorated by the use of curvature-based design variables.

Clearly, the difficulties encountered in the specification of desirable pressures are accentuated for multiple design point aircraft such as supersonic cruise/transonic maneuver fighters. For transport aircraft, consideration of wing weight and drag reduction must be balanced against one another. One possible solution to this problem is to conduct studies to identify sensible and desirable pressure distributions for different missions.

Another alternative is to use design objectives based on aerodynamic forces and moments. For this approach to be successful, the accuracy of computed aerodynamic forces and moments, in particular drag, must be improved. Experience with current numerical aerodynamic methods, even in two dimensions, has shown that inaccuracies in drag calculations can make realistic and reliable numerical optimization difficult. If sufficiently consistent and accurate drag calculation techniques can be developed, then the use of design objectives based on integrated aerodynamic parameters would best take advantage of the capabilities offered by numerical optimization.

Computation Time

Between 5 to 10 hours of computation time on a CDC 7600-class computer are needed to perform a wing design using the current numerical optimization scheme. These relatively large times are caused by the multitude of non-linear aerodynamic solutions required during the optimization process. The three obvious ways of reducing the computation times are (1) use more efficient computers, (2) use better solution algorithms, and (3) reduce the number of non-linear solutions.

The first two ways are related and they involve the use of new algorithms such as approximate factorization schemes on new vector computers such as the CRAY-1 and the CDC Cyber 203. Significant research is being devoted to this task.

The third way can be approached by at least two means. One approach is to develop a versatile and reliable 3-D inverse transonic method in which the wing geometry is computed directly from the specified pressures. Such a method would require about the same computation time used in transonic flow analysis. A deficiency in this approach is that constraints are difficult to impose. Nevertheless, an inverse method could produce a wing that is nearly an acceptable design. Numerical optimization could then be used for the final design refinements. The geometric changes might be expected to be less than for a complete optimization design, and fewer design variables might be required. Thus, the number of non-linear solutions needed in the optimization process should be reduced.

The second approach to reducing the number of non-linear solutions in fact involves the replacement of fine grid solutions with coarse grid results. To maintain accuracy, the coarse grid results are corrected to equivalent fine grid accuracy using Nixon's strained coordinate scheme¹⁸. The possibility of such an approach has already been explored by Lockheed-Georgia and Nielsen Engineering and Research scientists. In a proof of concept study, optimization, together with Nixon's strained coordinate scheme have been coupled to a 2-D transonic airfoil code. With this scheme, computer time for airfoil design using numerical optimization has been

reduced by close to a factor of 5.

By implementing a design procedure incorporating an inverse method together with numerical optimization and strained coordinates, we can expect to reduce wing design computation time from the current 5 to 10 hour range to approximately 1 to 2 hours on a CDC 7600. By using an algorithm which takes advantage of new vector processing computers, computer-aided wing transonic aerodynamic design in less than 1/2 hour can be forecast.

6. TASK 6 - FINAL DESIGN PROCEDURE

The wing design procedure involves the use of combinations of the following computer programs:

- o Full Potential Inviscid NCR
- o Extended Small Disturbance NCR and FCR
- o Numerical Optimization
- o Two-Dimensional Boundary Layer
- o Linking Codes
- o Subsonic Panel Code
- o Transonic Wing/Pylon/Nacelle Code

The steps involved in the procedure are shown in Figure 53.

a. Starting Wing

Starting wing geometry is not critical to the success of the method; however, computation costs can be reduced by selecting a wing with well-behaved flow near the design condition. For transonic transports the airfoil sections designed for this contract should be satisfactory for typical wing planforms. Alternatively, a wing with which the user has some previous experience can be used, or a wing with an airfoil section designed with 2-D design methods (e.g., ref. 12, 17) might be employed.

The wing geometry is defined by a number of spanwise geometric control stations connected by spanwise linear loft elements. We have found that this approach provides sufficient design flexibility and at the same time produces a wing which is easy to manufacture by avoiding compound curvature. Our experience shows that a four control station wing (root, break, mid-semispan, tip) is adequate. However, an additional station between the root and break might be needed in some applications.

b. Inviscid Solution

At this point, the user should select the transonic analysis code - FPE or ESD NCR/FCR. Based on our experience, FPE optimization is more reliable, but ESD NCR might be satisfactory if the wing leading edge is not being changed. Although we have not done a conclusive analysis, we believe ESD/FCR design should be avoided.

Having selected the analysis code, compute an inviscid solution for the starting wing at the design Mach number. The angle of attack should be selected to produce a lift coefficient which is about 10% greater than the design untrimmed lift coefficient. The geometry file must be cataloged for later use and the pressure distribution must be cataloged for use in the boundary layer analysis.

c. Boundary Layer Analysis

Attach the pressure distribution data file and use the 2-D boundary layer code to compute displacement thicknesses at the wing geometric control stations. At this point, the user should select the design Reynolds number. If the wing is being designed for technology demonstration, tunnel Reynolds number should be used. Flight Reynolds number is advisable for aircraft design applications.

Catalog the displacement thickness file for use in the next step.

d. Link Up

Using the Link-Up program with the geometry and displacement thickness files, compute the starting viscous pressure distribution.

NOTE: The inviscid solution, boundary layer analysis, and link-up steps could be replaced by a 3-D viscous analysis (e.g. the viscous FPE code available from NASA-Ames). However, this approach can introduce some inconsistency in the design procedure.

e. Design Pressures

Design pressures are specified near each geometric control station. The tip pressures should be defined near the 90% span station to avoid inaccuracies in solutions near the tip. Our experience shows that design pressures with a single weak shock wave outboard on the wing should be selected. The root upper surface pressures should have a mild re-compression gradient. For many applications, the upper surface pressure distributions used in this study should be quite satisfactory. The lower surface pressures should be selected to produce the desired aft loading and wing thickness.

The subsonic panel code is used to ascertain the fuselage/gearpod interference effects. These should be accounted for in the design pressures. The interference effects of the pylon/nacelle installation can be determined by running the transonic wing-pylon/nacelle code.

f. Design

Wing design is accomplished by designing the upper surface first and then the lower surface. Upper surface design is done station by station from root to tip. Specifically, the root station is designed to produce specified root pressures while keeping other stations fixed. The centerline station wing carry-through geometry is automatically changed to be the same as the root station. We have found that it is best to change the entire airfoil upper surface at a control station if the pressures at that control station are shock free. Otherwise, the design variables which affect geometric changes upstream of the shock should be used to produce the desired pressures ahead of the shock. Next, the recompression downstream of the shock is designed.

Once the pressure distribution at the root is satisfactory, the root airfoil geometry is fixed at the geometry that came out of the root design, and the next outboard station is designed.

After each upper surface station is designed, the lower surface is designed proceeding from root to tip. The lower surface pressures should be selected to produce the desired wing thickness and aft loading. The entire lower surface at a span station can be designed simultaneously.

After the entire wing has been modified, the procedure can be repeated, as required. Our experience shows that two iterations of the wing design procedure are generally required.

g. Inviscid Analysis

The designed fluid wing is next analyzed using the inviscid analysis code which was used during design. The resulting pressures and the wing geometry are cataloged for use in the next two steps.

h. Boundary Layer Analysis

The 2-D boundary layer code is used to compute displacement thickness distributions at each control station. The output of the analysis should be carefully reviewed to define separation locations. Separation in the cove should be avoided, but separation near the trailing edge (~97% chord) might be unavoidable and is not a serious problem. The user should use all separation indicators ($d\delta^*/dx$, C_f , form factor) in making an engineering judgment to define separation.

The displacement thickness file is cataloged for use in the next step.

i. Link-Down

The link-down program subtracts the δ^* from the fluid geometry to produce the solid wing. The user should carefully review the resulting solid wing geometry for smoothness. We have found that one or two smoothings are desirable.

j. Viscous Analysis

The last step of the procedure is a viscous analysis of the solid wing. The analysis should be done using both the linking technique of the design method and a coupled viscous analysis method. The results of this analysis should compare closely to the results of the inviscid analysis of the fluid wing.

k. A Final Note

The design procedure involves a great deal of user interactions with the computer codes. This was done on purpose. Engineering judgment is required in many key steps, and in particular, steps involving boundary layer analyses. We do not believe that our ability to compute separation, transition, and equivalent fluid geometry is at present, sufficiently reliable to permit hands-off design.

SECTION III

CONCLUDING COMMENTS

We have developed a new transonic wing design method using the numerical optimization scheme. We have also shown that new computational methods offer a means for the aerodynamic design of wings with transonic performance superior to that which could be obtained using previous design techniques. The method is relatively easy to use, and it is compatible with established industry design procedures. By using the new method, a 40% to 50% reduction in the cost associated with wing cruise aerodynamic design is obtainable. By incorporating the strained coordinate scheme into the method, cost reductions should approach 75%. Additionally, adapting a strained coordinate version of the method to the new vector processing computers should make possible efficient wing design using less than $\frac{1}{2}$ hour computation time.

REFERENCES

1. Boppe, C. W.: "Calculation of Transonic Wing Flows by Grid Embedding," AIAA Paper No. 77-207, January 1977.
2. Boppe, C. W.: "Computational Transonic Flow About Realistic Aircraft Configurations," AIAA Paper No. 78-104, January 1978.
3. Mason, W. H., et al.: "An Automated Procedure for Computing the Three-Dimensional Transonic Flow Over Wing-Body Combinations, Including Viscous Effects," AFFDL-TR-77-122, October 1977.
4. Jameson, A.: "Iterative Solution of Transonic Flows Over Airfoils and Wings," *Comm. Pure Appl. Math.*, Volume 27, 1974, pp. 283-309.
5. Jameson, A.; and Caughey, D. A.: "A Finite Volume Method for Transonic Potential Flow Calculation," AIAA Paper No. 77-635, June 1977.
6. Blackerby, W. T.; and Smith, P. R.: "Aerodynamic Investigation of C-141 Leading Edge Modification for Cruise Drag Reduction," AFFDL TR79-3059, June 1979.
7. Caughey, D. A.; and Jameson, A.: "Accelerated Iterative Calculation of Transonic Nacelle Flow Fields," *AIAA Journal*, Volume 15, No. 10, October 1977, pp. 1474-1480.
8. Vanderplaats, G. N.: "CONMIN - A Fortran Program for Constrained Function Minimization," NASA TM X-62282, August 1973.
9. McNally, W. D.: "FORTRAN Program for Calculating Compressible Laminar and Turbulent Boundary Layers in Arbitrary Pressure Gradients," NASA TN D-5681, 1970.
10. Bartlett, D. W.: "Wind Tunnel Investigation of Several High Aspect Ratio Supercritical Wing Configurations on a Wide-Body-Type Fuselage," NASA TM X-71996, 1977.
11. Kline, J.: "Wind Tunnel Tests of a 0.030 Scale Full-Span Model of the Lockheed-Georgia ATA Series 5 Transport," Calspan Rpt. AA-4007-W-7, 1978.
12. Carlson, L. A.: "Transonic Airfoil Analysis and Design Using Cartesian Coordinates," AIAA Proceedings, Second Computational Fluid Dynamics Conference, Hartford, Conn., 1975.
13. Bauer, F., et. al., "Supercritical Wing Section," *Lecture Notes in Economics and Mathematical Systems* 66, Springer-Verlag, 1972.
14. Jameson, A.: "Iterative Solution of Transonic Flows Over Airfoils and Wings," *Comm. Pure and Appl. Math.*, Volume 27, 1974, pp. 283-309.
15. Pounds, G. A.; and Stanewsky, E.: The Research Compressible Flow Facility. Lockheed-Georgia Company ER-9219, 1967.
16. Braslow, Albert L.; and Knox, Eugene C.: Simplified Methods for Determining of Critical Height of Distributed Roughness Particles for Boundary Layer

Transition at Mach Numbers from 0 to 5. NACA TN 4363, 1958.

17. Vanderplaats, G. N., Hicks, R. M. and Murman, E. M.: "Application of Numerical Optimization Techniques to Airfoil Design," NASA SP-347, Part II, 1975.
18. Nixon, D: "Techniques for Correcting Approximate Finite Difference Solutions," AIAA Paper No. 79-0277, 1979.

TABLE 2: C-141 PRESSURE TAP LOCATIONS

$\eta = .193$			$\eta = .389$		$\eta = .637$	
X/C	UPPER	LOWER	UPPER	LOWER	UPPER	LOWER
	.025	.025	.025	.025	.025	.025
	.05	.05	.05	.05	.05	.05
	.075	.075	.075	.10	.075	.075
	.10	.10	.10	.15	.10	.10
	.125	.15	.125	.20	.125	.15
	.15	.20	.15	.30	.15	.20
	.175	.30	.175	.40	.175	.30
	.20	.40	.20	.60	.20	.40
	.25	.50	.25	.70	.25	.50
	.3	.60	.30	.80	.30	.60
	.35	.70	.35	.90	.35	.80
	.40	.80	.40		.40	.90
	.45		.45		.45	
	.475		.475		.475	
	.50		.50		.50	
	.525		.525		.525	
	.55		.55		.55	
	.60		.575		.575	
	.625		.60		.60	
	.675		.625		.625	
	.70		.65		.65	
	.725		.675		.70	
	.75		.70		.725	
	.80		.725		.75	
	.85		.75		.775	
	.90		.775		.80	
			.80		.85	
			.85		.90	
			.90		.95	
			.95			

TABLE 3: C-141/AC2 PRESSURE TAP LOCATION

$\eta = .153$			$\eta = .253$		$\eta = .403$		$\eta = .653$		$\eta = .861$	
X/C	UPPER	LOWER	UPPER	LOWER	UPPER	LOWER	UPPER	LOWER	UPPER	LOWER
	.02	.05	.02	.05	.02	.05	.04	.04	.03	.04
	.05	.10	.05	.10	.05	.10	.10	.10	.10	.10
	.10	.20	.10	.20	.10	.20	.20	.20	.20	.20
	.15	.30	.15	.30	.15	.30	.30	.30	.30	.30
	.20	.40	.20	.40	.20	.40	.30	.45	.40	.45
	.25	.50	.25	.50	.25	.50	.45	.60	.48	.60
	.30	.60	.30	.60	.30	.60	.50	.75	.56	.75
	.35	.70	.35	.70	.35	.70	.55	.90	.64	.90
	.40	.80	.40	.80	.40	.80	.60		.72	
	.45	.85	.45	.85	.45	.85	.65		.80	
	.50	.90	.50	.90	.50	.90	.70		.90	
	.55	.95	.55	.95	.55	.95	.80		.97	
	.60		.60		.60		.90			
	.65		.65		.65		.97			
	.70		.70		.70					
	.75		.75		.75					
	.80		.80		.80					
	.85		.85		.85					
	.90		.90		.90					
	.95		.95		.95					
	.98		.98		.98					

TABLE 4: C-141B/AC2 MEASURED MODEL ORDINATES & ESTIMATED TWISTS

X/C	$\eta = 0$		$\eta = .0923$		$\eta = .2757$		$\eta = .6$		$\eta = 1.0$	
	ZU/C	ZL/C	ZU/C	ZL/C	ZU/C	ZL/C	ZU/C	ZL/C	ZU/C	ZL/C
0.0	.0179	.0179	.0131	.0131	.0162	.0162	.0085	.0085	0.0	0.0
.00241	.0322	-.0001	.0306	-.0012	.02281	.0035	.0162	-.00257	.00346	-.0161
.00961	.04282	-.0172	.0434	-.0204	.02973	-.0082	.0242	-.01349	.00931	-.0239
.02153	.05139	-.0316	.512	-.03437	.03649	-.01872	.0319	-.02385	.01445	-.0321
.03806	.05839	-.0434	.0579	-.04464	.04211	-.0253	.0384	-.03104	.02056	-.03875
.05904	.06441	-.05188	.06377	-.05253	.04799	-.03106	.04378	-.03683	.02708	-.04472
.08427	.0691	-.05833	.06931	-.05901	.05373	-.03663	.04975	-.04184	.03389	-.04947
.11349	.0739	-.06355	.07359	-.06316	.05913	-.04169	.0546	-.04633	.04034	-.05325
.14645	.07702	-.06717	.07695	-.06626	.06395	-.0463	.0584	-.0503	.0462	-.05658
.1828	.0795	-.06942	.07937	-.06966	.06818	-.05014	.06141	-.05358	.0512	-.05891
.22221	.08109	-.07011	.08059	-.07041	.07175	-.05312	.06384	-.05603	.0557	-.06021
.2643	.0812	-.06953	.08049	-.06966	.07465	-.05523	.0659	-.05763	.05966	-.06049
.30866	.07996	-.06743	.07918	-.06749	.07688	-.05625	.06758	-.05812	.06314	-.05981
.35486	.07751	-.06403	.07698	-.06395	.07816	-.05633	.06878	-.05729	.0657	-.05788
.40245	.0744	-.05948	.07401	-.05913	.07837	-.05513	.06967	-.05527	.0678	-.05459
.45099	.07066	-.0538	.07041	-.05332	.07758	-.05223	.07042	-.05172	.06903	-.04976
.5	.06637	-.04739	.06625	-.04663	.07585	-.04744	.07058	-.04635	.06907	-.04351
.54901	.06153	-.04056	.0616	-.0395	.07314	-.04124	.07005	-.03965	.06817	-.03626
.59755	.05643	-.03341	.05657	-.03227	.06954	-.03396	.06863	-.03189	.06619	-.02856
.64514	.05105	-.02642	.05122	-.02538	.06529	-.02627	.06625	-.02362	.063	-.02095
.69134	.04544	-.02003	.04566	-.01905	.06053	-.01883	.06265	-.01586	.05855	-.01344
.7357	.03976	-.01468	.04004	-.01362	.0552	-.01239	.05775	-.00914	.05298	-.00733
.77779	.03422	-.01057	.03451	-.00932	.04937	-.00736	.05165	-.00398	.04643	-.00262
.8172	.02891	-.0073	.02919	-.00603	.04305	-.00371	.04461	-.00061	.03889	-.00066
.85355	.02388	-.00474	.02414	-.00366	.036318	-.00127	.03724	.00125	.03091	-.000237
.88651	.01913	-.00296	.01939	-.0021	.02956	.00011	.03011	.00211	.02334	.00188
.91573	.01466	-.00191	.01495	-.00122	.023	.0005	.02353	.00198	.01659	.00078
.94096	.01068	-.00155	.01094	-.00087	.01706	.00034	.01742	.00128	.01053	-.00024
.96194	.00728	-.00141	.00743	-.00091	.01201	-.00005	.01215	.00024	.0049	-.00074
.97847	.00451	-.00104	.00473	-.00109	.00795	-.00047	.00791	-.00082	.00152	-.00155
.99039	.00242	-.00089	.00289	-.00128	.00494	-.00084	.00472	-.00151	.00032	-.00117
.99759	.00111	-.00082	.00181	-.00142	.003	-.00098	.00255	-.00178	.00009	-.00043
1.0	.00067	-.00067	.00145	-.00147	.00232	-.00226	.00178	-.0018	.00009	-.00009

ZU = UPPER SURFACE
ZL = LOWER SURFACE

TABLE 4: C-141B/AC2 MEASURED MODEL ORDINATES & ESTIMATED TWISTS (CONTINUED)

C-141B/AC2 TWIST DISTRIBUTIONS

(Estimated Twist To Be Used With Measured Model Ordinates)

	$\eta = 0$	$\eta = .0923$	$\eta = .2757$	$\eta = 6$	$\eta = 1.0$
Design Twist	4.911°	4.911°	3.368°	2.336°	.646°
Estimated Twist $M = .8; C_L = .6$	3.764°	3.617°	2.096°	.725°	-.724°
Estimated Twist $M = .8; C_L = .445$	3.764°	3.657°	2.227°	.999°	-.42°
Estimated Twist $M = .8; C_L = .33$	3.764°	3.678°	2.294°	1.14°	-.2683°
Estimated Twist $M = .78; C_L = .6$	3.764°	3.619°	2.105°	.743°	-.705°
Estimated Twist $M = .78; C_L = .445$	3.764°	3.657°	2.227°	.999°	-.42°
Estimated Twist $M = .78; C_L = .33$	3.764°	3.681°	2.303°	1.158°	-.247°

TABLE 5: TEST MATRIX

TEST MATRIX FOR TESTS
 CFWT052 = C-141B CONFIGURATION
 CFWT053 = C-141B/AC2 CONFIGURATION

W₁ = C-141B Wing
 W₂ = C-141B/AC2 Wing
 F = Fuselage
 GP = Gear Pod
 PN = Pylon/Nacelle

CONFIGURATION	TEST	SERIES	.6	.7	.75	.78	.79	.80	.81	.82	.84
W ₁ + F + GP	CFWT052	3	A	A	A	A	A	A	A	A	A
W ₂	CFWT053	0		B		B		B	B		
W ₂ + PN	CFWT053	1		B		B		B	B		
W ₂ + PN + F	CFWT053	5		B		B		B	B		
W ₂ + PN + F + GP	CFWT053	4	B	B	B	B	B	A	B	B	B
W ₂ + F + GP	CFWT053	3	A	A	A	A	A	A	A	A	
W ₂ + F	CFWT053	6		B		B		B	B		

α Schedules:

A: -2, -1, -0.5, 0.0, 0.5, 1.0, 1.5, 2.0, 3.0, 4.0

B: -1, 0.0, 0.5, 1.0, 1.5, 2.0, 3.0

TABLE 6: RUN SUMMARY TEST CFWT053
C-141B/AC2 CONFIGURATION

CONFIGURATION: W₂; SERIES 0; R = 5 X 10⁶

M	-2	-1	-0.5	0	0.5	1.0	1.5	2.0	3.0	4.0
.60										
.70		10		11	12	13	14	15	16	
.75										
.78		29		28	23	24	25	26	27	
.79										
.80		31		32	33	34	35	36	37	
.81		38		39	40	41	42	43	44	
.82										
.84										

R = 2.5 X 10⁶

.70	1	2	3	4	5	6	7
-----	---	---	---	---	---	---	---

TABLE 6: RUN SUMMARY TEST CFWT053 C-141B/AC2 CONFIGURATION (CONTINUED)

CONFIGURATION: $W_2 + PN$; SERIES 1; $R \approx 5 \times 10^6$

M	α									
	-2	-1	-0.5	0	0.5	1.0	1.5	2.0	3.0	4.0
.60										
.70		47		48	49	50	51	52	53	
.75										
.78		55		57	58	59	60	61	62	
.79										
.80		64		65	66	67	68	69	70	
.81		71		72	73	74	75	76	77	
.82										
.84										

TABLE 6: RUN SUMMARY TEST CFWT053 C-141B/AC2 CONFIGURATION (CONTINUED)

CONFIGURATION: $W_2 + F + GP$; SERIES 3; $R \approx 5 \times 10^6$

M	α									
	-2	-1	-0.5	0	0.5	1.0	1.5	2.0	3.0	4.0
.60	112	131	132	133	134	135	136	138	139	140
.70	113	142	143	144	145	146	149	150	151	152
.75	141	155	156	157	158	160	161	162	163	164
.78	165	166	167	168	169	170	171	172	173	174
.79	175	176	177	196	197	198	199	200	201	202
.80	102	103	104	105	106	107	108	109	110	111
.81	204	205	207	208	209	210	211	212	213	214
.82	216	219	220	221	222	223	224	225	226	227
.84	229	230	231	232	233	235	236	237	238	239

$R \approx 2.5 \times 10^6$

R Sweep At $M = 0.80$, $\alpha = 2.0$

$R \times 10^{-6}$	RUN NO.
1.6	127
2.5	122
3.1	128
4.04	129
5.0	109

TABLE 6: RUN SUMMARY TEST CFWT053 C-141B/AC2 CONFIGURATION (CONTINUED)

CONFIGURATION: $W_2 + PN + F + GP$; SERIES 4; $R \approx 5 \times 10^6$

M	α									
	-2	-1	-0.5	0	0.5	1.0	1.5	2.0	3.0	4.0
.60		251		252	253	254	255	256	257	
.70				259						
		258		260	262	263	264	265	266	
.75		268		269	270	271	272	273	274	
.78		276		277	279	280	281	284	285	
.79		287		288	289	290	291	292	293	
.80										
	241	242		244	245	246	247	248	249	250
.81										
		295		296	298	299	304	305	307	
.82										
		310		311	312	313	314	315	316	
.84										
		318		319	320	321	322	323	324	

TABLE 5: RUN SUMMARY TEST CFWT053 C-141B/AC2 CONFIGURATION (CONTINUED)

CONFIGURATION: $W_2 + PN + F$; SERIES 5; $R \approx 5 \times 10^6$

M	α									
	-2	-1	-0.5	0	0.5	1.0	1.5	2.0	3.0	4.0
.60										
.70		333		336	337	338	339	340	341	
.75										
.78		343		344	345	346	347	348	349	
.79										
.80		351		352	353	354	355	356	357	
.81		359		360	361	362	363	364	365	
.82										
.84										

TABLE 6: RUN SUMMARY TEST CFWT053 C-141B/AC2 CONFIGURATION (CONTINUED)

CONFIGURATION: $W_2 + F$; SERIES 6; $R \approx 5 \times 10^6$

M	α									
	-2	-1	-0.5	0	0.5	1.0	1.5	2.0	3.0	4.0
.60										
.70		370		371	372	373	374	375	376	
.75										
.78		377		378	379	380	381	382	383	
.79										
.80		384		385	386	387	388	389	390	
.81		391		392	393	394	395	396	397	
.82										
.84										

TABLE 7: RUN SUMMARY TEST CFWT052
C-141B CONFIGURATION

CONFIGURATION: $W_1 + F + GP$; SERIES 3; $R \approx 5 \times 10^6$

M	α									
	-2	-1	-0.5	0	0.5	1.0	1.5	2.0	3.0	4.0
.60	196	197	198	199, 200 201, 236	202	203	204	205	206	207
.70	208	209	210	211, 212	213	214	215	216	217	218
.75	224	225	227	228	229 230	231	232	233	234	235
.78	237	238	239	240	241	242	243	244	245	246
.79	247	248	249	250, 251	252	253	254	255	256	257
.80	258	259	260	261, 262	263	264	265	266	267	268
.81	269	271	272	273, 274	275	276	277	278	279	280
.82	281	282	283	284, 285	286	287	288	289	290	291
.84	292	293	294	295, 296	297	298	299	300	301	302

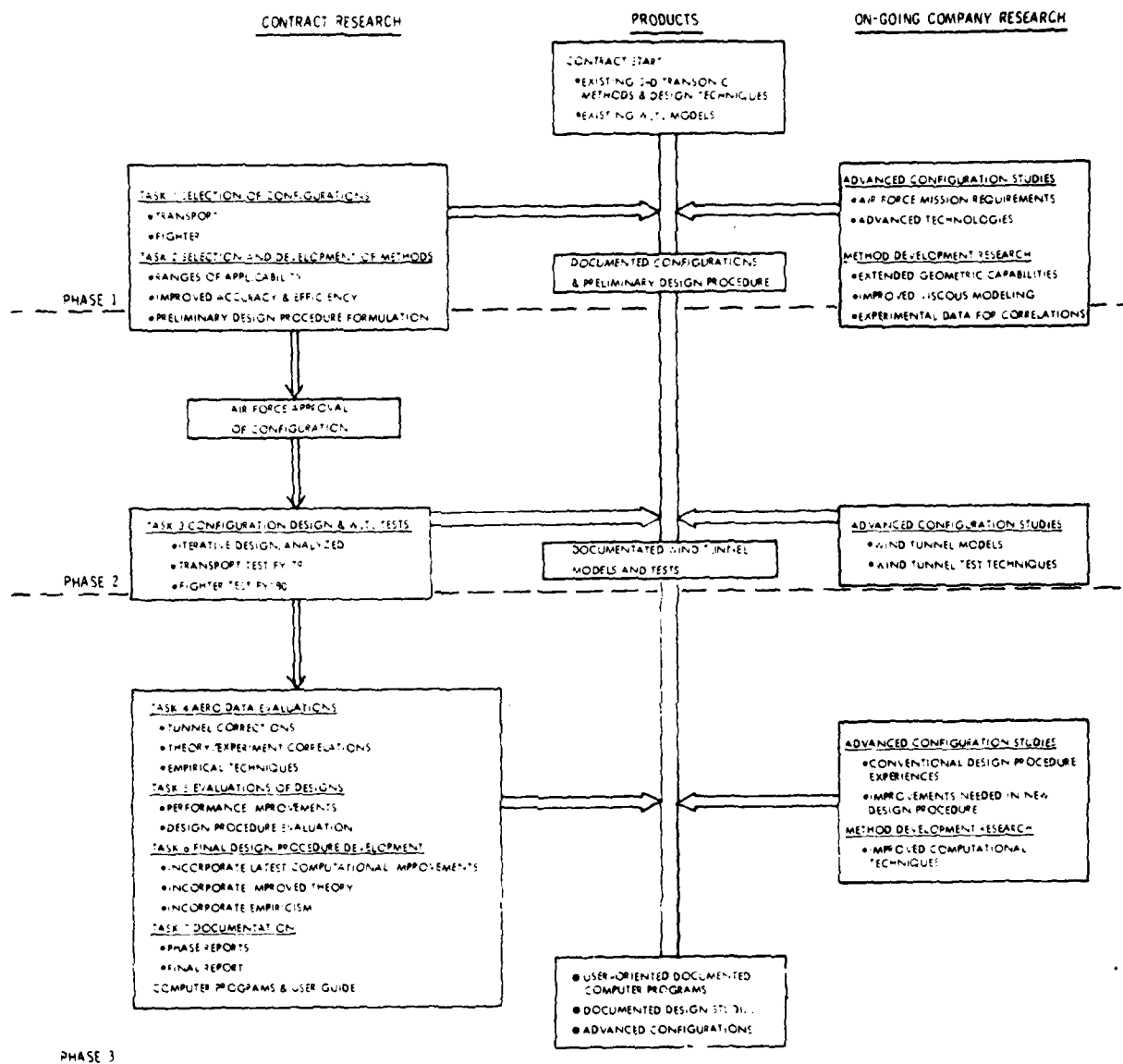
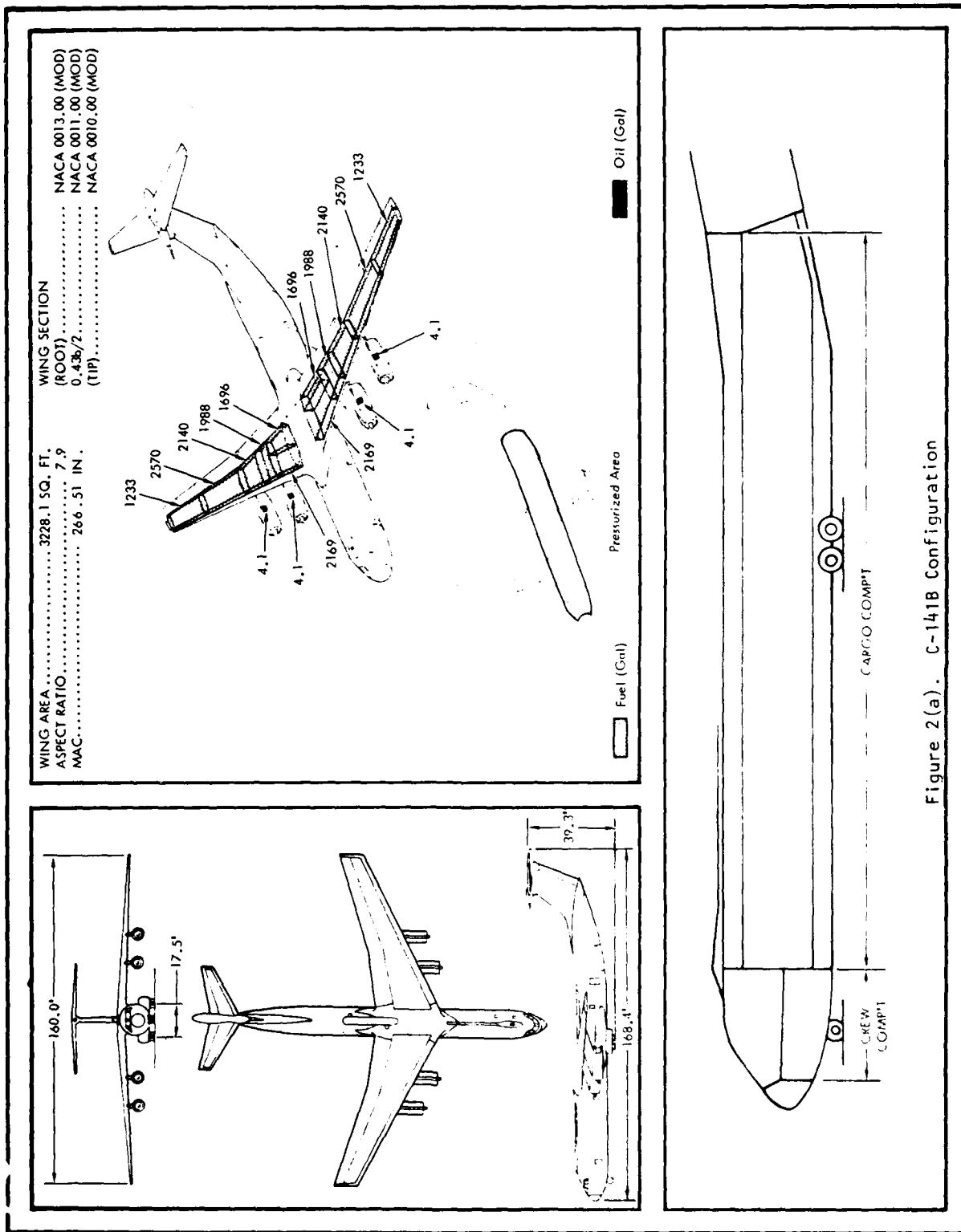


Figure 1. Program Plan



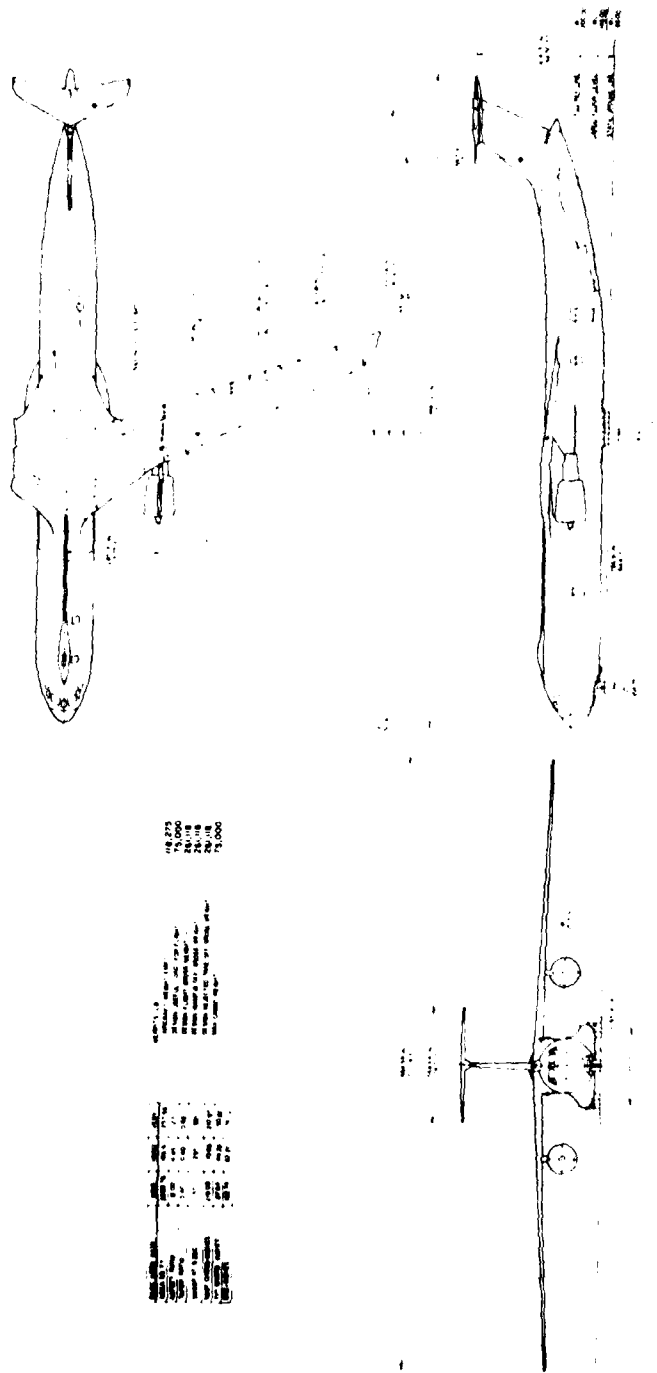


Figure 2(b). C-141B AC2 Configuration

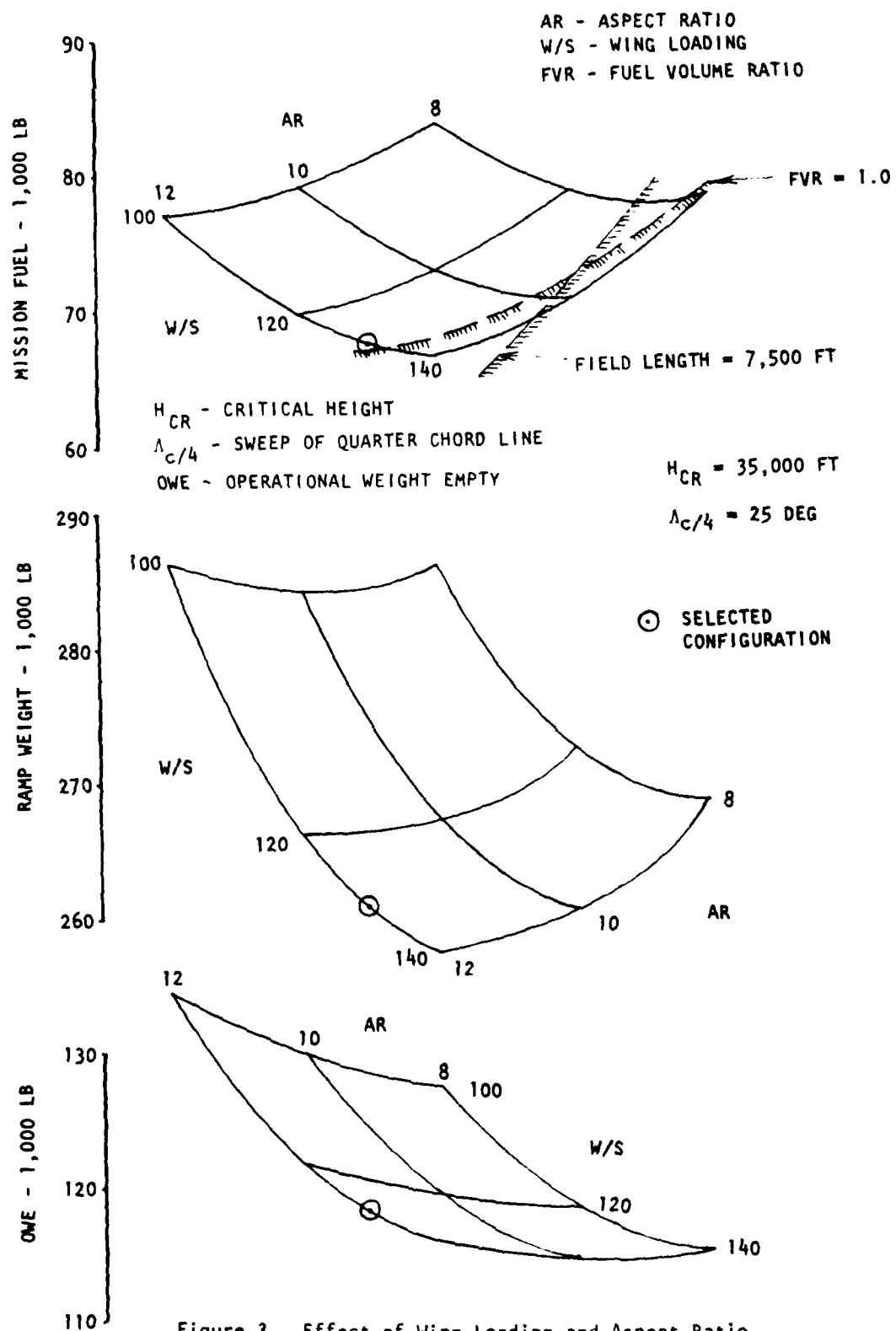


Figure 3. Effect of Wing Loading and Aspect Ratio on C-141B/AC2 Fuel and Weight

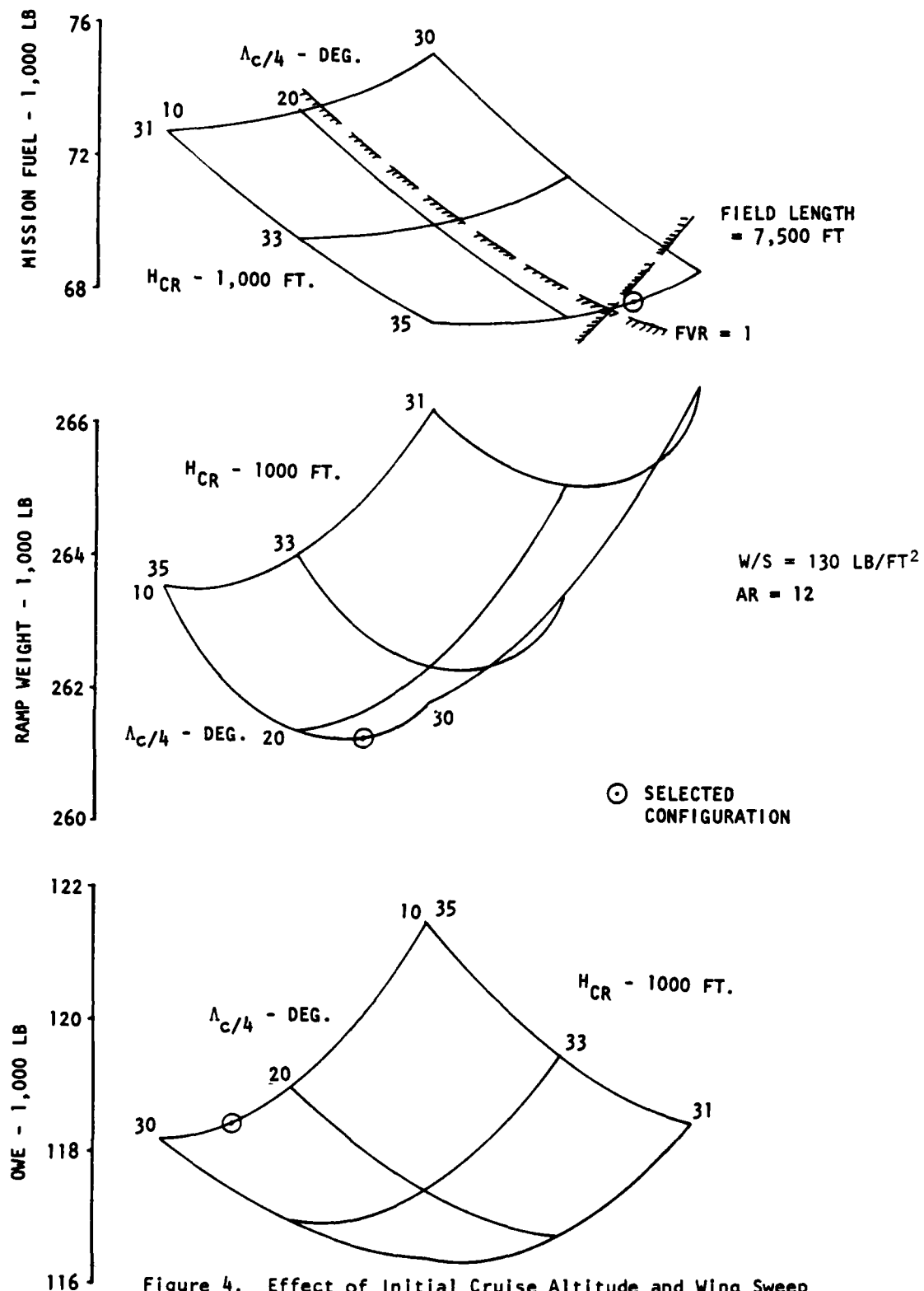


Figure 4. Effect of Initial Cruise Altitude and Wing Sweep on C-141B/AC2 Fuel and Weight

C-141B/AC2 SELECTED TRANSPORT CONFIGURATION
 RANGE= 3500. N.M. PAYLOAD= 75000. CRUISE MACH= .800 DELTA MACH= .000
 CENTER SECTION FUEL WAS USED IN Y-RANGE CALCULATION. MISC. DRAG= 17.0 COUNTS.
 .0 PERCENT 2-ND SEGMENT L/D

THRUST	ETA	II-1000	W/S	CL	AR	SWEEP	T/C	SW	W-RAMP	OW	CR-L/D	FVR
38774.	.80	35.	130.00	.56312.00	25.00	.1087	1960.	261118.	119275.	21.17	1.059	
/---DESIGN POINT DATA---/												
W-RAMP	DOC/SM	WTO	WTLND	FAAFL	LOIST	T/W	ORAD	CLMXT	CLMXL	FLPT	FLML	
261118.	.000	261118.	227196.	7512.	4115.	.2970	.0423	1.76	2.25	10.0	40.0	
WPR	TRATE	FNTTO	TCRUS	SFC	EDWT	DENG	LNAC	MISFUEL	HLKFUEL	CD	LFCWT	
					(IN)	(IN)						
4.50	38774.	36112.	7521.	.725	6019.	81.6	149.	67842.	61490.	.0275	0.	

DRAG BUILDUP, MACH NO. = .8000
 BASE DES MACH NO. = .8093 DEL MACH NO. = -.0093

WETTED AREA/WING AREA

WING= 1.8302 FUSELAGE= 3.4101 PYLON= .0203
 HOR TAIL= .1918 VERT TAIL= .2664

SHIT= 185.4 SVT= 257.6 ENDPLATE/SIDE= .0
 INITIAL CRUISE LIFT COEFFICIENT= .5828

WING= .00581 FUSELAGE= .00550 UPSWEEP= .00026 ENDPLATE= .00000

PYLON= .00006 NACELLE= .00000 HOR TAIL= .00061 VERT TAIL= .00075

TAIL BOOM= .00000 SWIRL DRAG = .00000 SCRUJ DRAG = .00000 PROP WETTED = .0

CDC= .00100 DELCDP= .00012 CDNACINT= .00000 CDCREEP= .00000

TRIM= .00120 MISC= .00170 INTERFERENCE= .00065 ROUGHNESS= .00039

TOTAL PROFILE DRAG= .01522 INDUCED= .00948 TOTAL DRAG= .02753

Figure 5. C-141B/AC2 Configuration Data and Target Performance

GEOMETRIC SUMMARY

FUSELAGE

LENGTH	MAX HEIGHT	MAX WIDTH	WETTED AREA	FLOOR LENGTH	FLOOR WIDTH
155.630	14.160	14.160	6683.30		

BASIC WING

TAPER	SPAN	US SWP	LE SWP	TE SWP	RT CID	TP CID	M.A.C.	X APEX	X LE	Y LE	AREA	X25MAC	AR
.4000	153.36	25.000	26.658	19.757	18.257	7.303	13.562	53.881	70.378	32.862	1959.86	.4740	12.0000
TOTAL WING													
							15.040				2083.78		11.2863

COMPLETE WING

LE HAT SWEEP	TE HAT SWEEP	ROOT TOTAL	OUTURK ETA	OUTURK CHORD	INURK ETA	INURK CHORD	GLOVE AREA	TOTAL AREA	SPOILER AREA	SPOILER % CID	LE FLP AREA	LE FLP % CID	TE FLP AREA	TE FLP % CID
37.930	19.757	24.119	.2757	15.237	.2757	15.237	54.82	2014.68	118.04	.0800	168.83	.1000	285.75	.2500

EMPERIAGE (IF NHING=2, 'HOR' IS ONE EMPLATE)

T/C	TAPER	VUAR	SWEEP	AR	ROOT	TIP	MAC	YUAR	ARM	SPAN	AREA	
HOR	.0950	.4000	.5720	25.000	4.450	9.221	3.688	6.850	6.155	82.00	28.72	185.41
VER	.0950	.6200	.0617	35.000	1.270	17.581	10.900	14.502	8.336	72.00	18.09	257.56

ENGINES & NACELLES

NUMBER ENGINES	ENGINE LOC	PROP DIA	ENGINE LENGTH	ENGINE DIA	NACELLE DIA	NACELLE LENGTH	INSTLD LENGTH	ENGINE SPANWISE LOCATIONS
2	.000	.000	12.457	6.804	7.892	12.457	23.716	-27.79
NUMBER PYLONS	PYLON THICK	PYLON CHORD	PYLON HEIGHT	PYLON AREA				
2.0	.0800	12.457	.789	19.66				

Figure 5. Continued

CONDITION	WT	C G	% MAC
WEIGHT EMPTY	116405.68	860.71	9.94
OPERATING WEIGHT	116275.24	861.29	10.29
ZERO FUEL WEIGHT	193275.23	853.18	5.31
GROSS WEIGHT	261117.59	868.70	14.04
GROSS WT NO PAYLOAD	186117.59	880.10	21.85

APEX = 646.57

LEMAC = 844.54

MAC = 162.75

Figure 5. Concluded

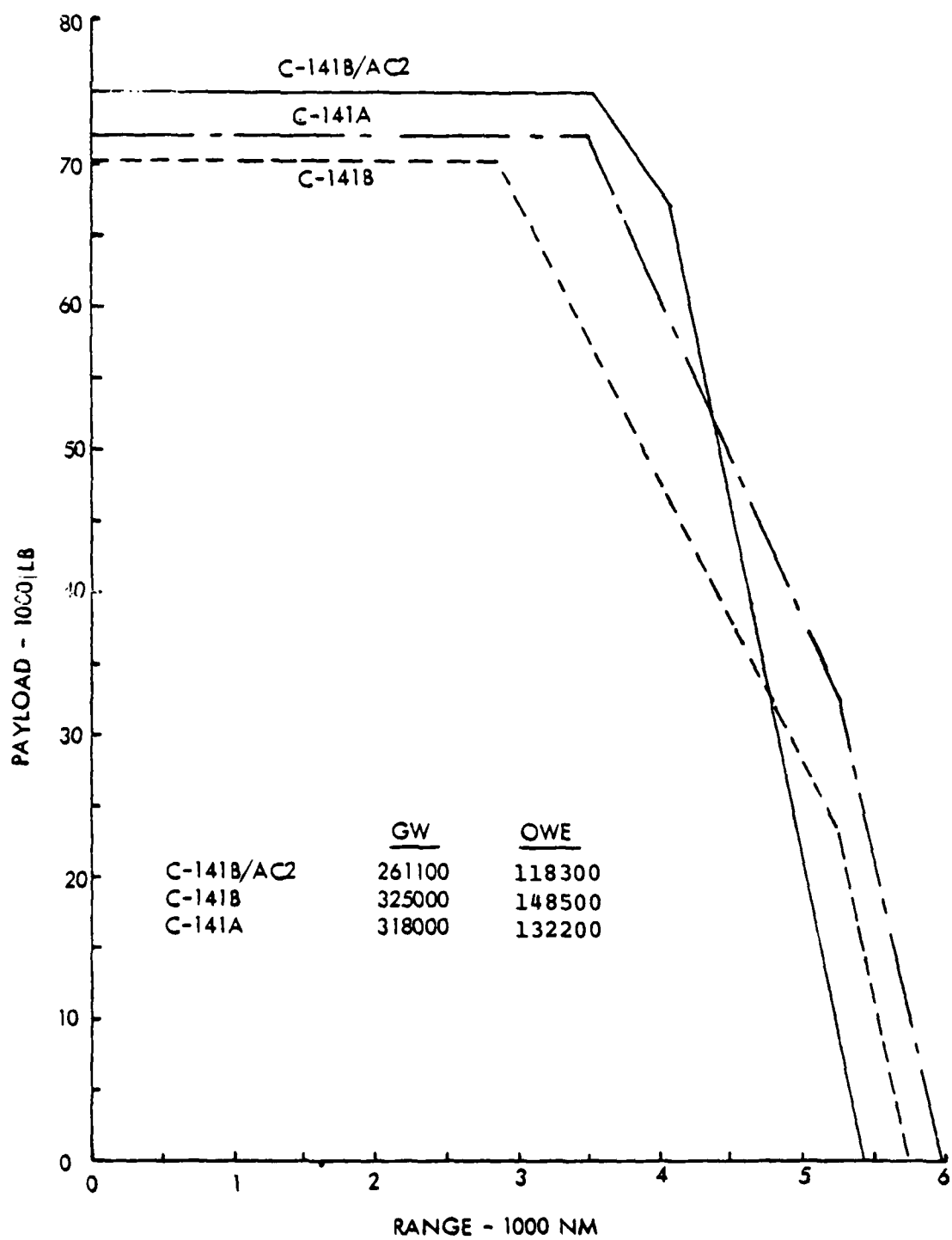


Figure 6. Payload/Range Comparison

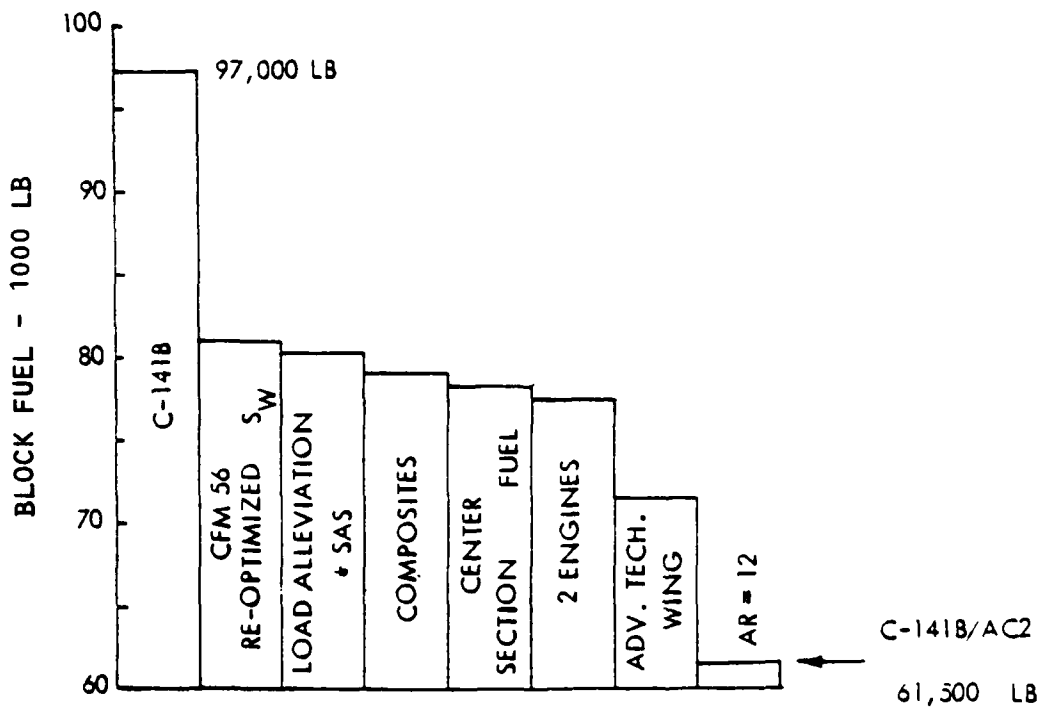
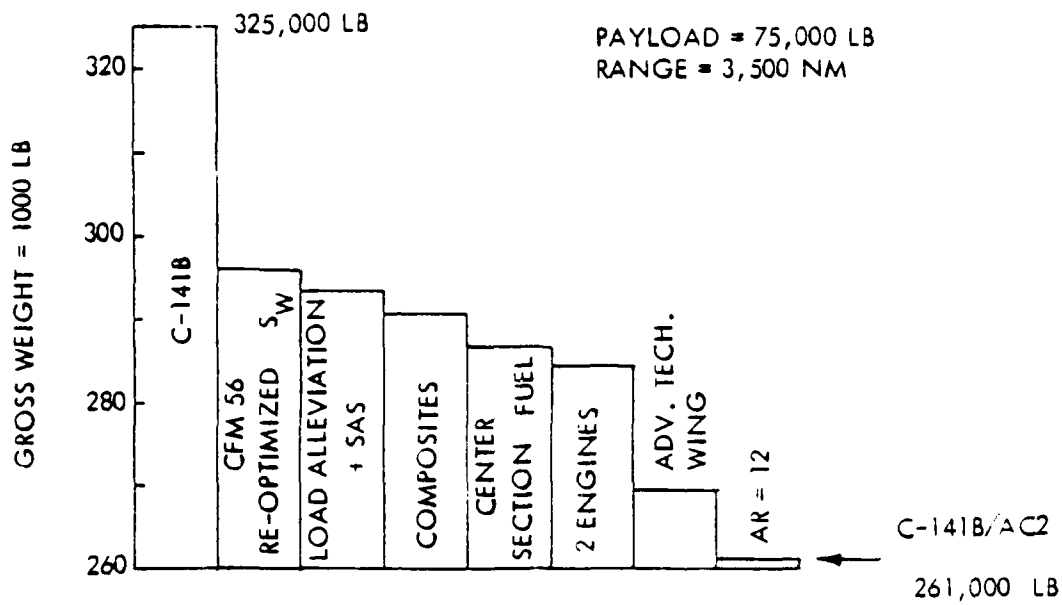


Figure 7. Impact of Advanced Technologies on the C-141B/AC2

NOTES:

1. AEDC 16T, TF-481, R 221
2. MEASURED MODEL ORDINATES, PYLON/NACELLES OFF

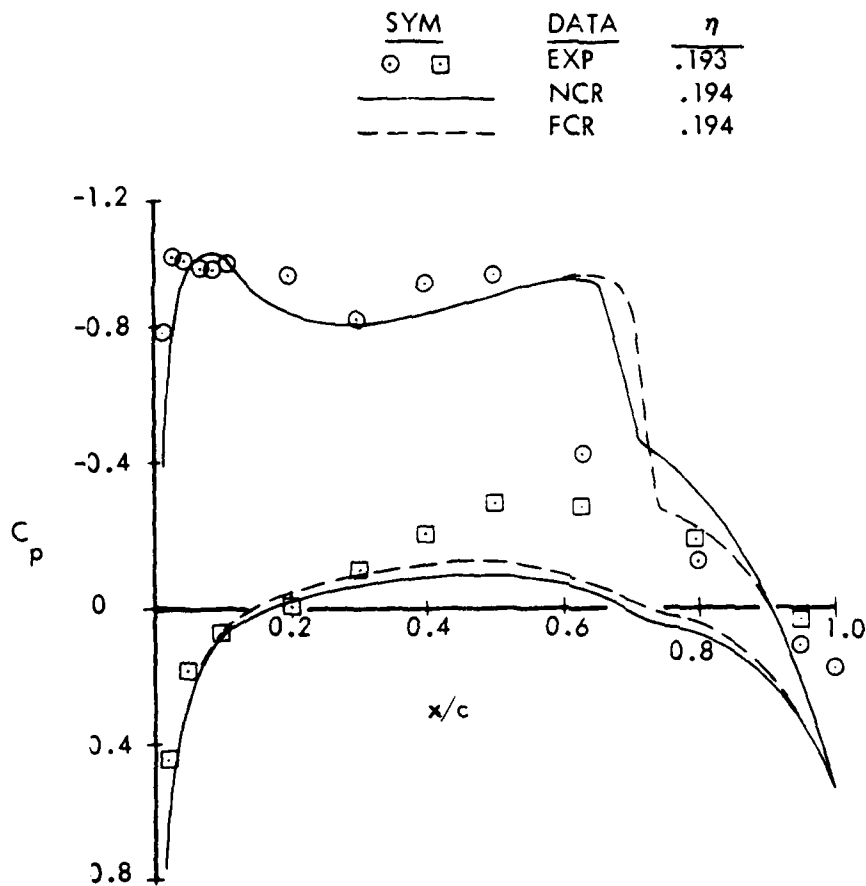


Figure 8. Inviscid Pressure Correlations for C-141
Mach = .77, $\alpha_F = 1.2^\circ$

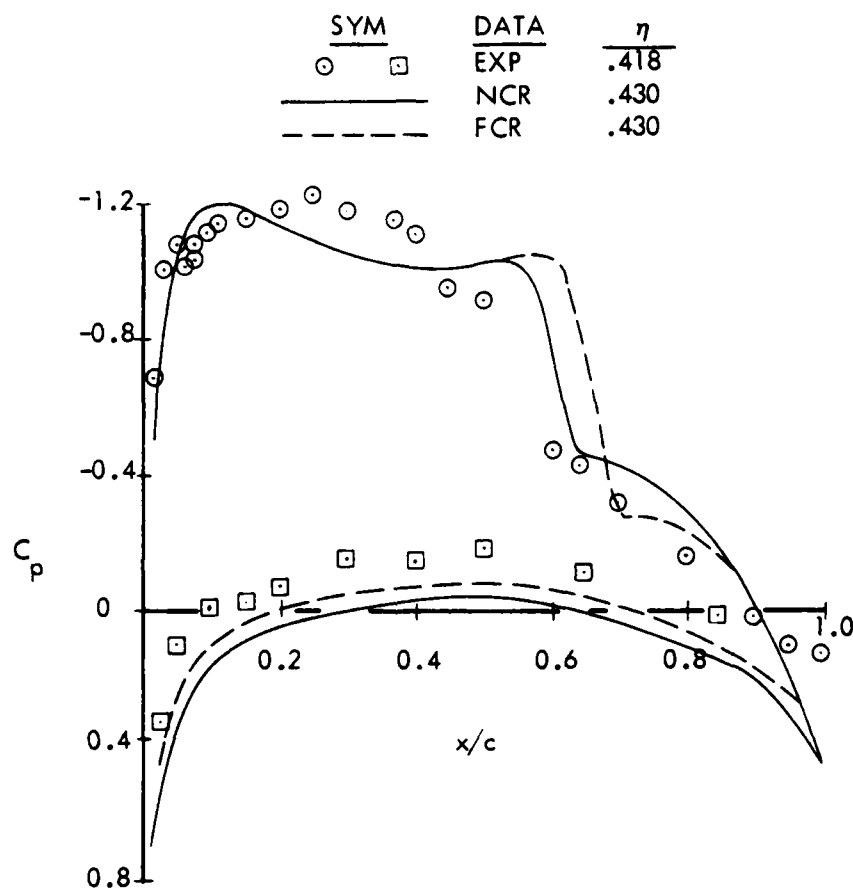


Figure 8. (Continued) (2)

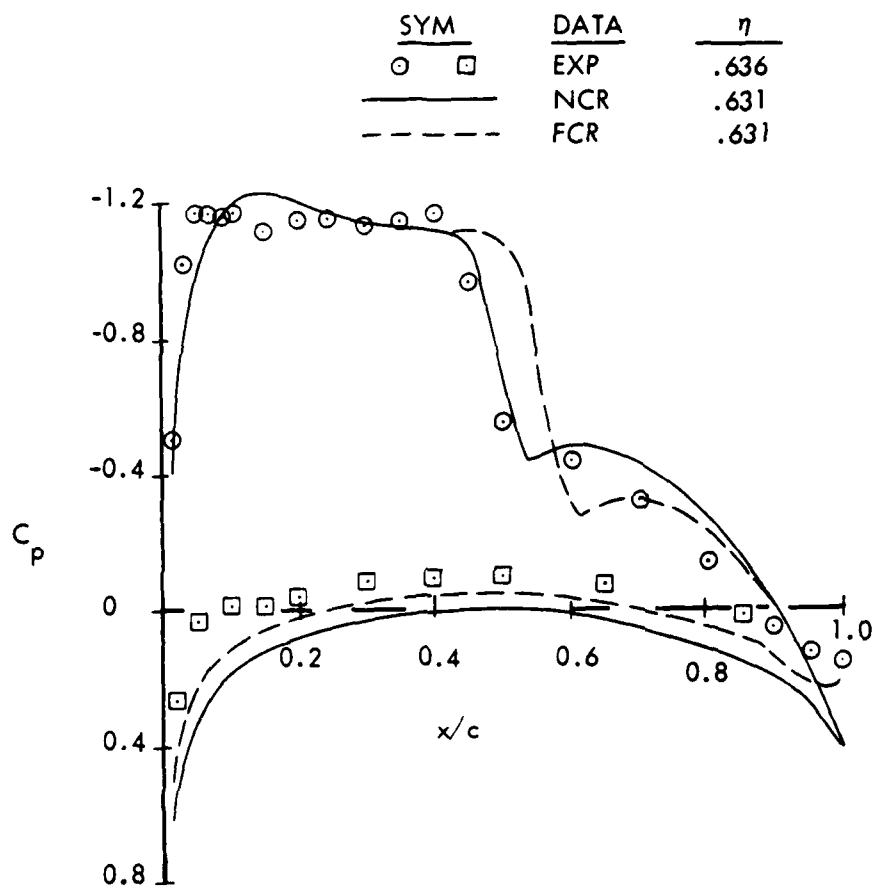


Figure 8. (Continued) (3)

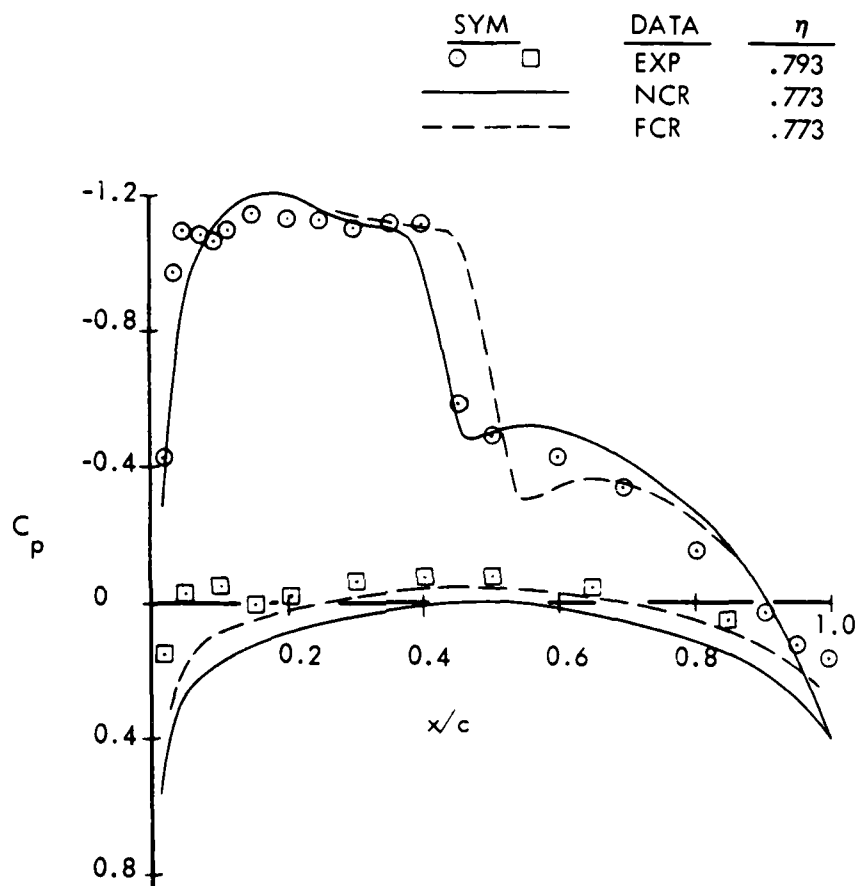


Figure 8. (Concluded) (4)

NOTES:

1. AECD 16T, TF-481, R227
2. MEASURED MODEL ORDINATES, PYLON/NACELLES OFF

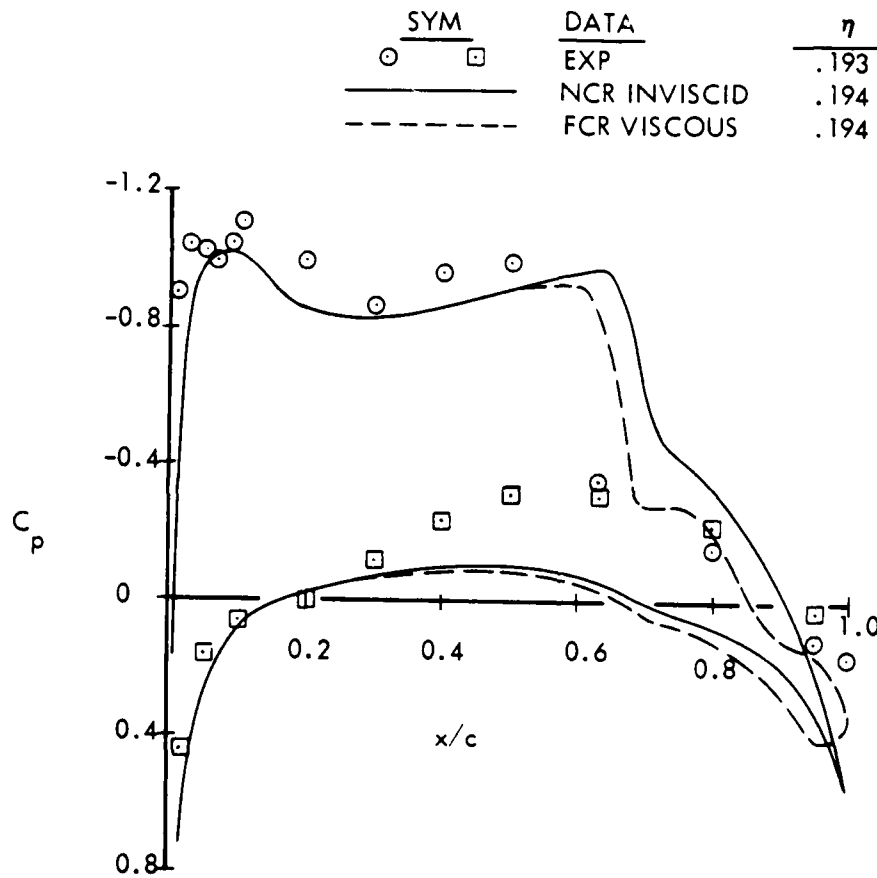


Figure 9. Pressure Correlations for C-141 with Weak Viscous Interaction. Mach = .77, $\alpha_F = 1.2^\circ$

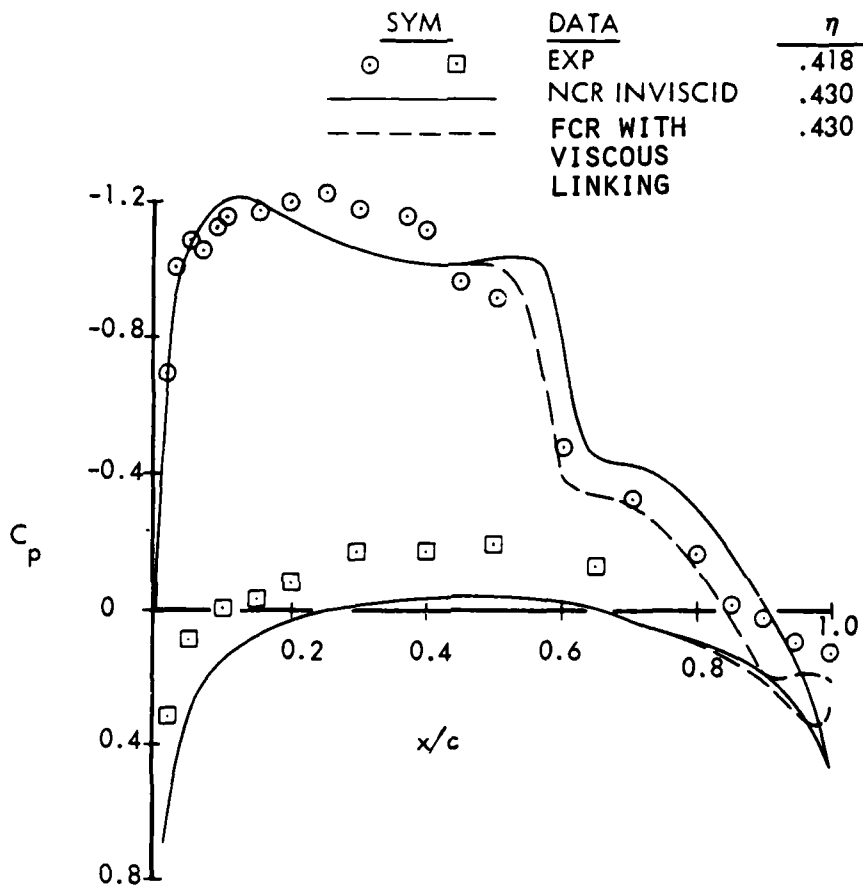


Figure 9. (Continued) (2)

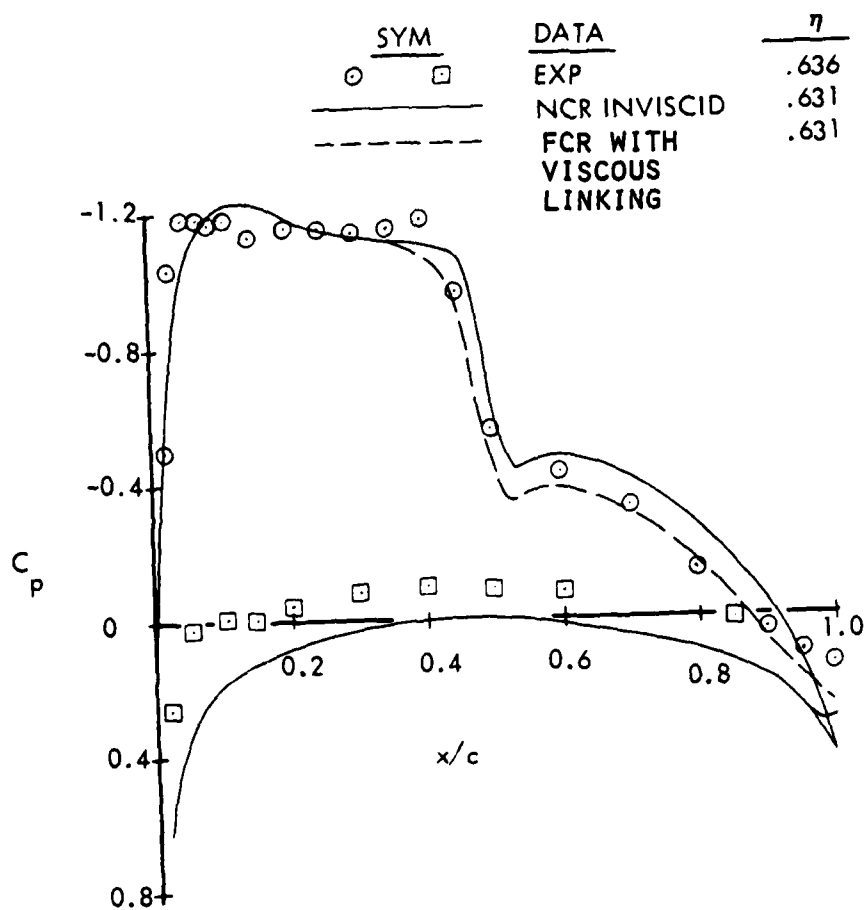


Figure 9. (Continued) (3)

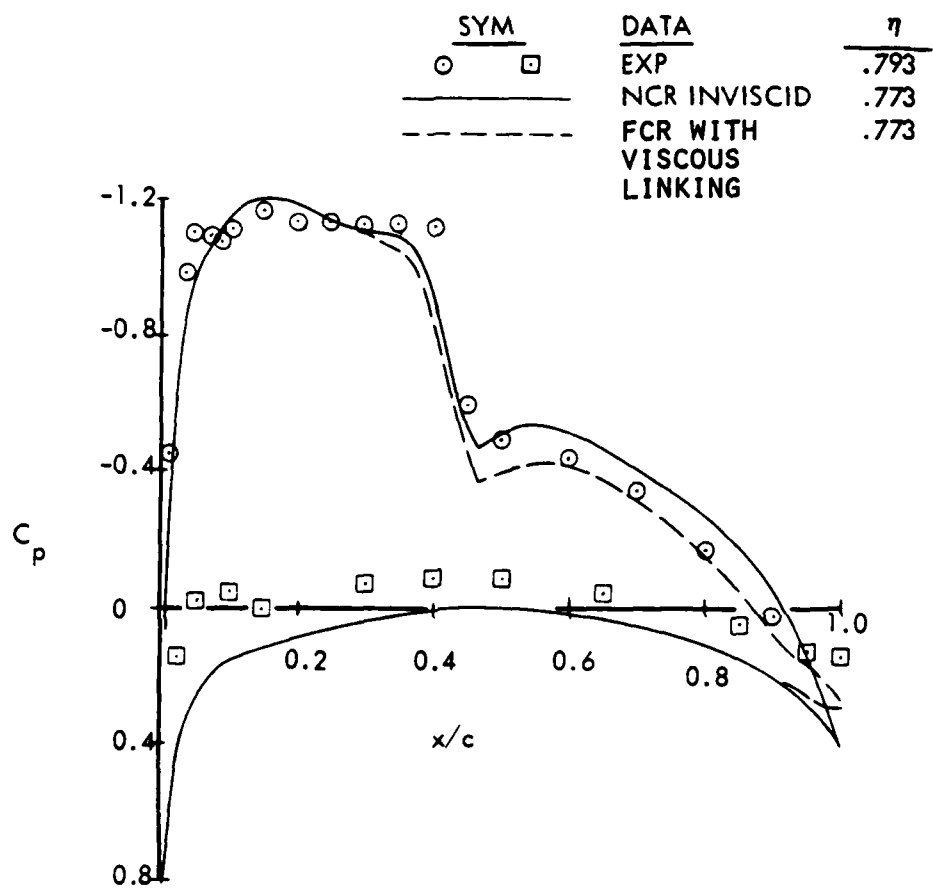


Figure 9. (Concluded) (4)

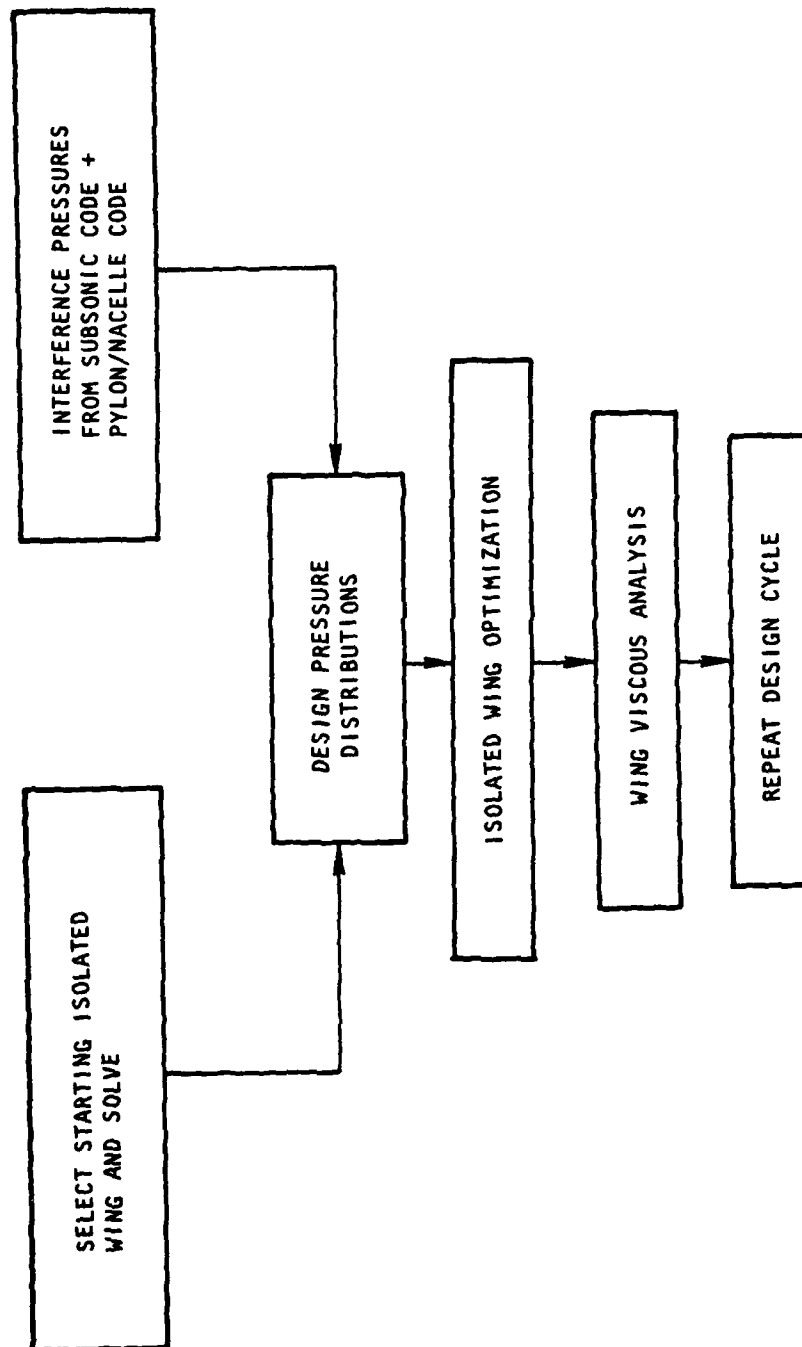


Figure 10. Transport Wing Design Procedure

MACH = .80 $C_L = .60$

LRC ———

ATA - - - -

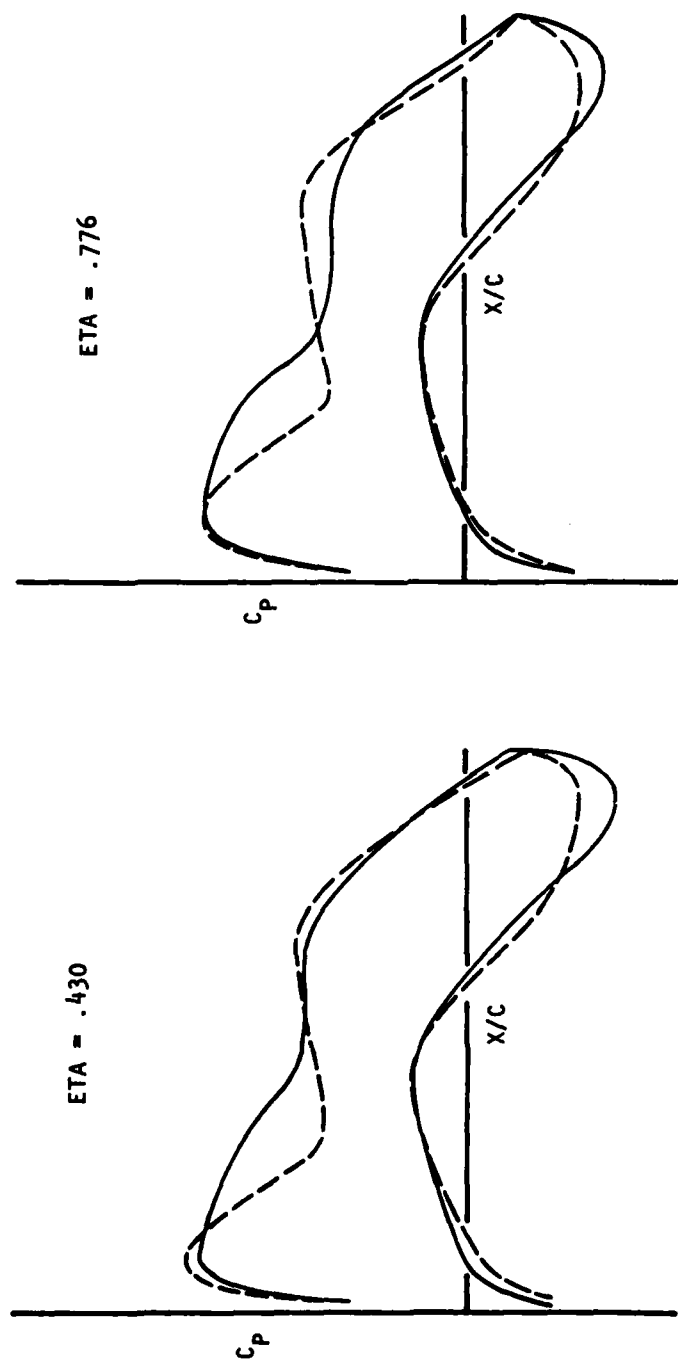


Figure 11. Starting Wing Selection

C-141B/AC2 SUBSONIC
CODE PANELING

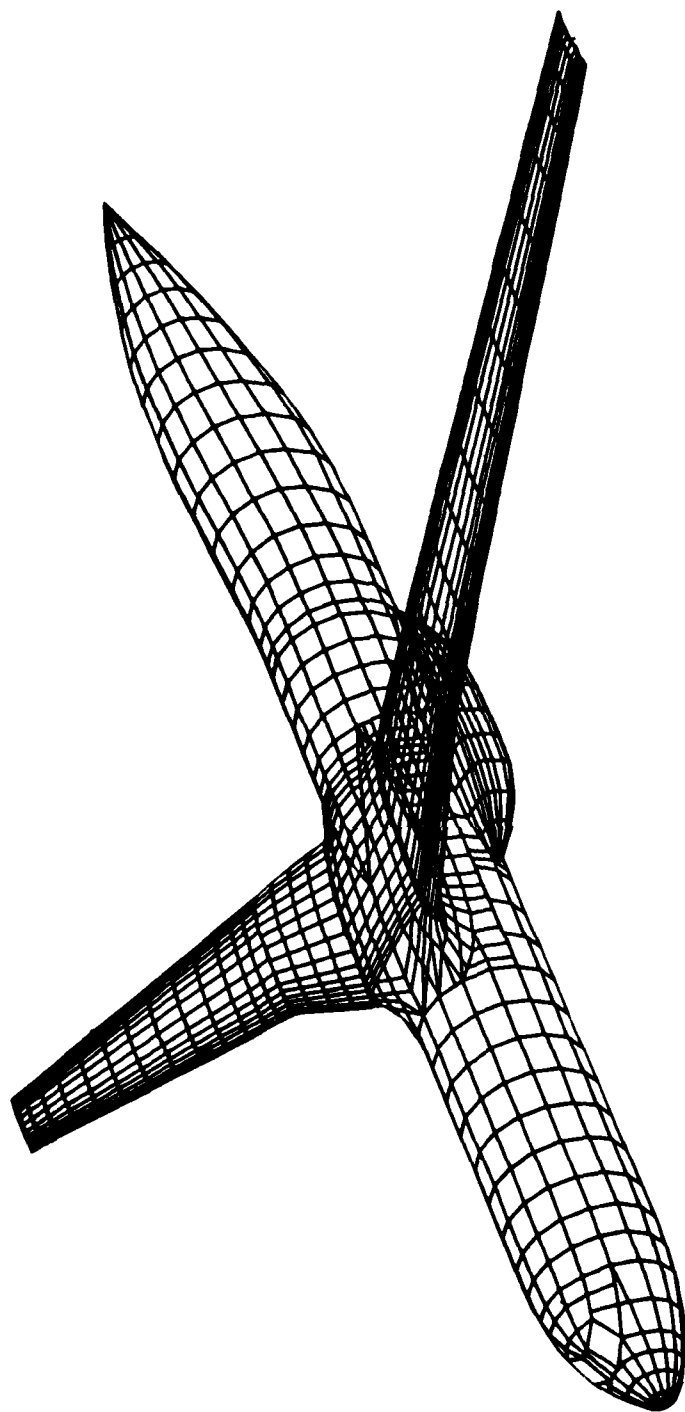


Figure 12. C-141B/AC2 Paneling

INTERFERENCE EFFECTS

MACH = .70
 $\alpha = .50$ DEG

— ISOLATED
 - - - CONFIGURATION

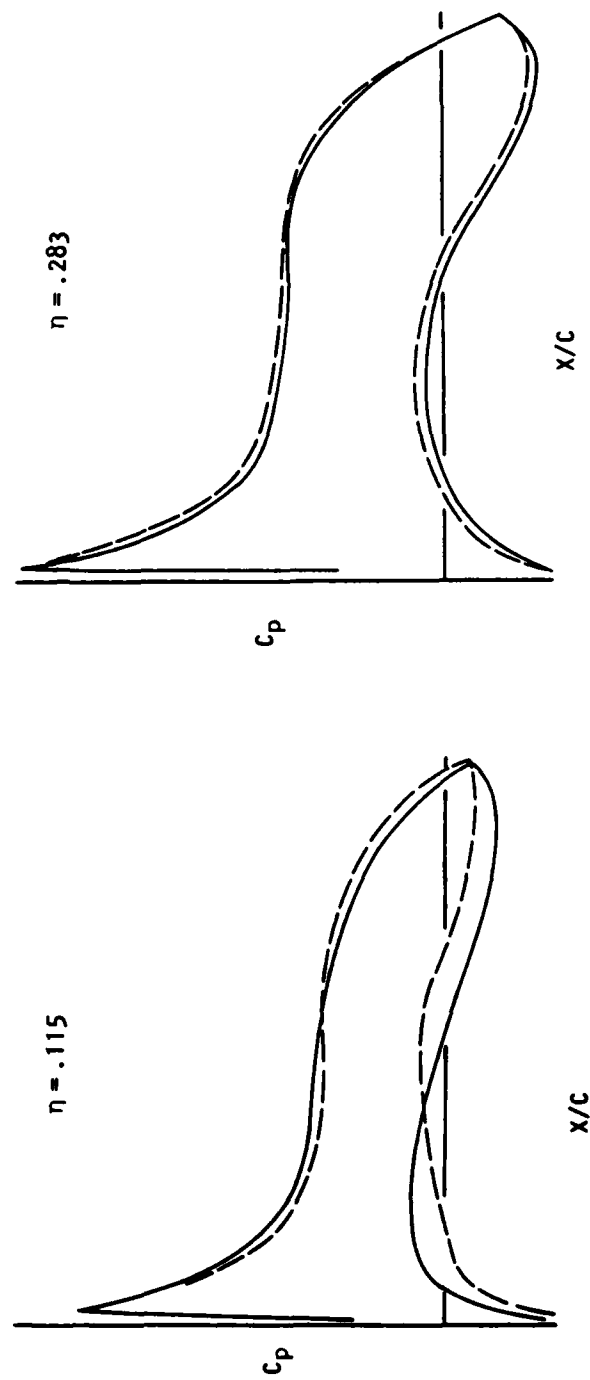


Figure 13. Interference Pressures

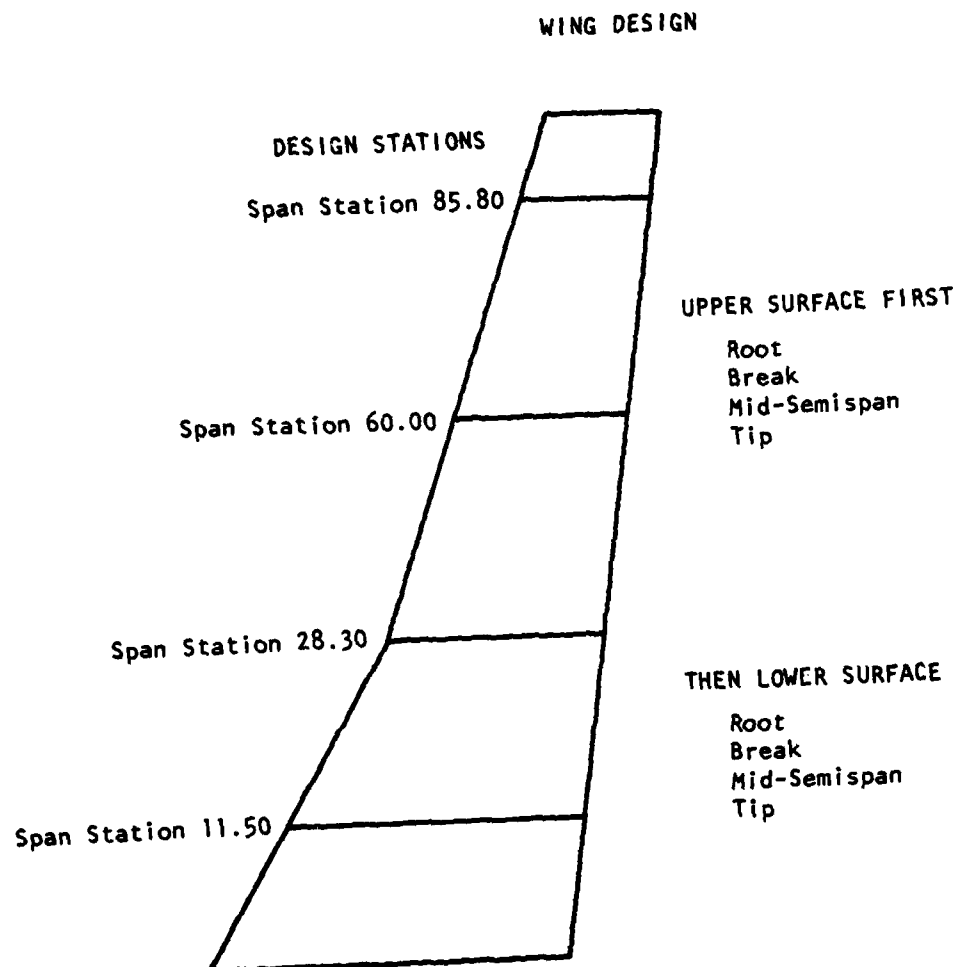


Figure 14. Wing Design Stations

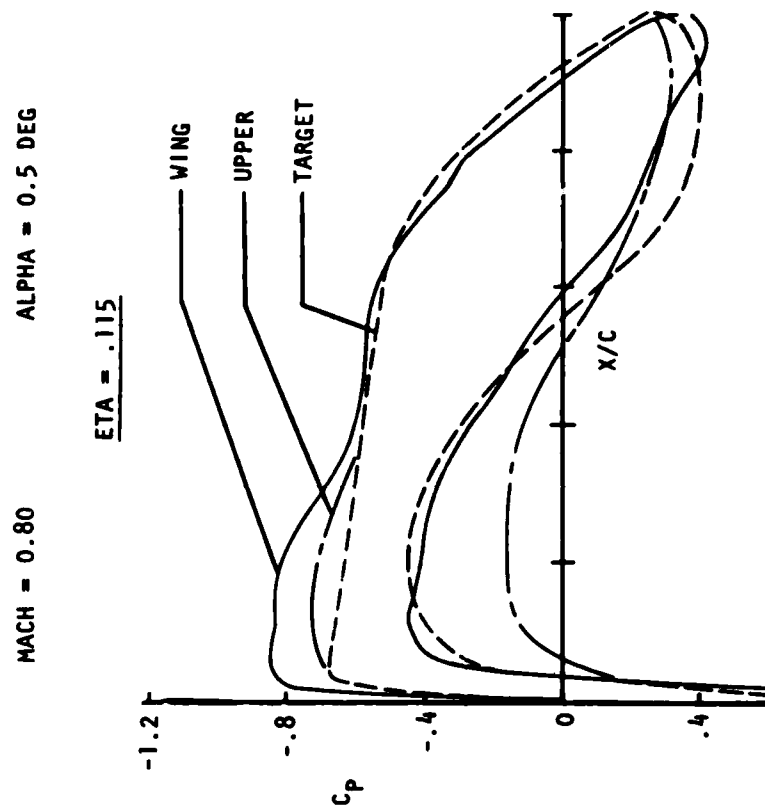


Figure 15. Comparison of ESD Design Pressures

MACH = 0.80 ALPHA = 0.5 DEG

ETA = .284

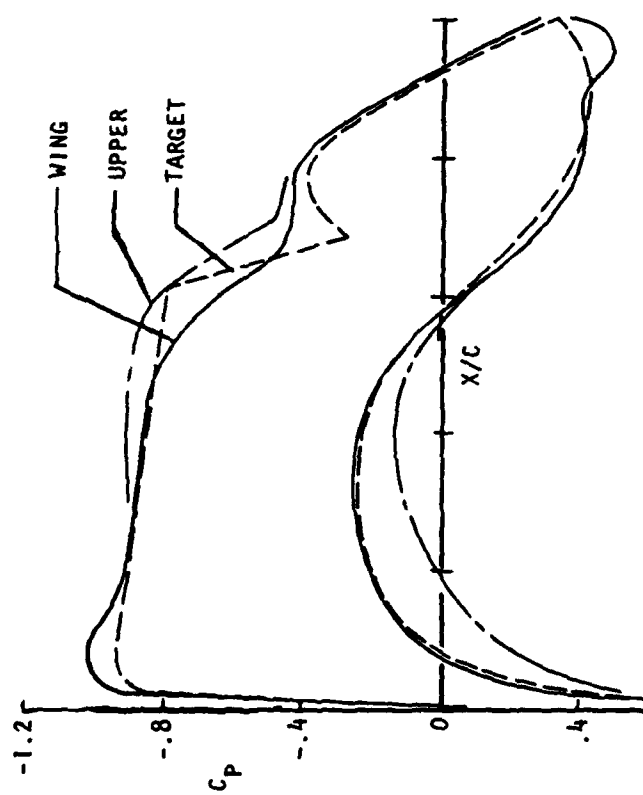


Figure 15. Continued

MACH = 0.80 ALPHA = 0.5 DEG

ETA = .858

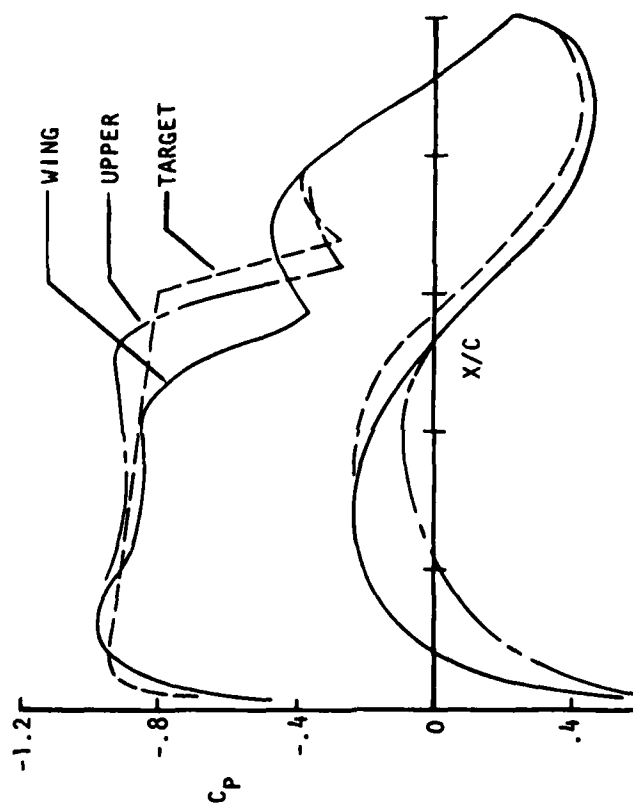


Figure 15. Concluded

MACH = 0.80 ALPHA = 0.5 DEG

ETA = .115

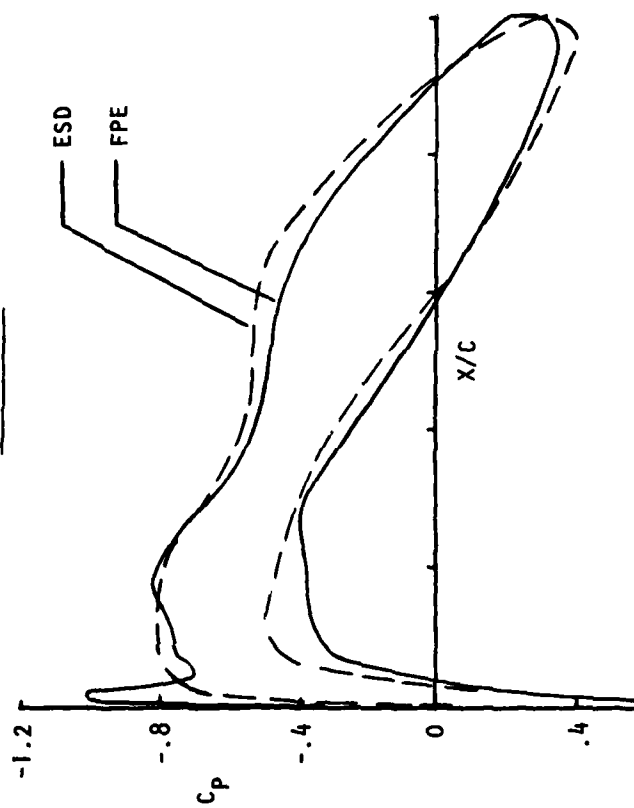


Figure 16. ESD and FPE Fluid Wing Analysis

MACH = 0.80 ALPHA = 0.5 DEG

ETA = .284

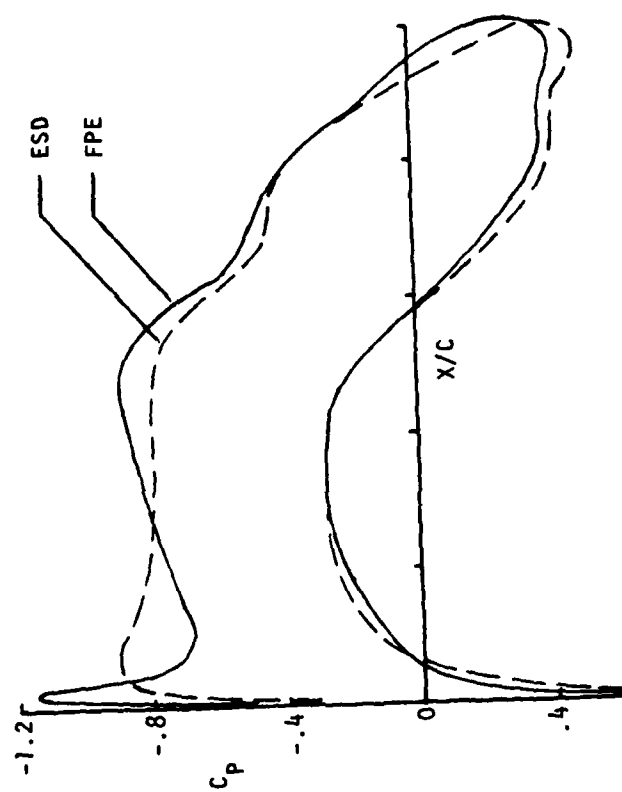


Figure 16. Continued

MACH = 0.80 ALPHA = 0.5 DEG

ETA = .858

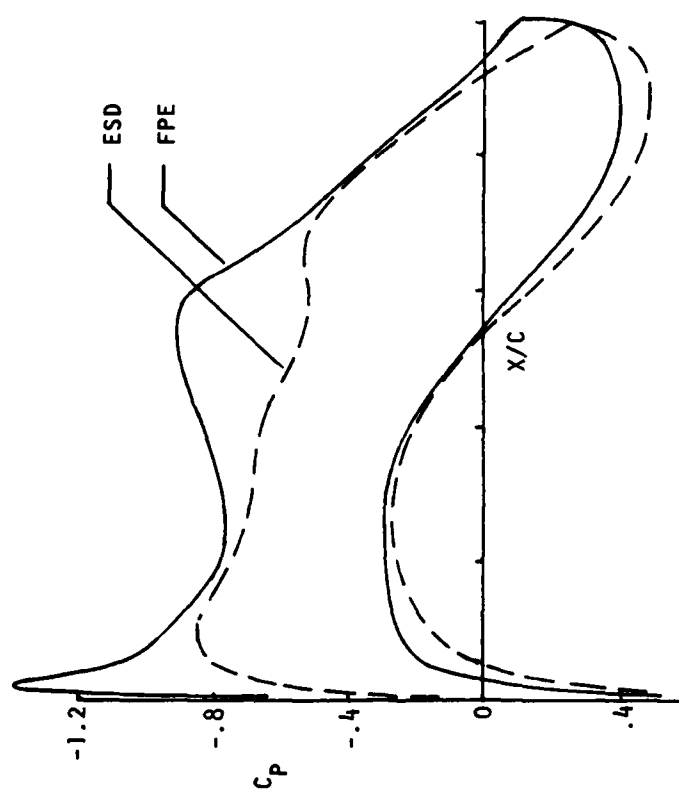


Figure 16. Concluded

MACH = 0.80 ALPHA = 0.0 DEG

ETA = .115

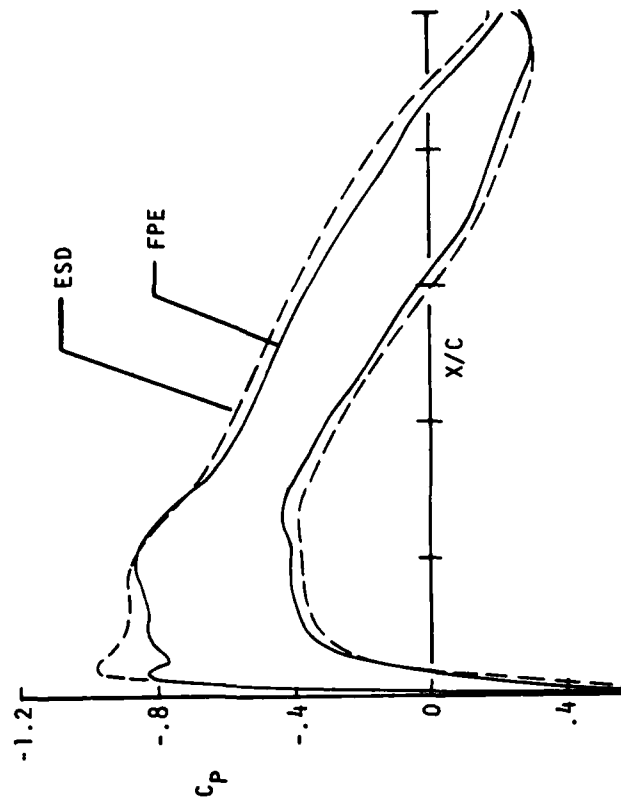


Figure 17. Calculated Pressures for Final Wing

MACH = 0.80 ALPHA = 0.0 DEG

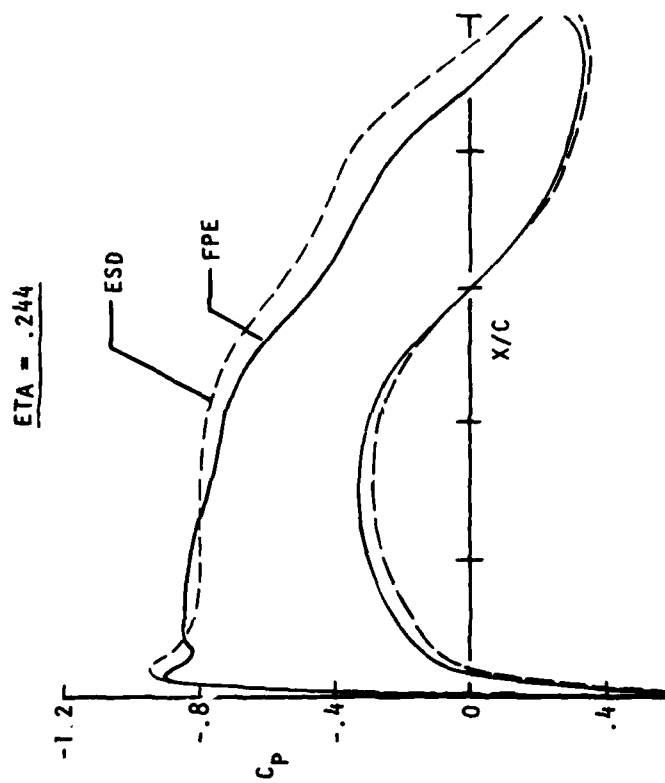


Figure 17. Continued

MACH = 0.80 ALPHA = 0.0 DEG

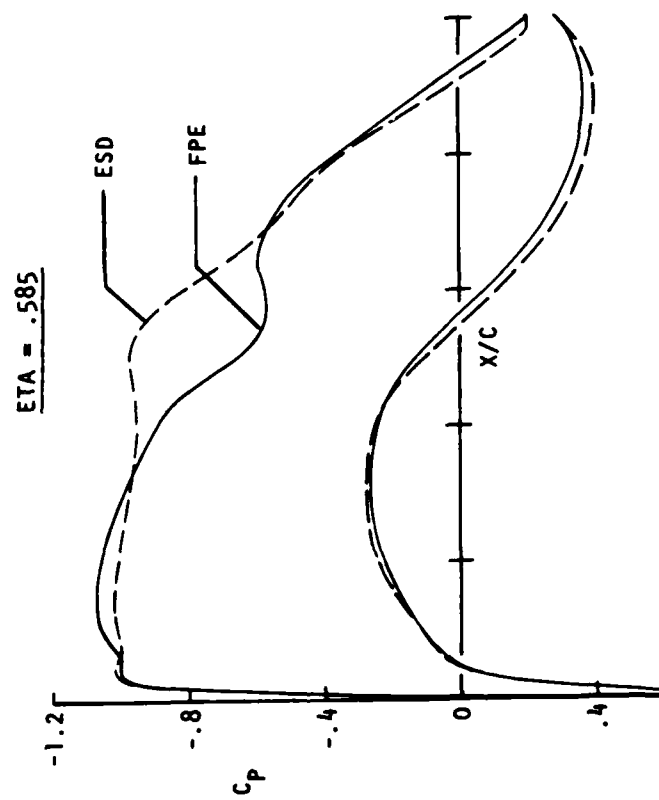


Figure 17. Continued

MACH = 0.80 ALPHA = 0.0 DEG

ETA = .878

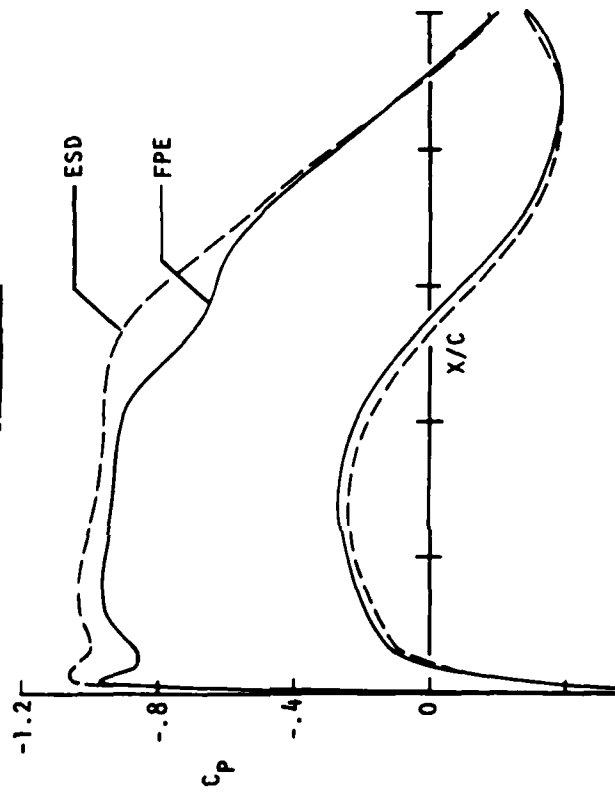


Figure 17. Concluded



76

Figure 18. C-141 Fuselage

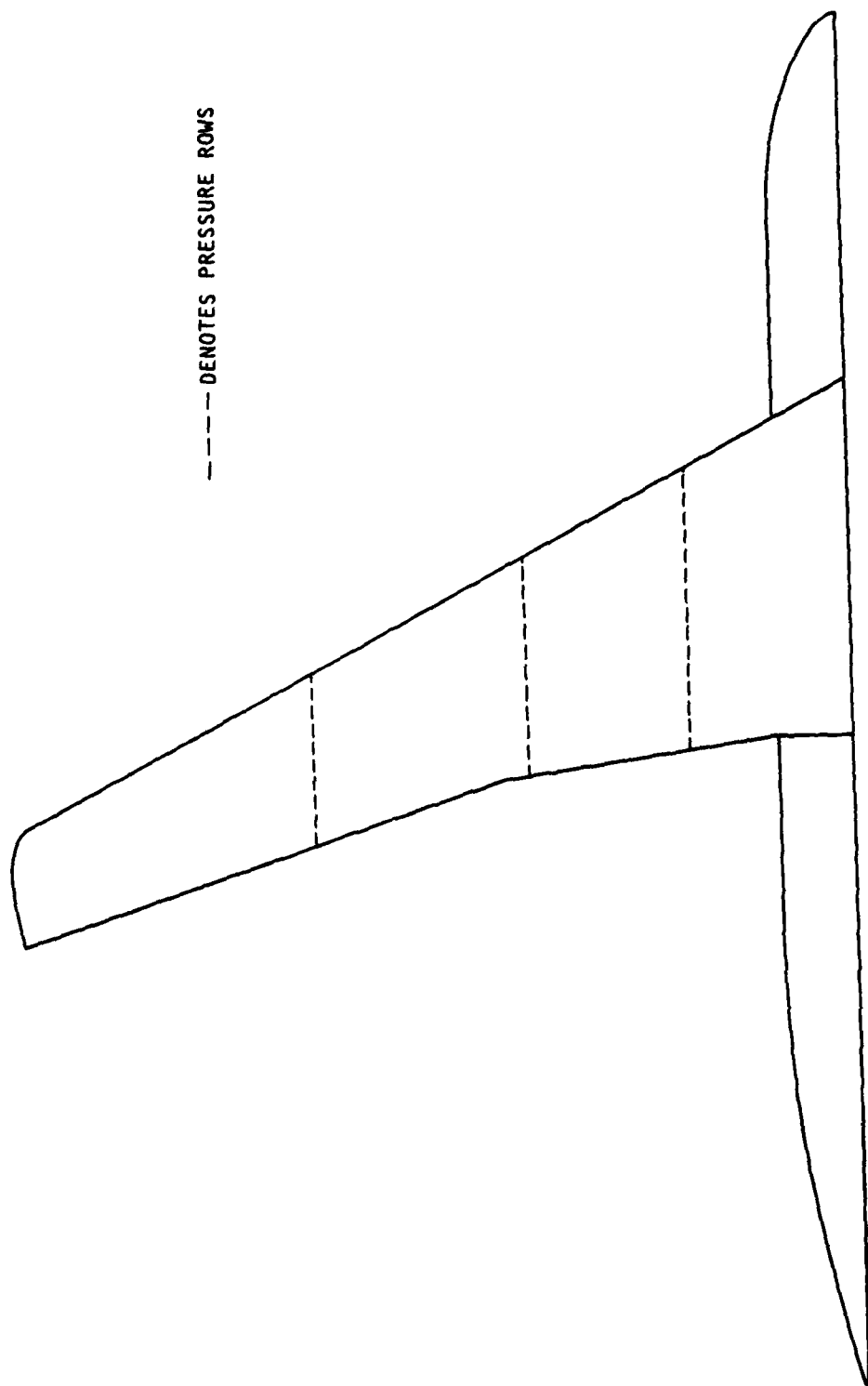


Figure 19. C-141 Planform

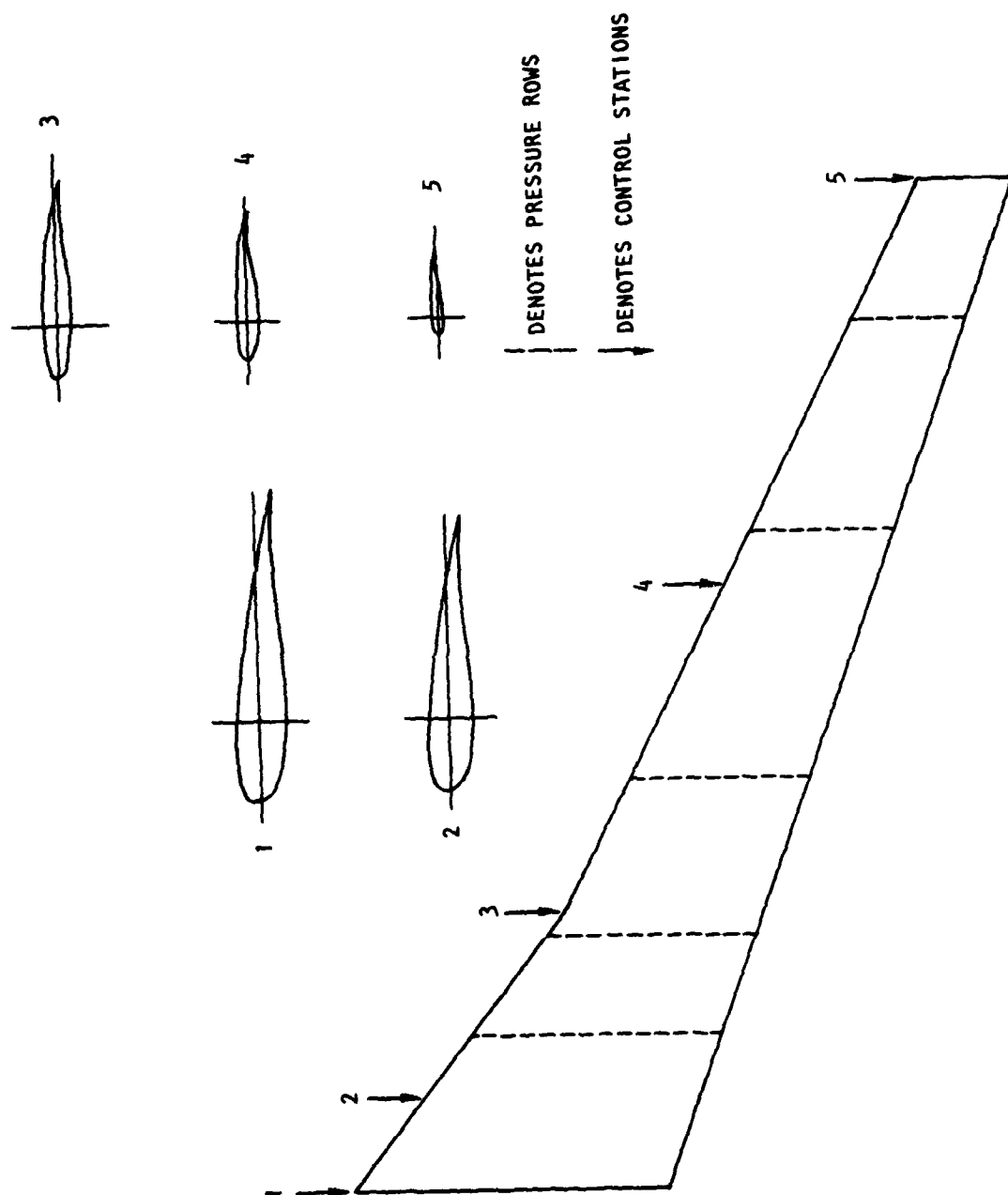


Figure 20. C-141B/AC2 Wing Planform

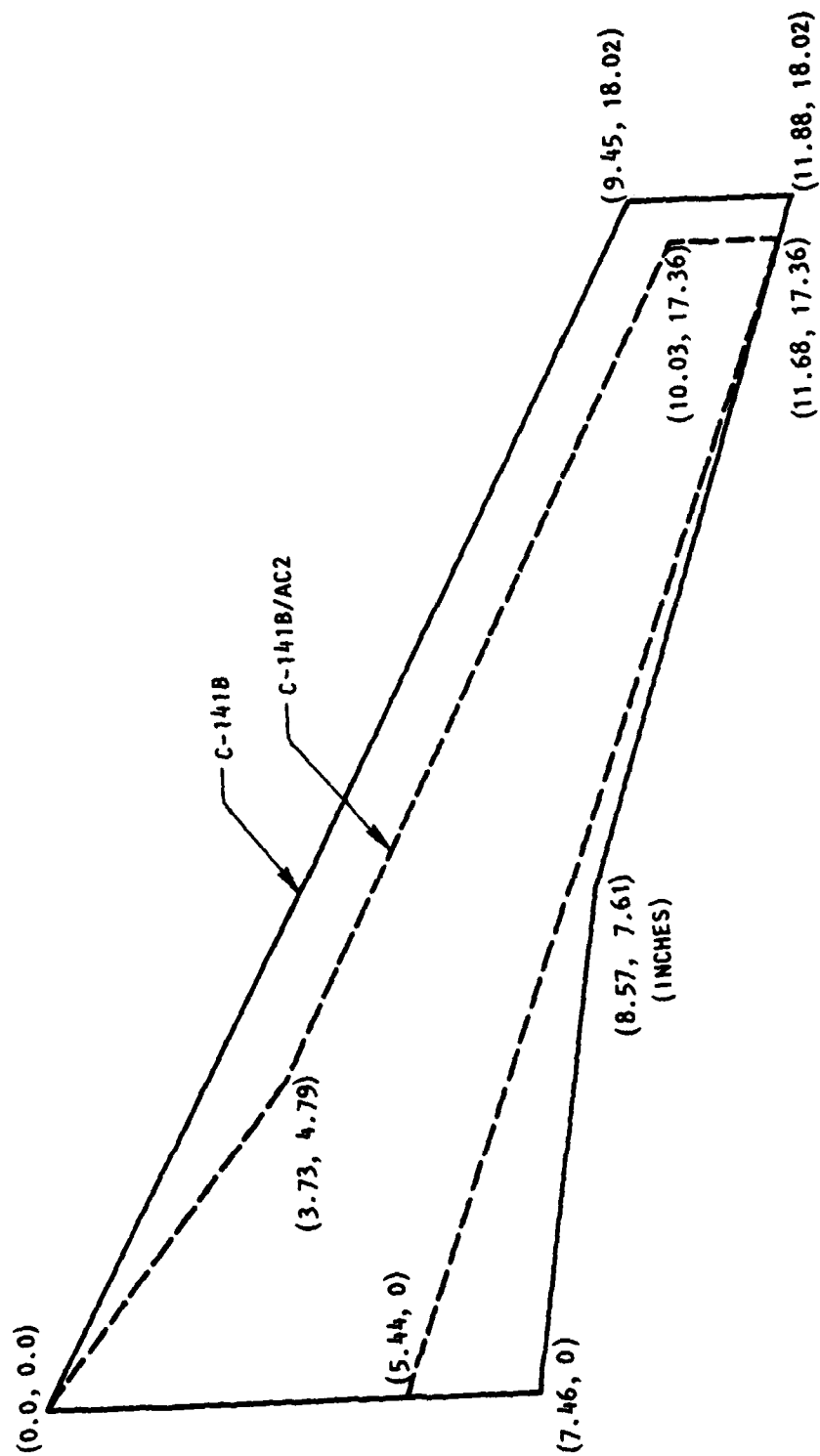


Figure 21. Comparison of C-141B and C-141B/AC2 Planforms

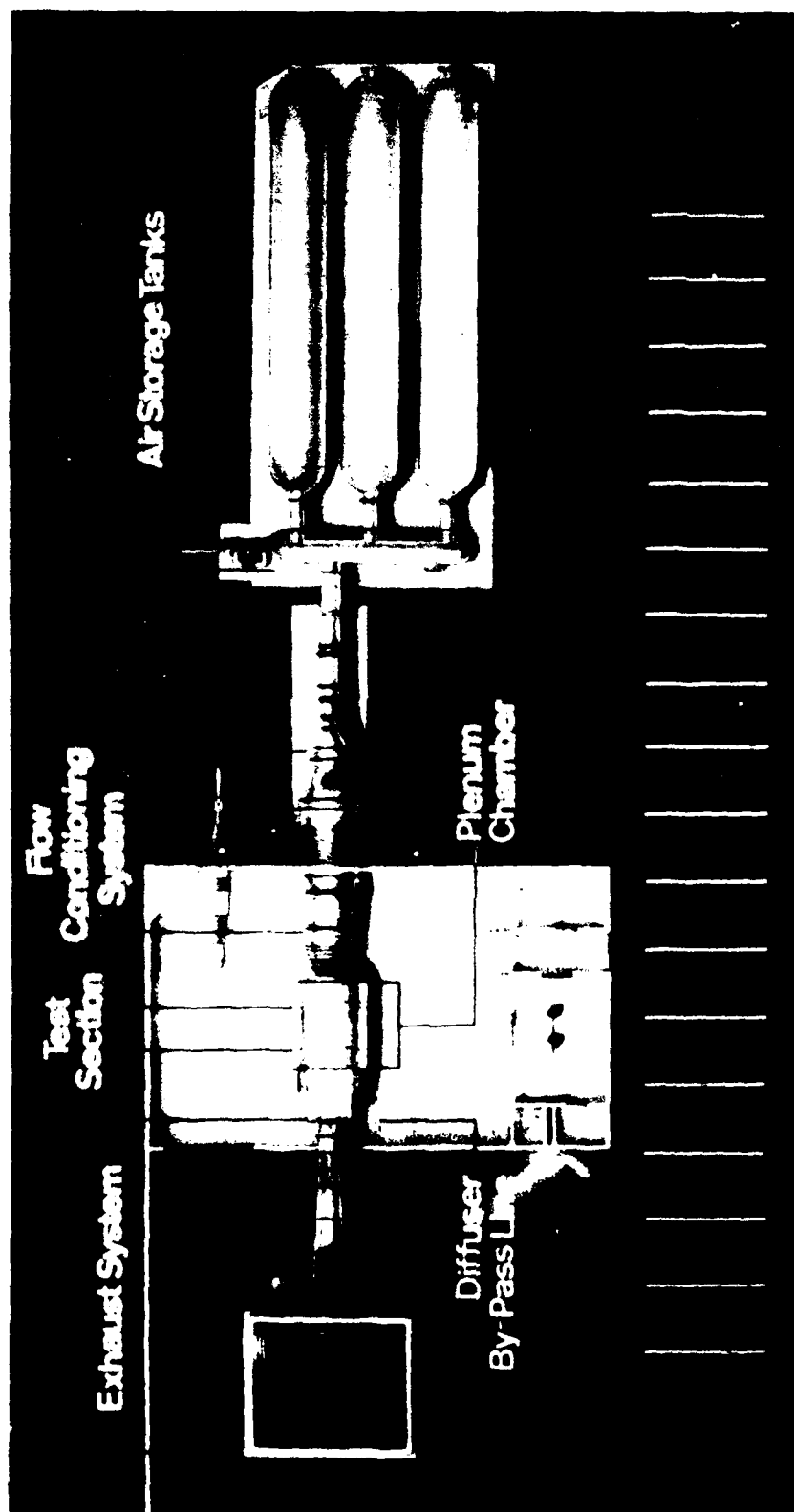


Figure 22. Lockheed-Georgia Compressible Flow Wind-Tunnel



Figure 23. Photograph of Test Apparatus

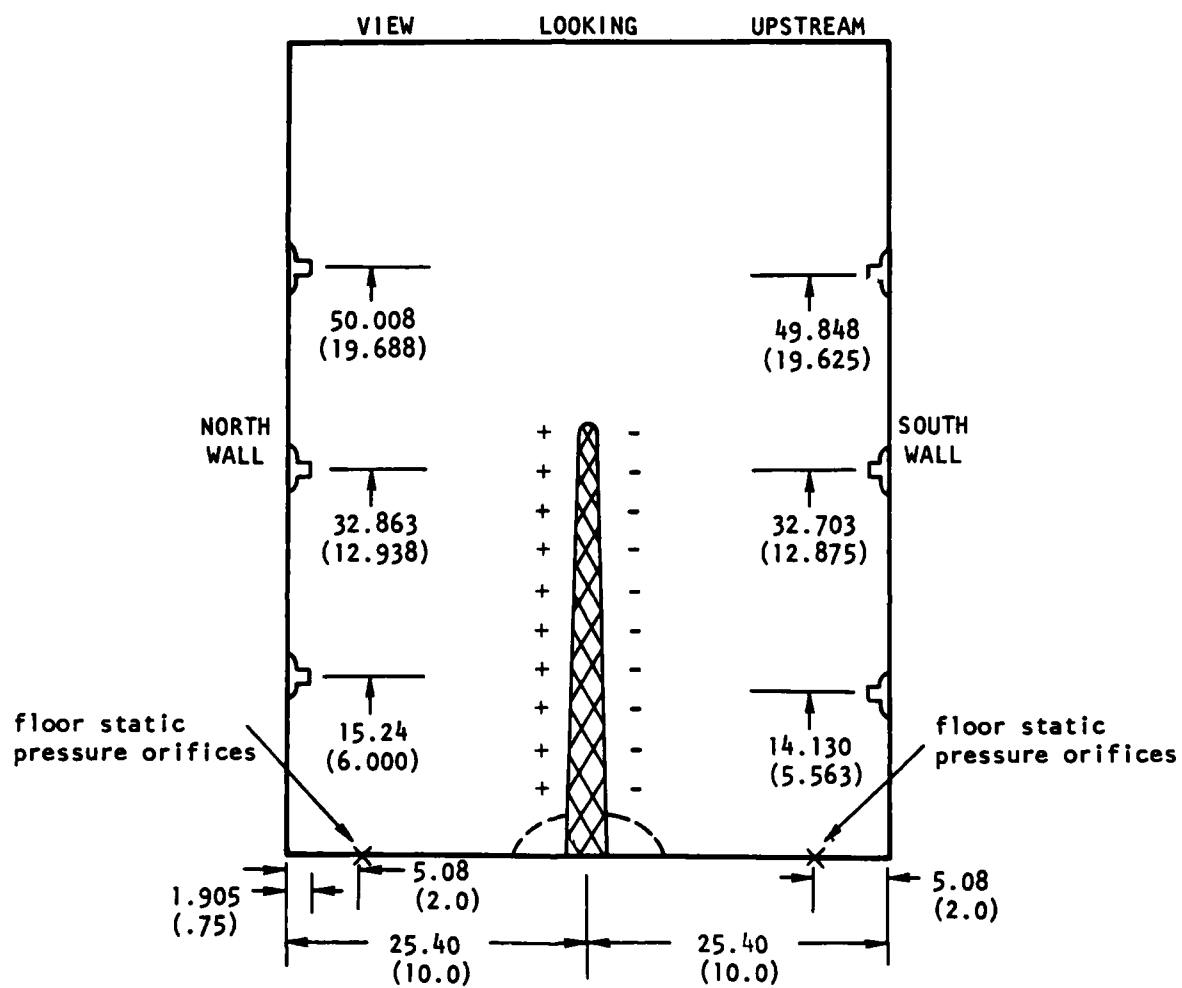


Figure 24. Far-field rail locations - cm (inches).

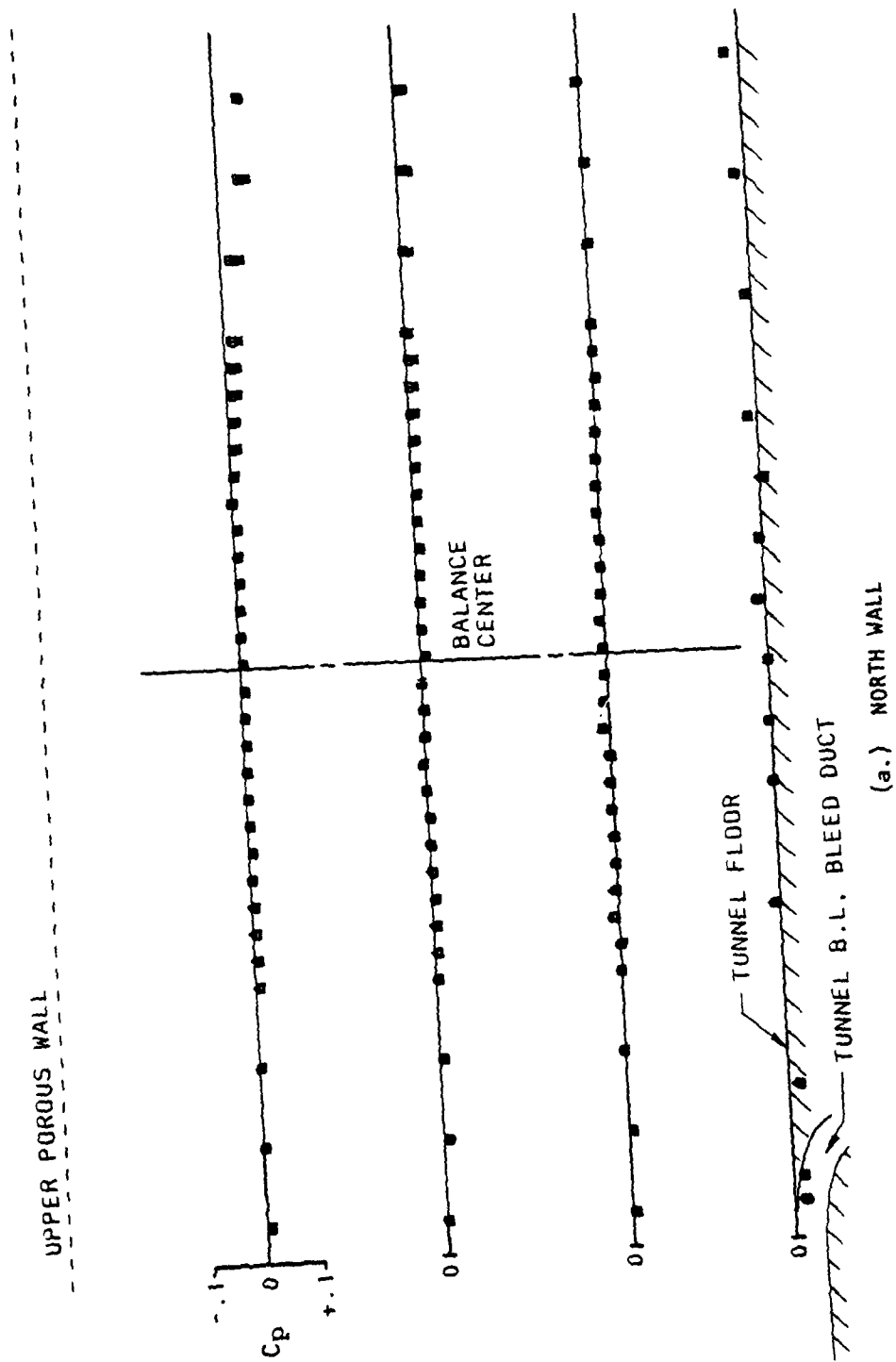
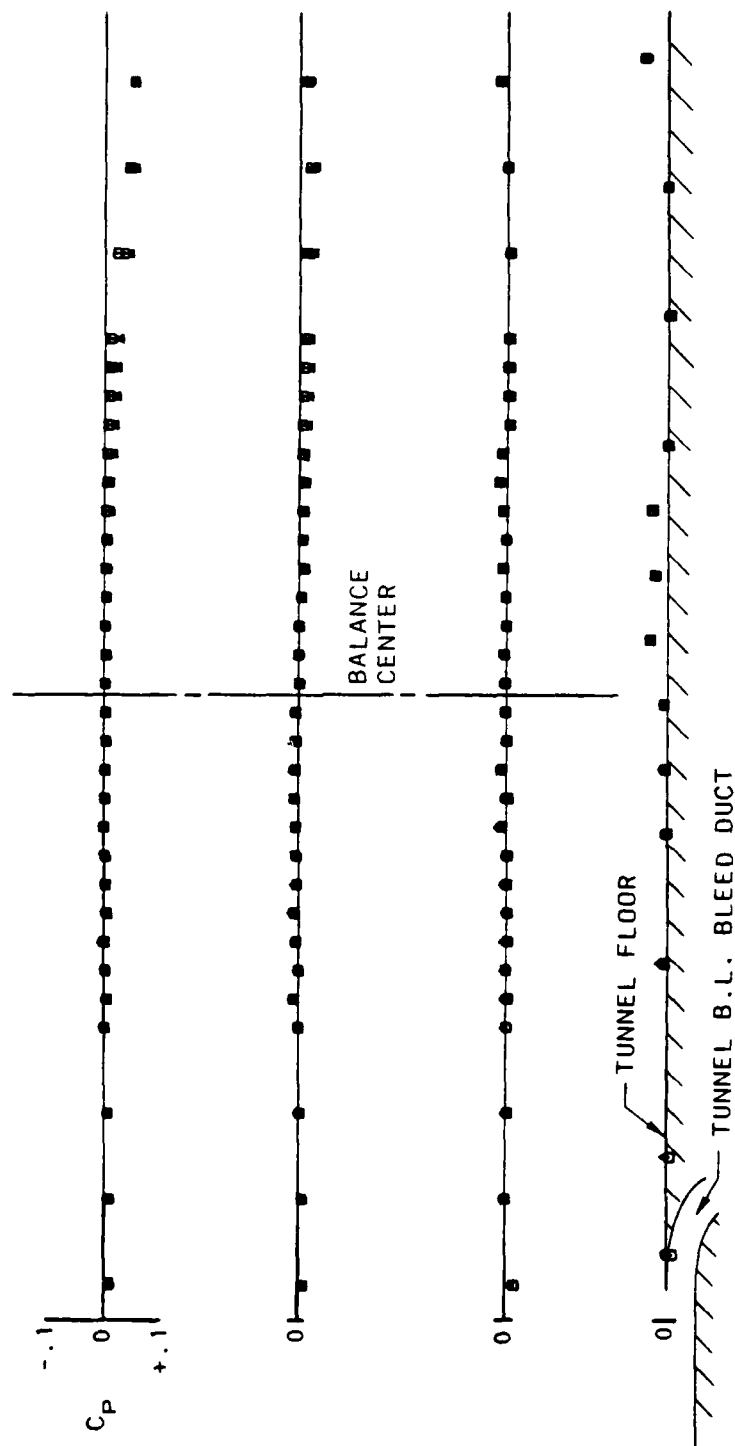


Figure 25. Calibration of Floor Static Pressure Orifices and Far-field Rails

UPPER POROUS WALL



(b.) SOUTH WALL

Figure 25. (Concluded)

CFWT052
 SERIES 3
 $R_N = 5 \times 10^6$

- ∇ $M = .60$
- \circ $M = .70$
- \square $M = .75$
- \triangle $M = .78$
- \diamond $M = .79$
- \square $M = .80$
- \diamond $M = .81$
- \diamond $M = .82$
- \circ $M = .84$

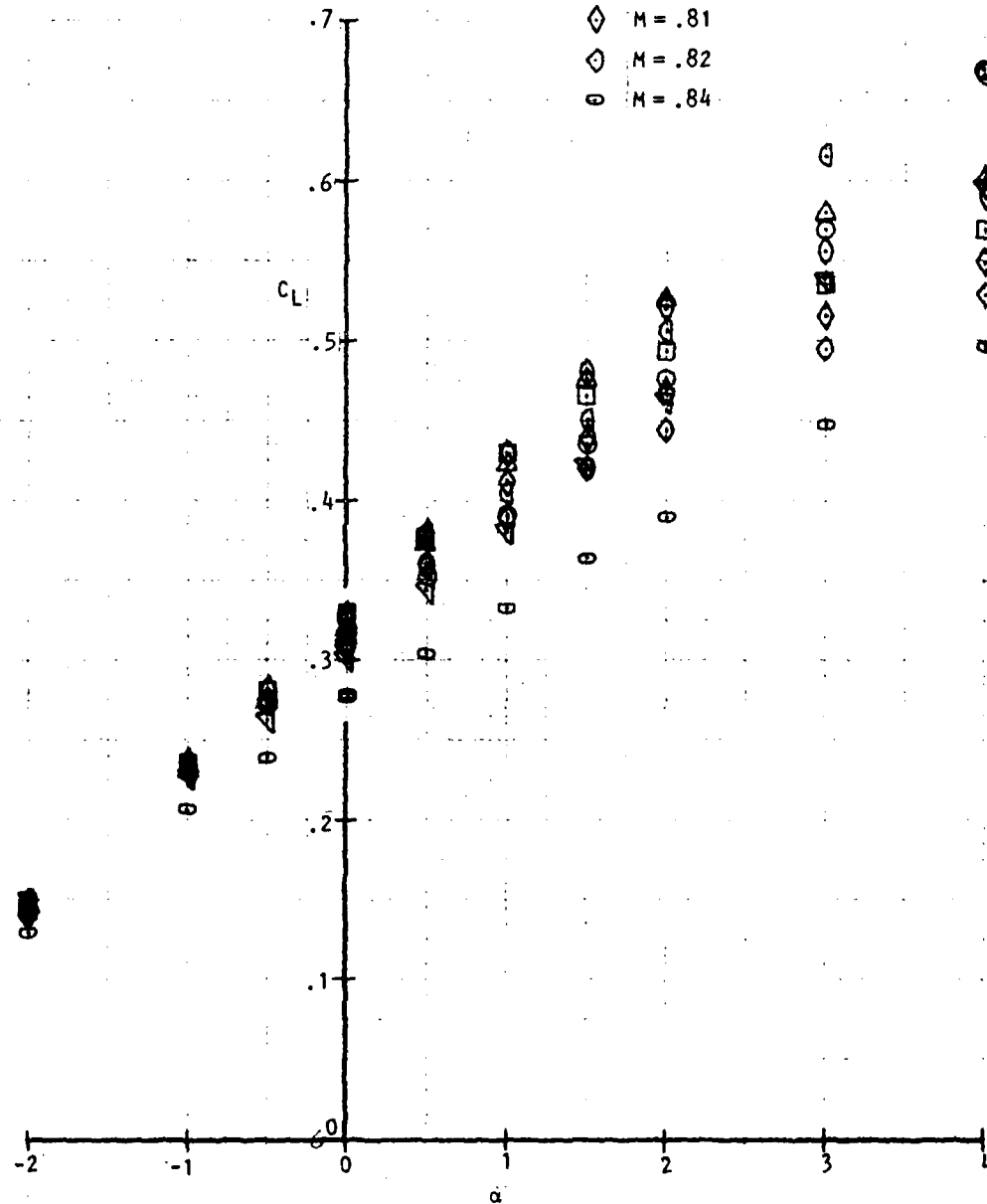


Figure 26a. C_L vs. α C-141 Baseline Configuration

AD-A110 231

LOCKHEED-GEORGIA CO MARIETTA

F/6 1/3

NUMERICAL AIRCRAFT DESIGN USING 3-D TRANSONIC ANALYSIS WITH OPT--ETC(U)

AUG 81 A J SROKOWSKI, M E LORES, R A WEED

F33615-78-C-3014

UNCLASSIFIED

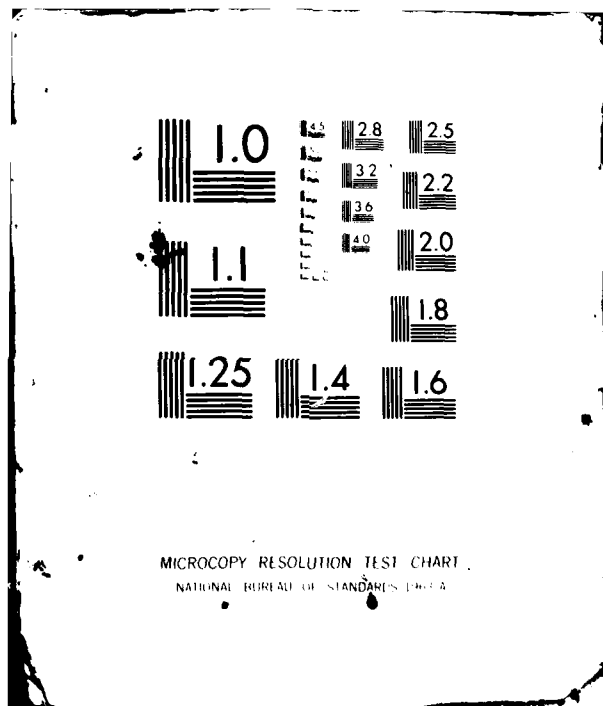
LG81ER0107-VOL-2-PT-1

AFWAL-TR-81-3091-VOL-2-PT- NL

2 + 2

2 0 0 0

END
DATE
FILMED
2 82
DTIC



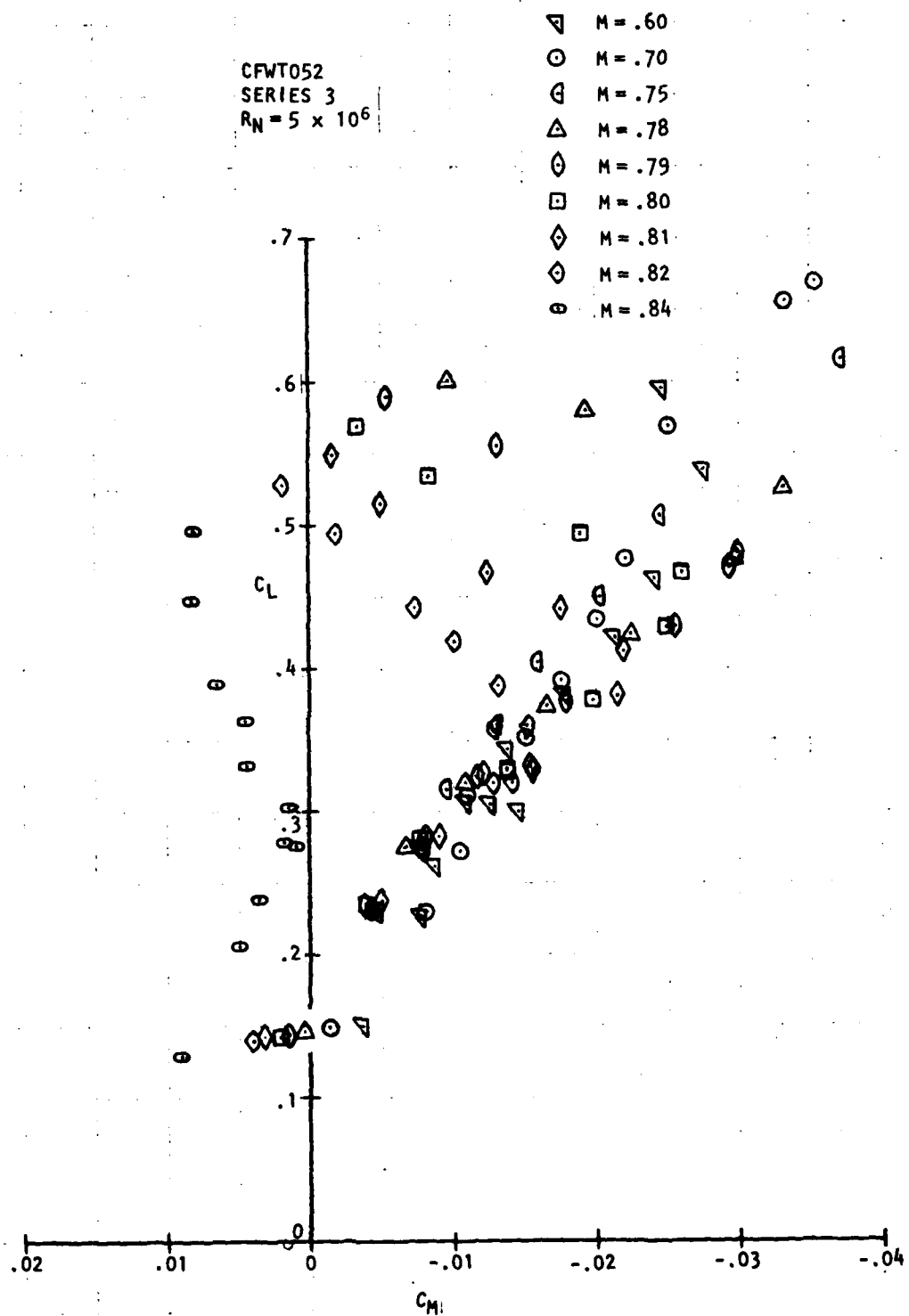


Figure 26b. C_L vs. C_M C-141 Baseline Configuration

∇ $M = .60$
 \circ $M = .70$
 \square $M = .75$
 \triangle $M = .78$
 \diamond $M = .79$
 \square $M = .80$
 \diamond $M = .81$
 \diamond $M = .82$
 \circ $M = .84$

CFWT052
 SERIES 3
 $Re = 5 \times 10^6$

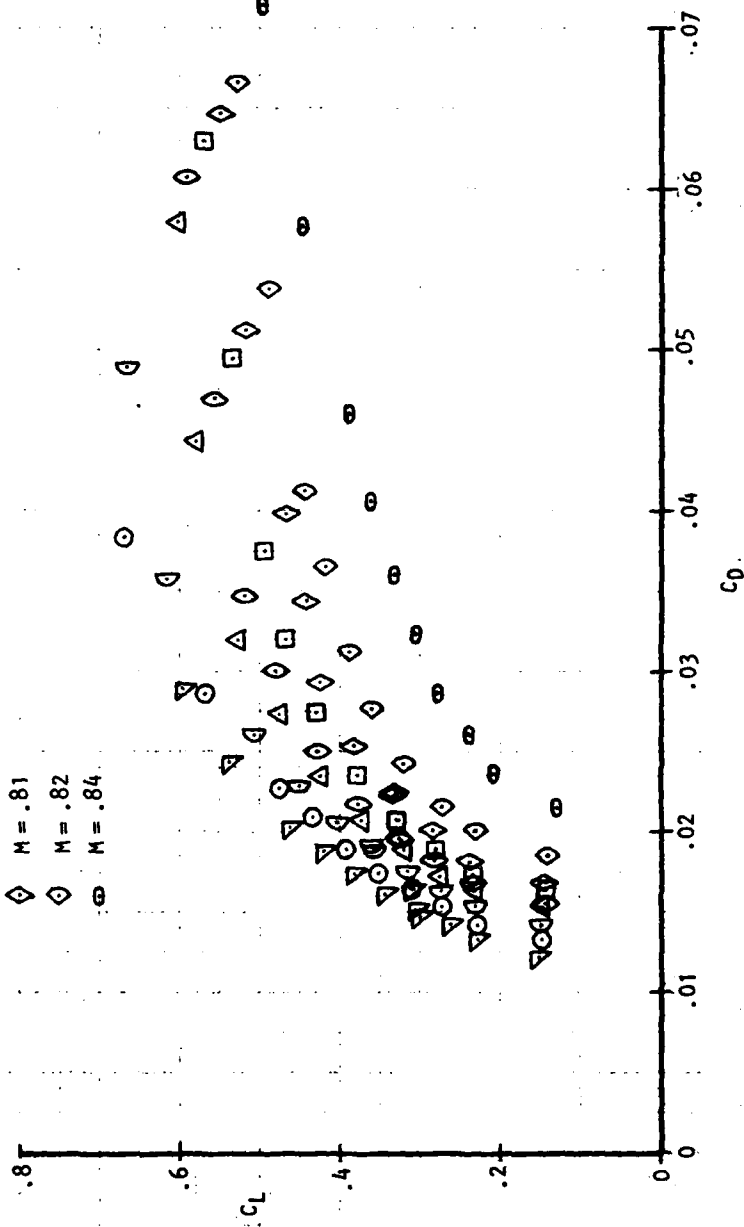


Figure 26c. C_L vs. C_D C-141 Baseline Configuration

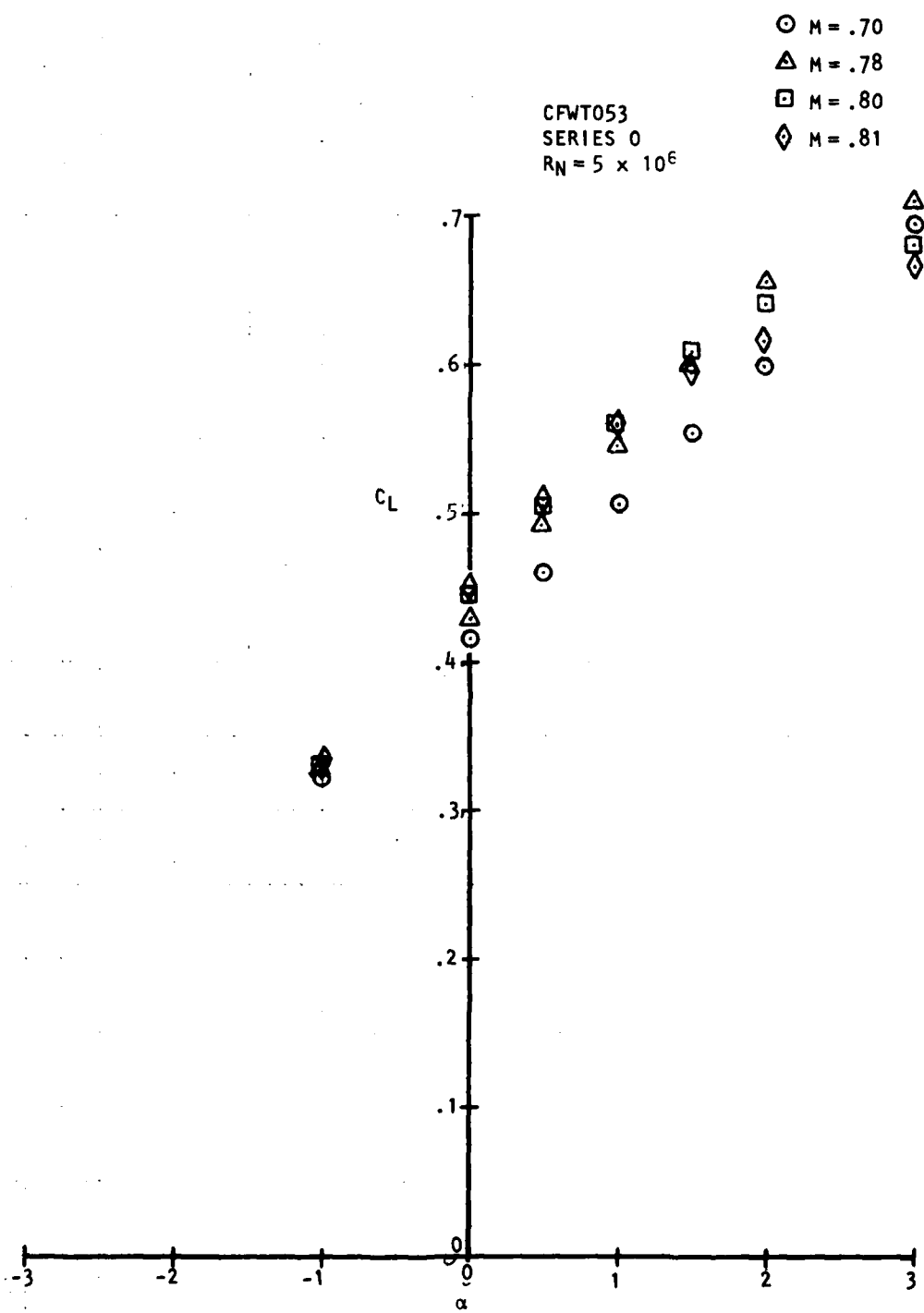


Figure 27a. C_L vs. α C-141B/AC2 Wing Alone

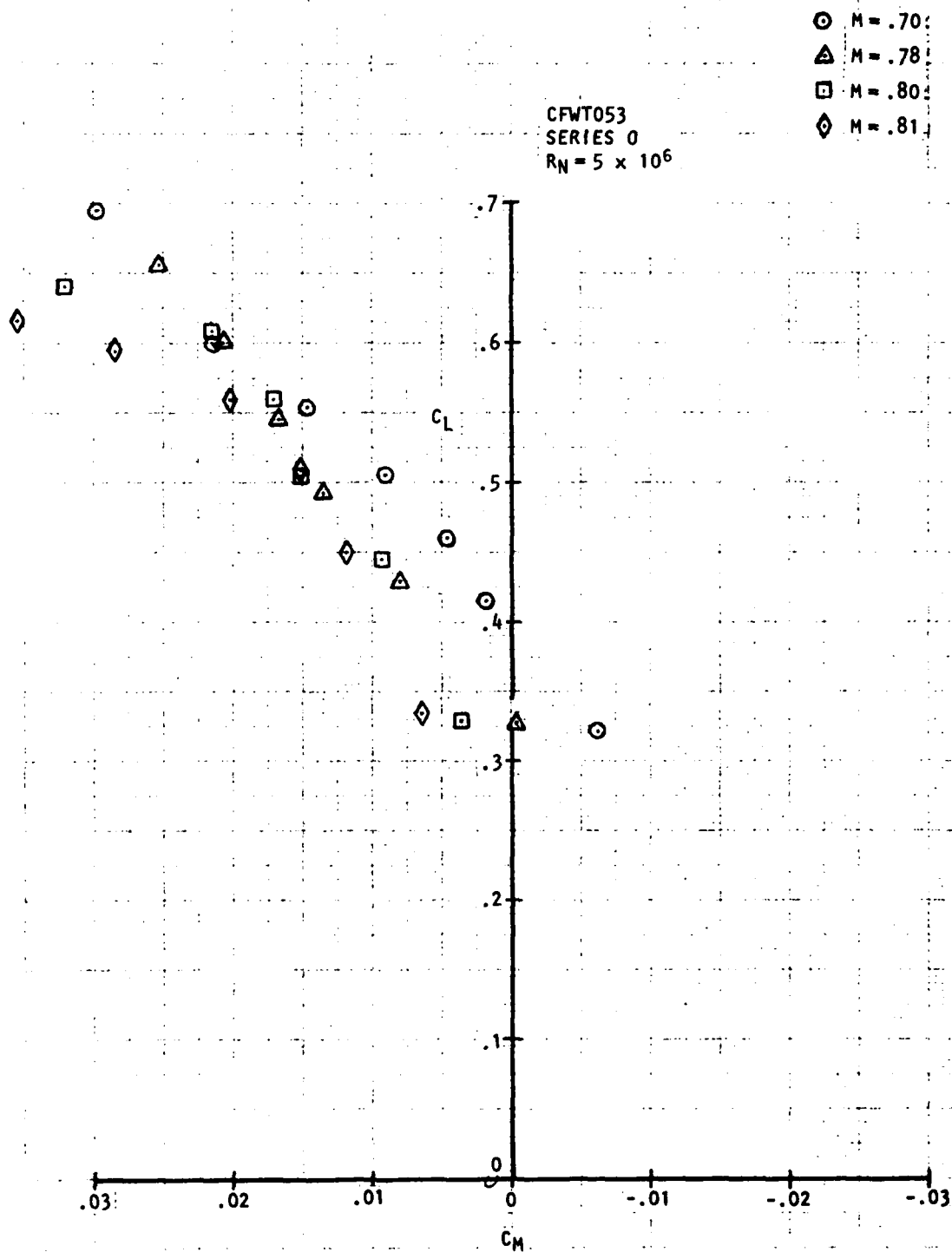


Figure 27b. C_L vs. C_M C-141B/AC2 Wing Alone

○ $M = .70$
 △ $M = .78$
 □ $M = .80$
 ◇ $M = .81$

CFWT053
 SERIES 0
 $R_N = 5 \times 10^6$

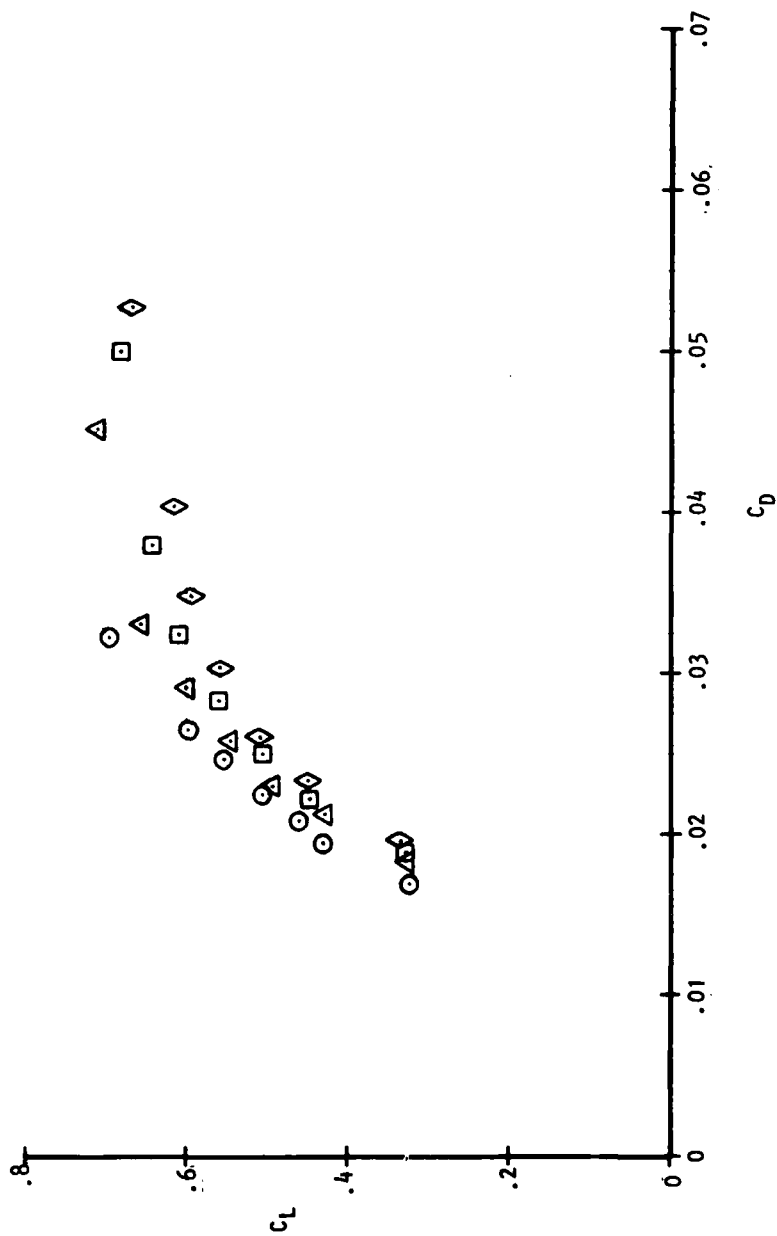


Figure 27c. C_L vs. C_D C-141B/AC2 Wing Alone

CFWT053
 SERIES 1
 $R_N = 5 \times 10^6$

○ $M = .70$
 △ $M = .78$
 □ $M = .80$
 ◇ $M = .81$

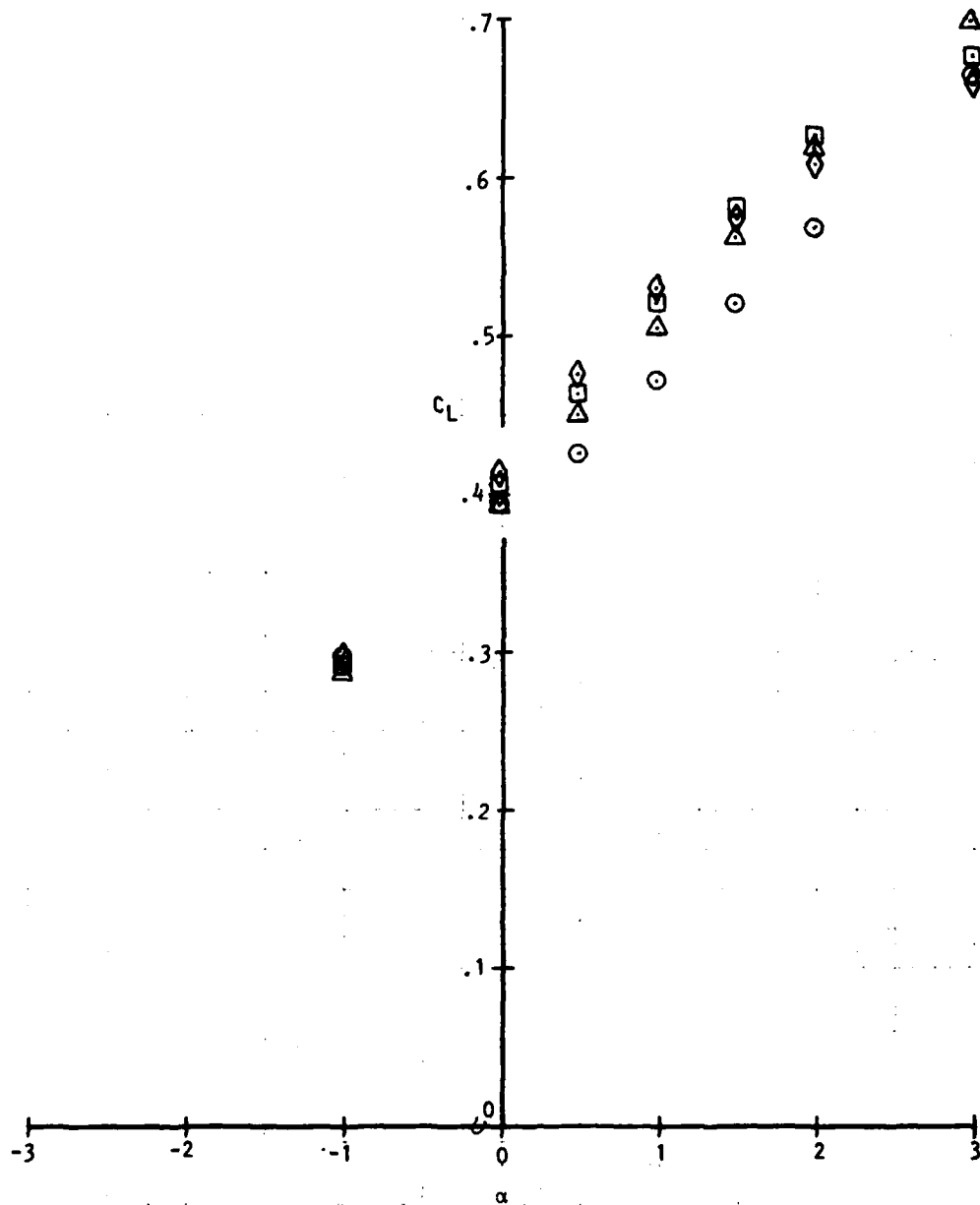


Figure 28a. C_L vs. α C-141B/AC2 Wing + Pylon/Nacelle

CFWT053
 SERIES 1
 $R_N = 5 \times 10^6$

- $M = .70$
- △ $M = .78$
- $M = .80$
- ◇ $M = .81$

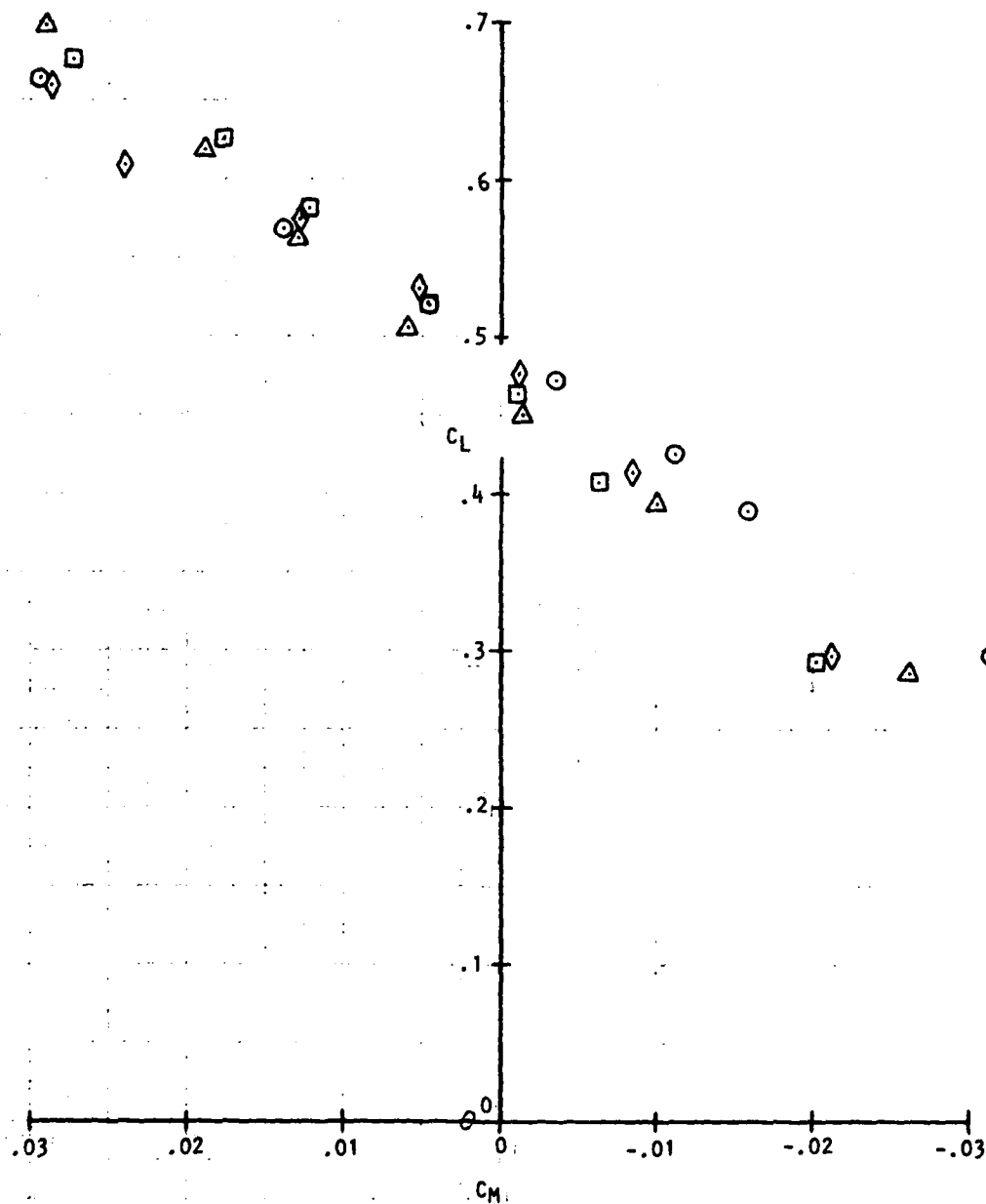


Figure 28b. C_L vs. C_M C-141B/AC2 Wing + Pylon/Nacelle

\circ $M = .70$
 \triangle $M = .78$
 \square $M = .80$
 \diamond $M = .81$

CFMT053
 SERIES 1
 $R_N = 5 \times 10^6$

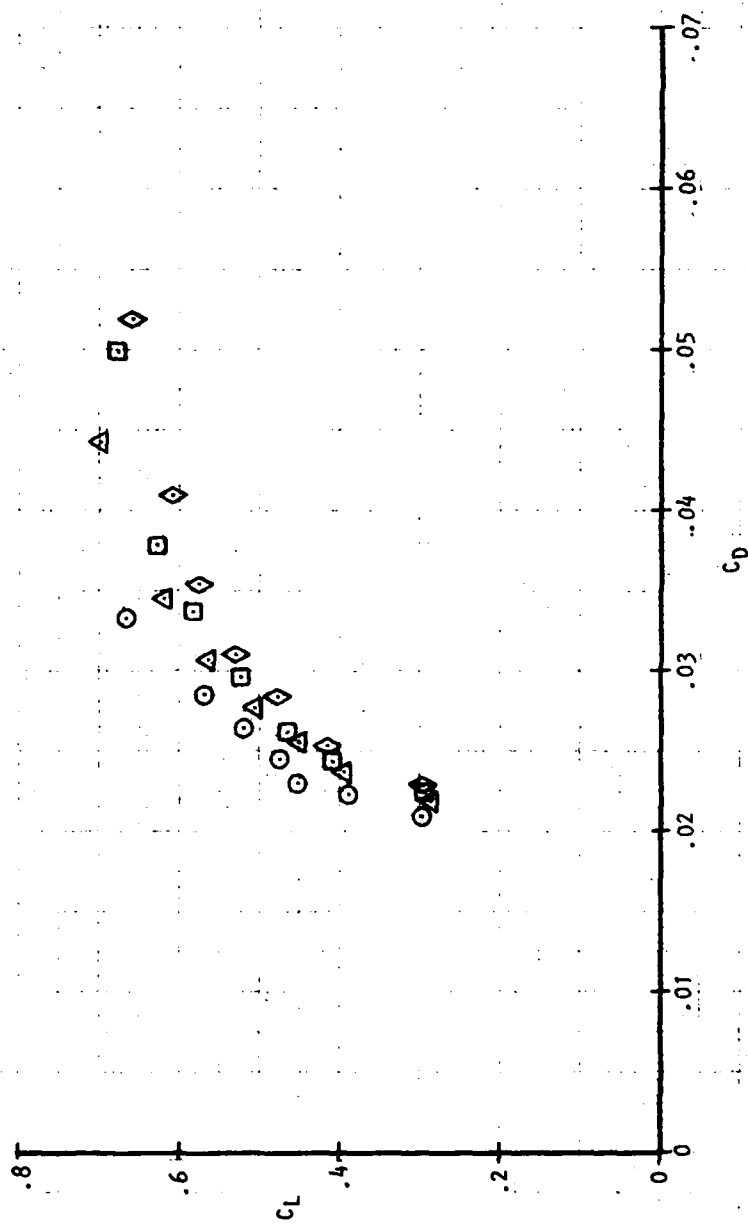


Figure 28c. C_L vs. C_D C-141/AC2 Wing + Pylon/Nacelle

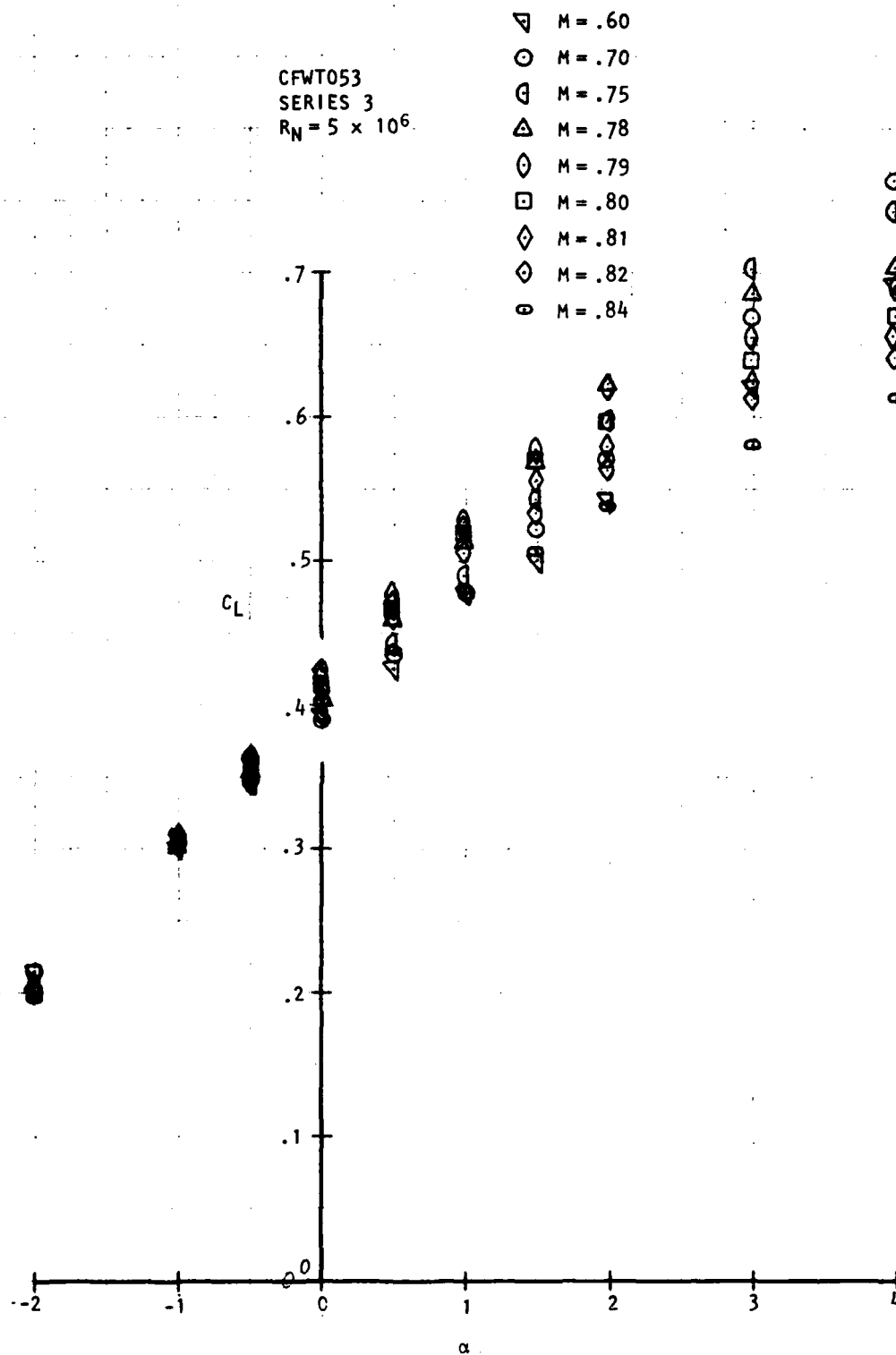
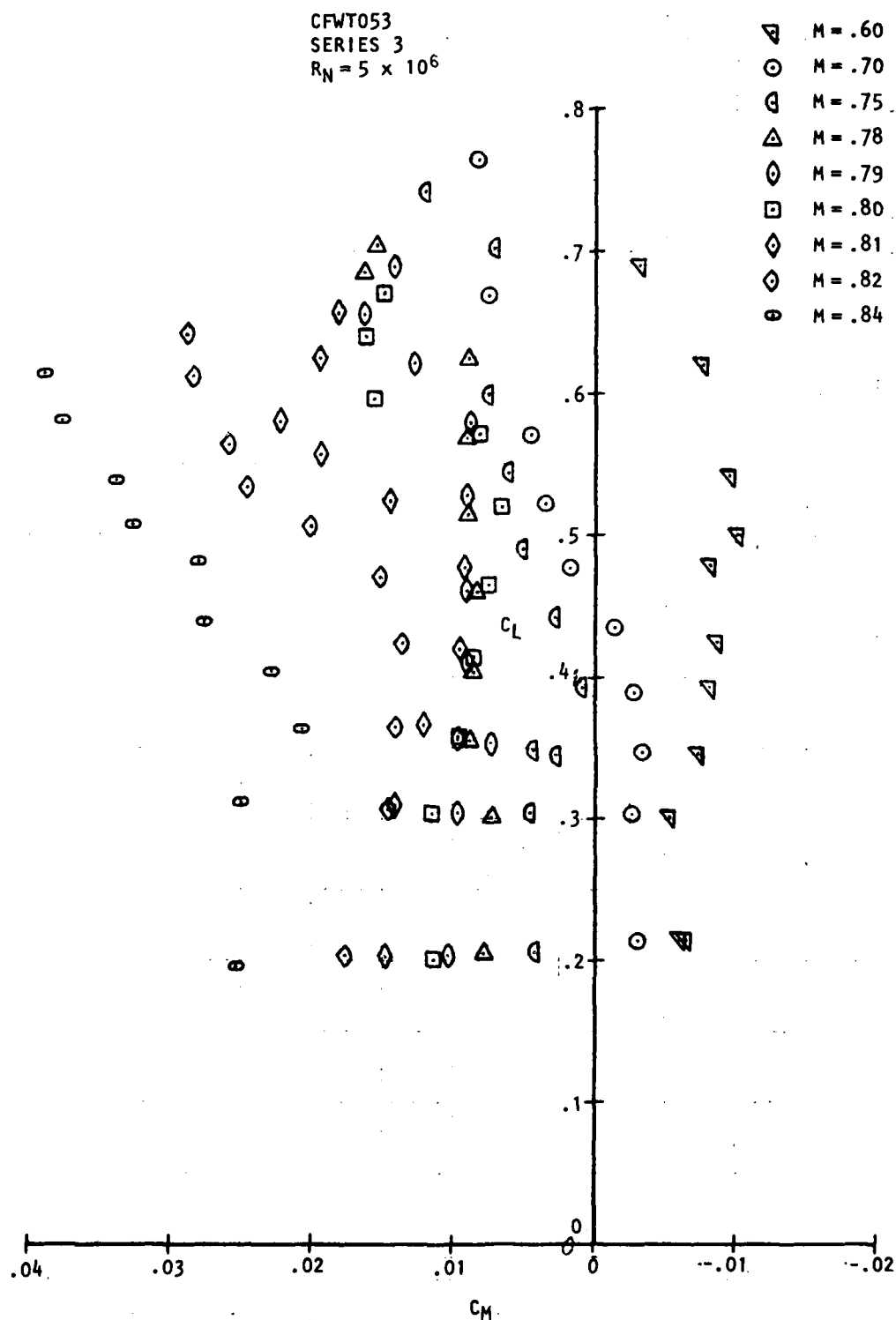


Figure 29a. C_L vs. α C141/AC2 Wing + Fuselage + Gearpod



∇ M = .60
 \circ M = .70
 \diamond M = .75
 \triangle M = .78
 \diamond M = .79
 \square M = .80
 \diamond M = .81
 \diamond M = .82
 \circ M = .84

CFWT053
 SERIES 3
 $R_N = 5 \times 10^6$

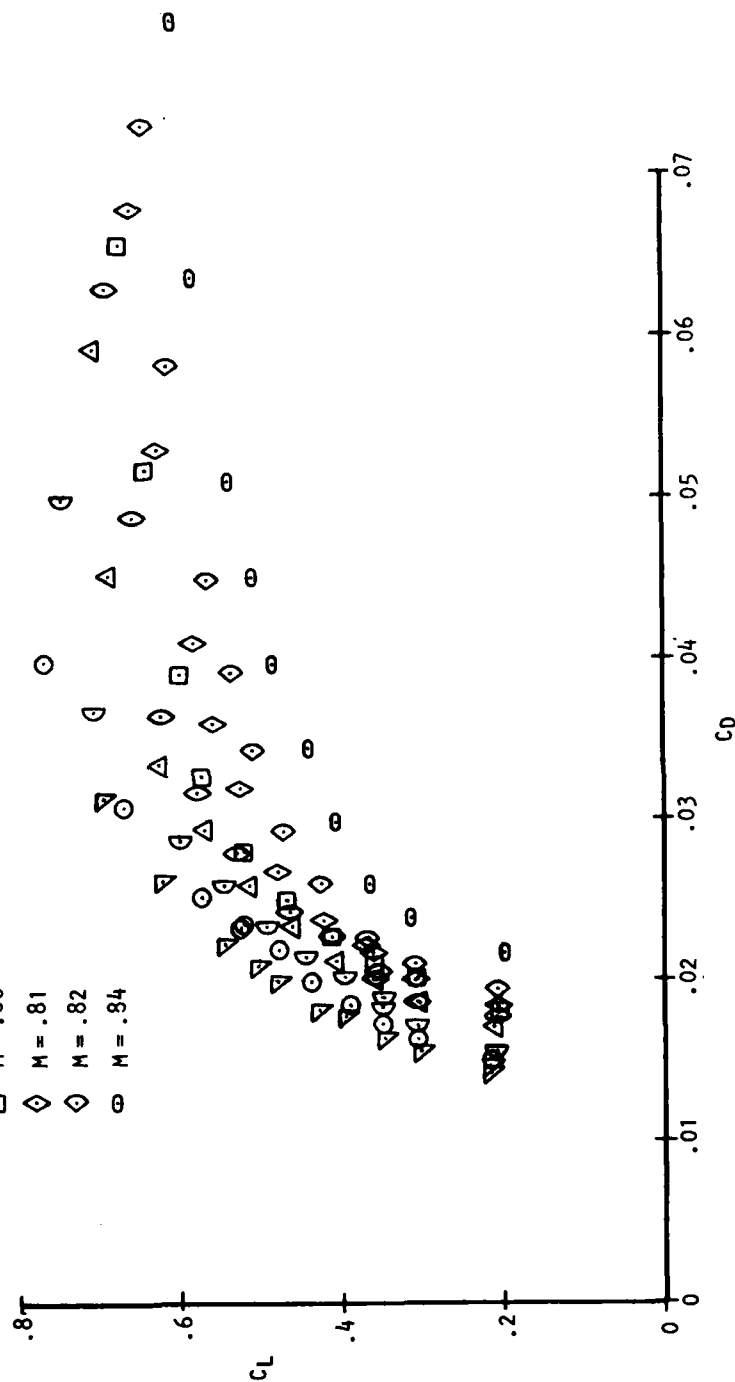


Figure 29c. C_L vs. C_D C-141/AC2 Wing + Fuselage + Gearpod

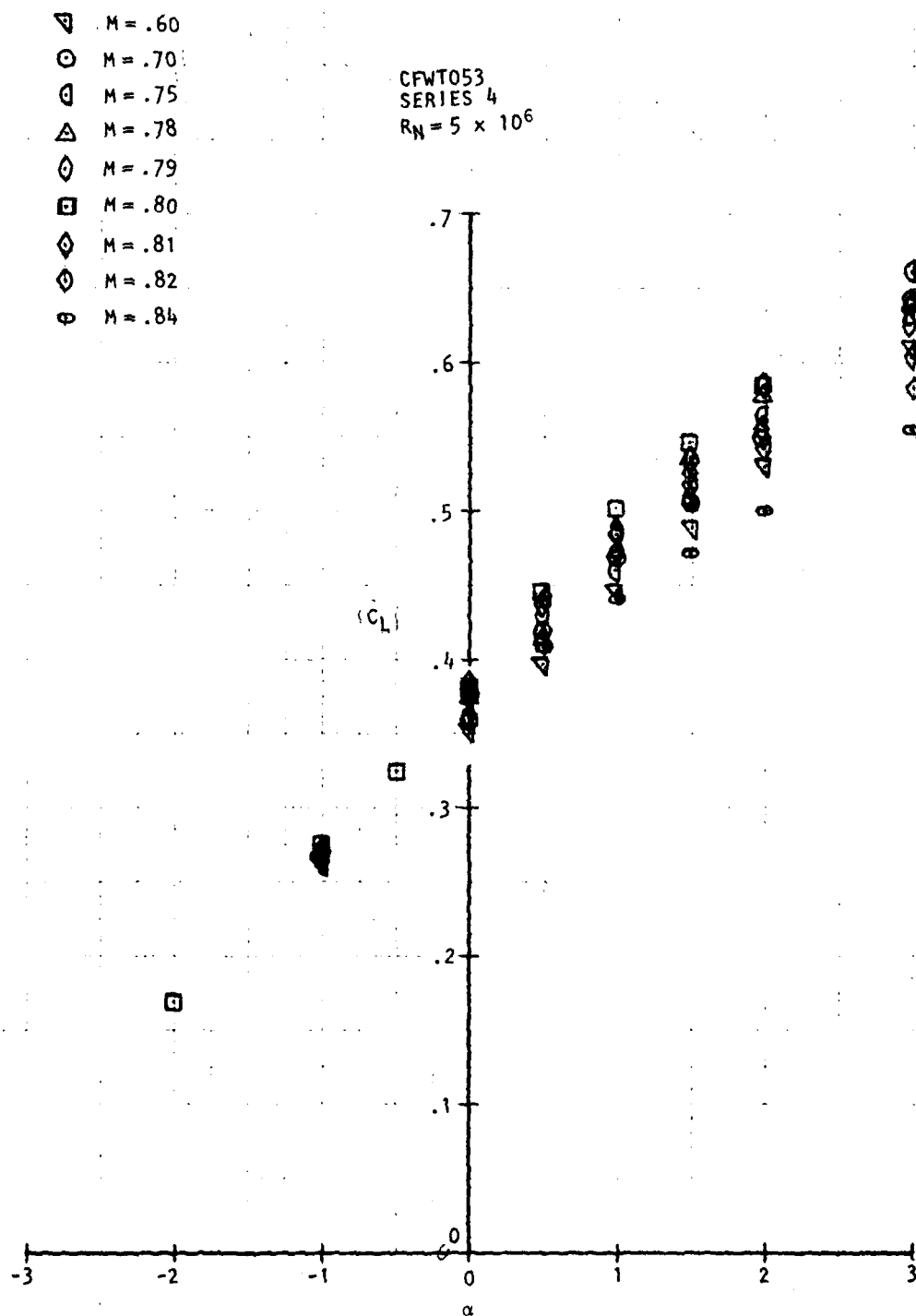


Figure 30a. C_L vs. α - C-141B/AC2 Wing + Fuselage + Gearpod + Pylon/Nacelle

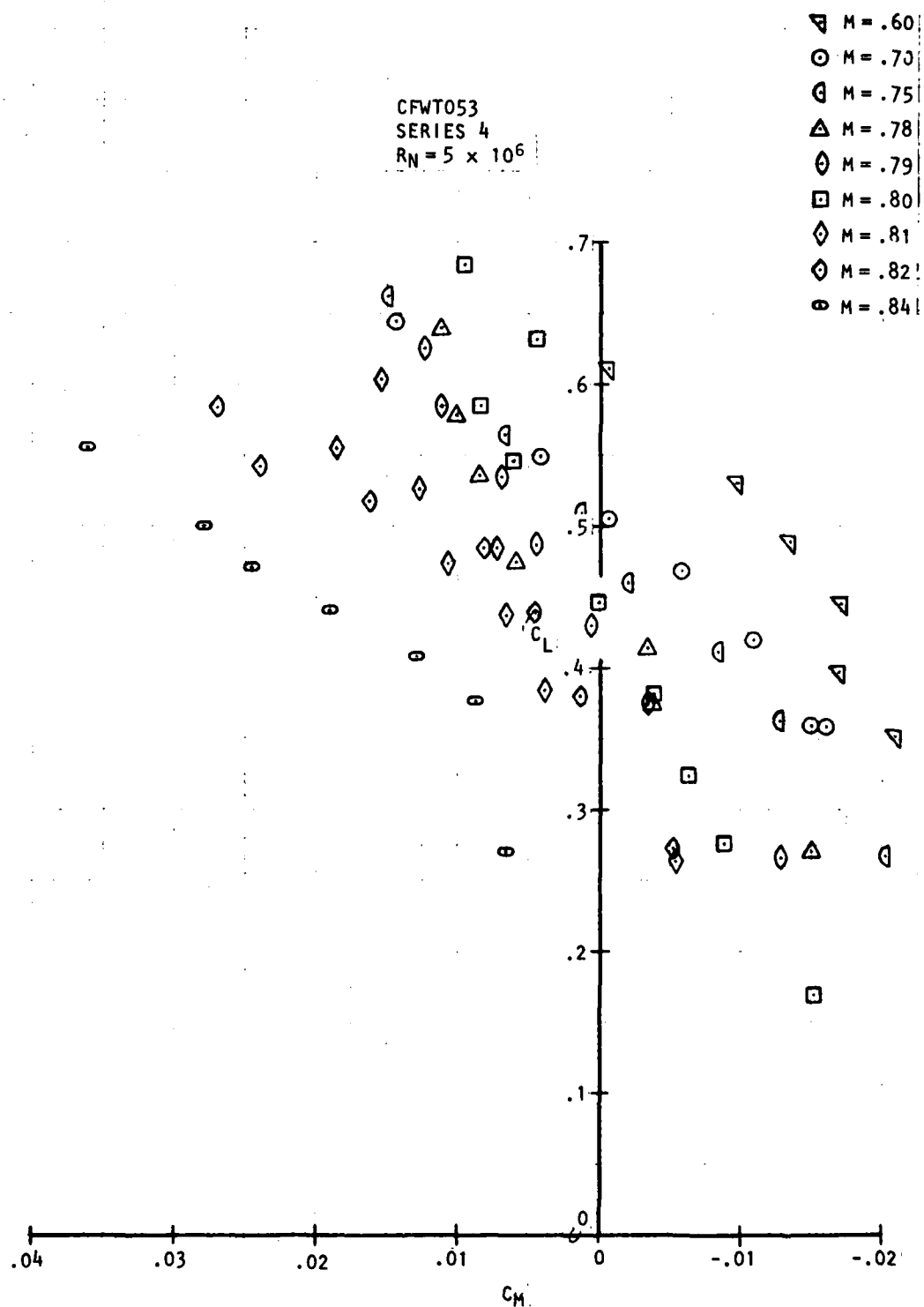


Figure 30b. C_L vs. C_M C-141B/AC2 Wing + Fuselage + Gearpod + Pylon/Nacelle

∇ $M = .60$
 \circ $M = .70$
 \square $M = .75$
 \triangle $M = .78$
 \diamond $M = .79$
 \square $M = .80$
 \diamond $M = .81$
 \diamond $M = .82$
 \circ $M = .84$

CFJ1053
 SERIES 4
 $R_N = 5 \times 10^6$

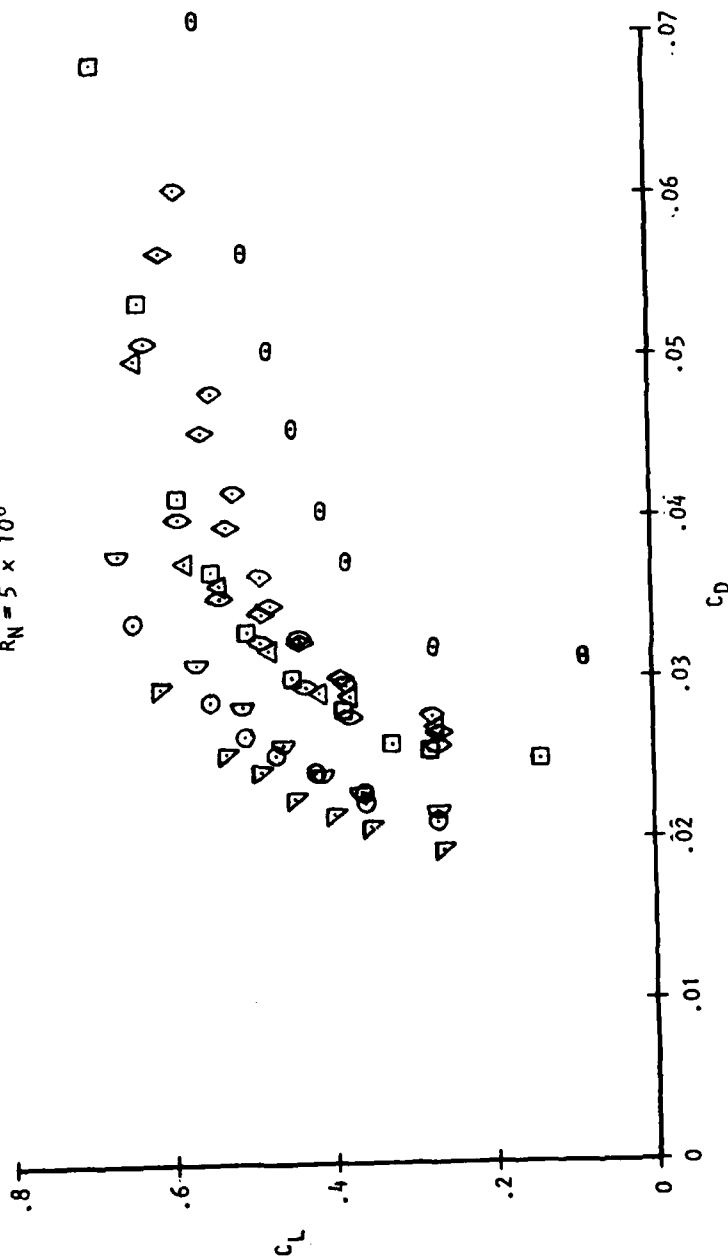


Figure 30c. C_L vs. C_D C-141B/AC2 Wing + Fuselage + Gearpod + Pylon/Nacelle

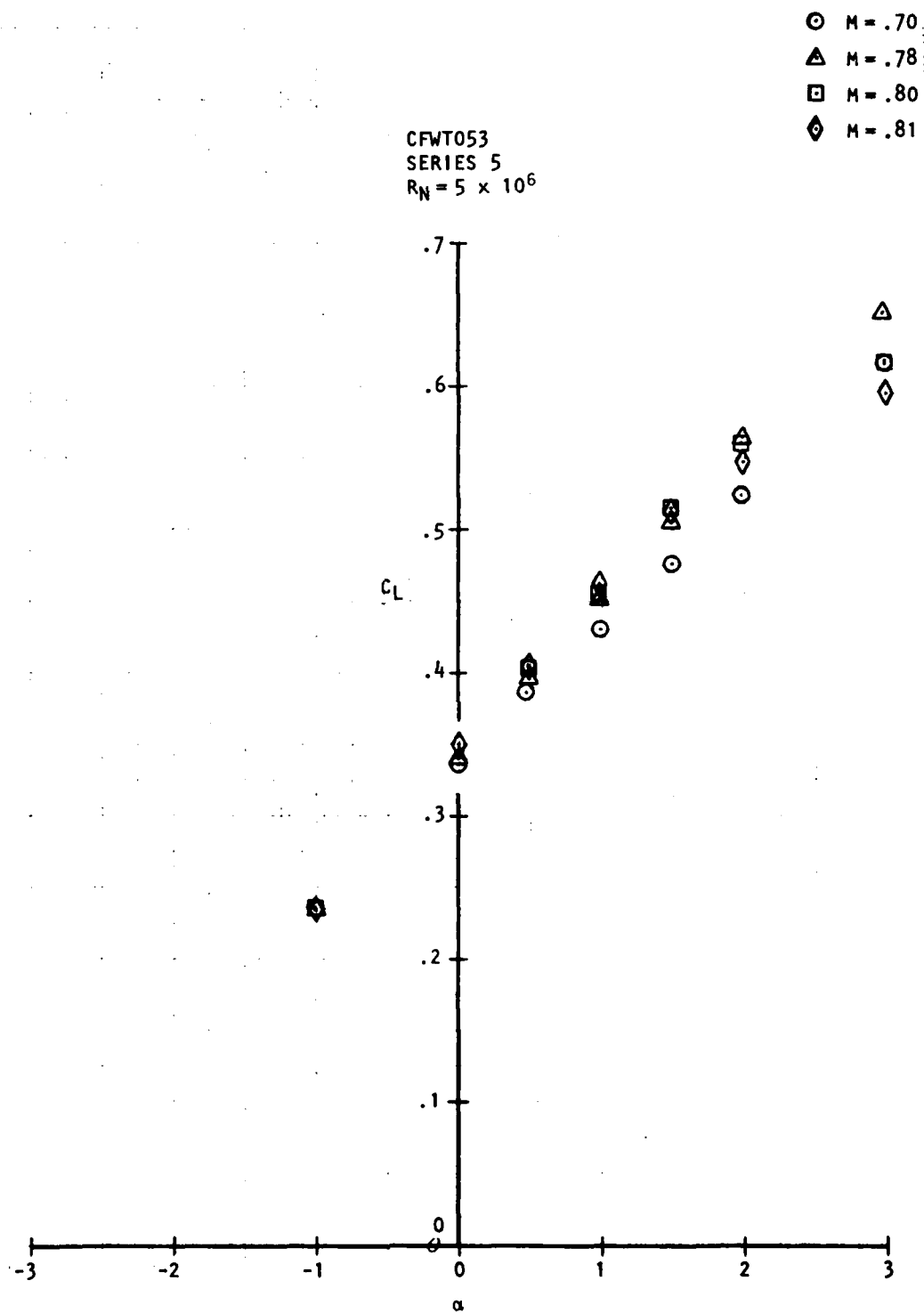


Figure 31a. C_L vs. α C-141B/AC2 Wing + Fuselage + Pylon/Nacelle

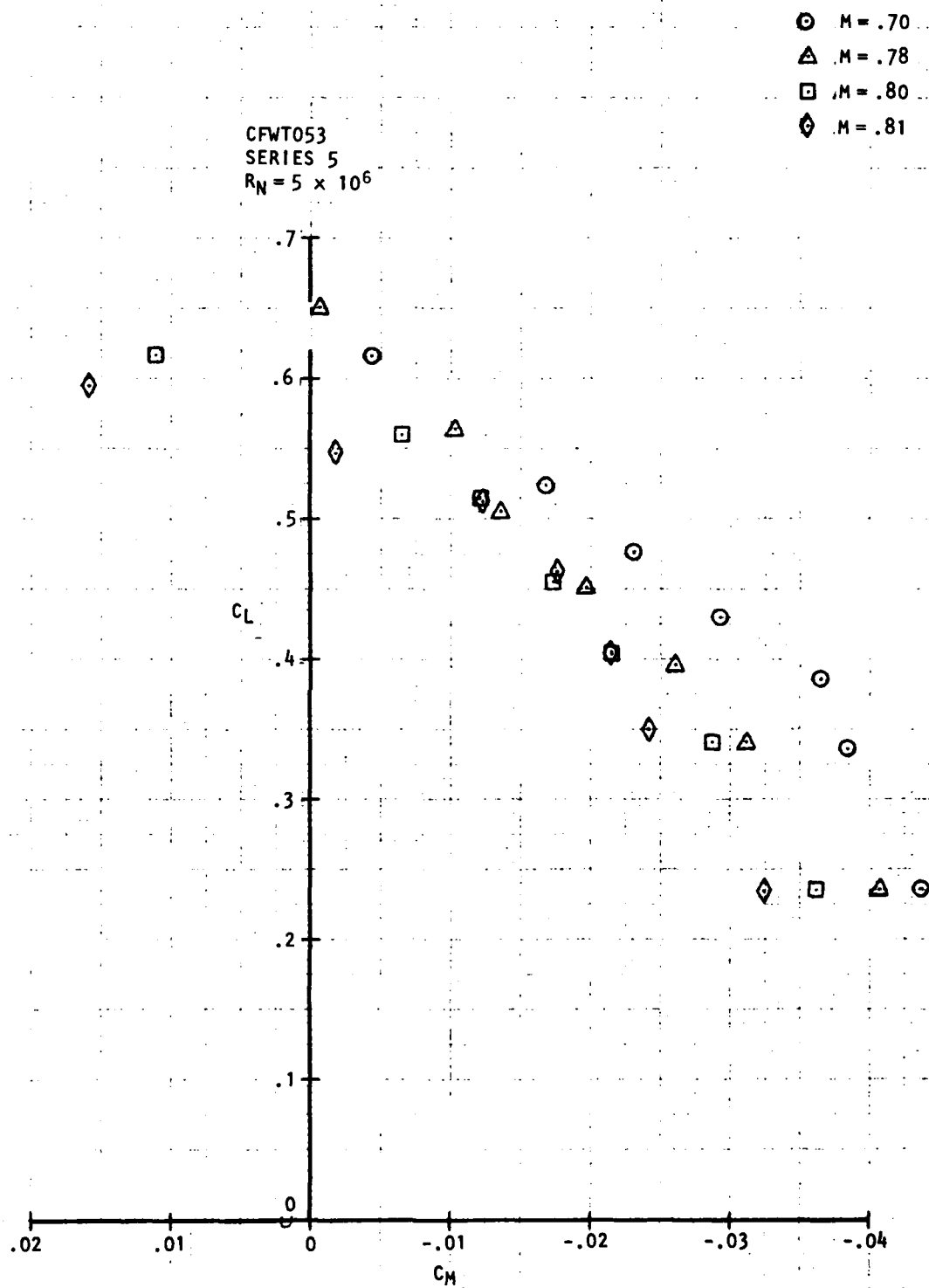


Figure 31b. C_L vs. C_M C-141B/AC2 Wing + Fuselage + Pylon/Nacelle

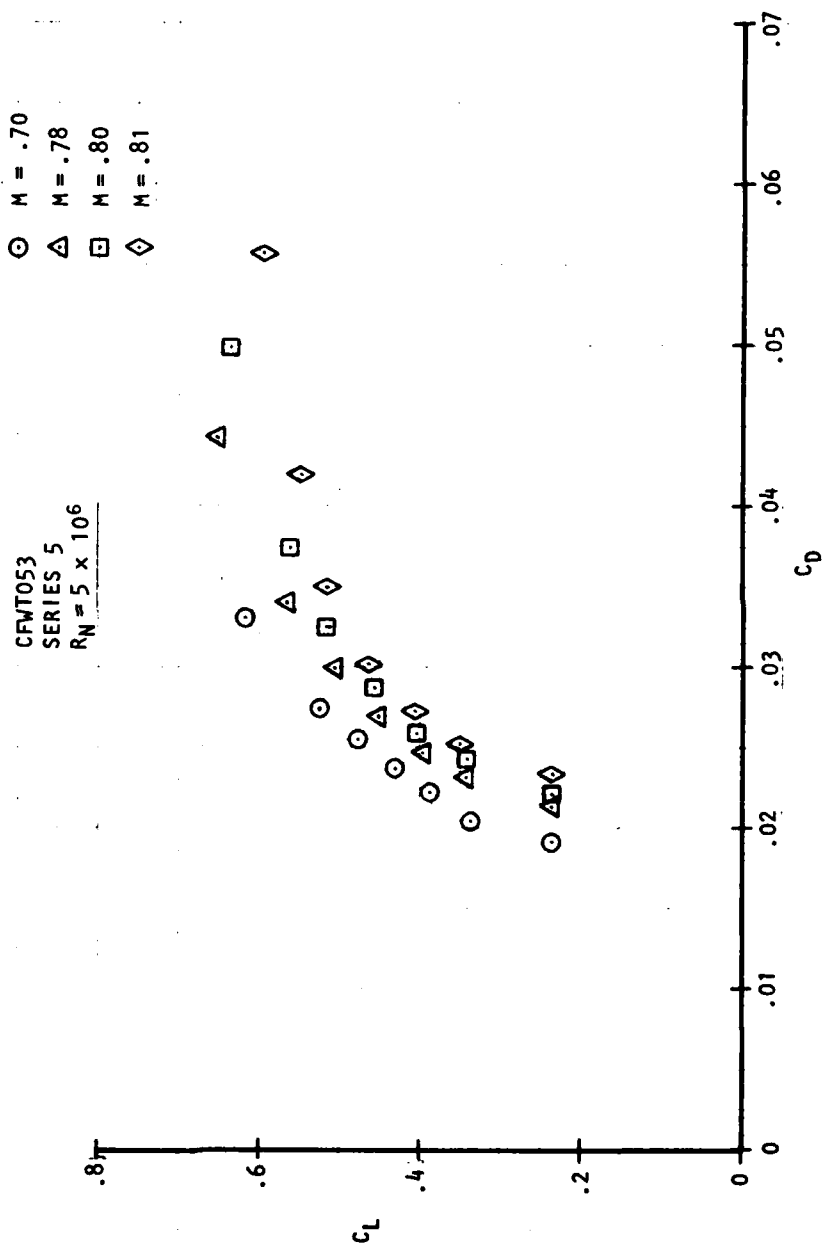


Figure 31c. C_L vs. C_D C-141B/AC2 Wing + Fuselage + Pylon/Nacelle

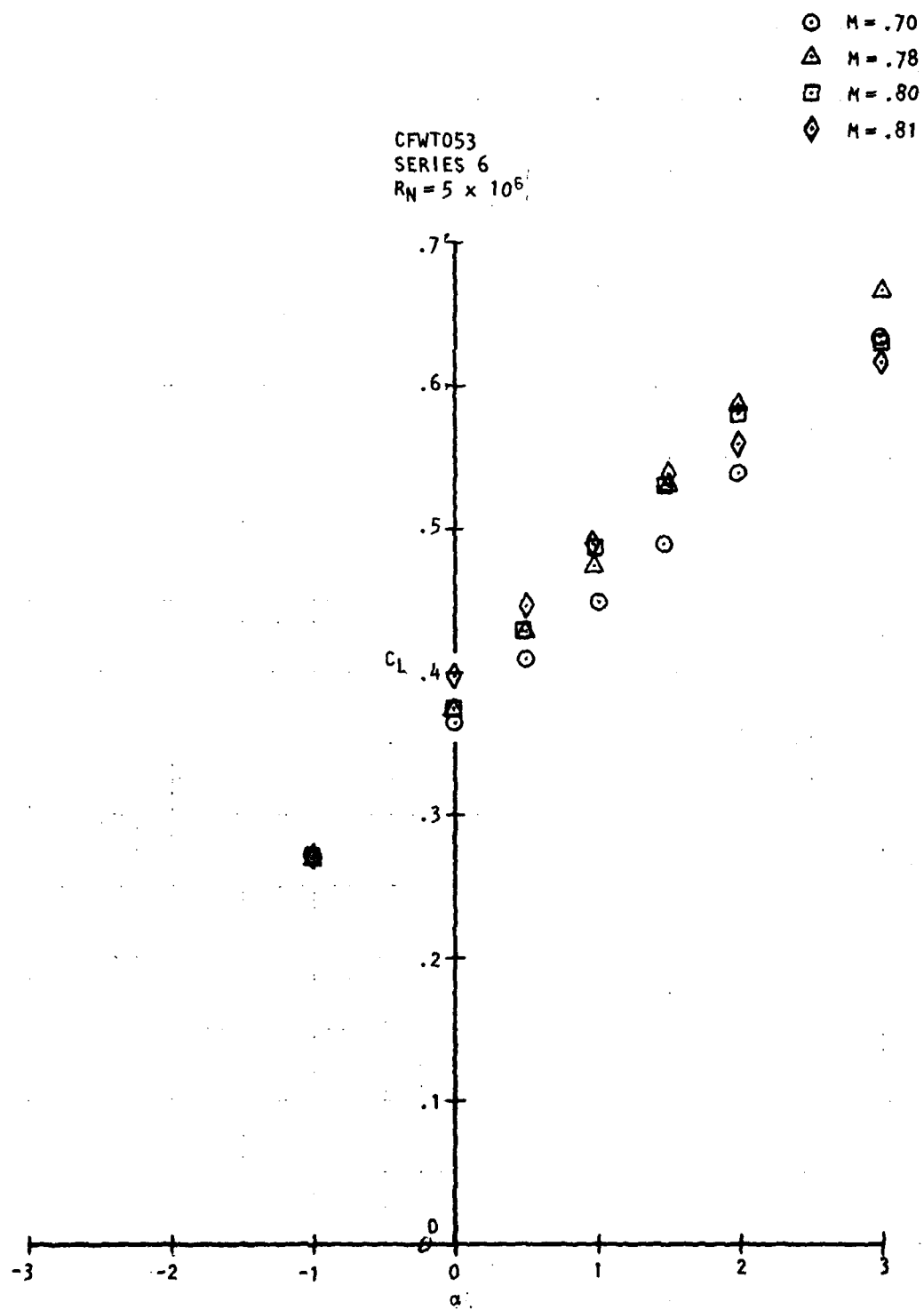


Figure 32a. C_L vs. α C-141B/AC2 Wing + Fuselage

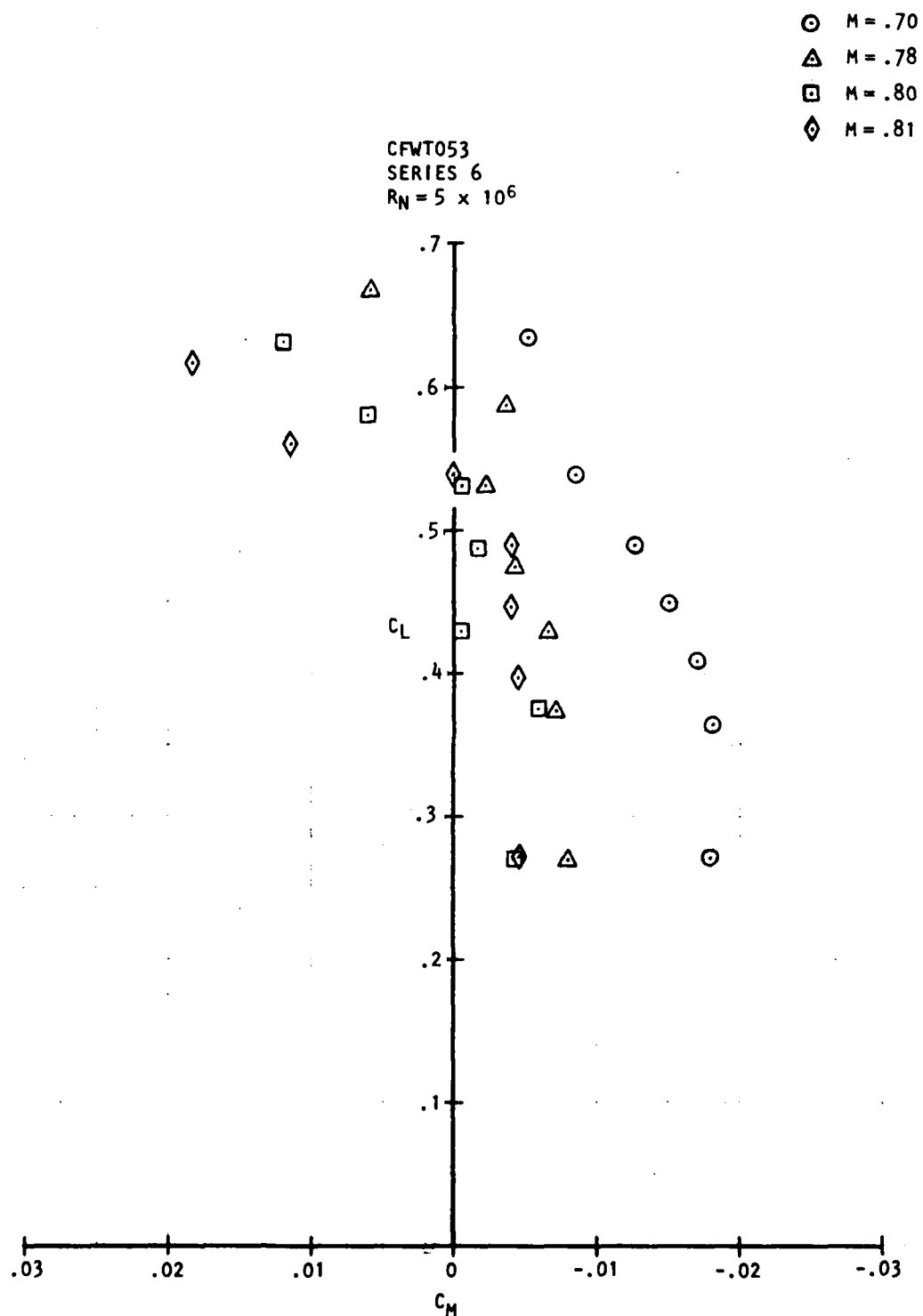
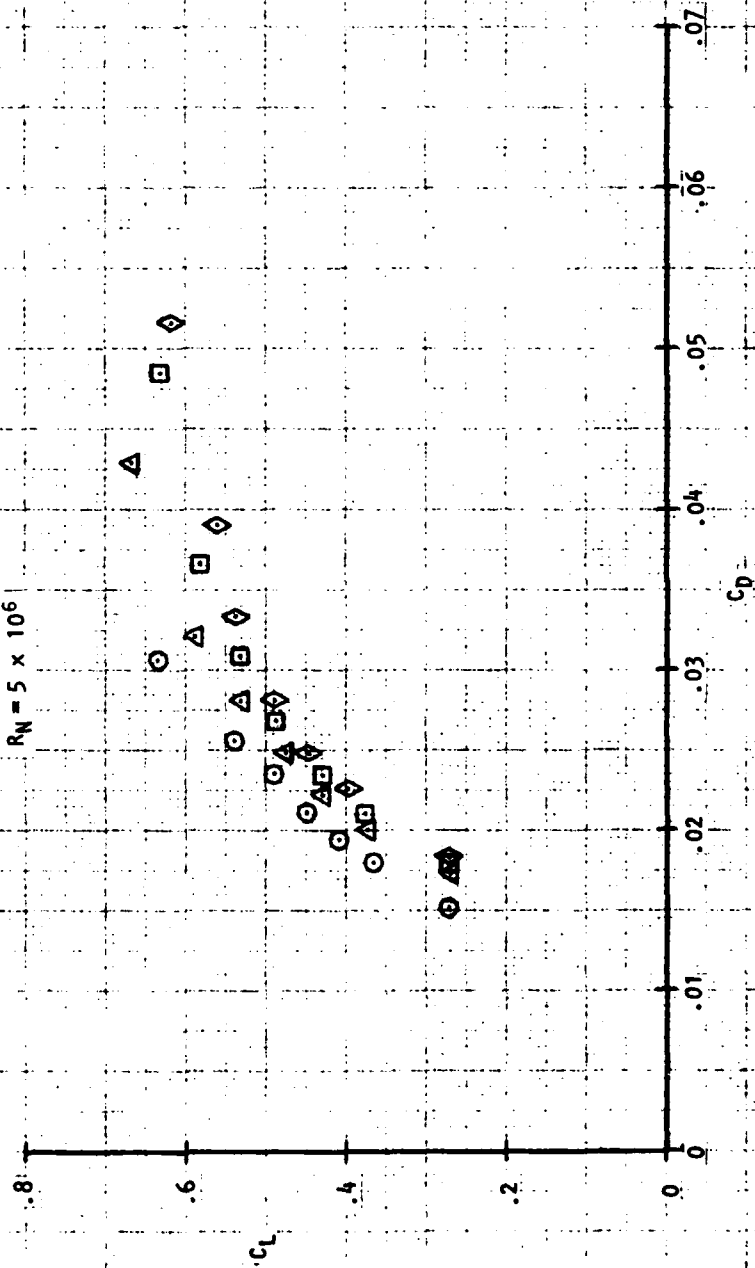
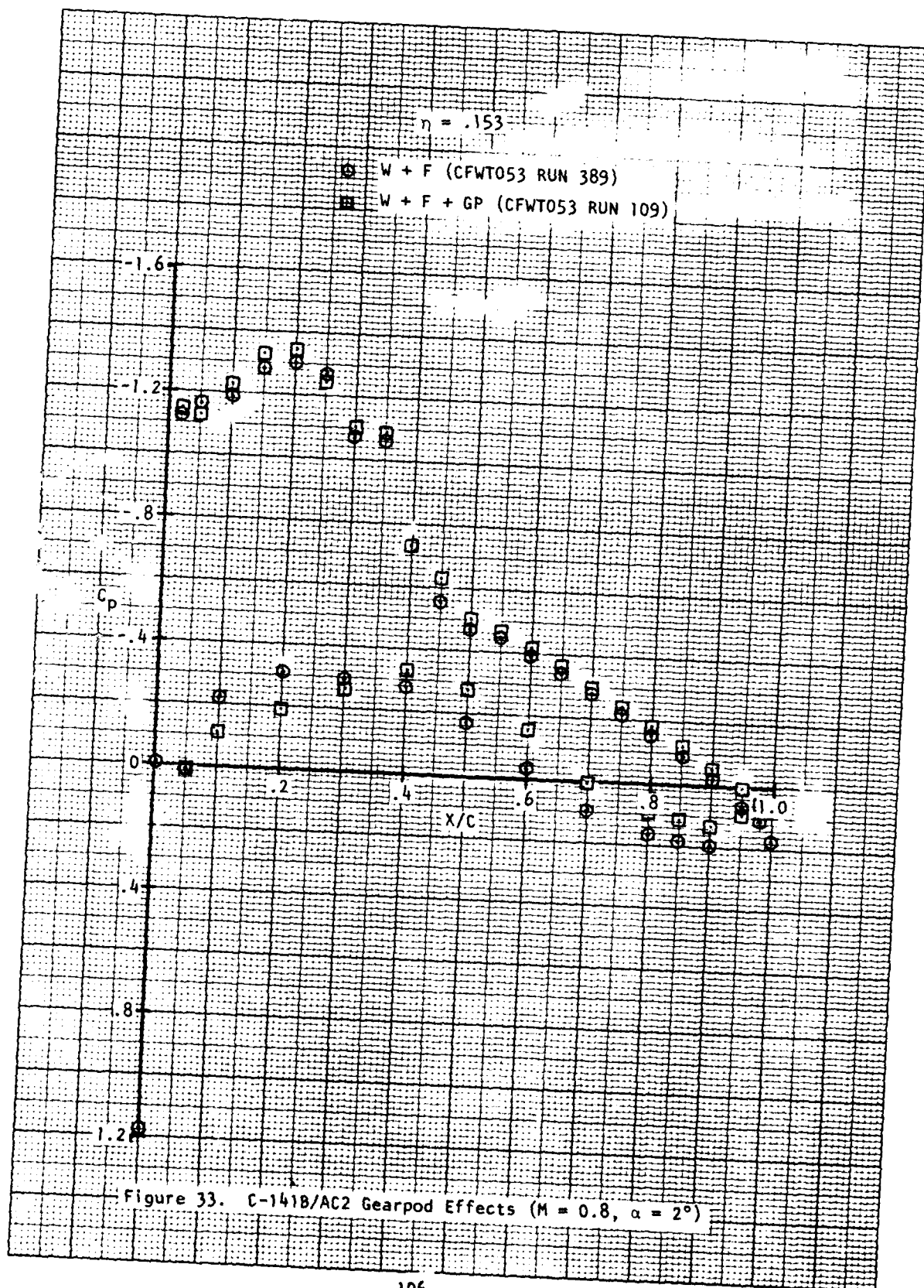


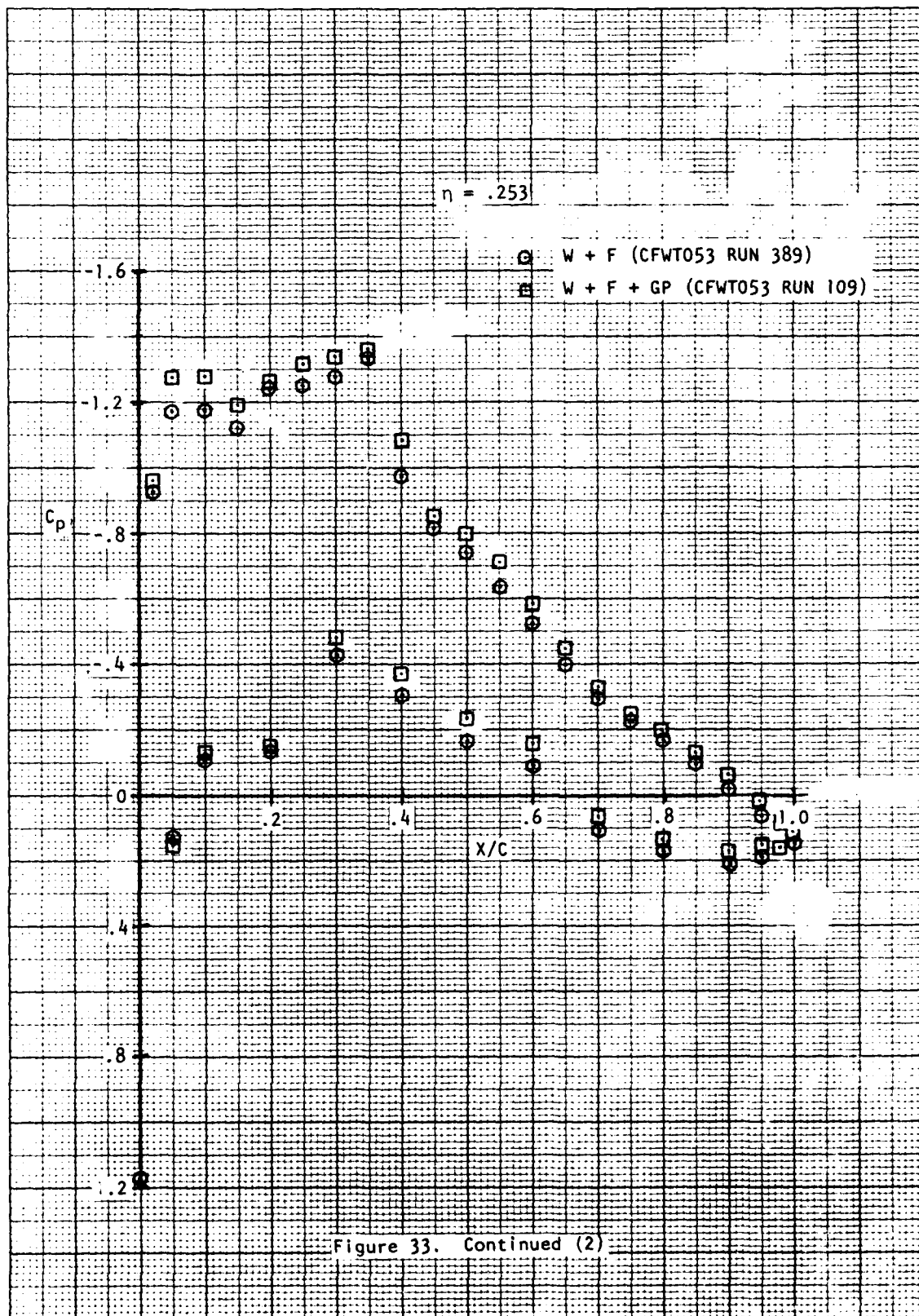
Figure 32b. C_L vs. C_M C-141B/AC2 Wing + Fuselage

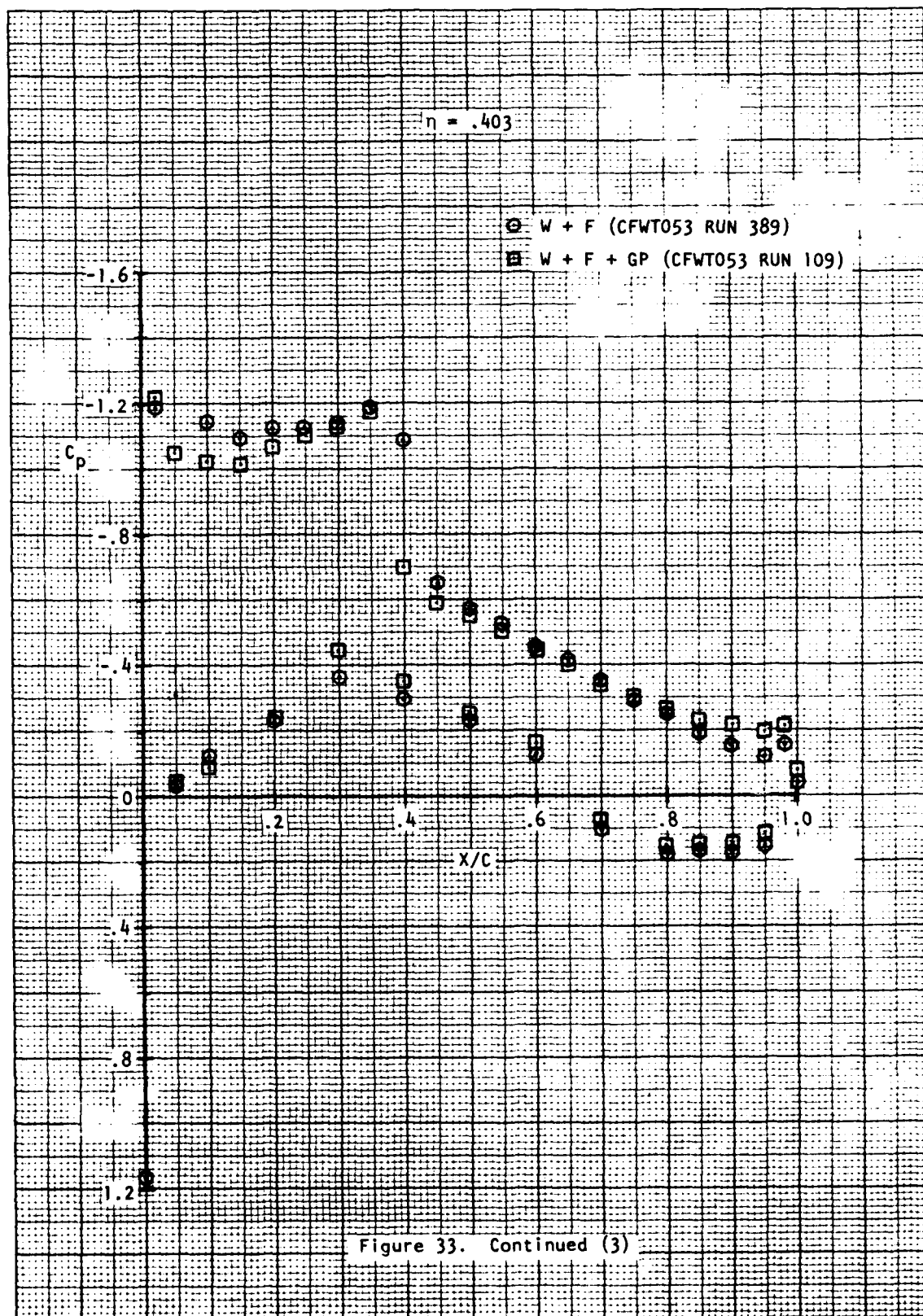
\bigcirc $M = .70$
 \triangle $M = .78$
 \square $M = .80$
 \diamond $M = .81$

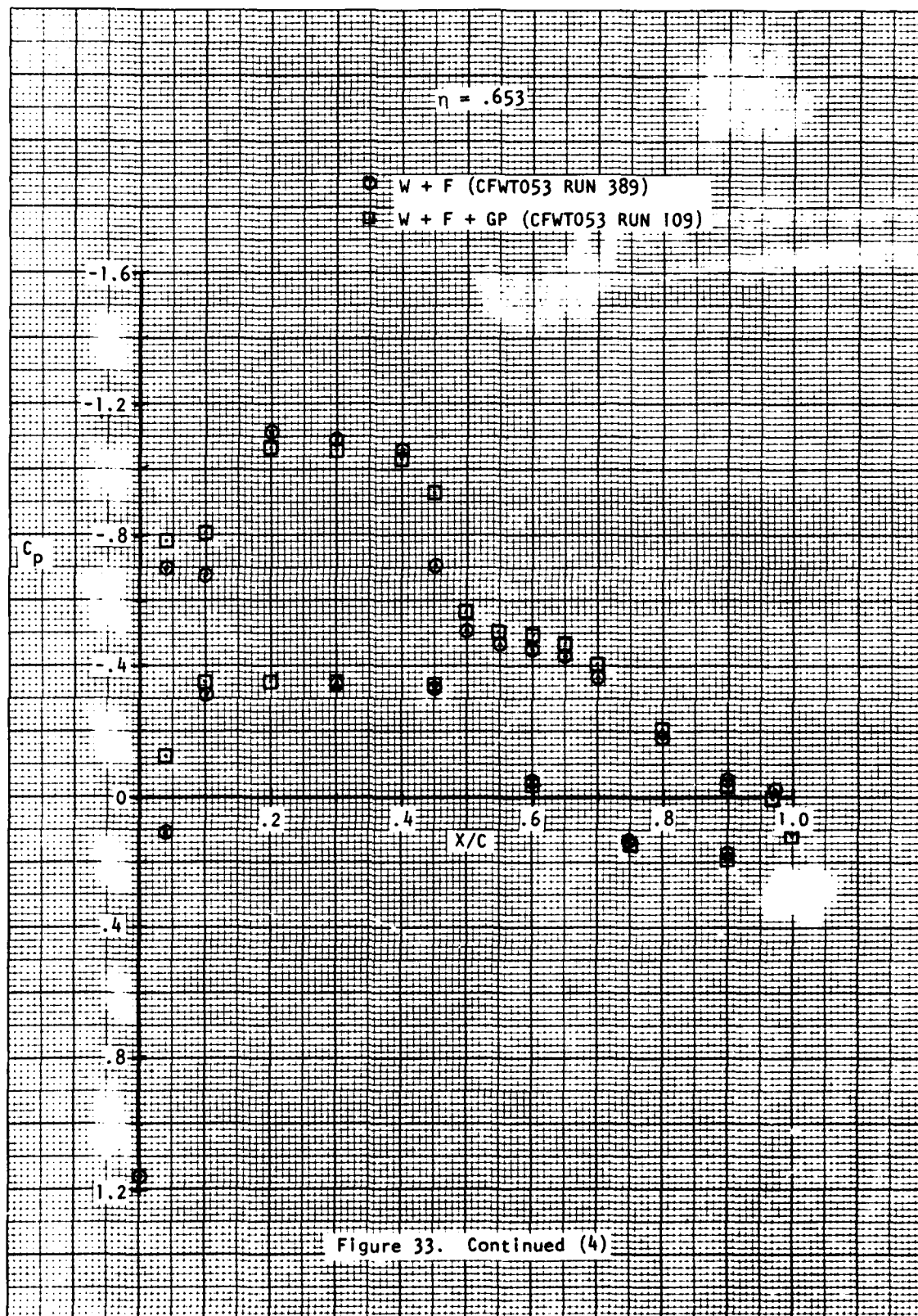
CFWT053
 SERIES 6
 $R_N = 5 \times 10^6$

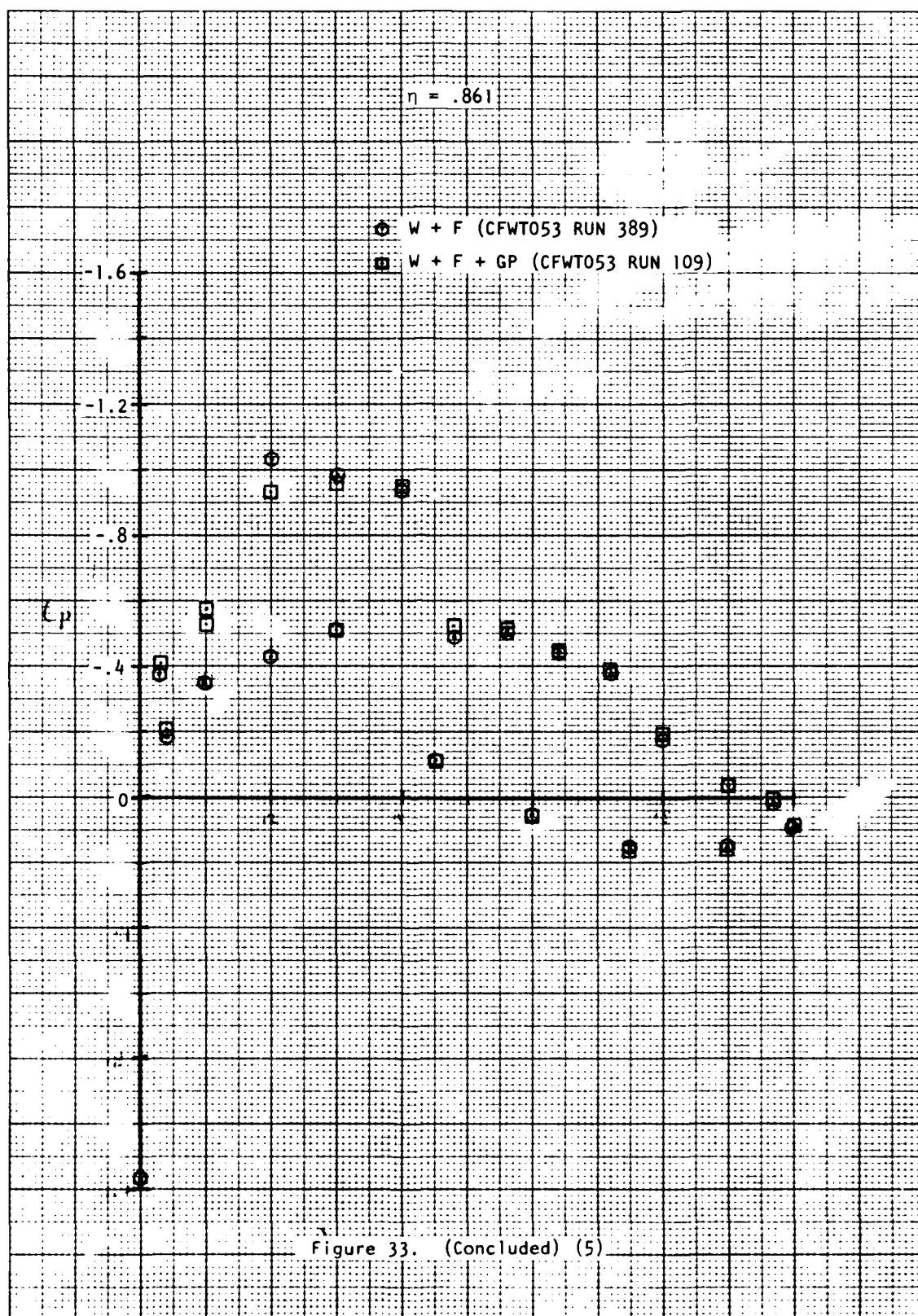












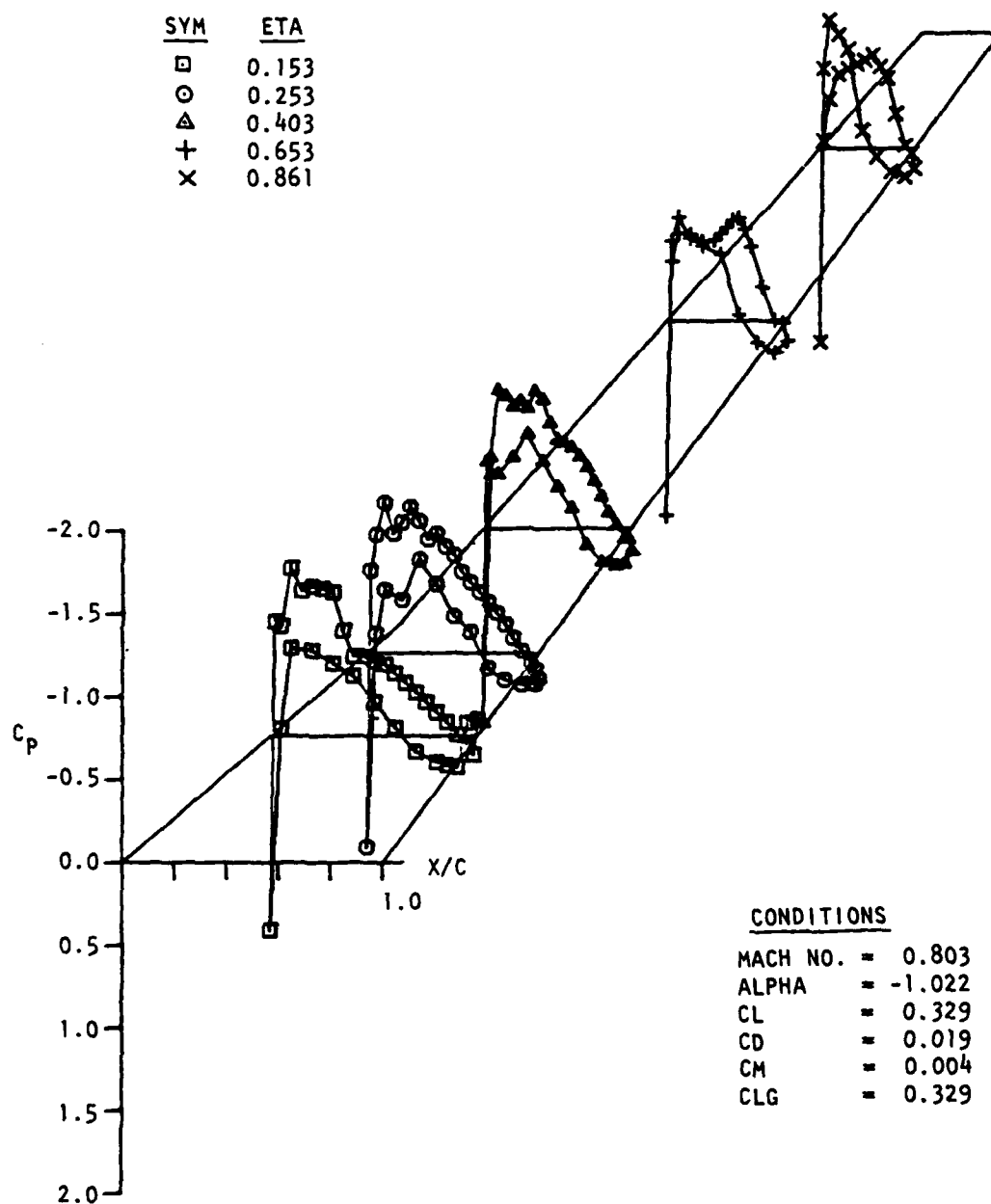


Figure 34. C-141B/AC Wing Alone Isometric Pressure Plots
Mach = 0.80 ($\alpha = -1^\circ$)

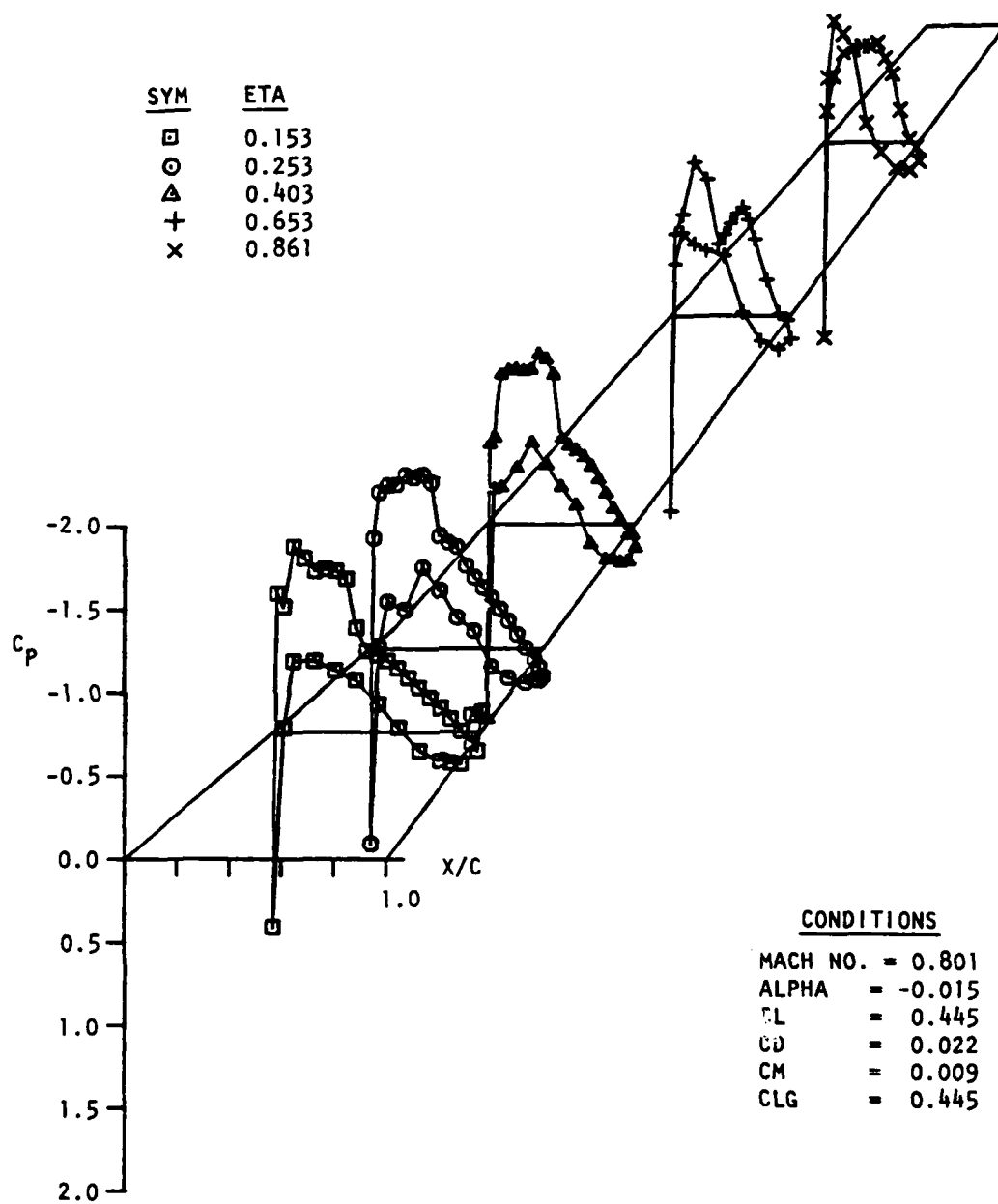


Figure 34. (Continued) ($\alpha \sim 0^\circ$)

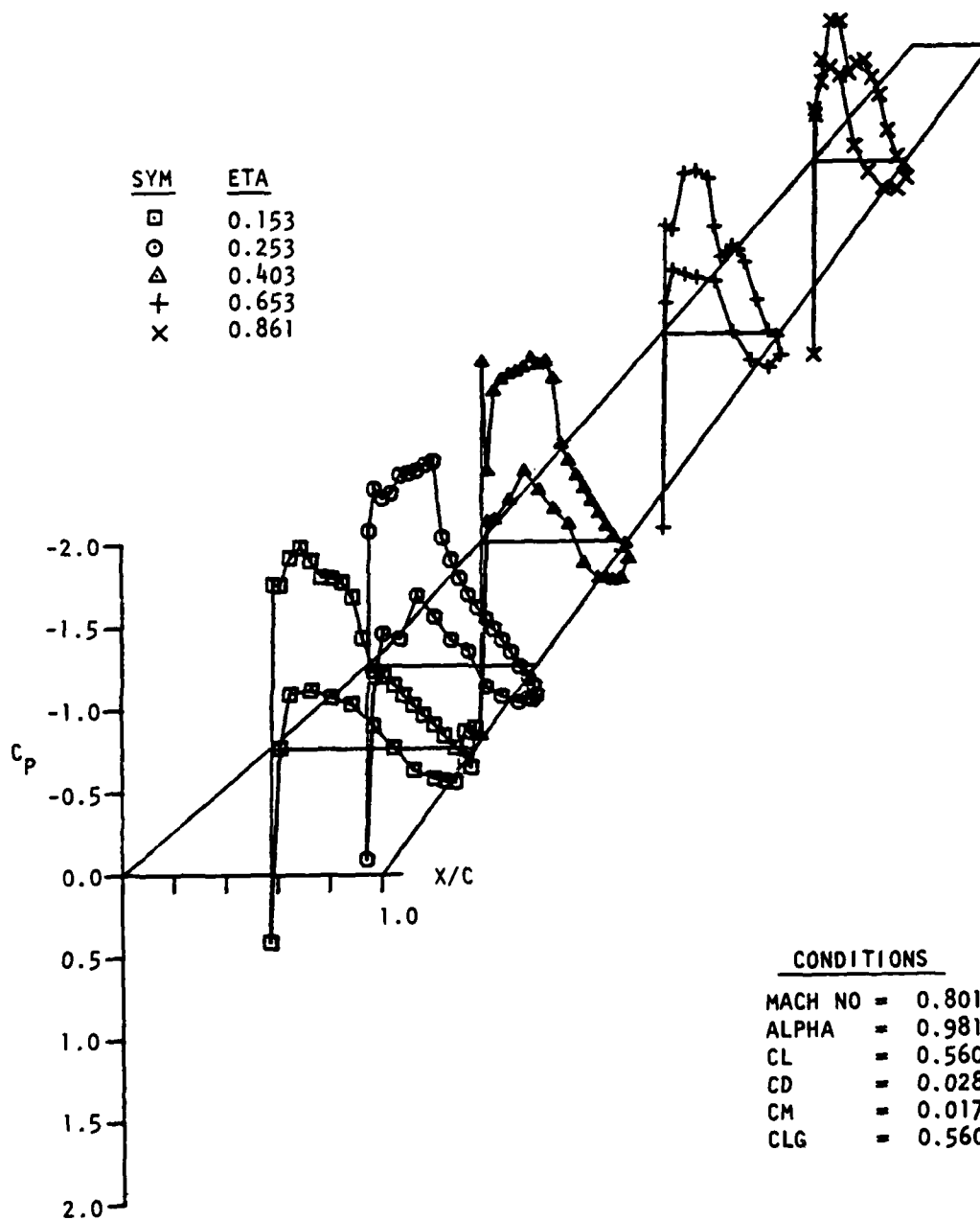


Figure 34. (Continued) ($\alpha = 1^\circ$)

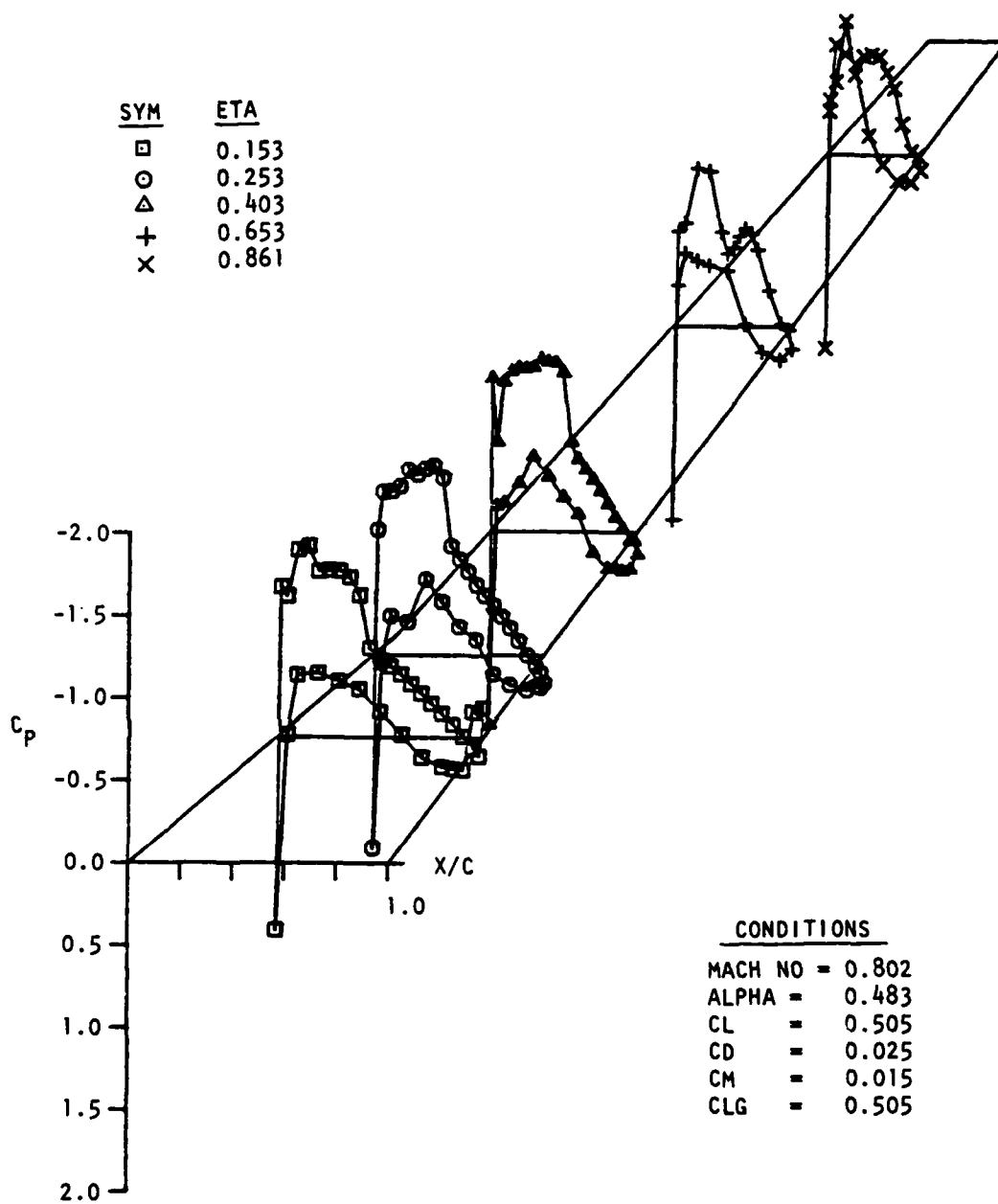


Figure 34. (Continued) ($\alpha \sim 5^\circ$)

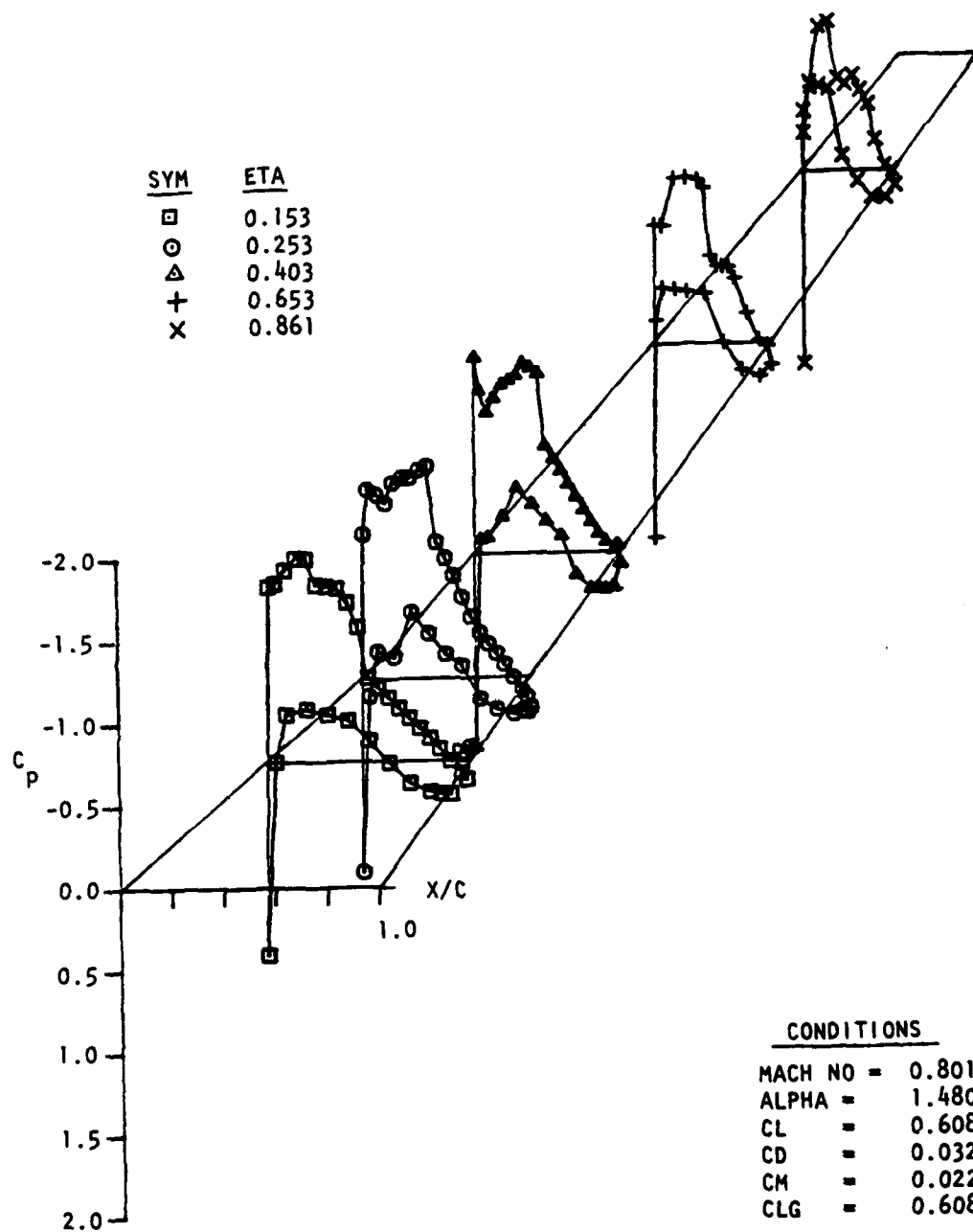


Figure 34. (Continued) ($\alpha = 1.5^\circ$)

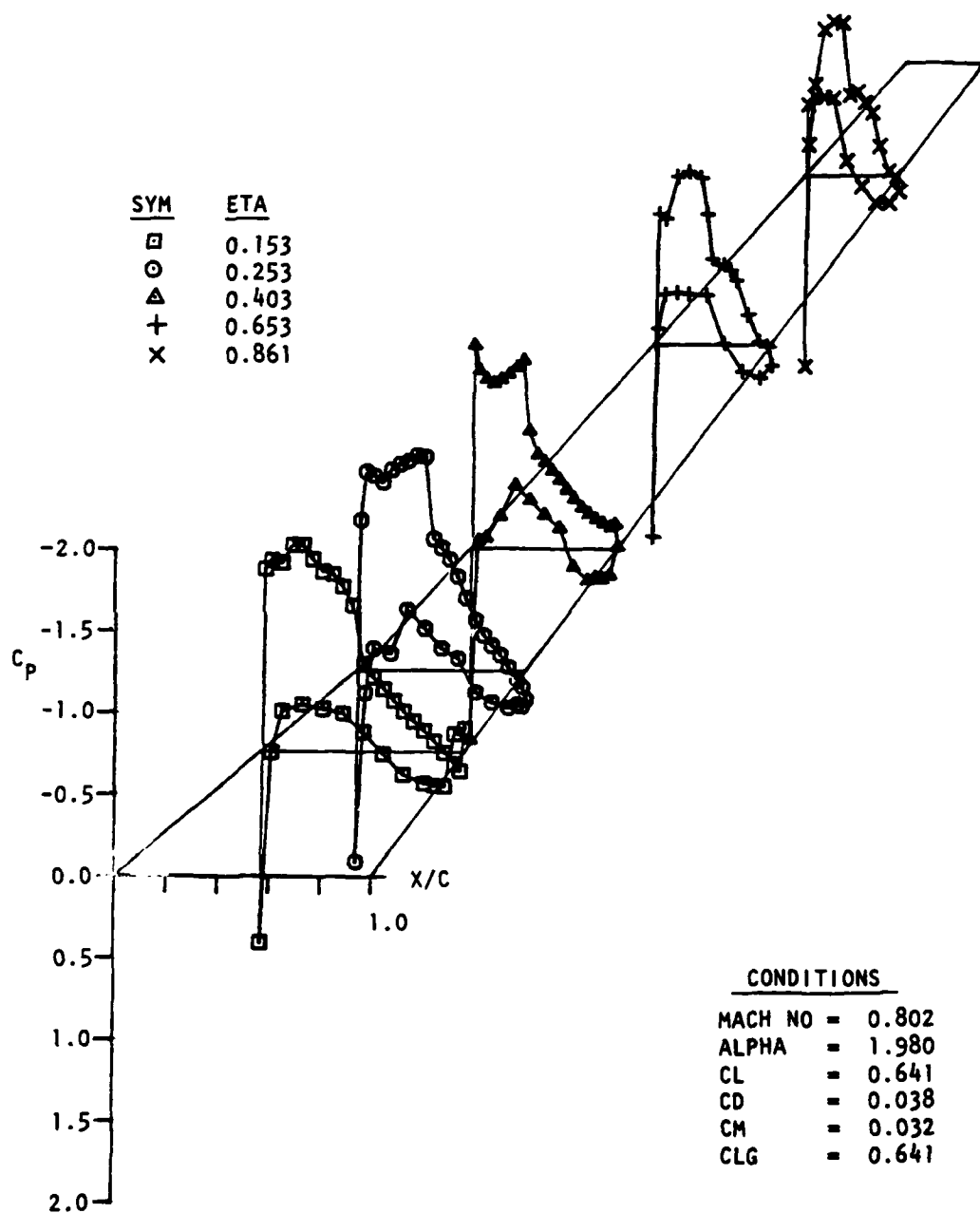


Figure 34. (Continued) ($\alpha = 2^\circ$)

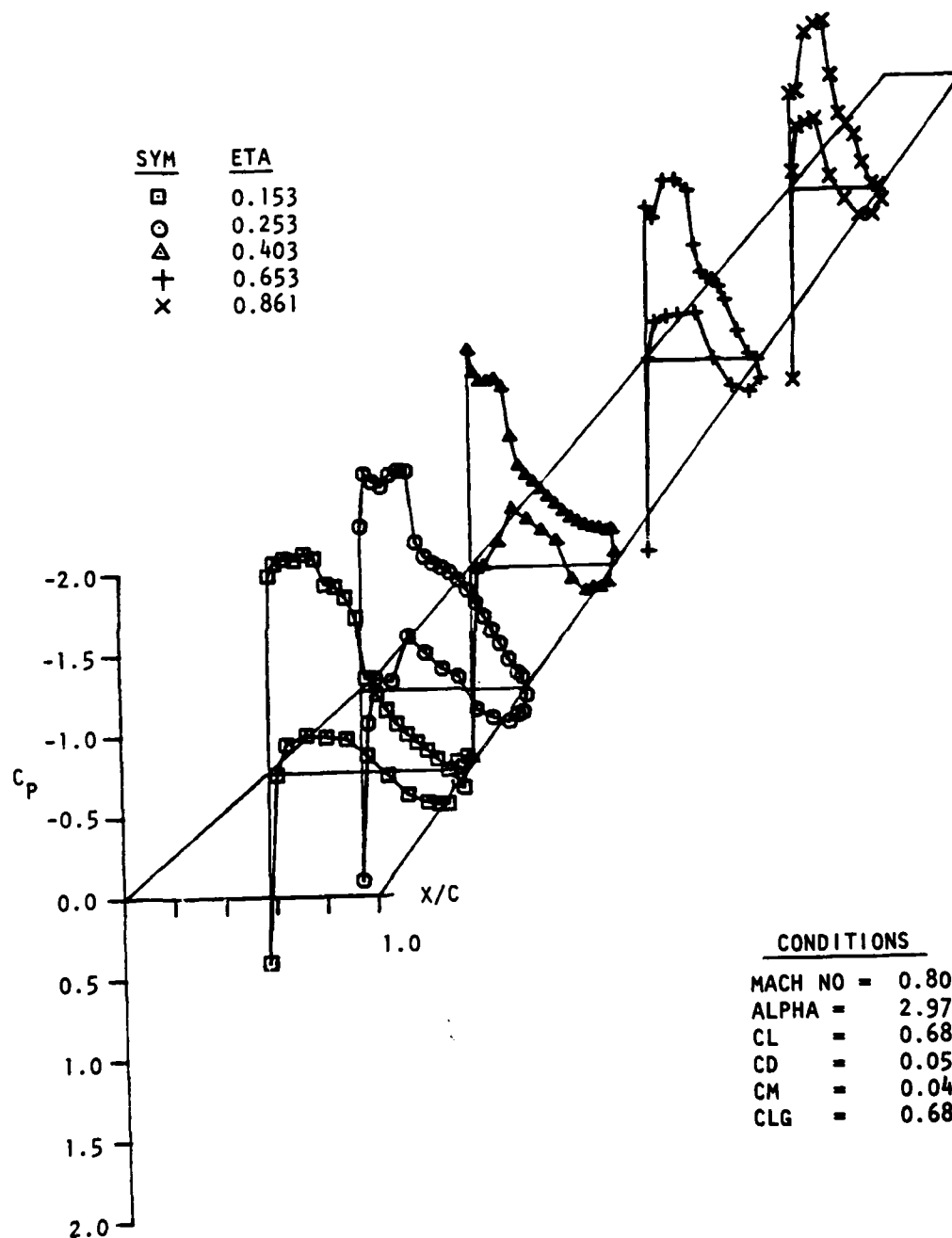


Figure 34. (Concluded) ($\alpha = 3^\circ$)

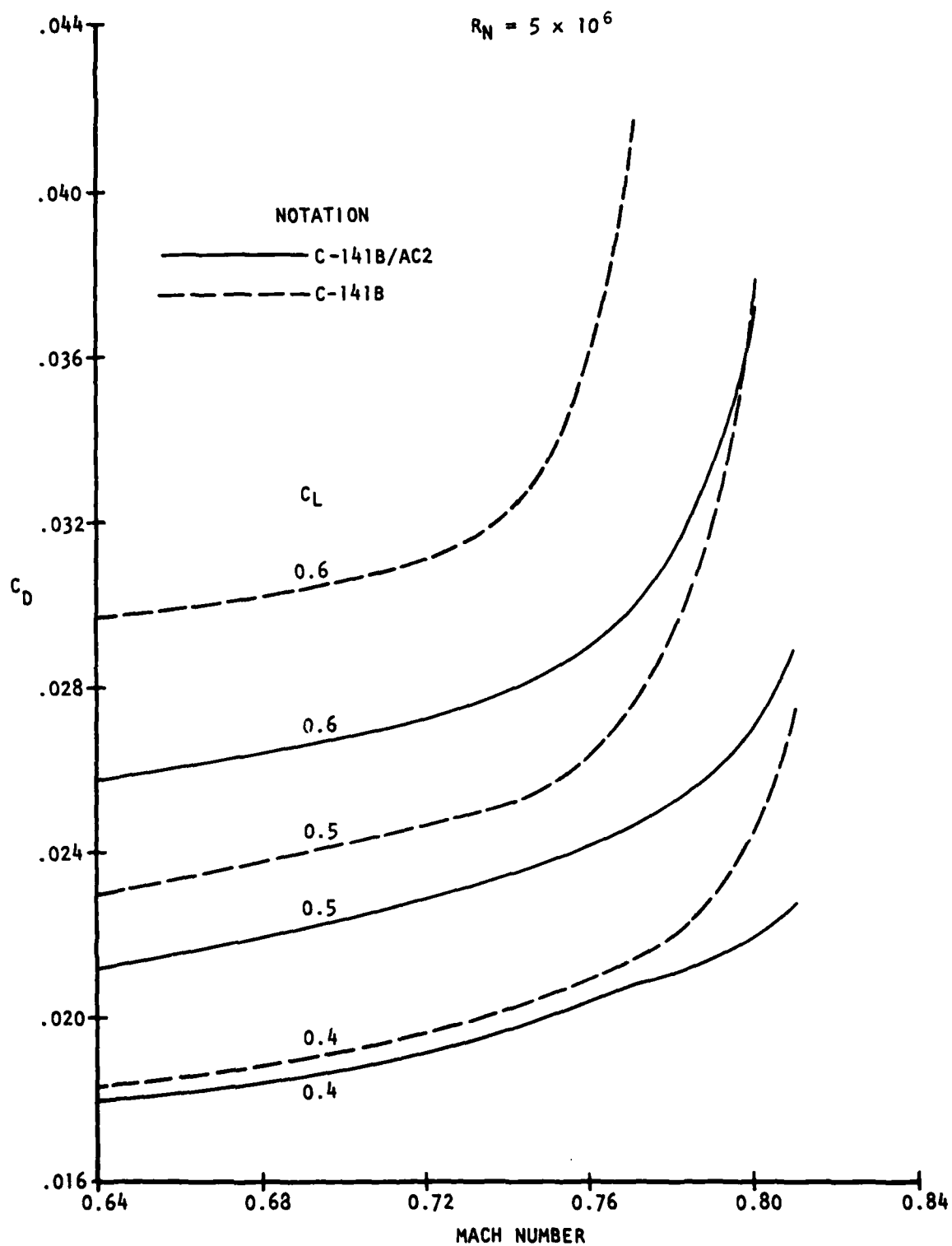


Figure 35. Measured Drag Rise Characteristics

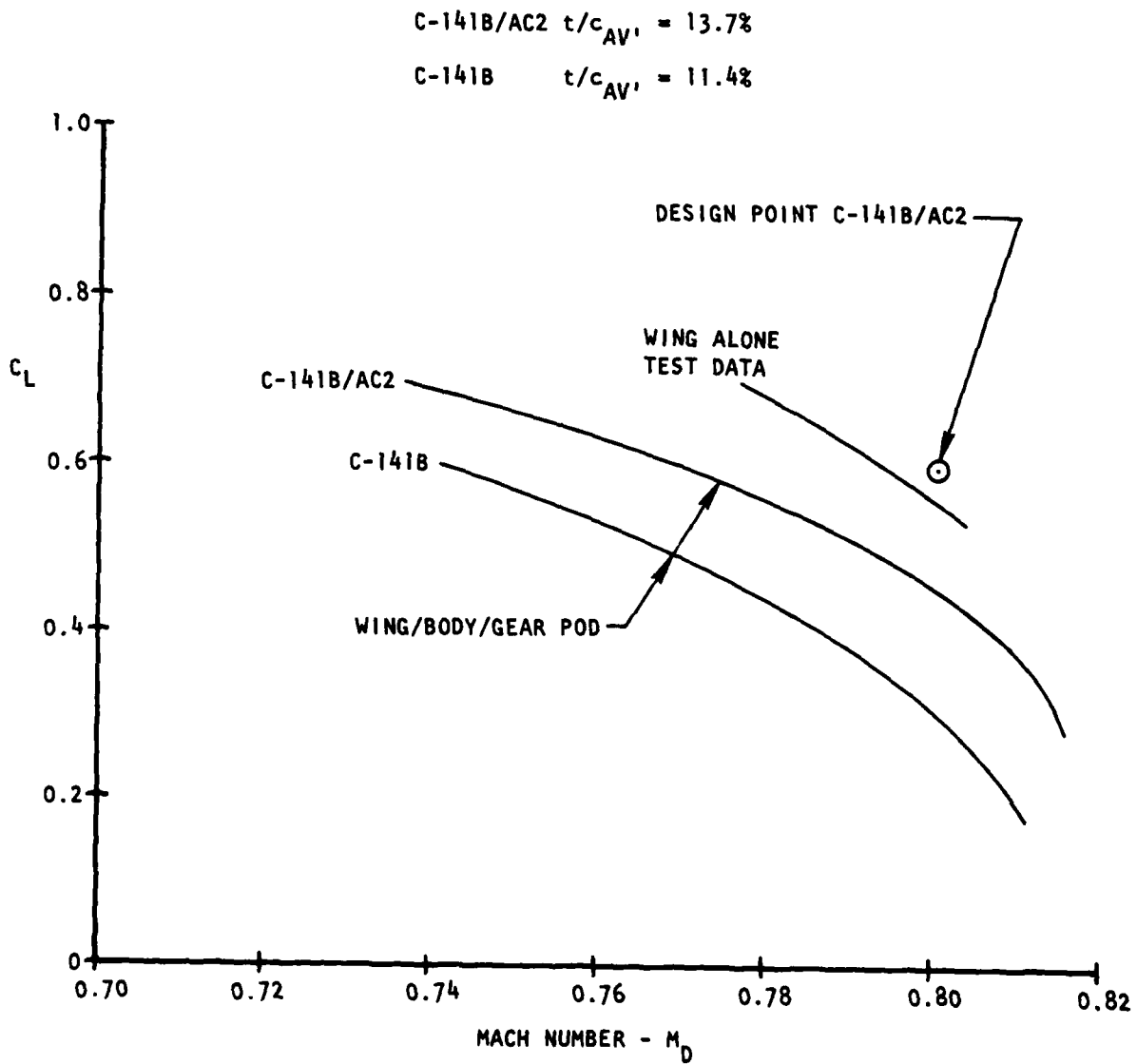


Figure 36. Measured Drag Divergence Mach Numbers

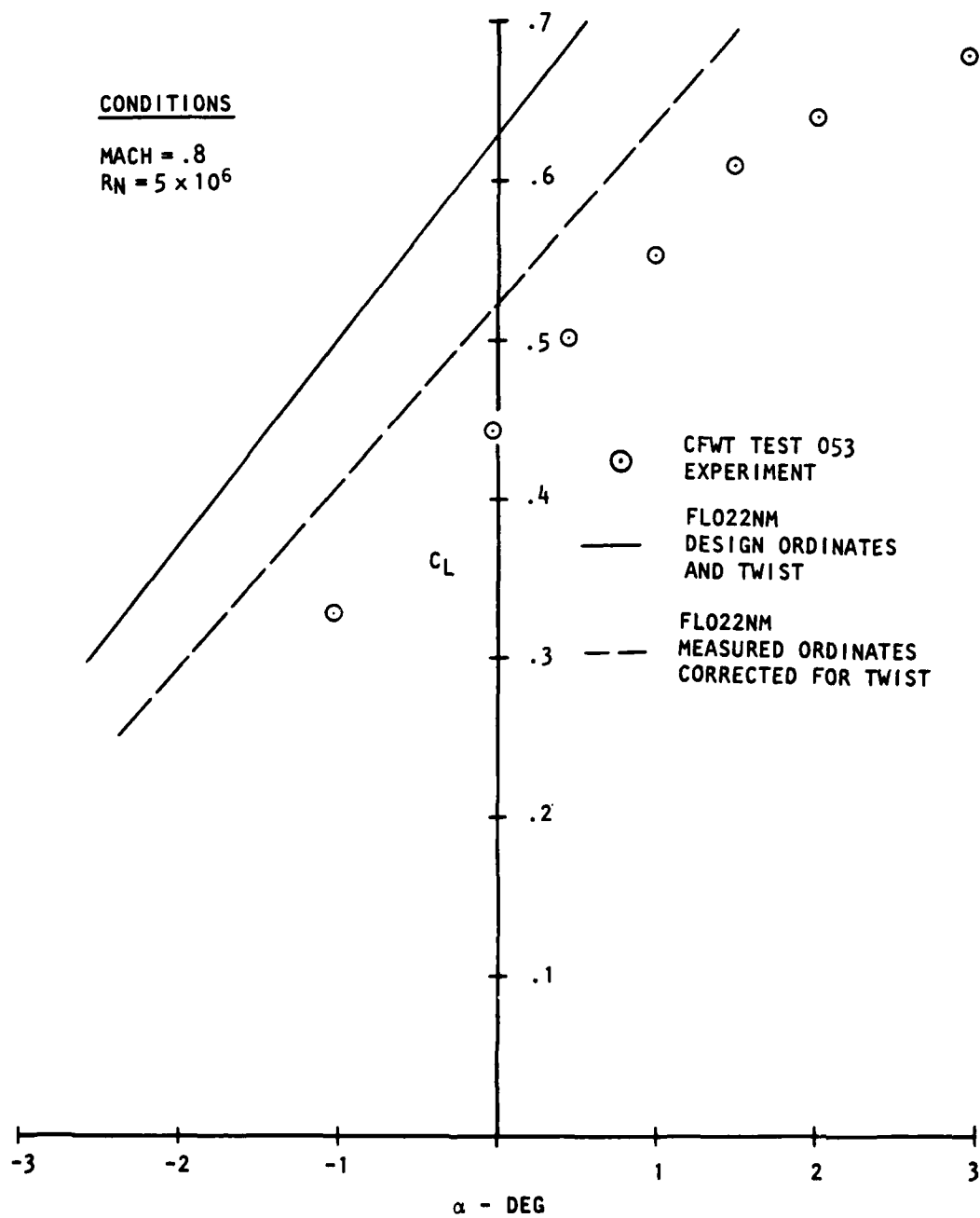


Figure 37. C-141B/AC2 Measured and Computed Lift

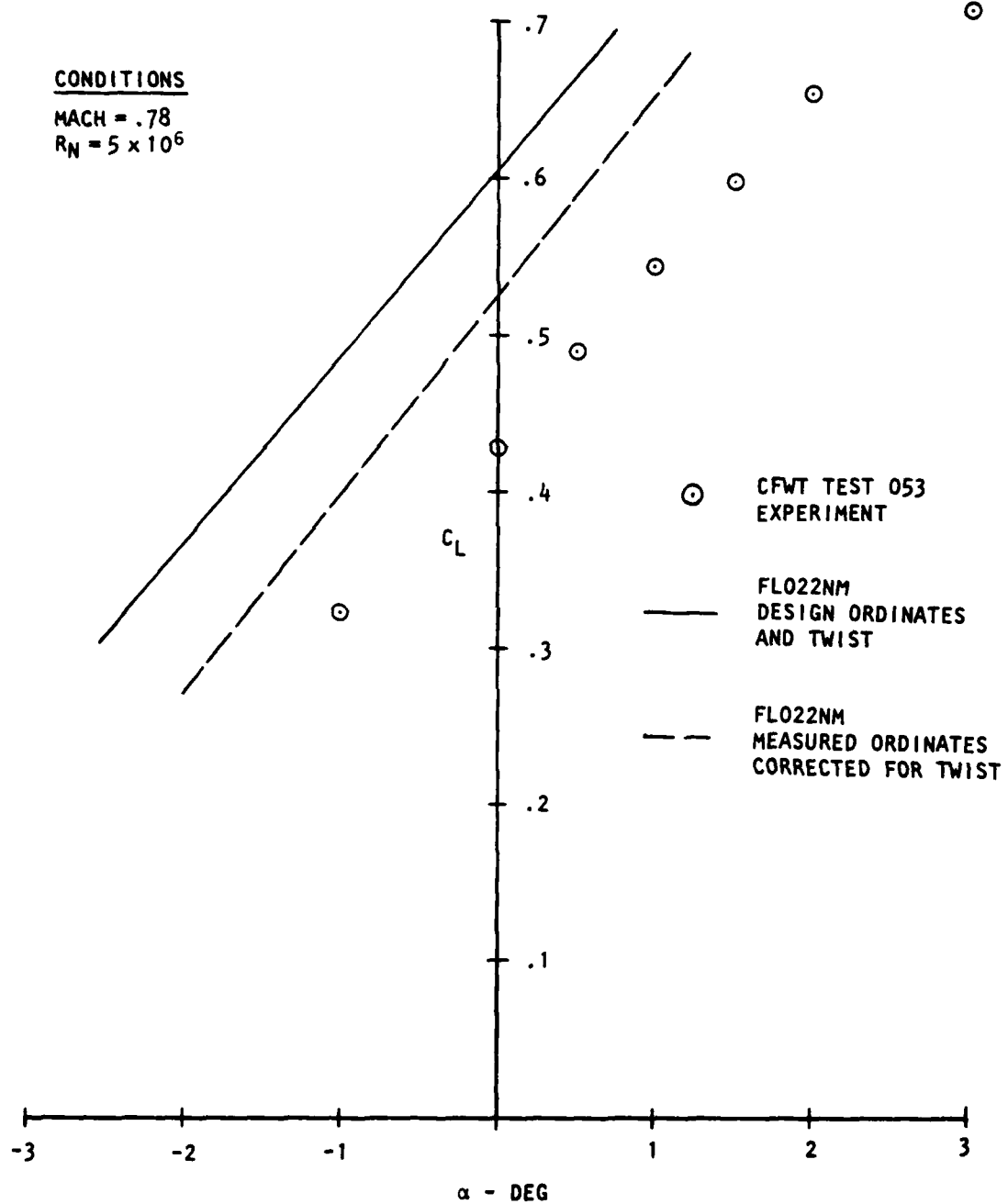


Figure 37. (Concluded) (2)

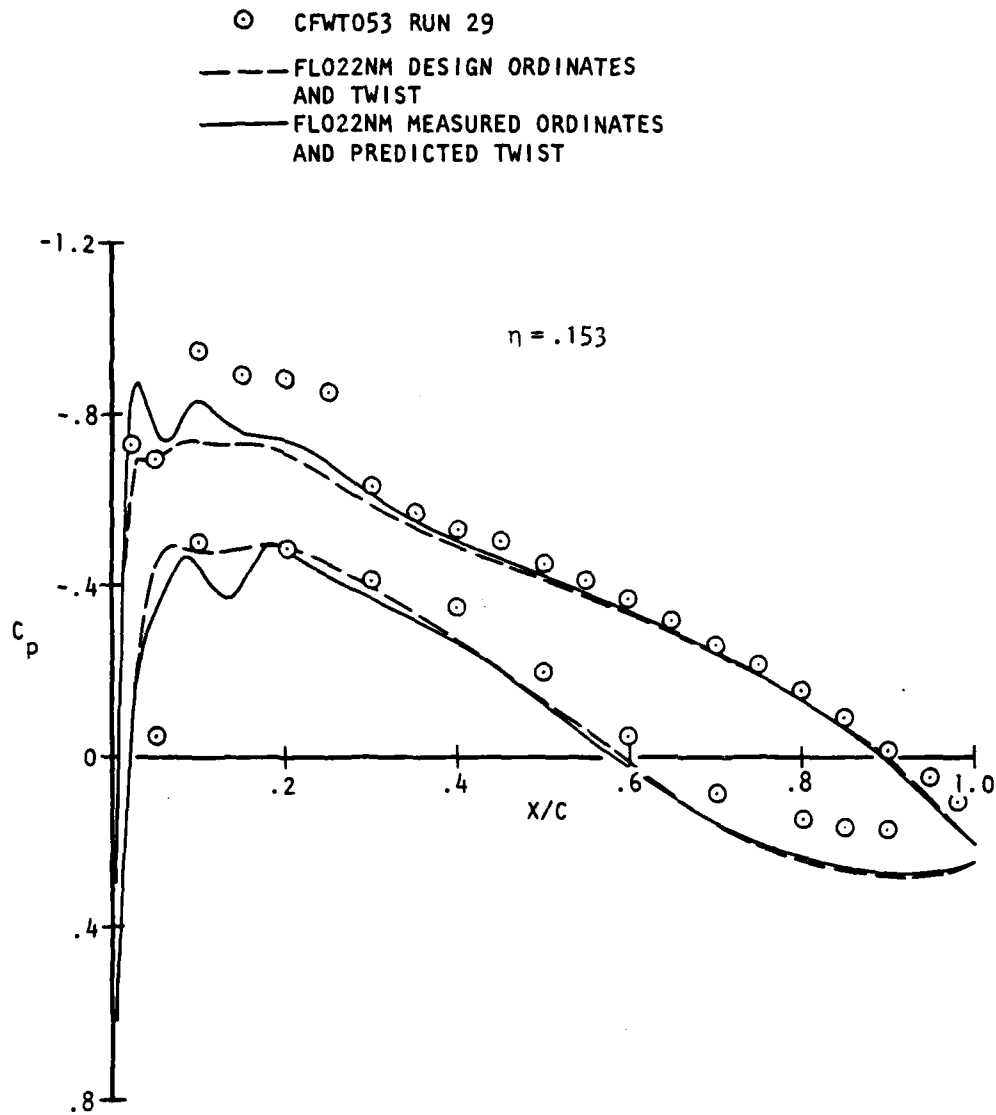


Figure 38. Full Potential Correlation: $M = 0.78$, $C_L = .33$

○ CFWT053 RUN 29
 --- FLO22NM DESIGN ORDINATES
 AND TWIST
 — FLO22NM MEASURED ORDINATES
 AND PREDICTED TWIST

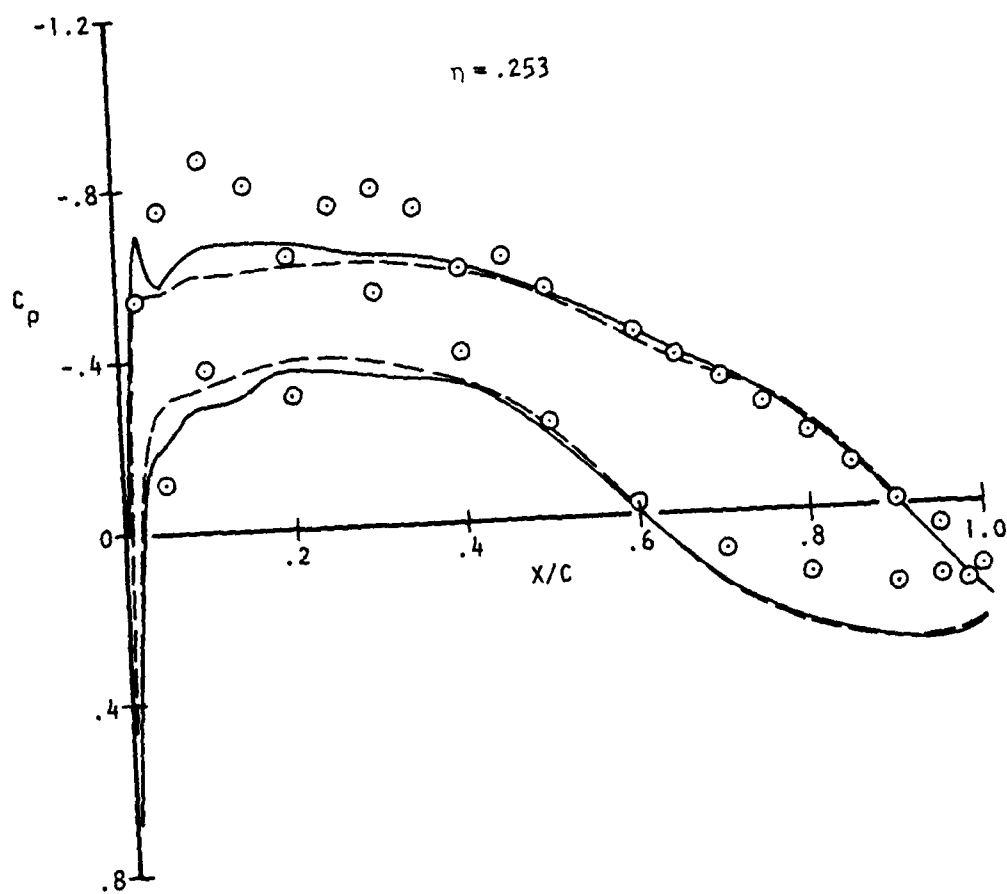


Figure 38. (Continued) (2)

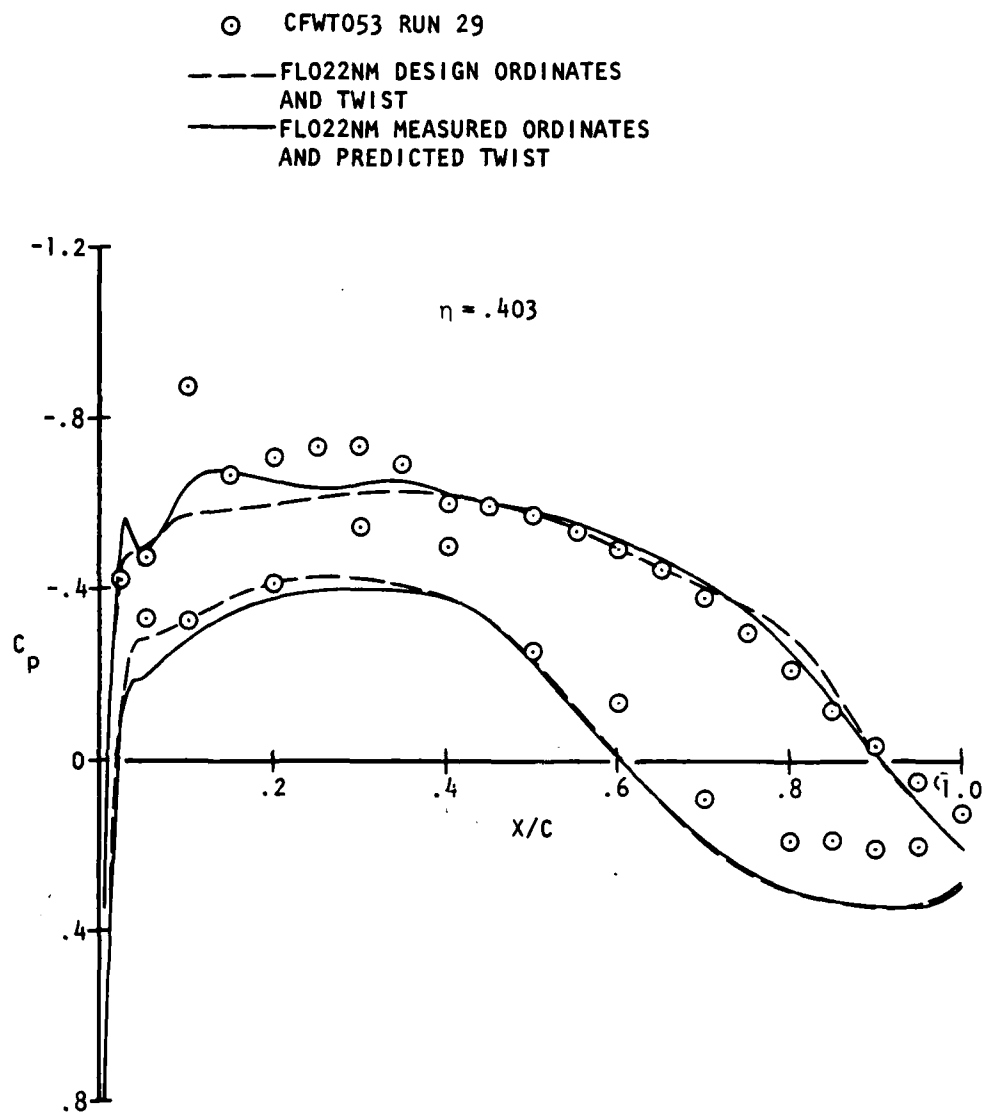


Figure 38. (Continued) (3)

- CFWT053 RUN 29
- FLO22NM DESIGN ORDINATES AND TWIST
- FLO22NM MEASURED ORDINATES AND PREDICTED TWIST

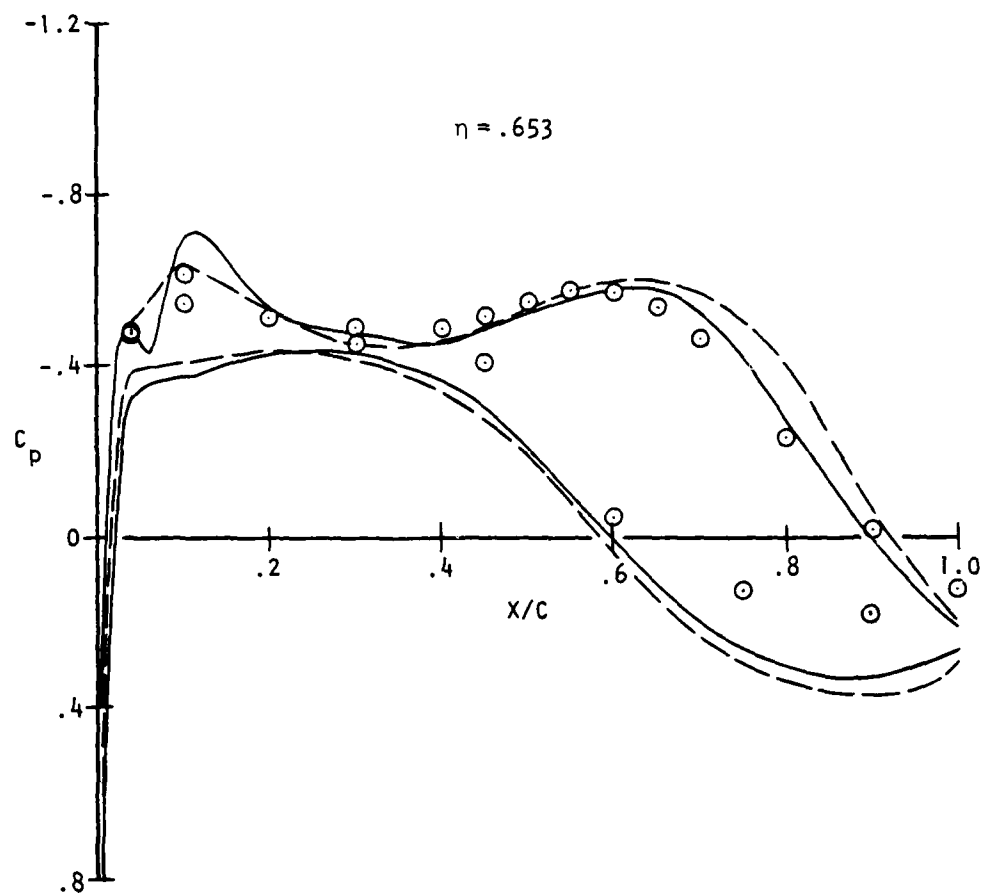


Figure 38. (Continued) (4)

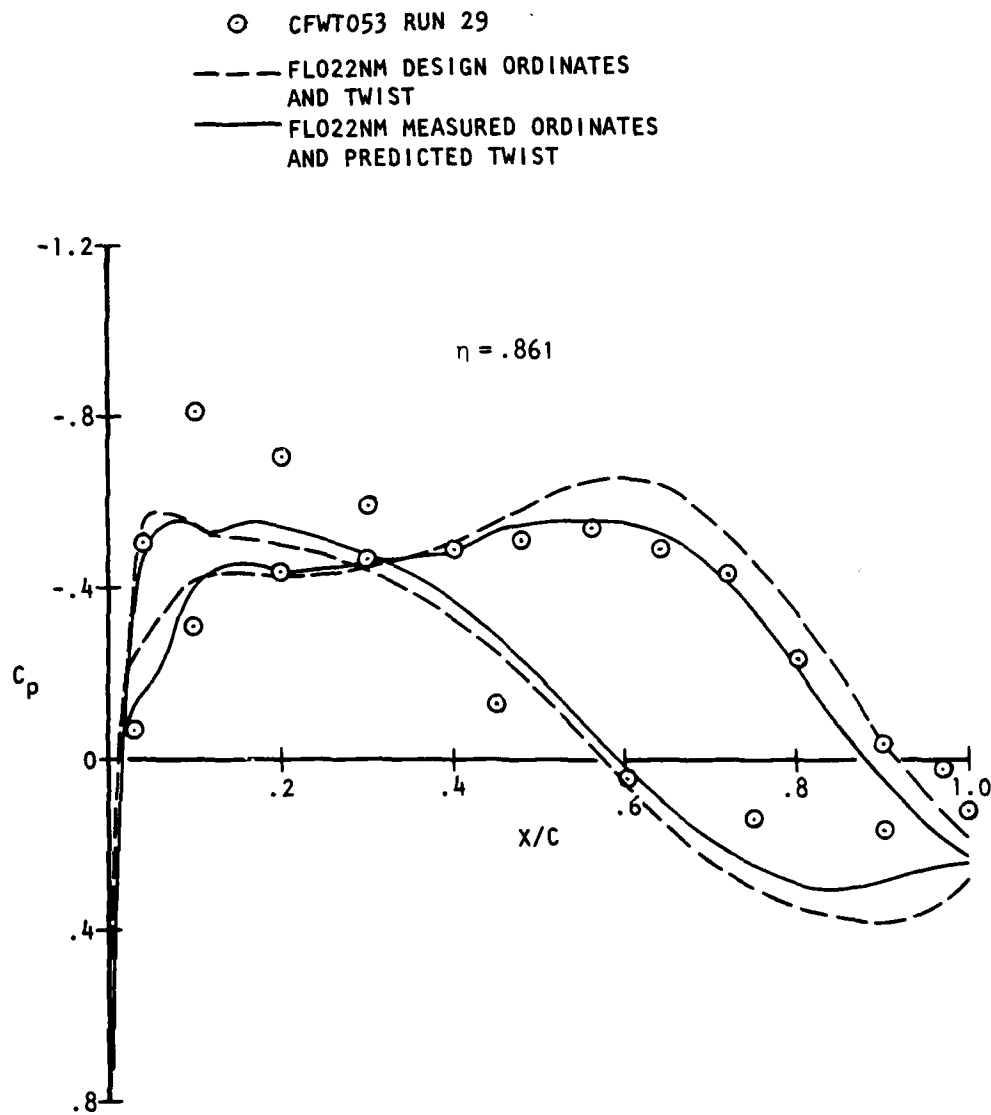


Figure 38. (Concluded) (5)

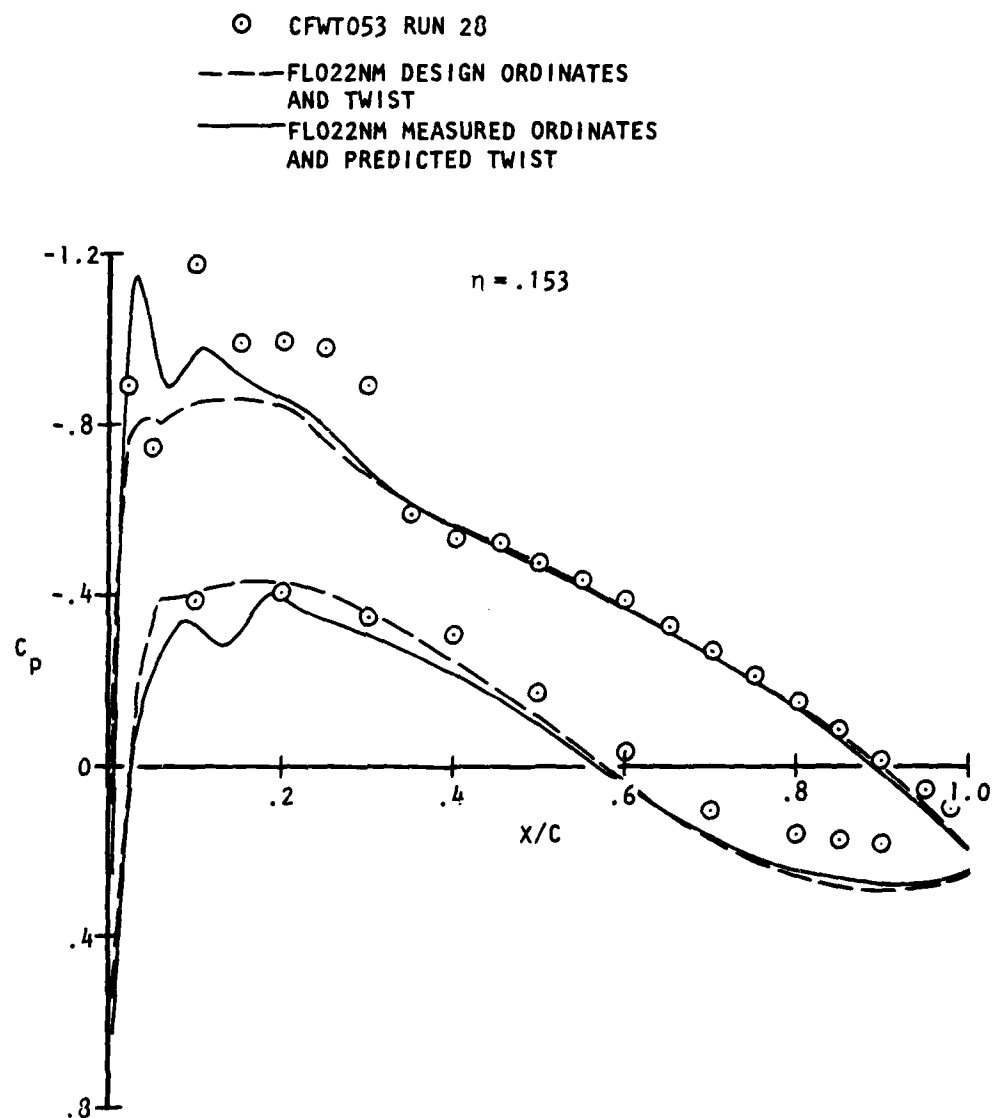


Figure 39. Full Potential Correlation: $M = 0.78$, $C_L = 0.43$

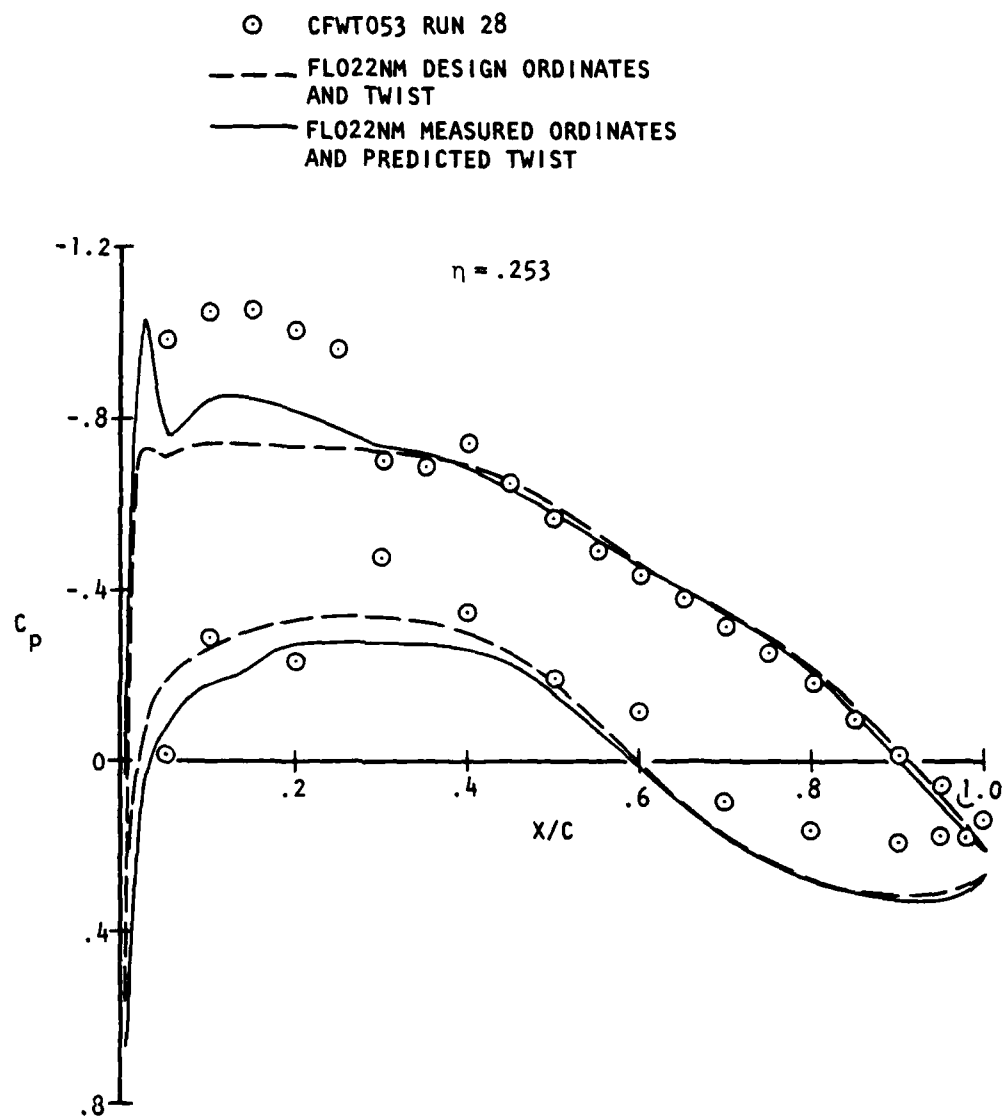


Figure 39. (Continued) (2)

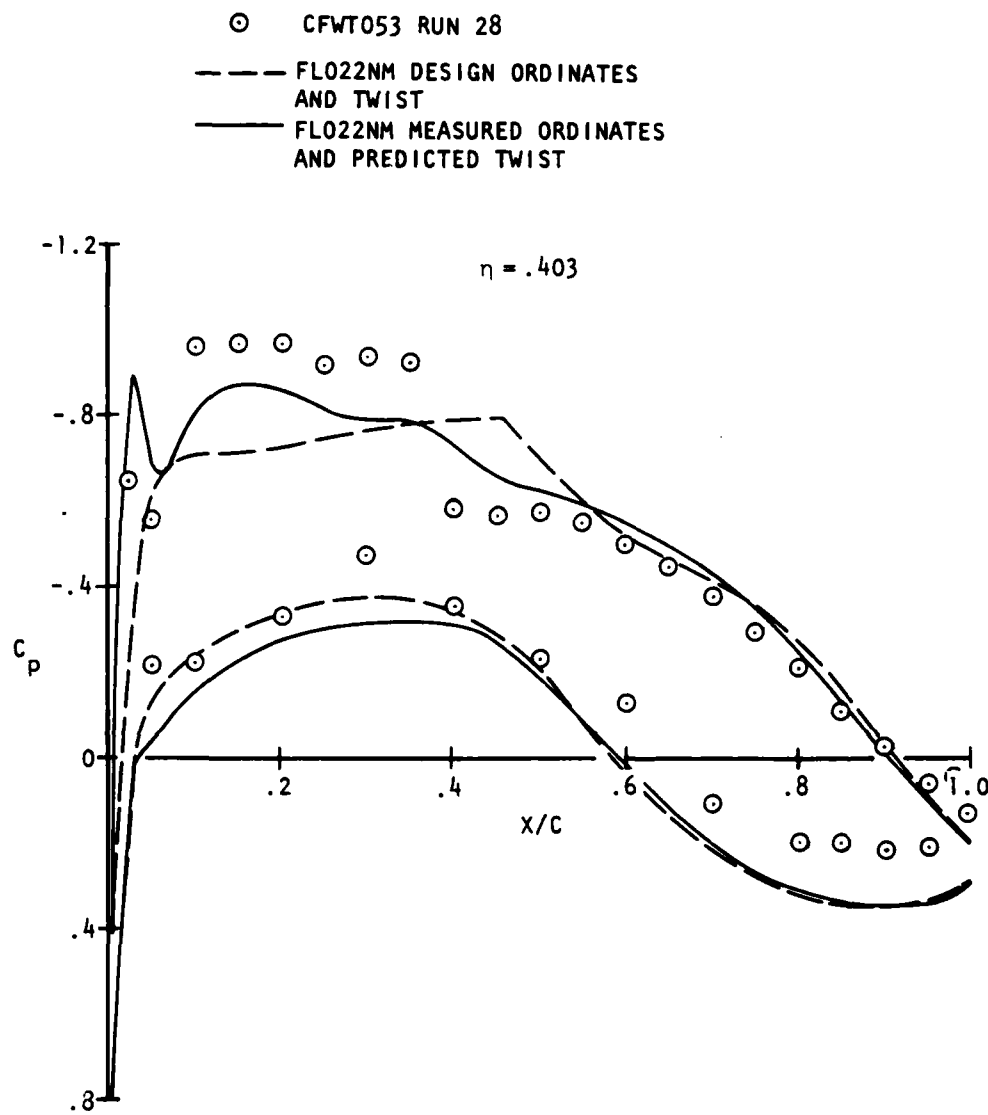


Figure 39. (Continued) (3)

○ CFWT053 RUN 28
 --- FLO22NM DESIGN ORDINATES
 AND TWIST
 — FLO22NM MEASURED ORDINATES
 AND PREDICTED TWIST

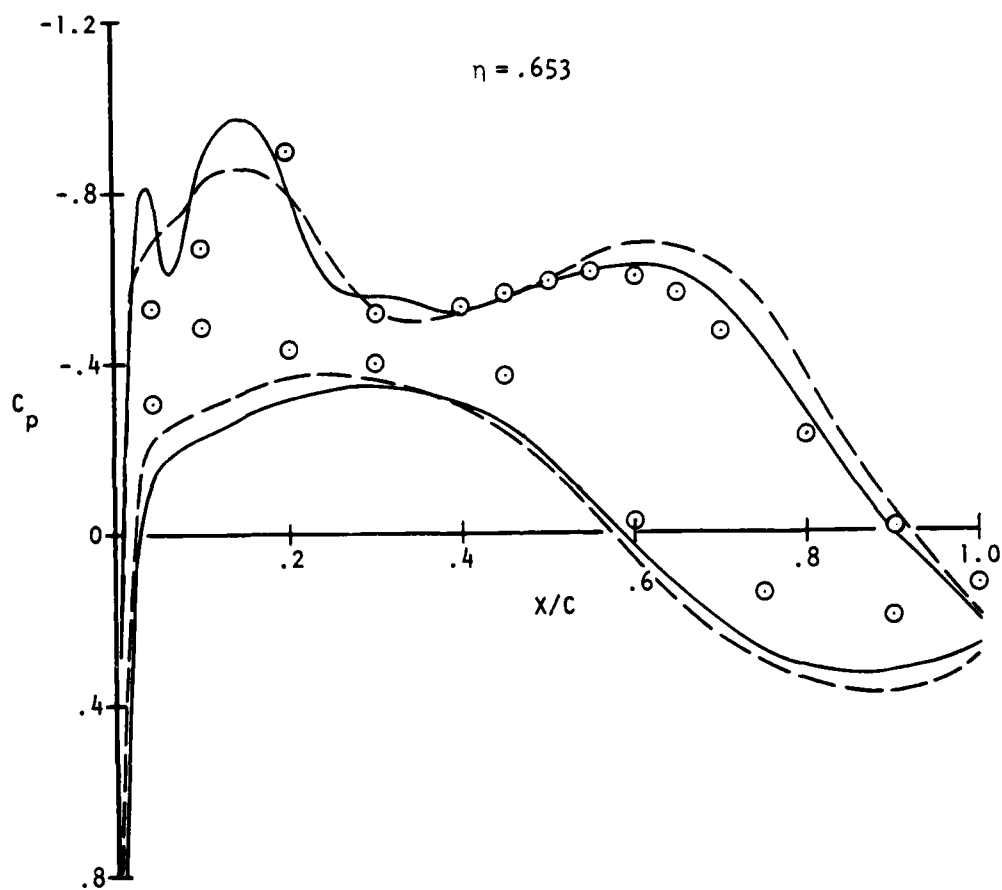


Figure 39. (Continued) (4)

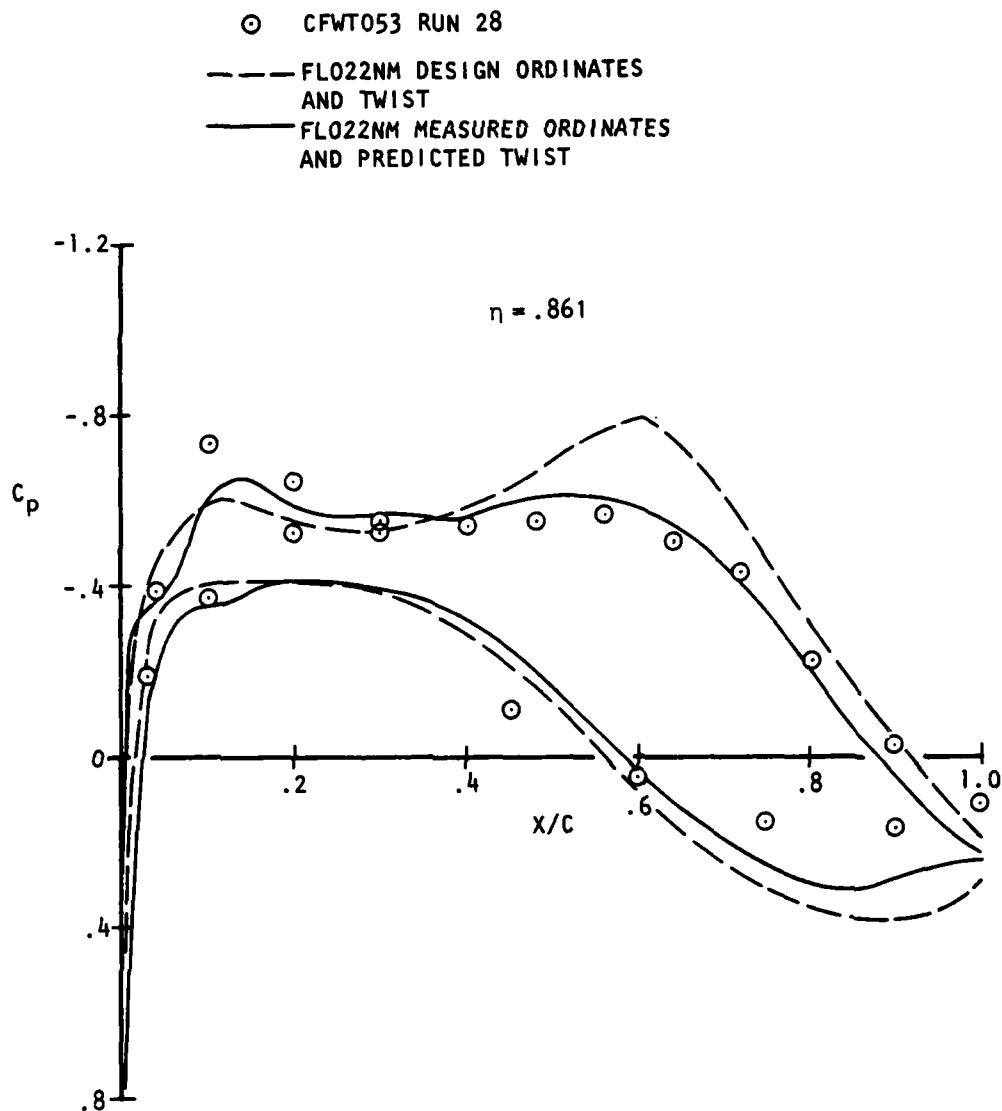


Figure 39. (Concluded) (5)

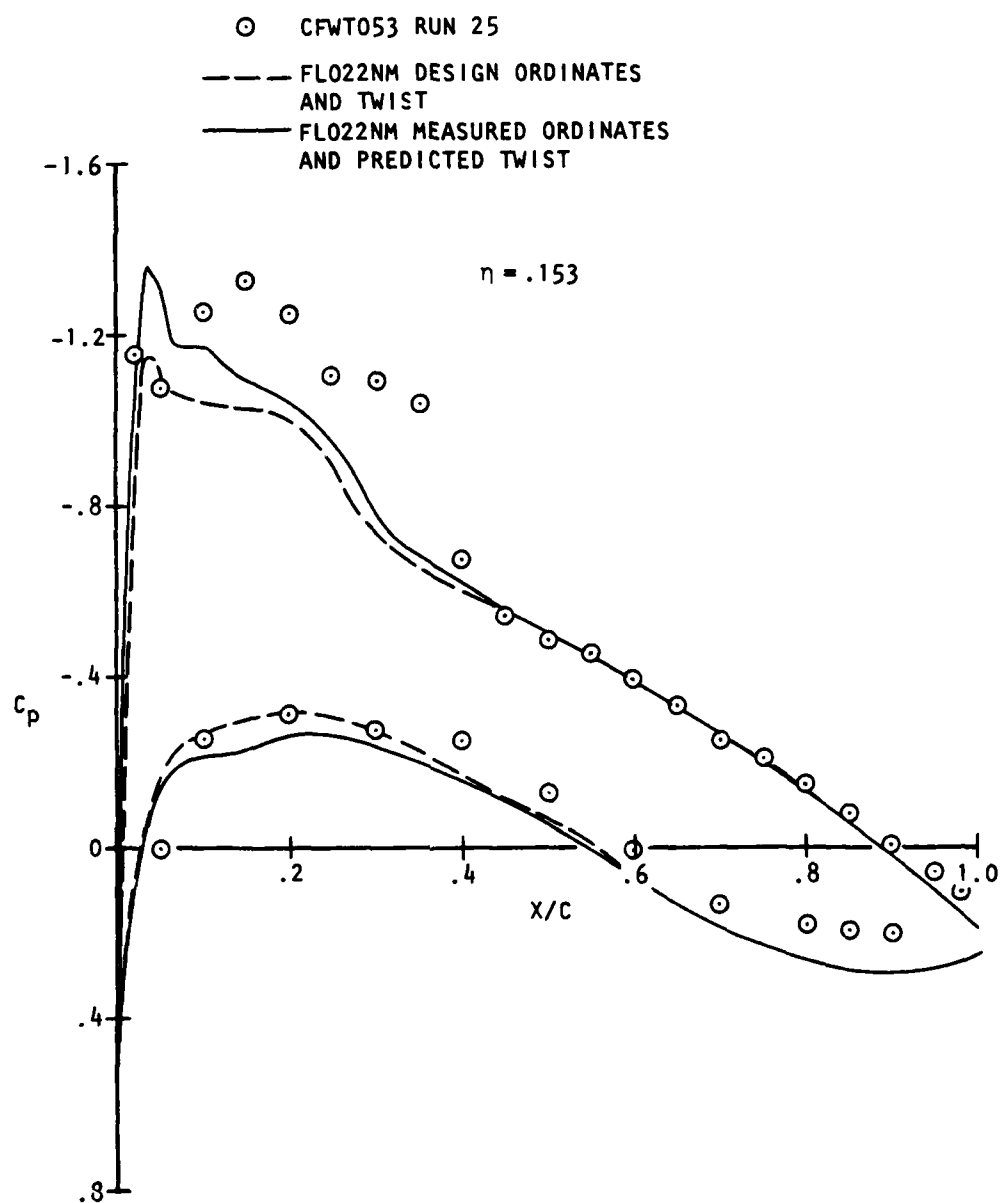


Figure 40. Full Potential Correlation, $M = 0.78$, $C_L = 0.60$

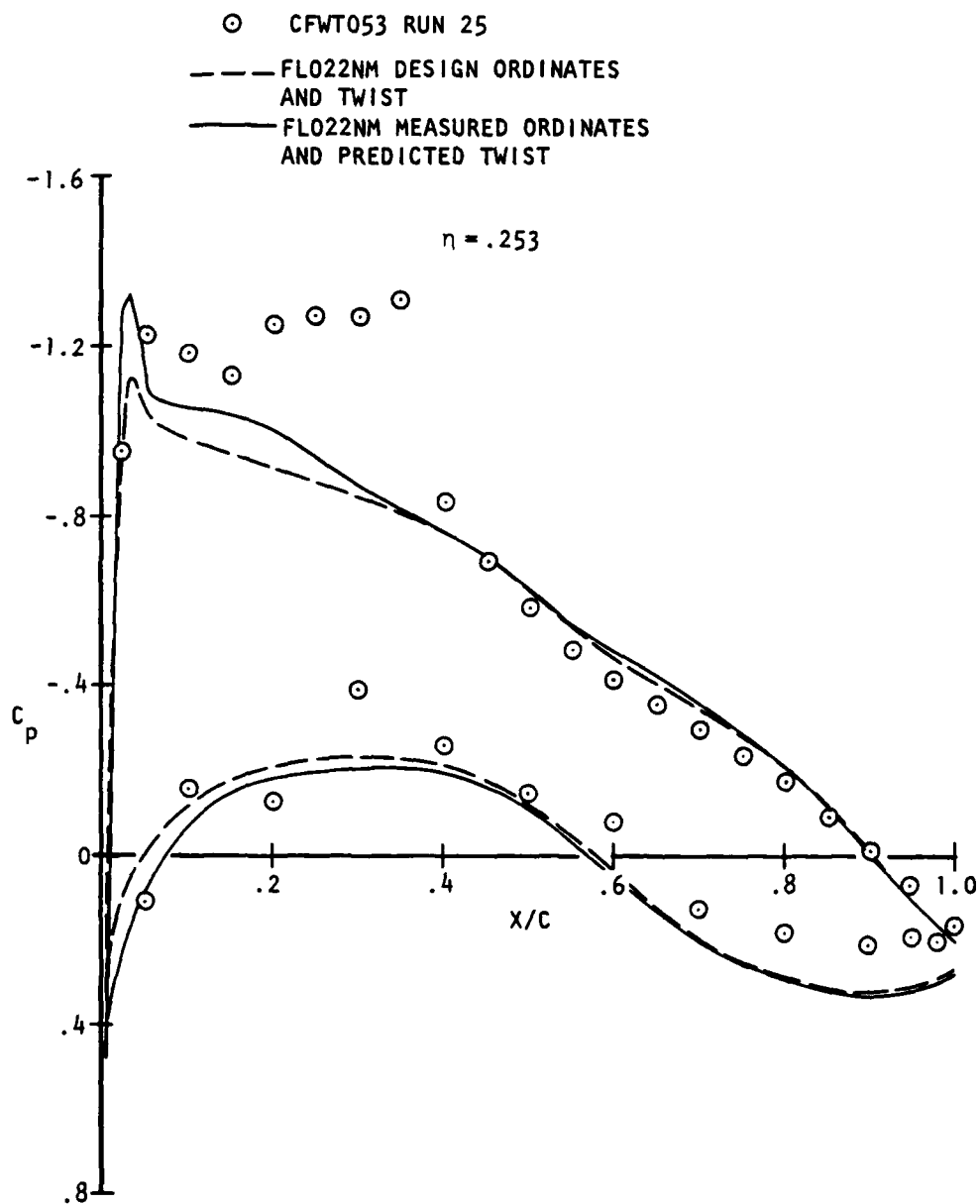


Figure 40. (Continued) (2)

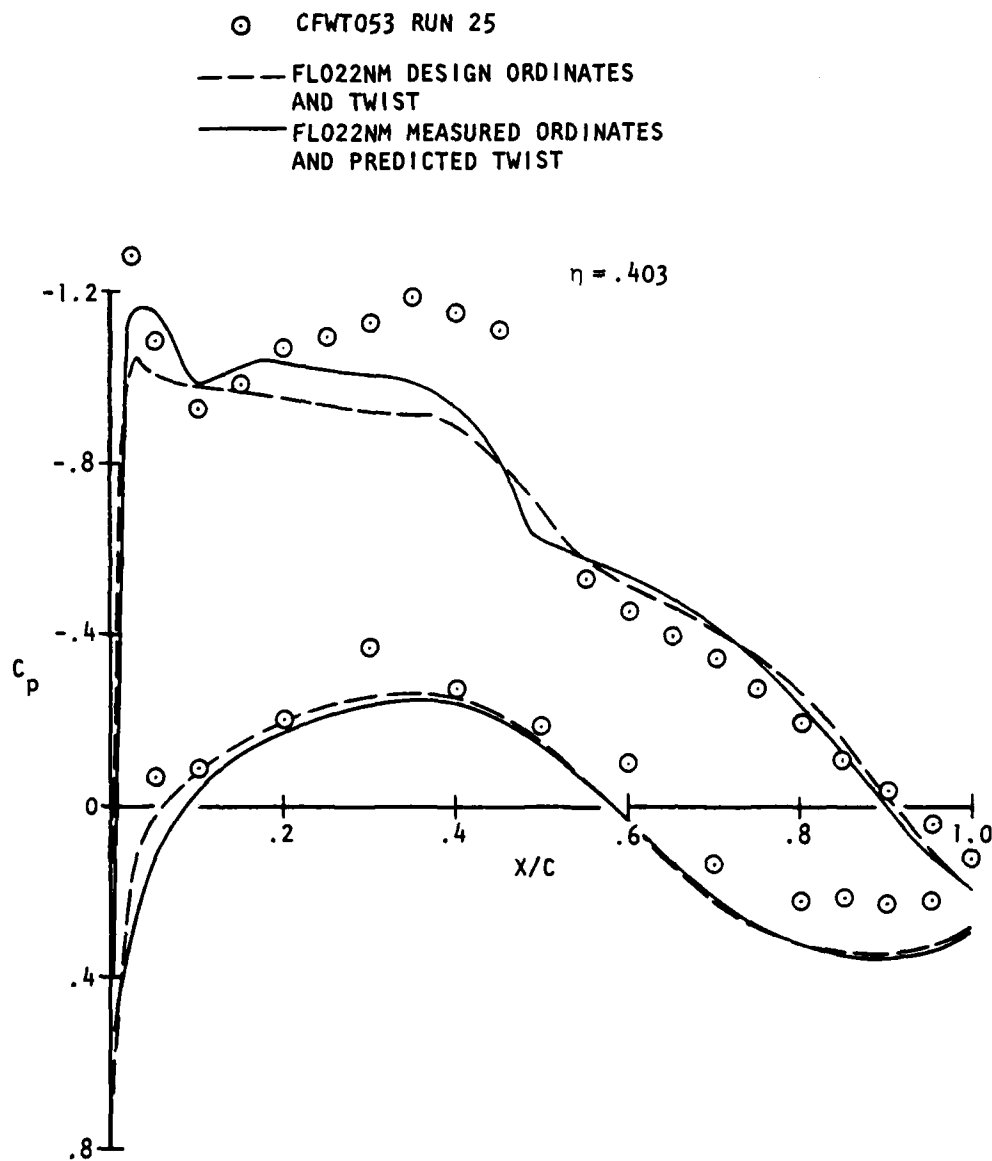


Figure 40. (Continued) (3)

○ CFWT053 RUN 25

--- FLO22NM DESIGN ORDINATES
AND TWIST

— FLO22NM MEASURED ORDINATES
AND PREDICTED TWIST

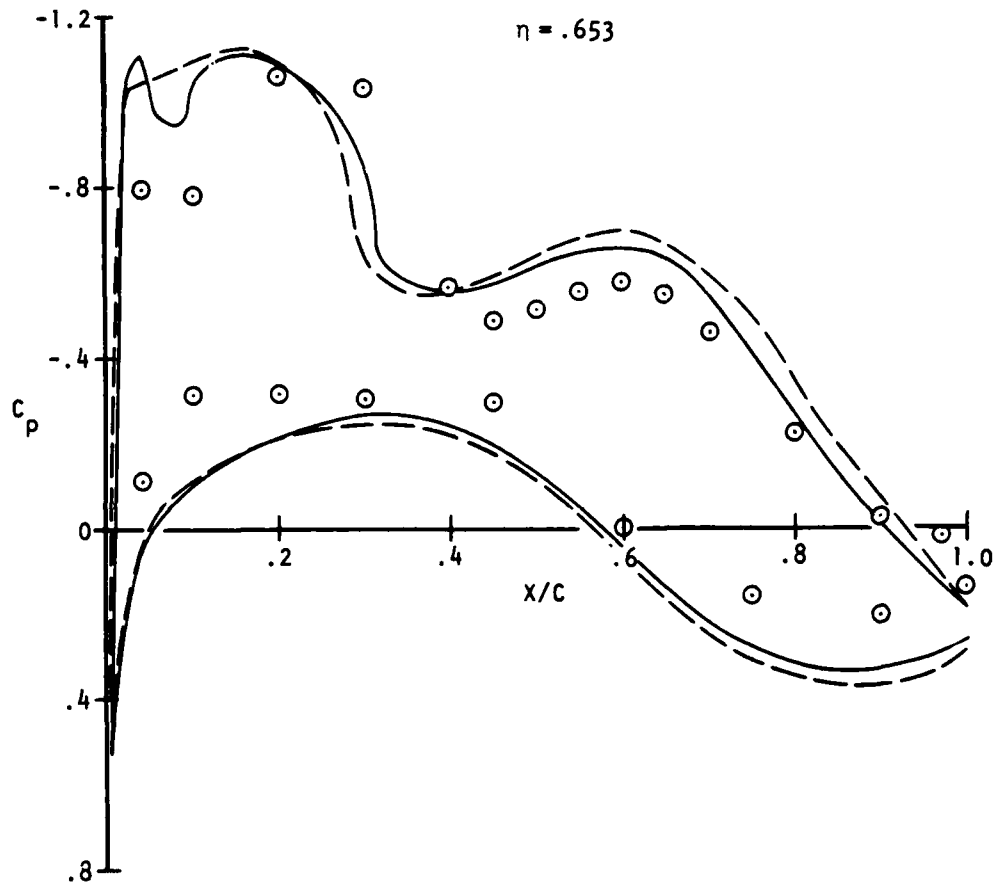


Figure 40. (Continued) (4)

⊙ CFWT053 RUN 25
 --- FLO22NM DESIGN ORDINATES
 AND TWIST
 — FLO22NM MEASURED ORDINATES
 AND PREDICTED TWIST

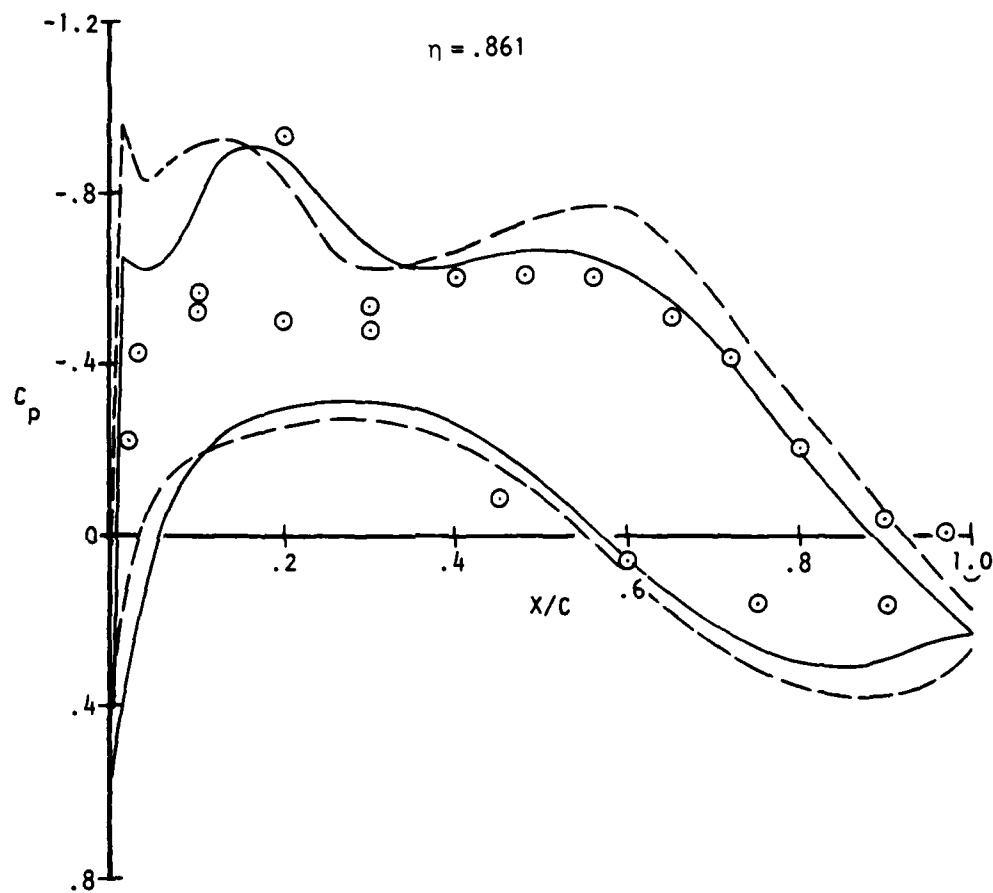


Figure 40. (Concluded) (5)

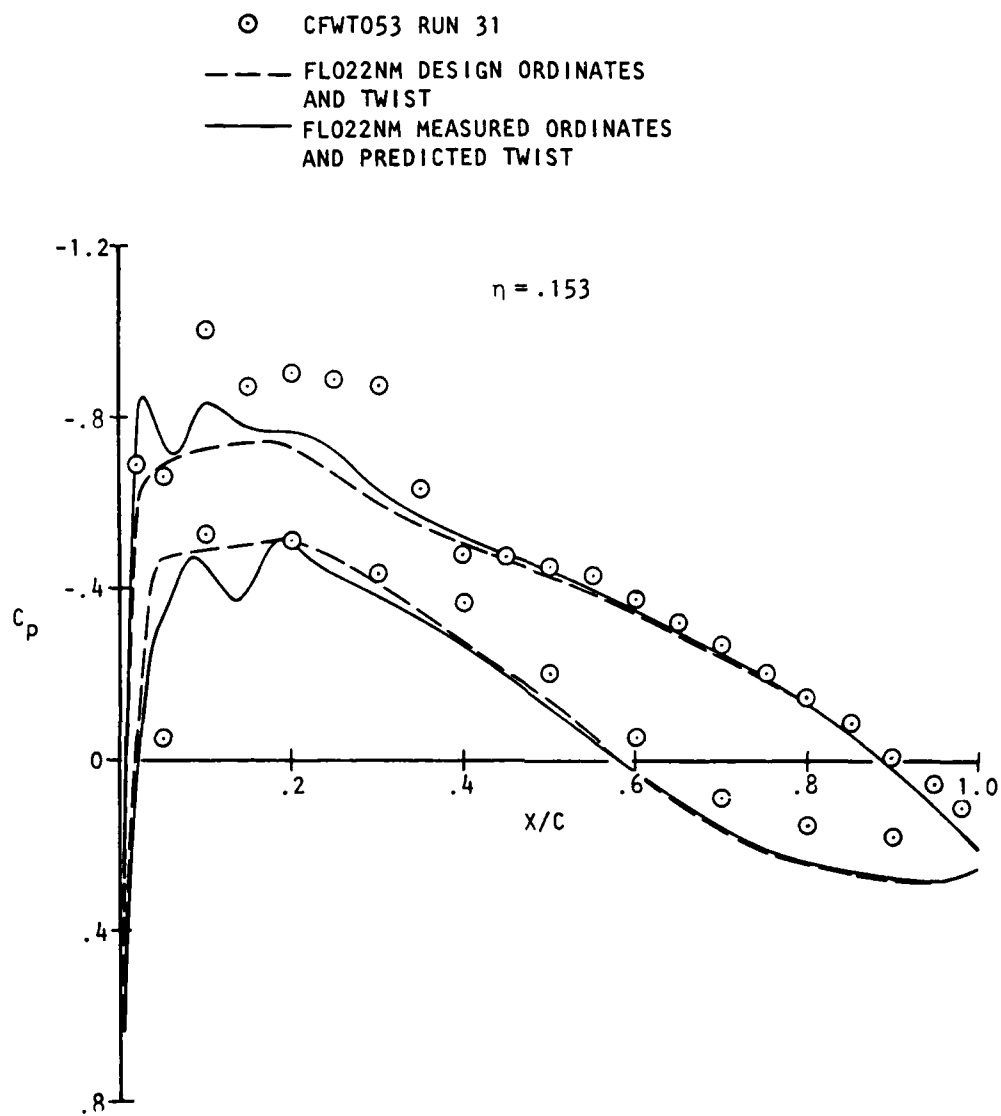


Figure 41. Full Potential Correlation, $M = 0.80$, $C_L = 0.330$

○ CFWT053 RUN 31
 --- FLO22NM DESIGN ORDINATES
 AND TWIST
 — FLO22NM MEASURED ORDINATES
 AND PREDICTED TWIST

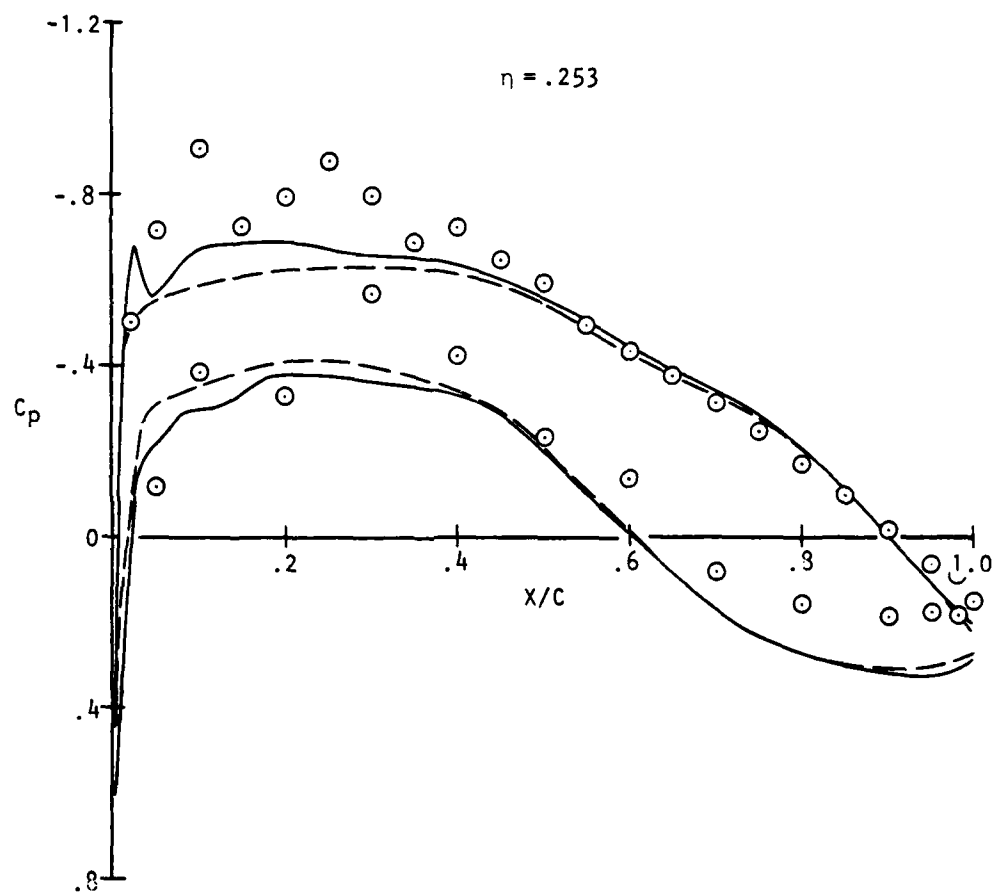


Figure 41. (Continued) (2)

⊙ CFWT053 RUN 31

--- FLO22NM DESIGN ORDINATES
AND TWIST

— FLO22NM MEASURED ORDINATES
AND PREDICTED TWIST

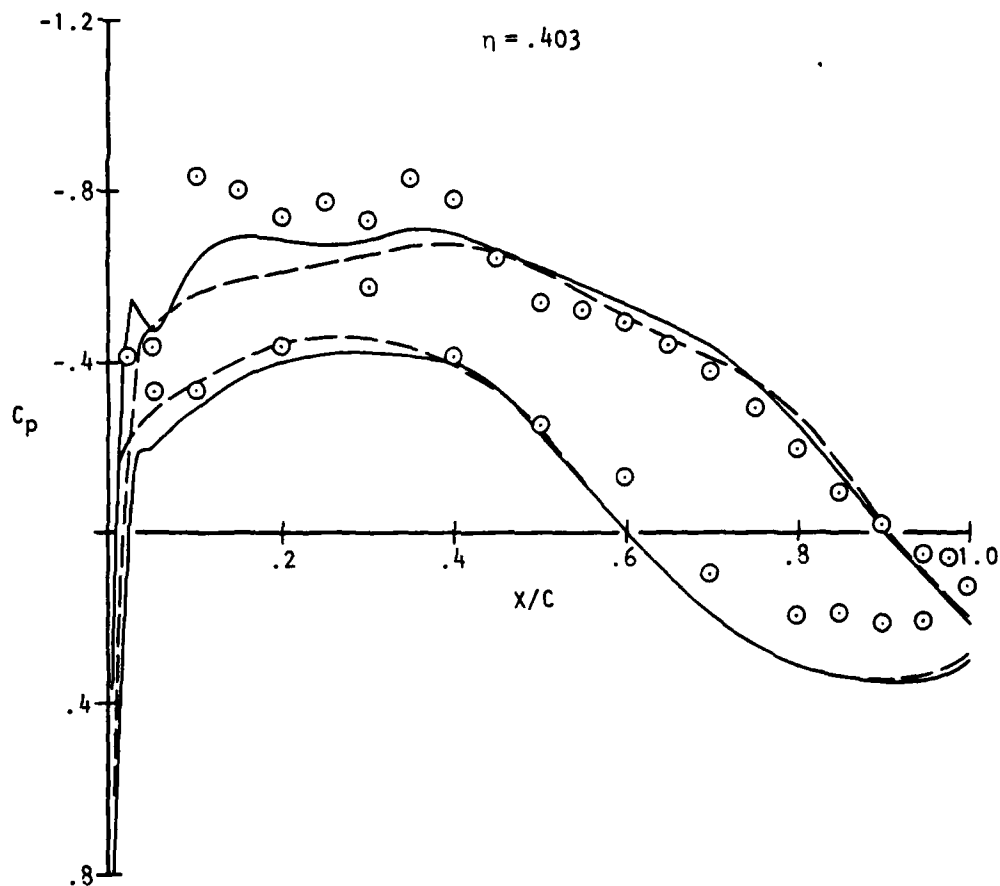


Figure 41. (Continued) (3)

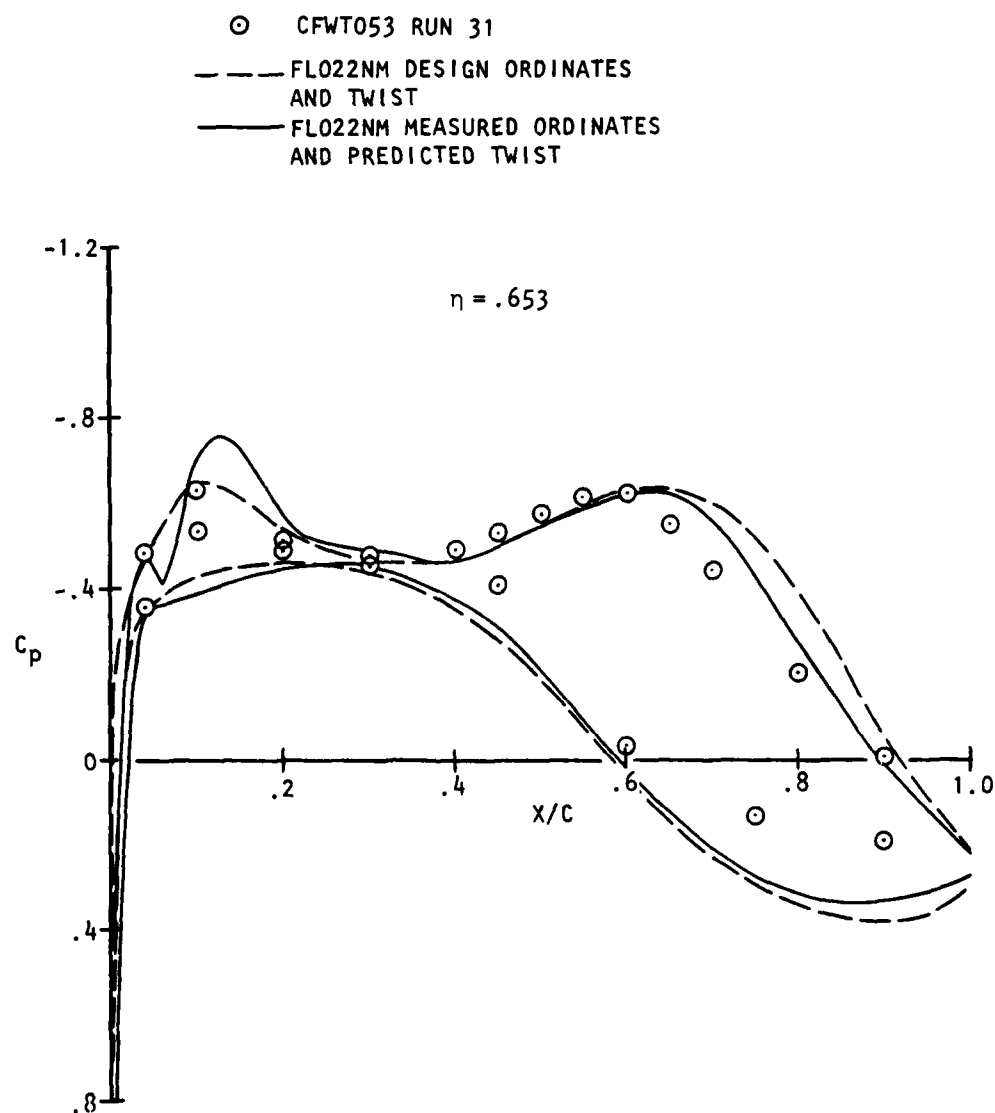


Figure 41. (Continued) (4)

○ CFWT053 RUN 31

--- FLO22NM DESIGN ORDINATES
AND TWIST

— FLO22NM MEASURED ORDINATES
AND PREDICTED TWIST

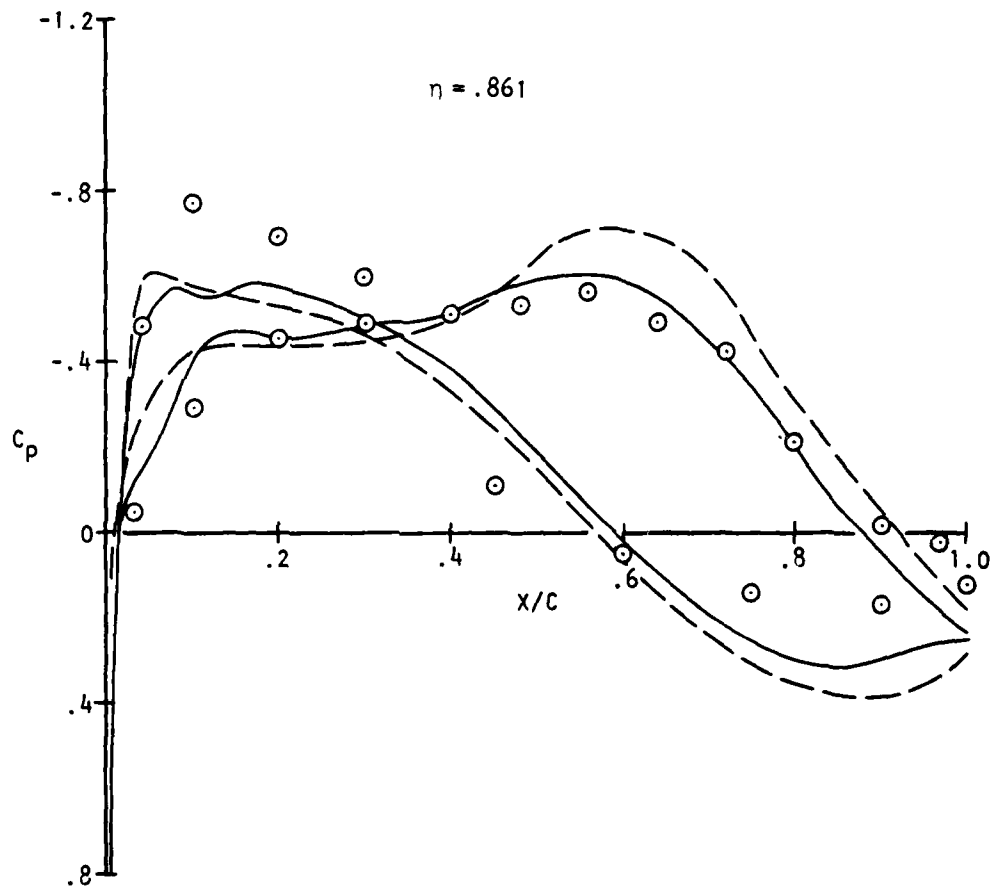


Figure 41. (Concluded) (5)

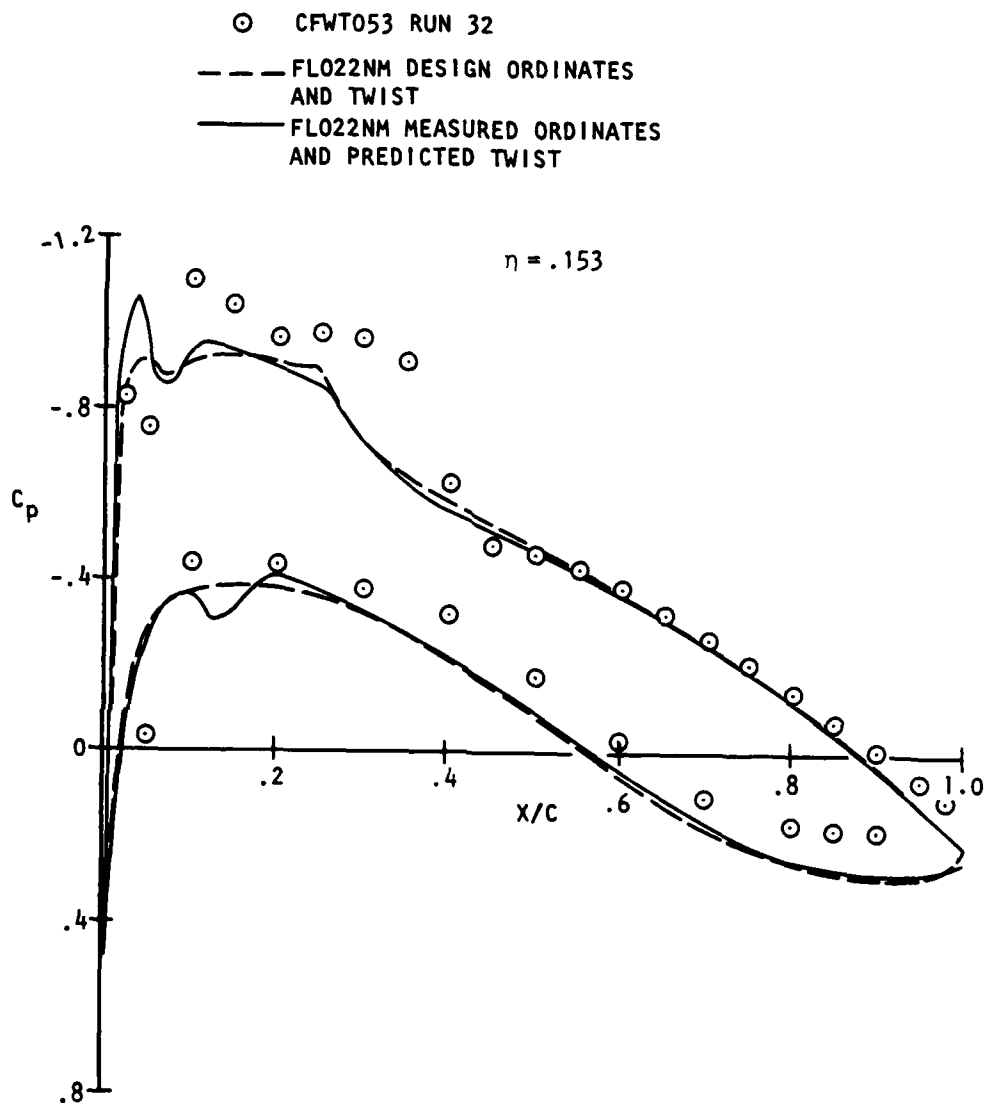


Figure 42. Full Potential Correlation, $M = 0.80$, $C_L = 0.445$

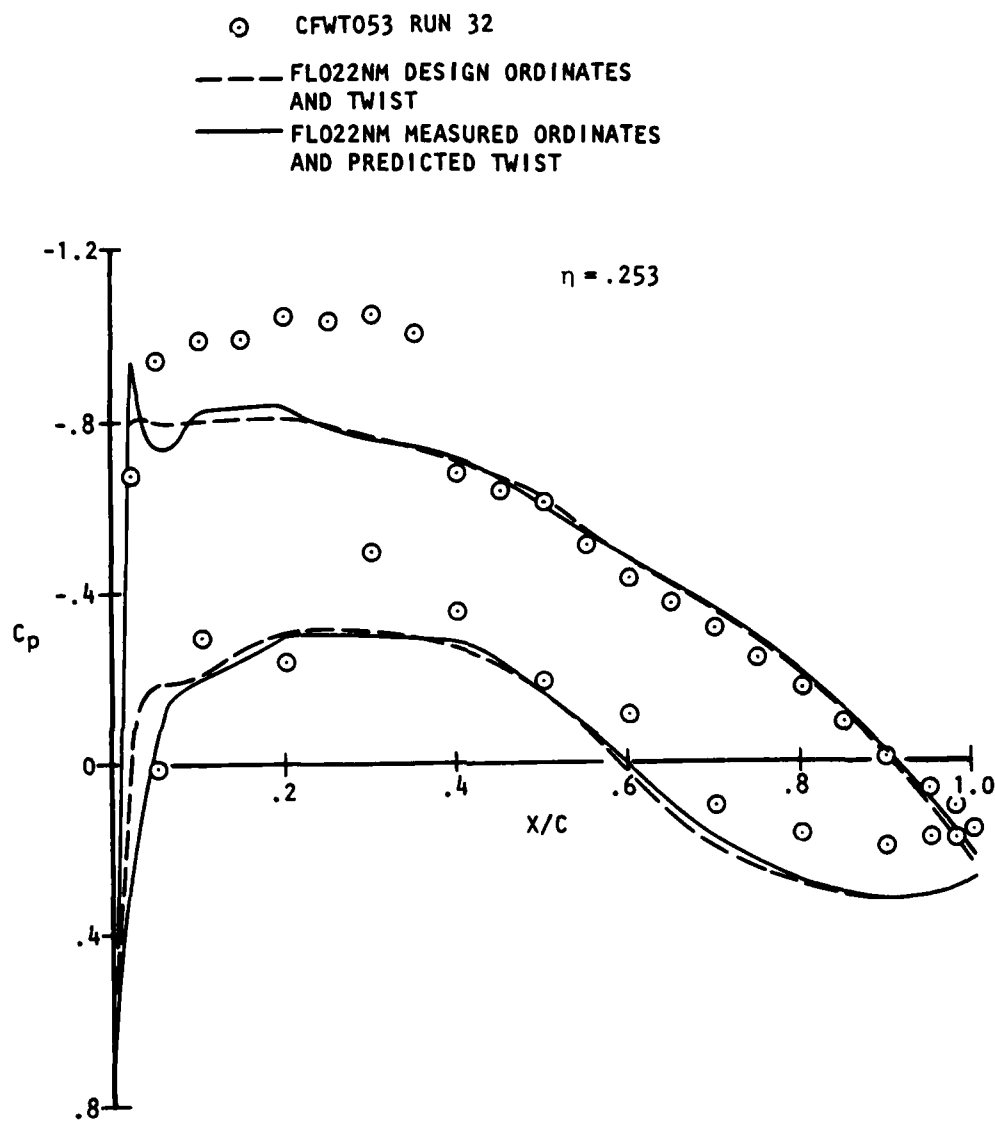


Figure 42. (Continued) (2)

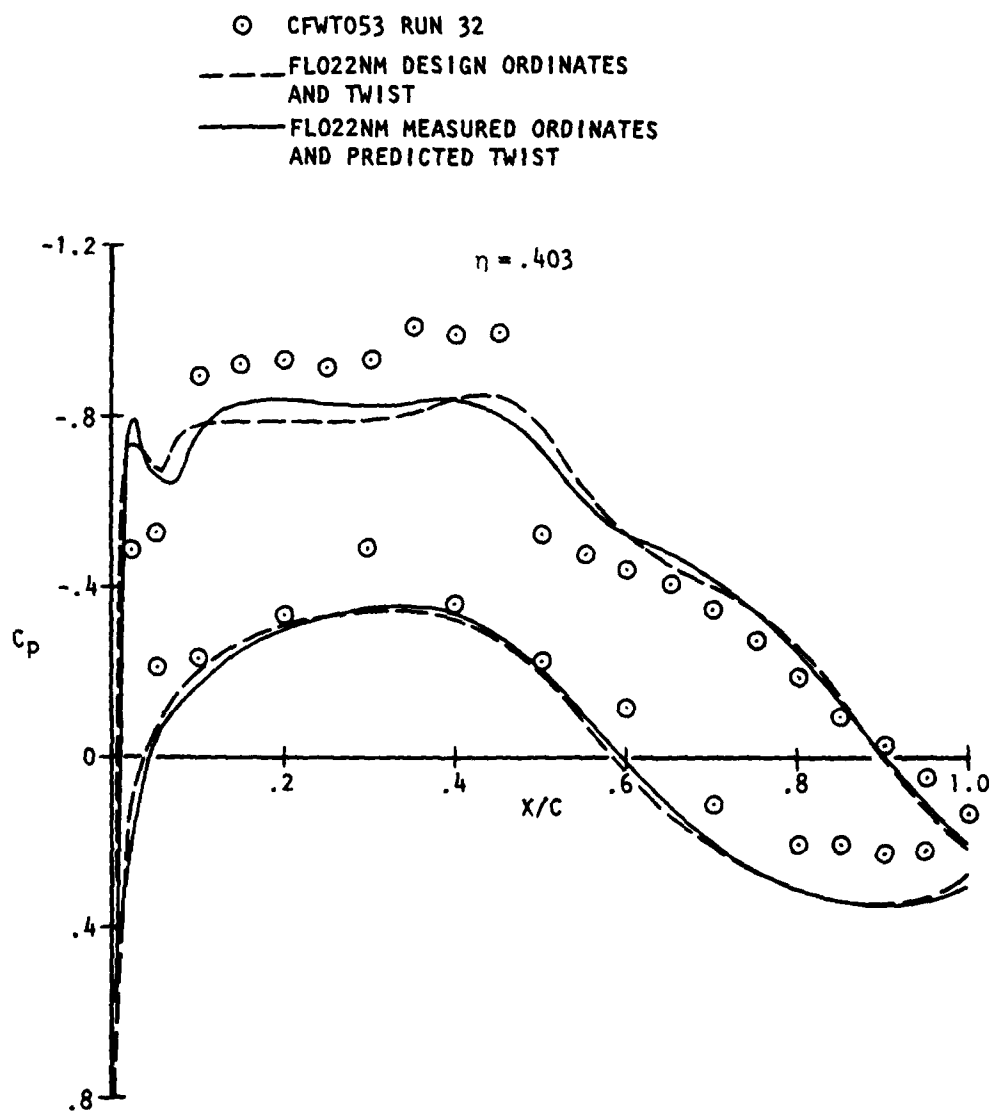


Figure 42. (Continued) (3)

○ CFWT053 RUN 32

--- FLO22NM DESIGN ORDINATES
AND TWIST

— FLO22NM MEASURED ORDINATES
AND PREDICTED TWIST

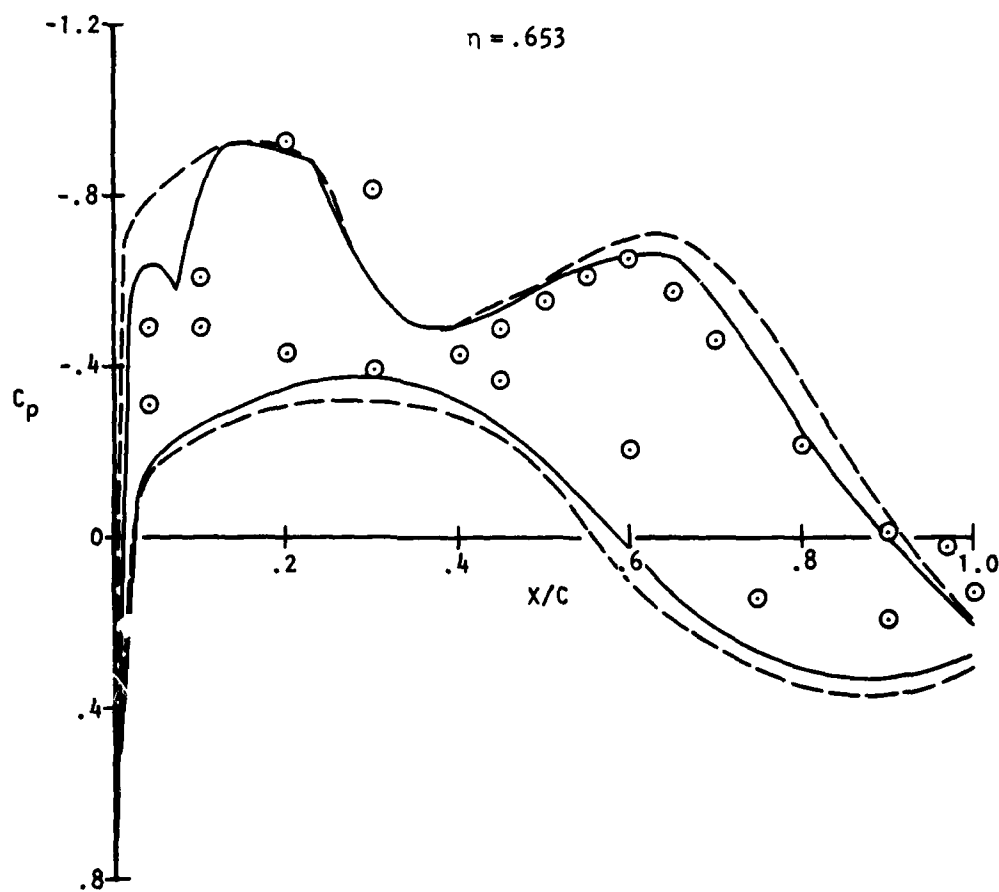


Figure 42. (Continued) (4)

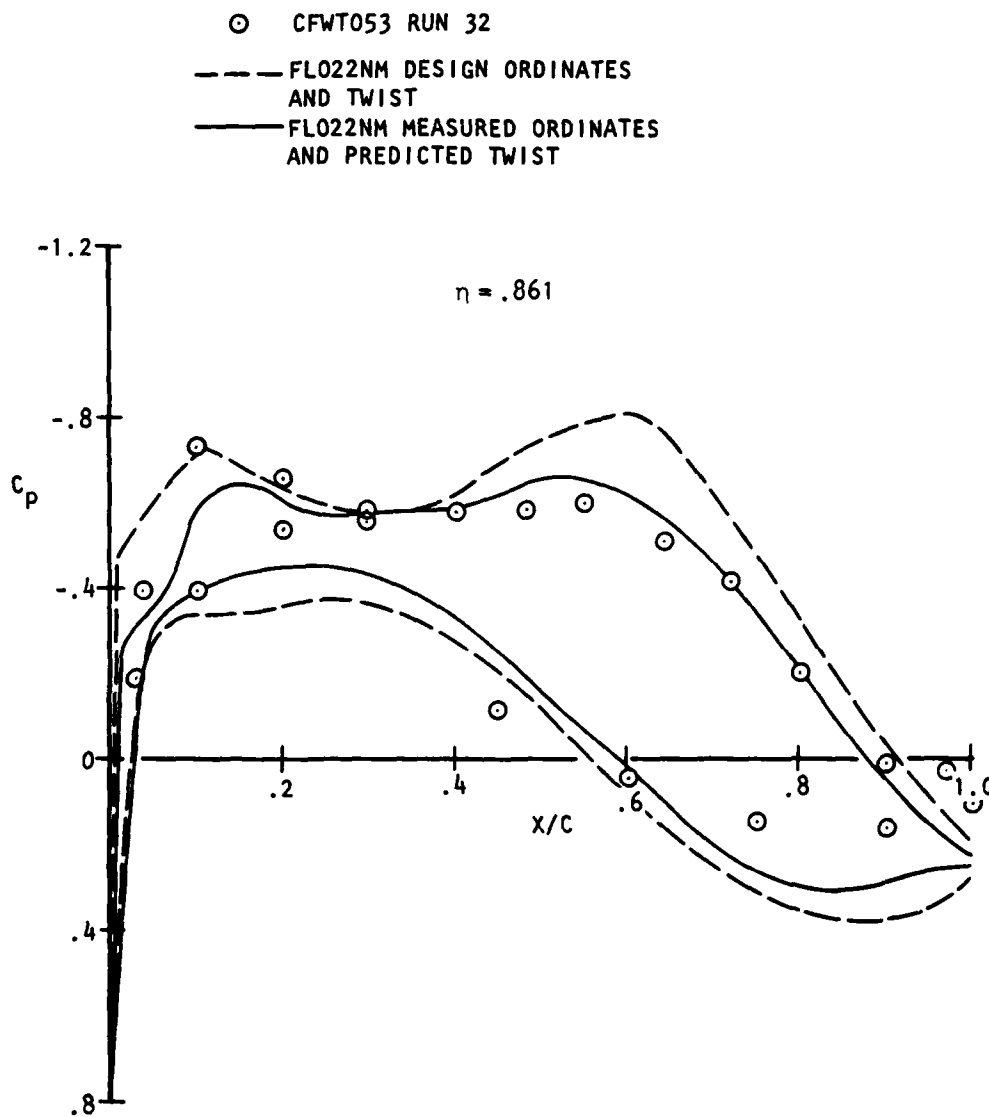


Figure 42. (Concluded) (5)

○ CFWT TEST 053 RUN 35
 --- FLO22NM DESIGN ORDINATES
 AND TWIST
 — FLO22NM MEASURED ORDINATES
 AND PREDICTED TWIST

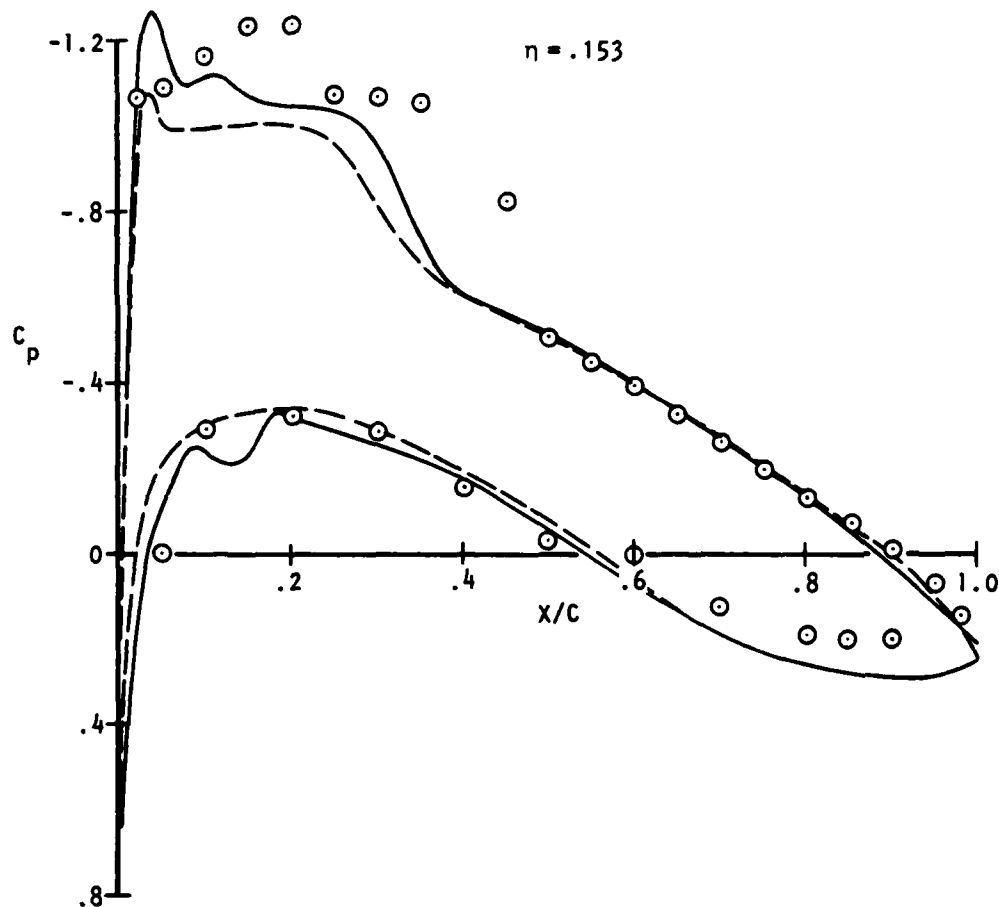


Figure 43. Full Potential Correlation, $M = 0.80$, $C_L = 0.60$

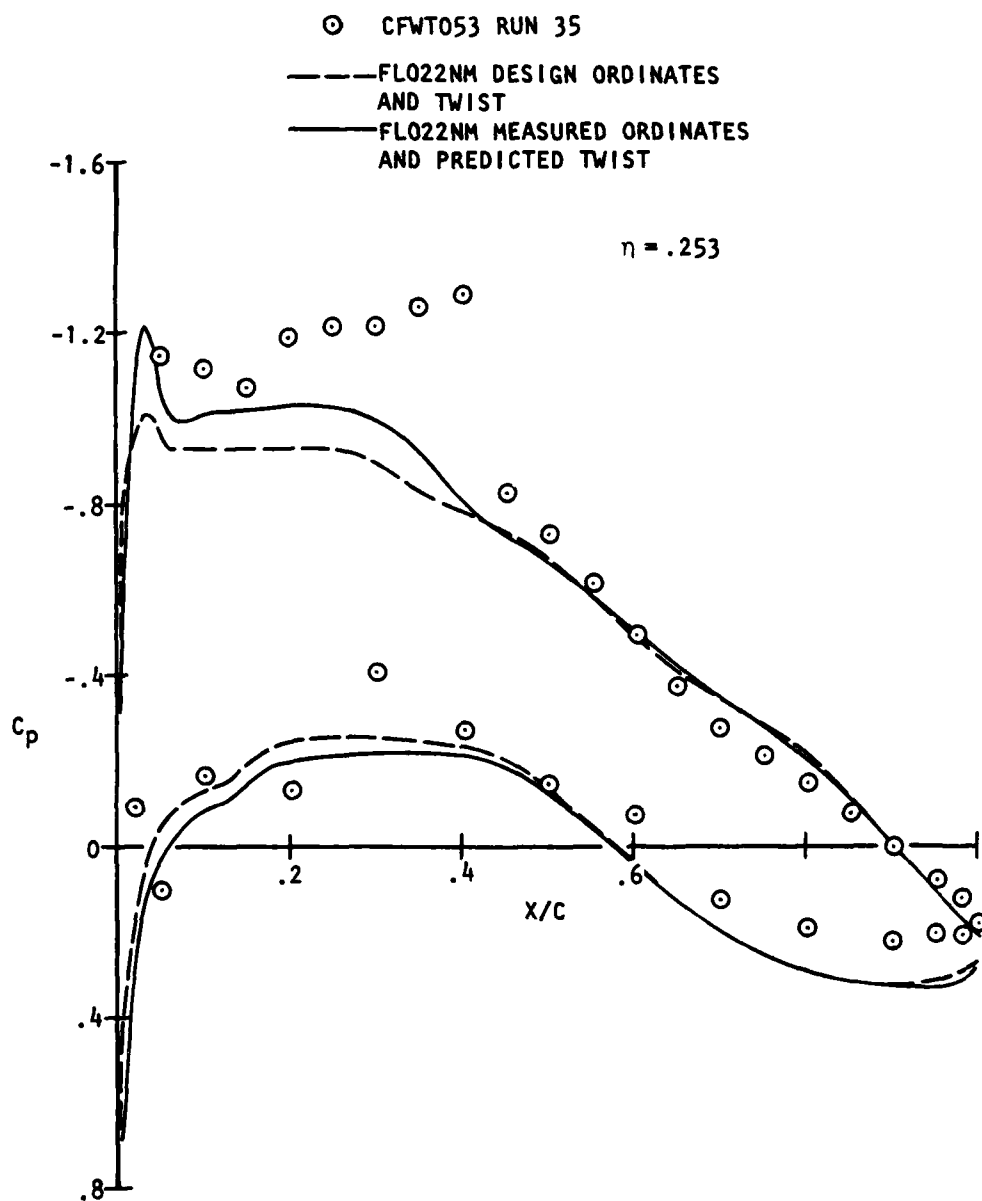


Figure 43. (Continued) (2)

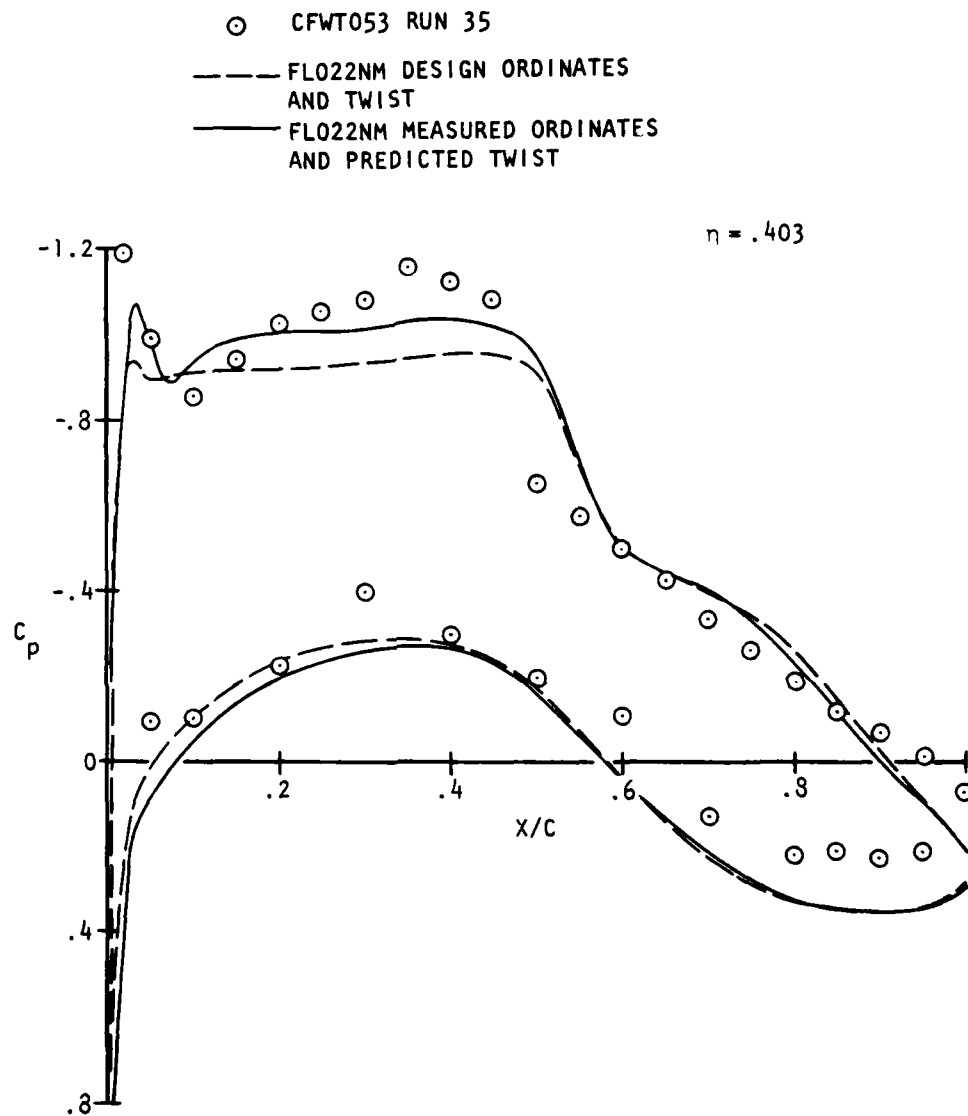


Figure 43. (Continued) (3)

⊙ CFWT053 RUN 35

--- FLO22NM DESIGN ORDINATES
AND TWIST

— FLO22NM MEASURED ORDINATES
AND PREDICTED TWIST

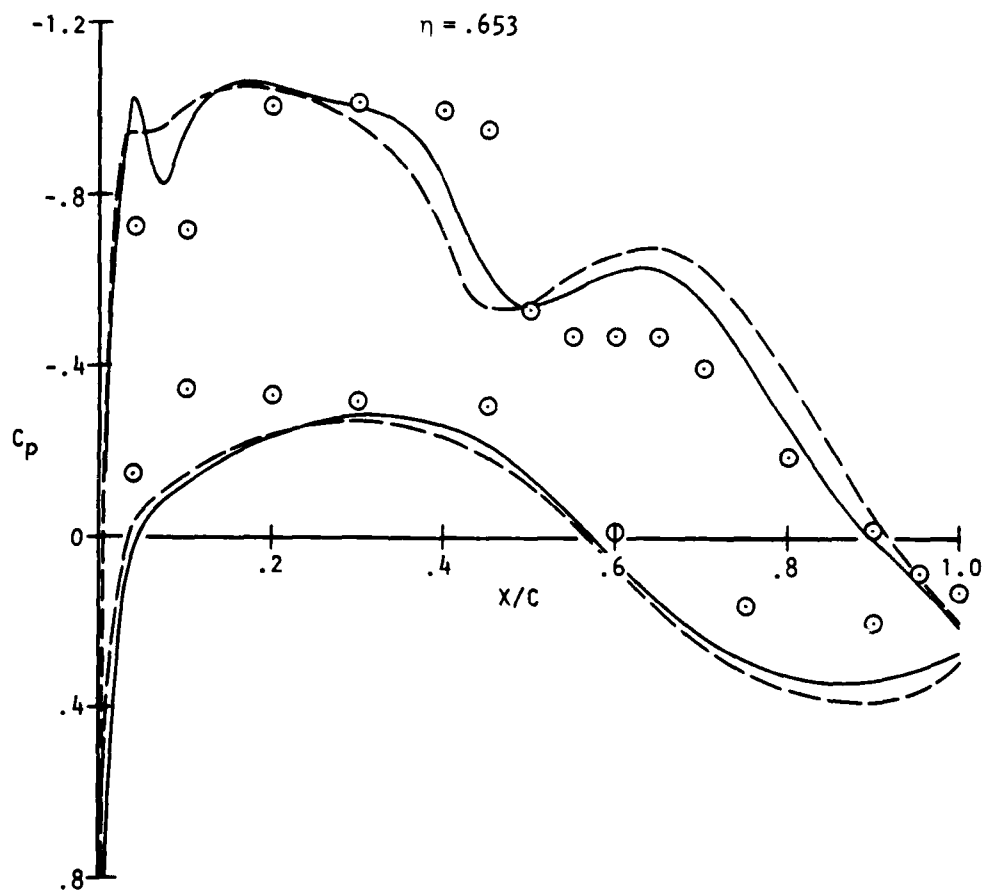


Figure 43. (Continued) (4)

○ CFWT053 RUN 35

--- FLO22NM DESIGN ORDINATES
AND TWIST

— FLO22NM MEASURED ORDINATES
AND PREDICTED TWIST

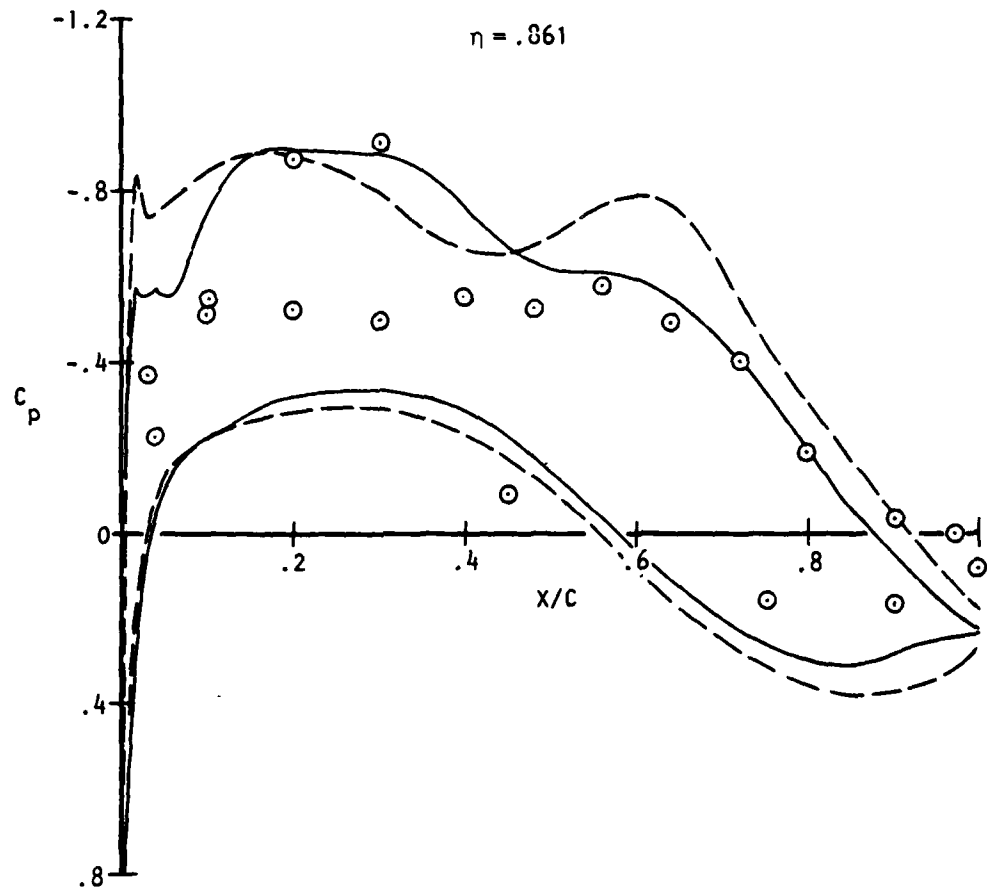


Figure 43. (Concluded) (5)

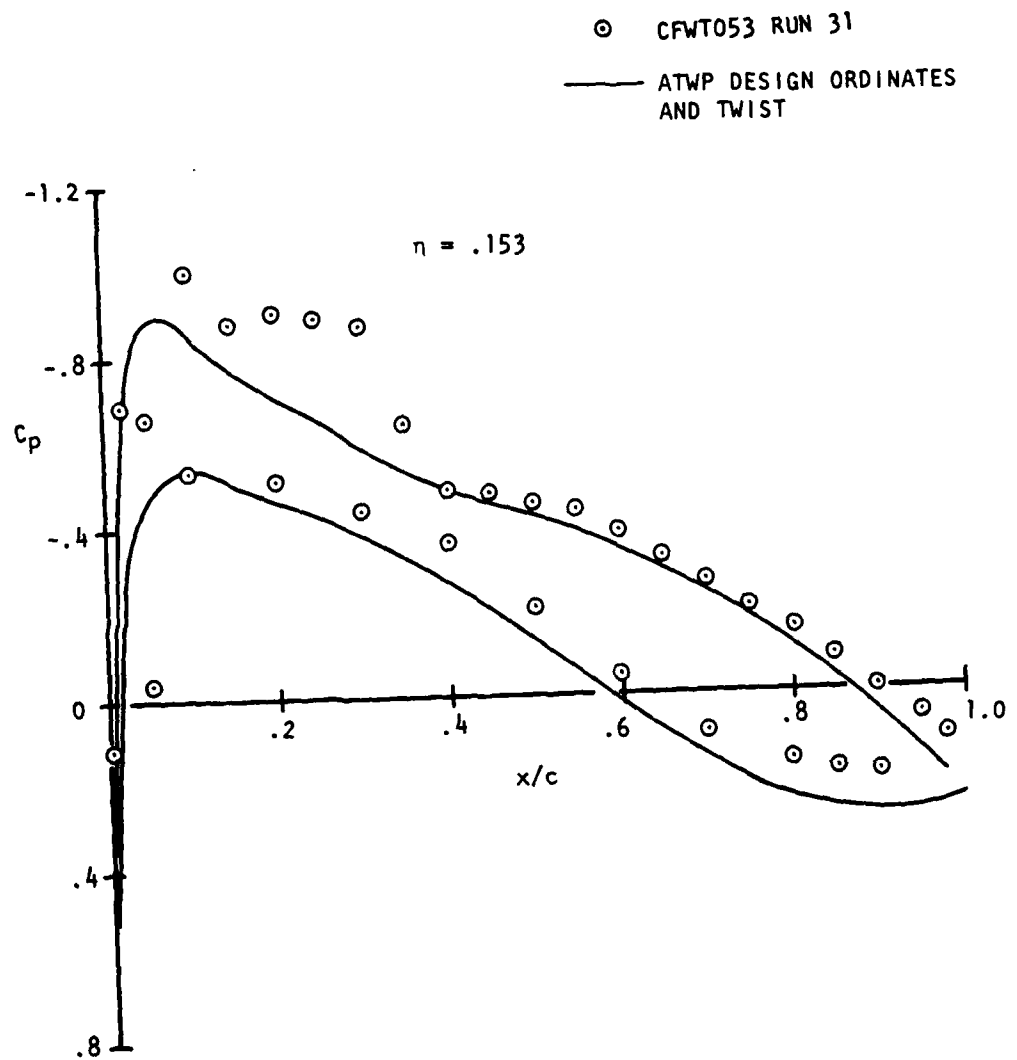


Figure 44. Extended Small Disturbance Correlation, $M = 0.80$, $C_L = 0.32$

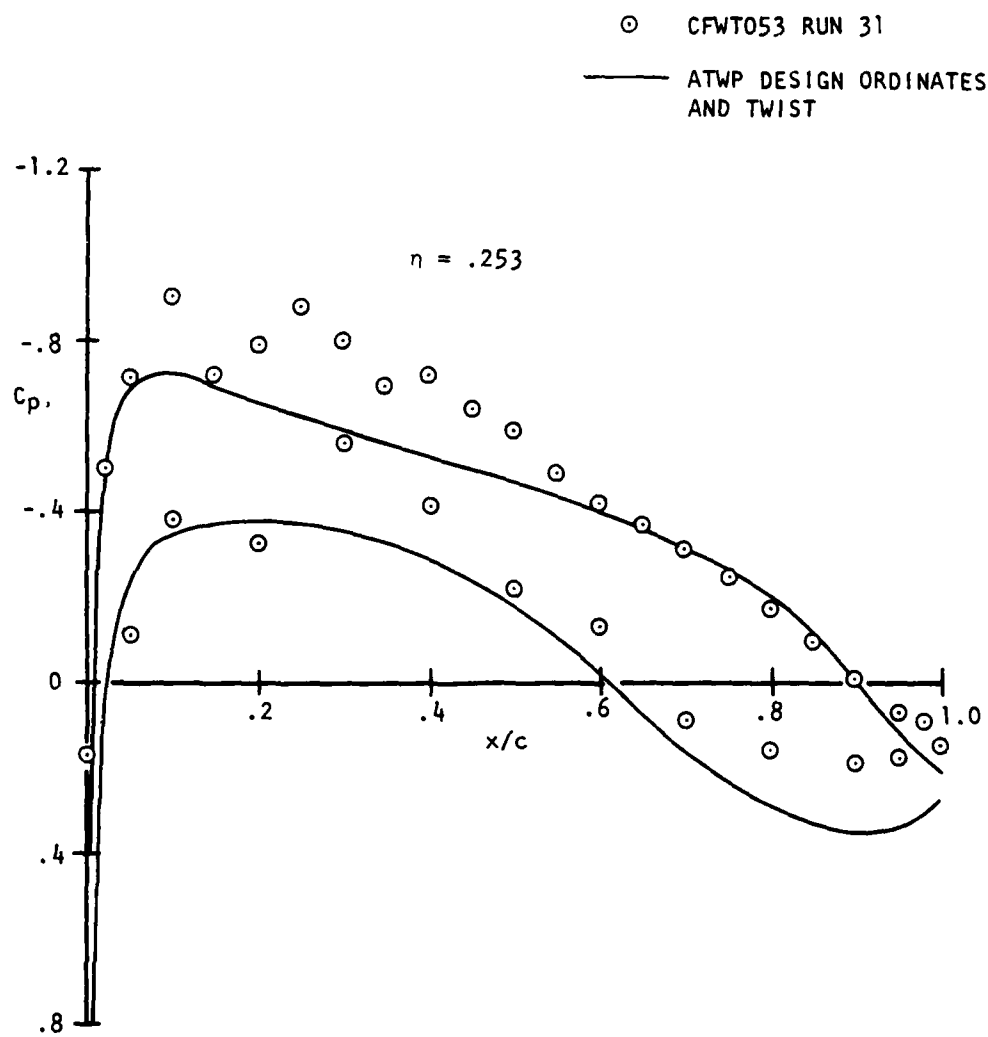


Figure 44. Continued (2)

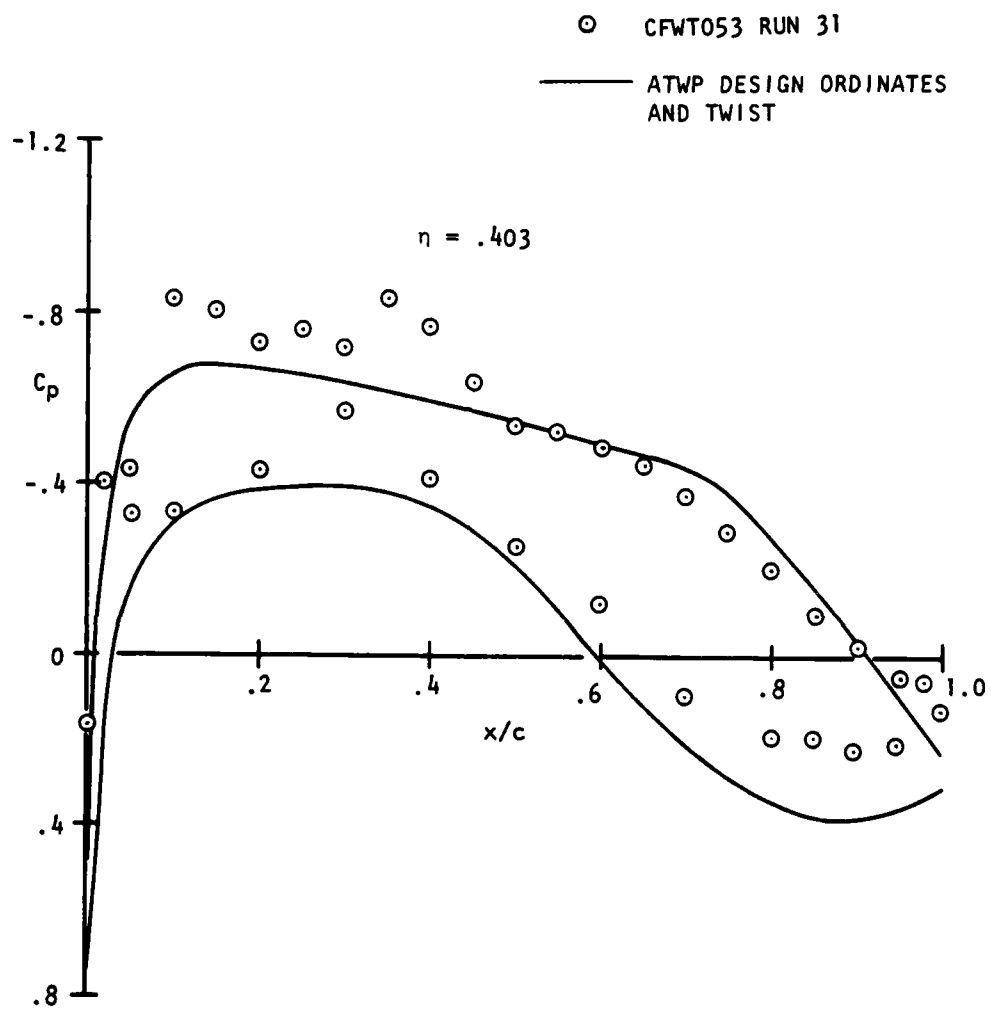


Figure 44. Continued (3)

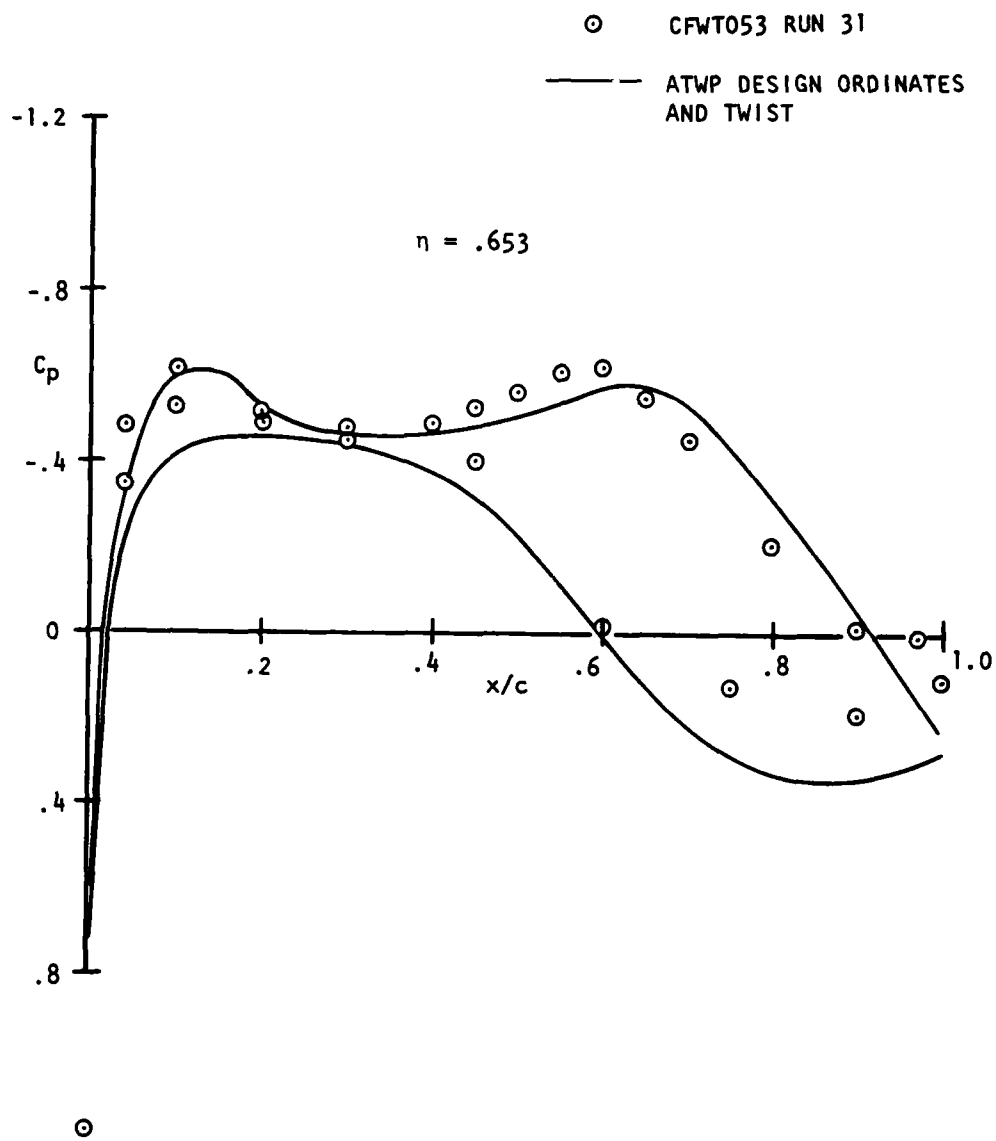


Figure 44. (Continued) (4)

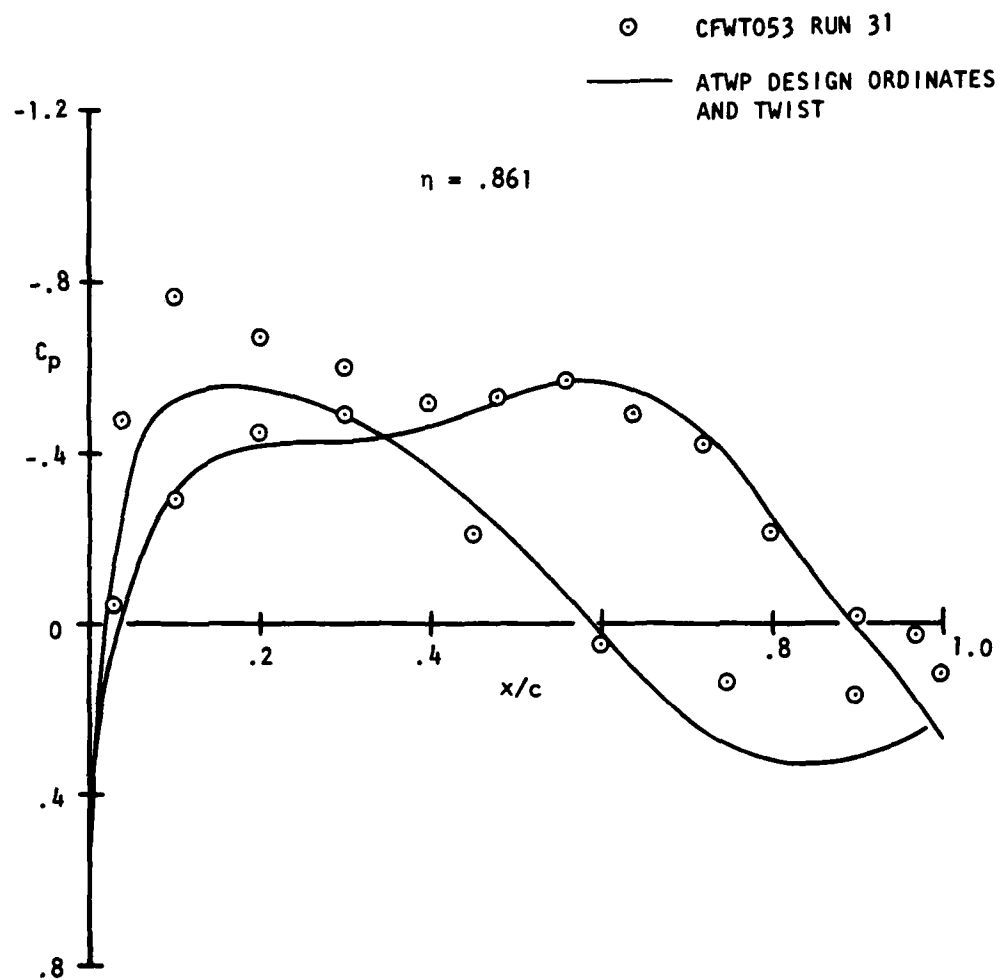


Figure 44. (Concluded) (5)

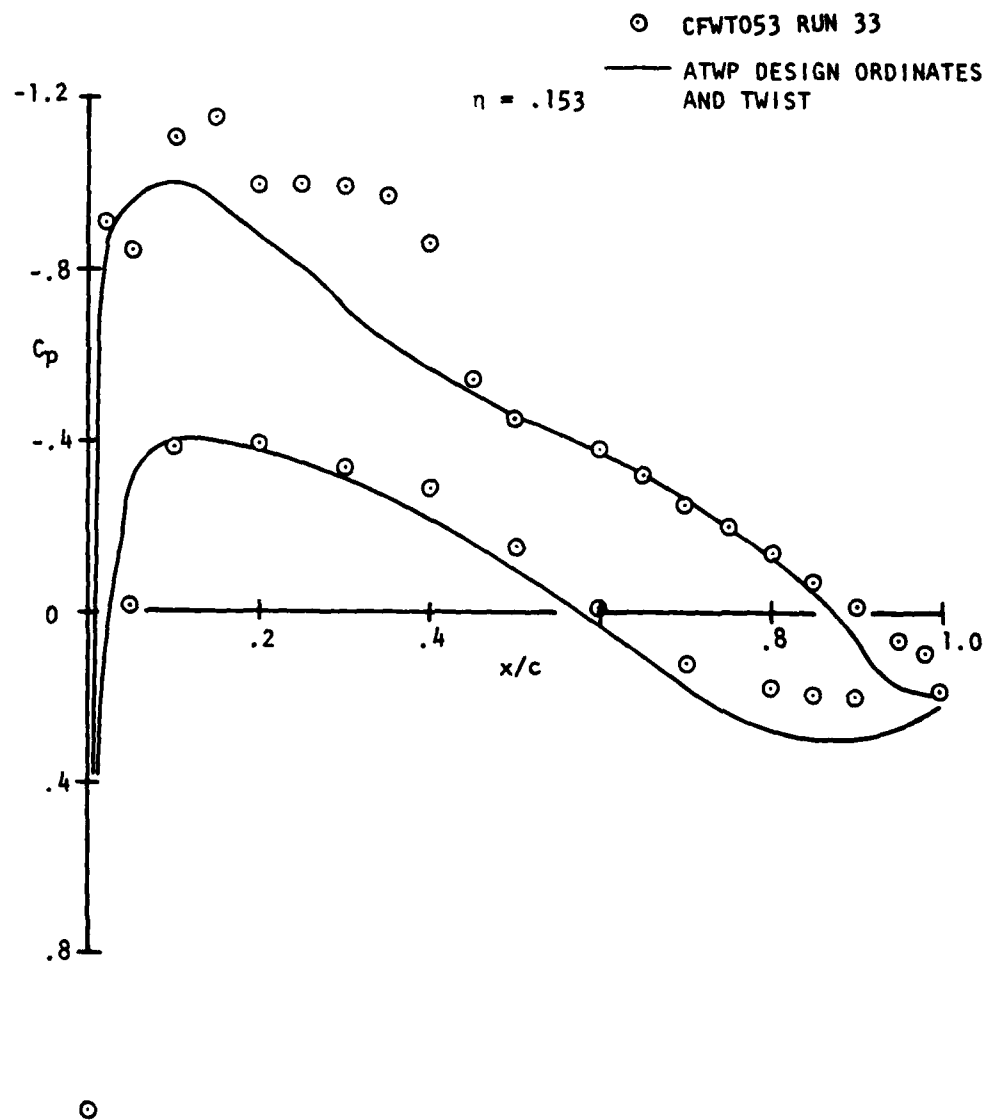


Figure 45. Extended Small Disturbance Correlation, $M = 0.80$, $C_L = .49$

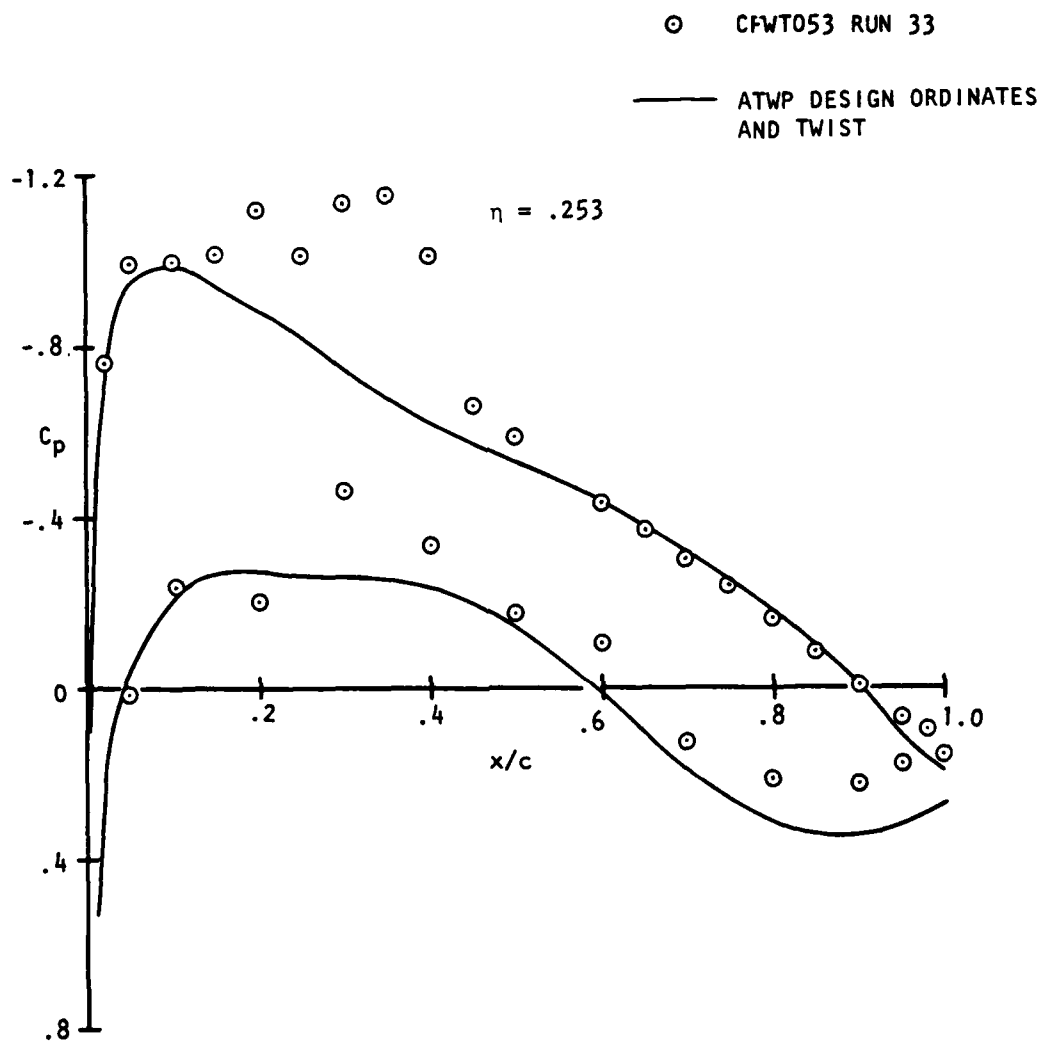


Figure 45. (Continued) (2)

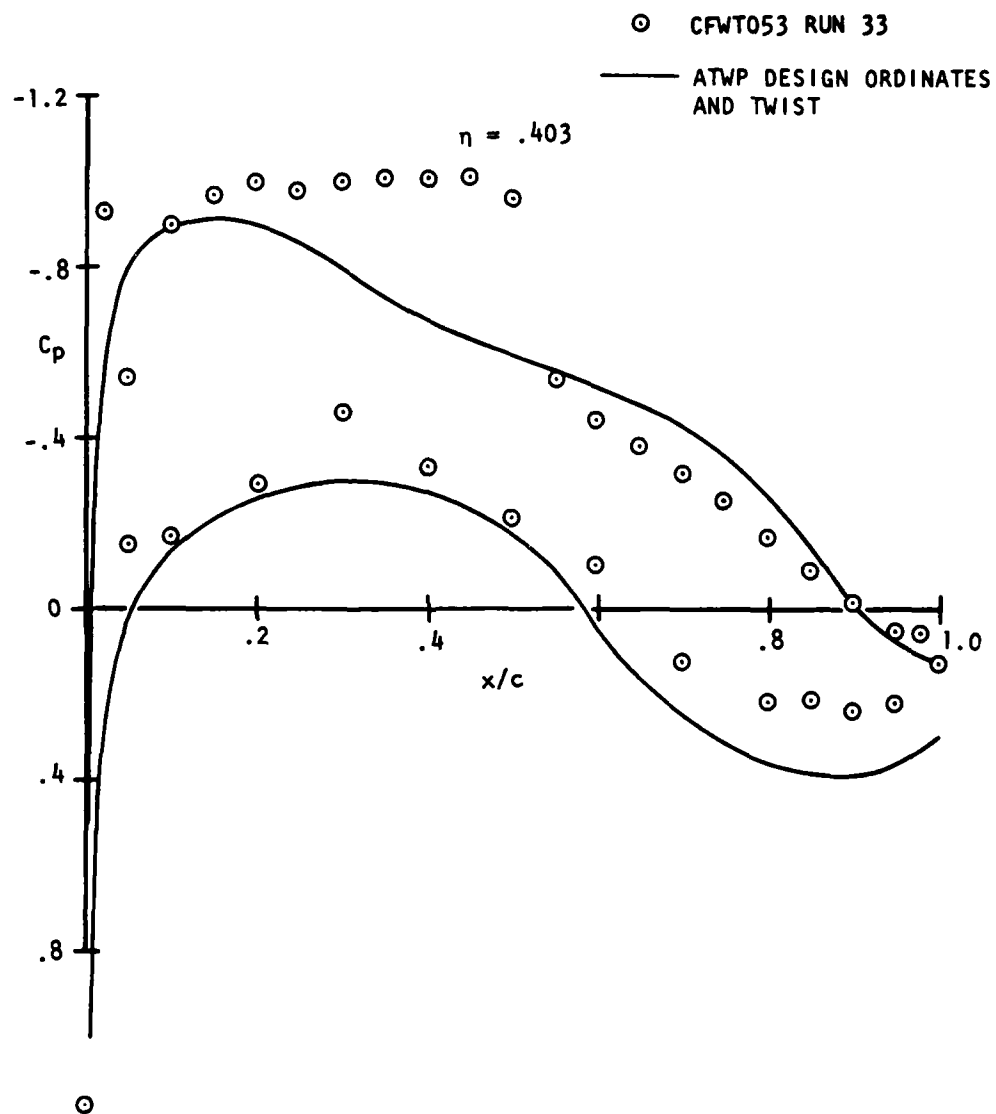


Figure 45. (Continued) (3)

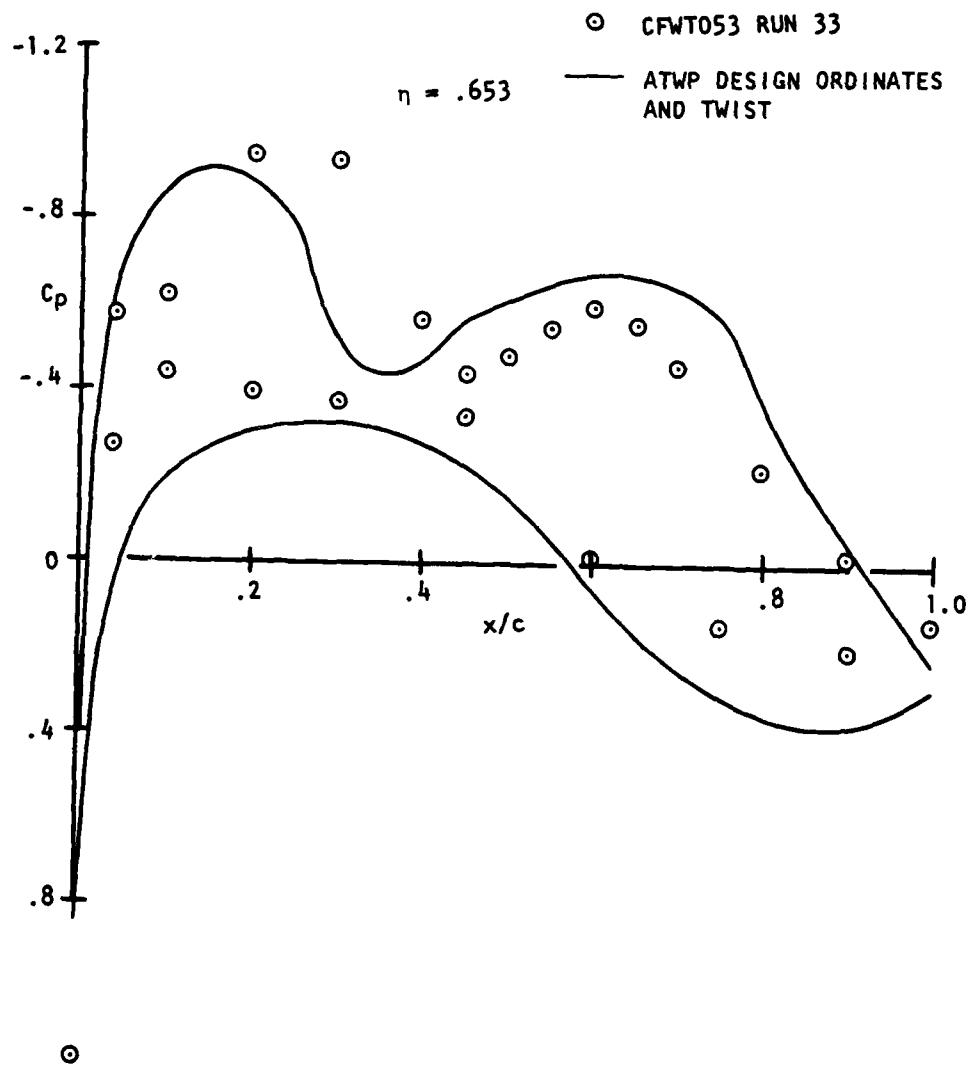


Figure 45. (Continued) (4)

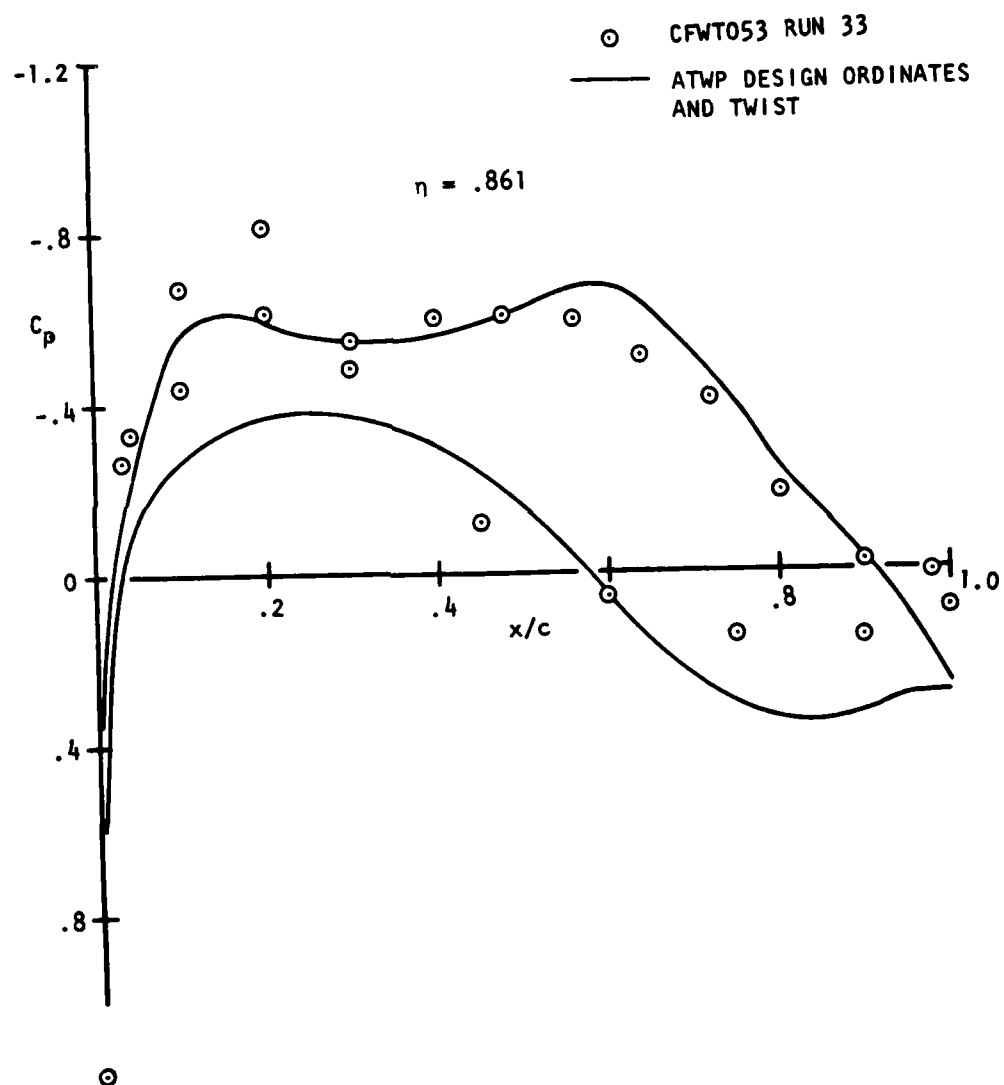


Figure 45. (Concluded) (5)

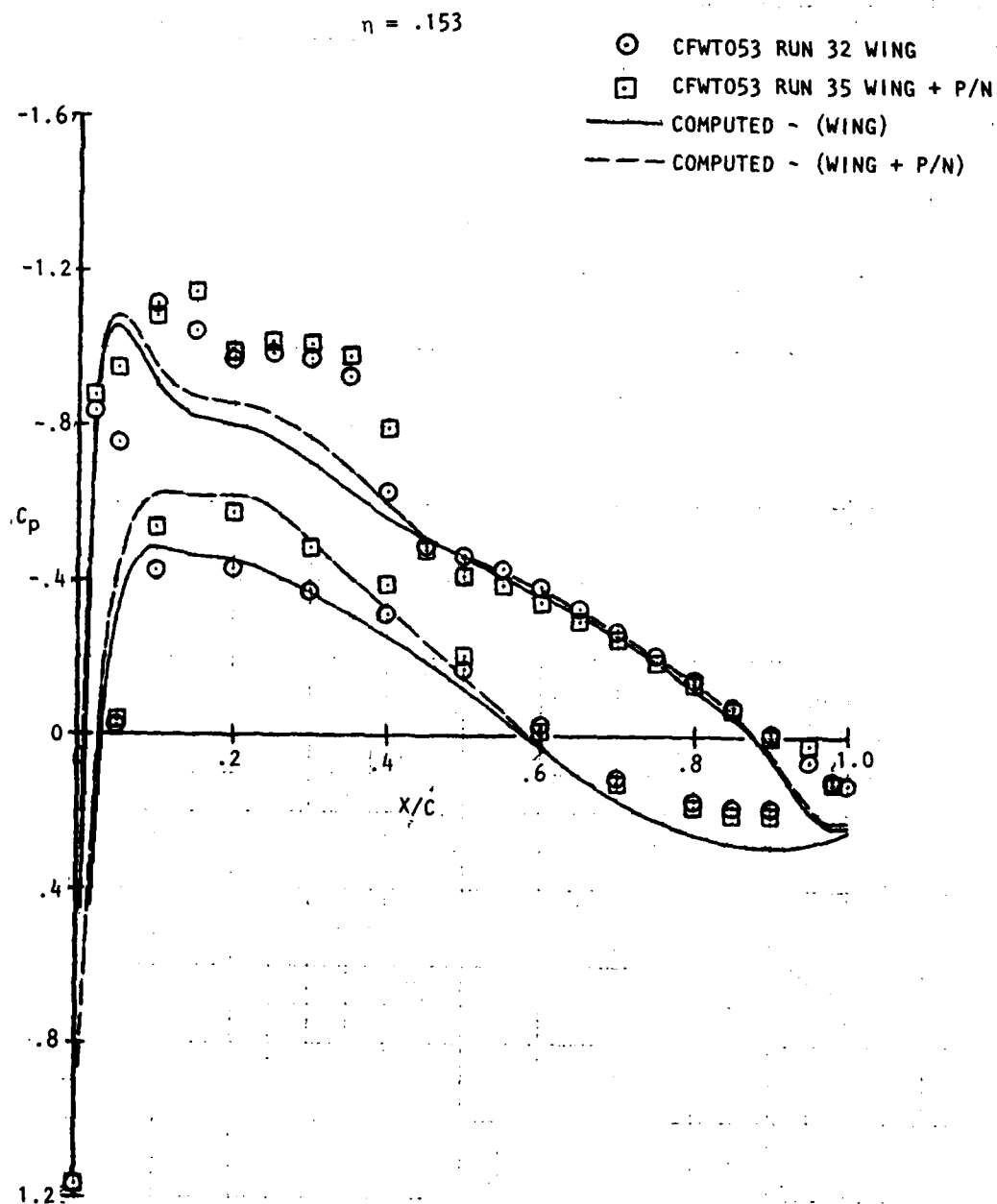


Figure 46. Correlation of Pylon/Nacelle Interference Effects
 $M = 0.80$, (Wing Alone $C_L = .445$)

$\eta = .253$

- CFWT053 RUN 32 WING
- CFWT053 RUN 35 WING + P/N
- COMPUTED - (WING)
- - - COMPUTED - (WING + P/N)

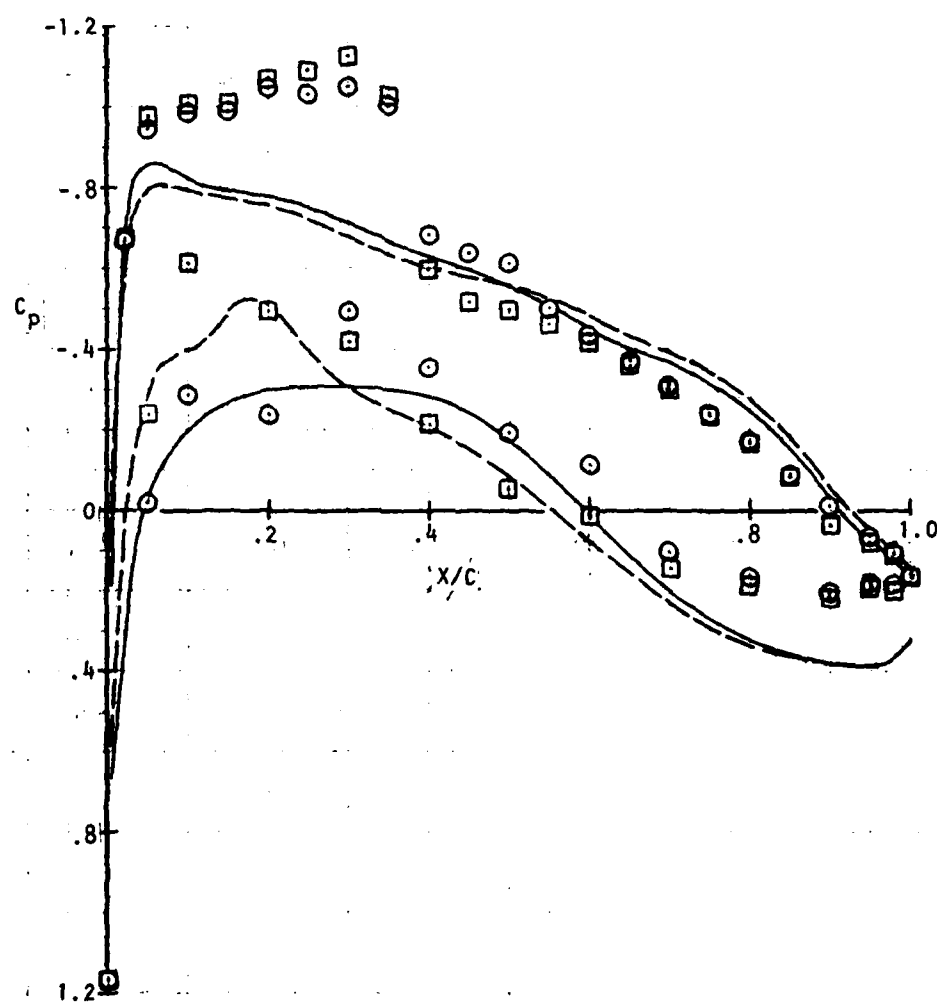


Figure 46. (Continued) (2)

$\eta = .403$

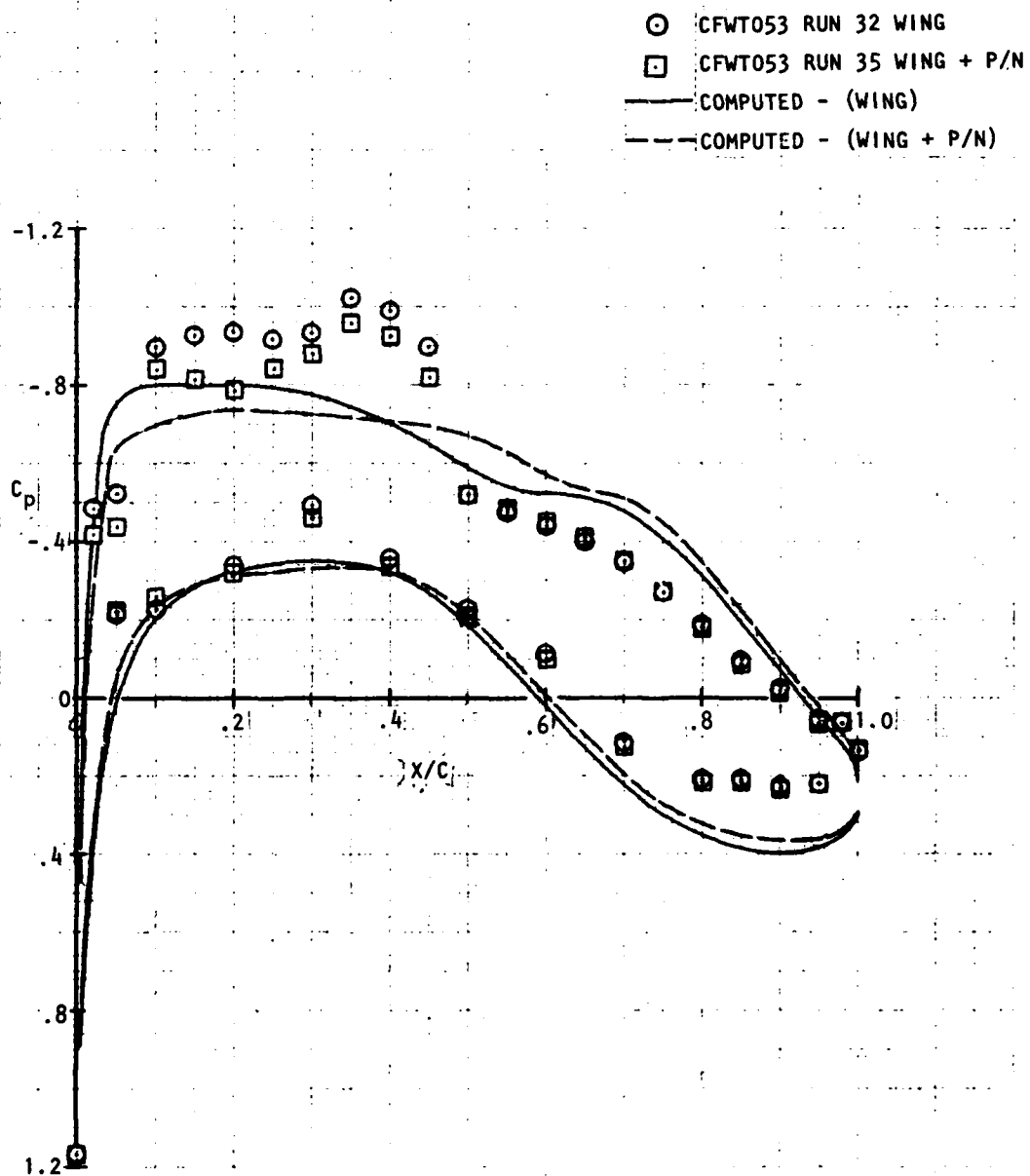


Figure 46. (Continued) (3)

$$\eta = .653$$

- CFWT053 RUN 32 WING
- CFWT053 RUN 35 WING + P/N
- COMPUTED - (WING)
- - - COMPUTED - (WING + P/N)

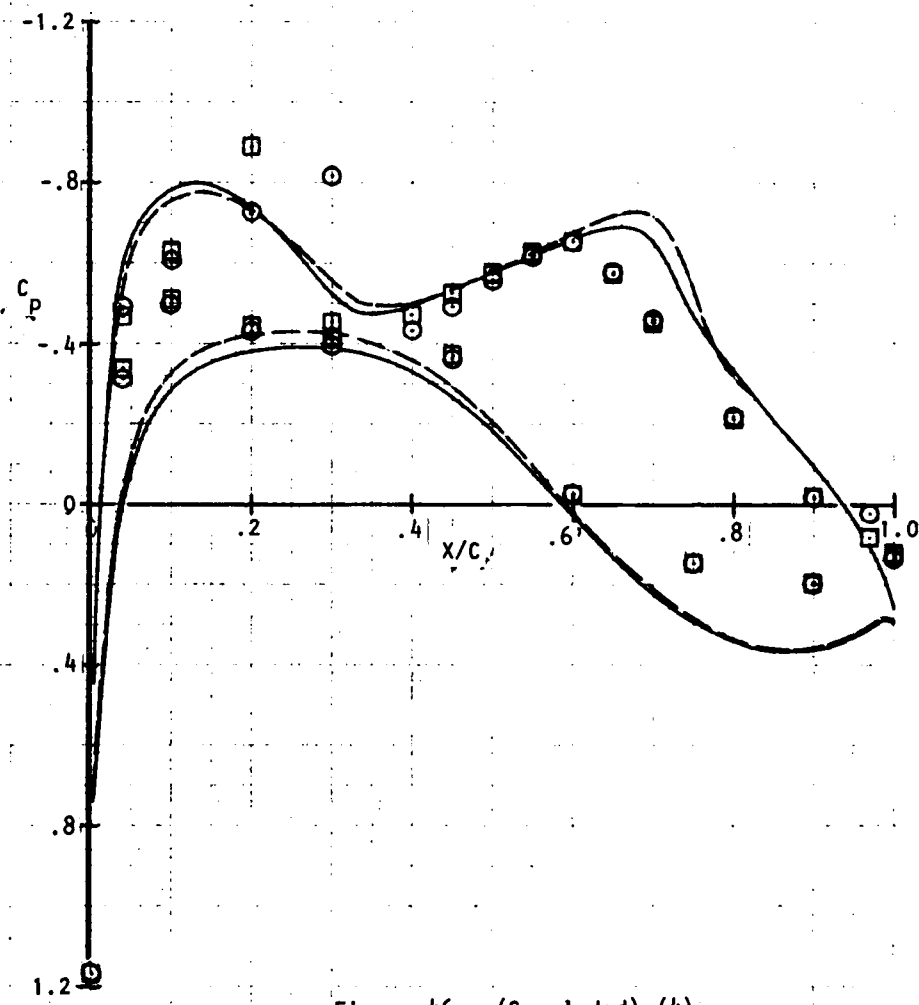


Figure 46. (Concluded) (4)

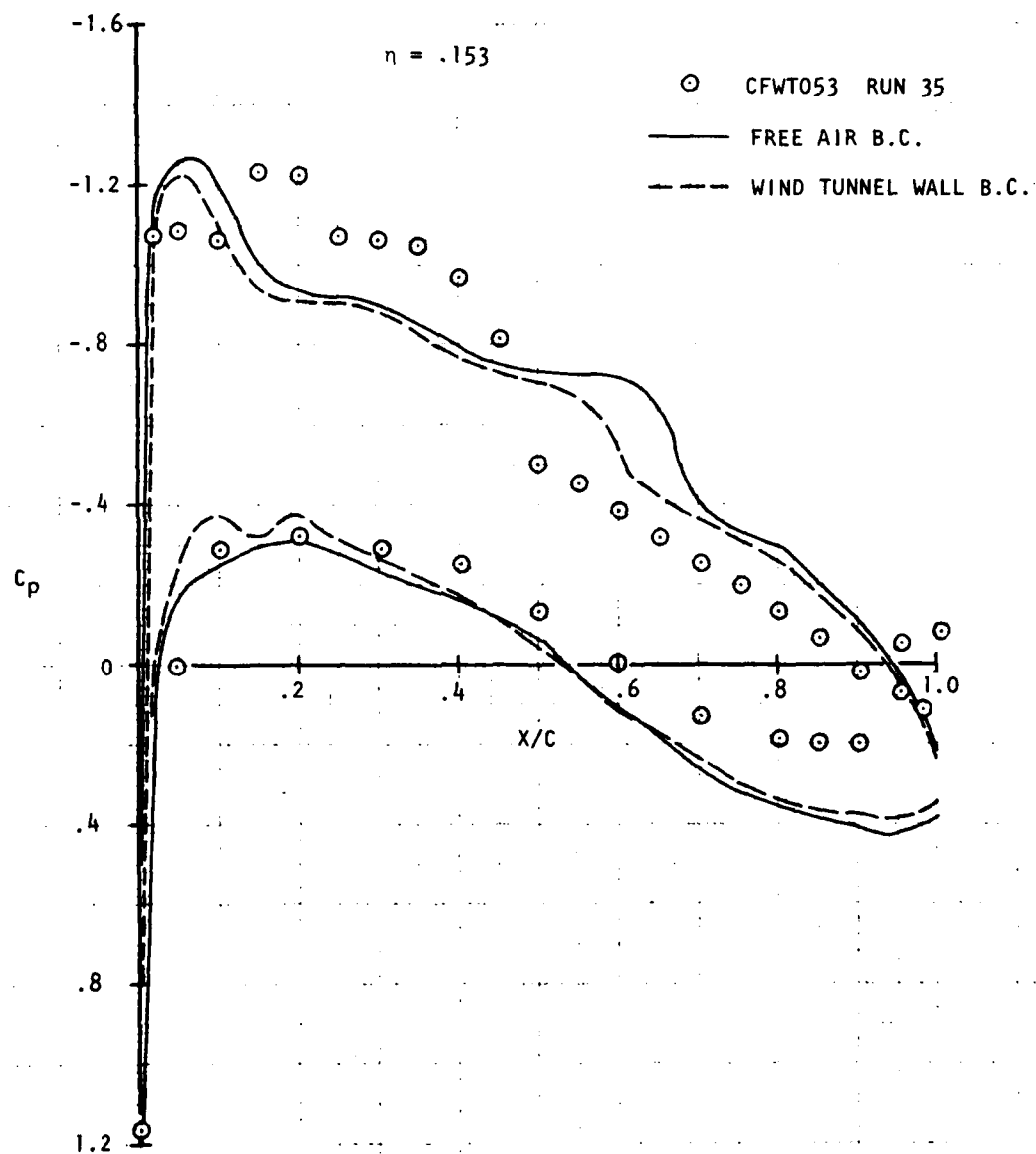


Figure 47. Effect of Wind Tunnel Wall Boundary Conditions,
 $M = 0.80$, $\alpha = 0.7^\circ$.

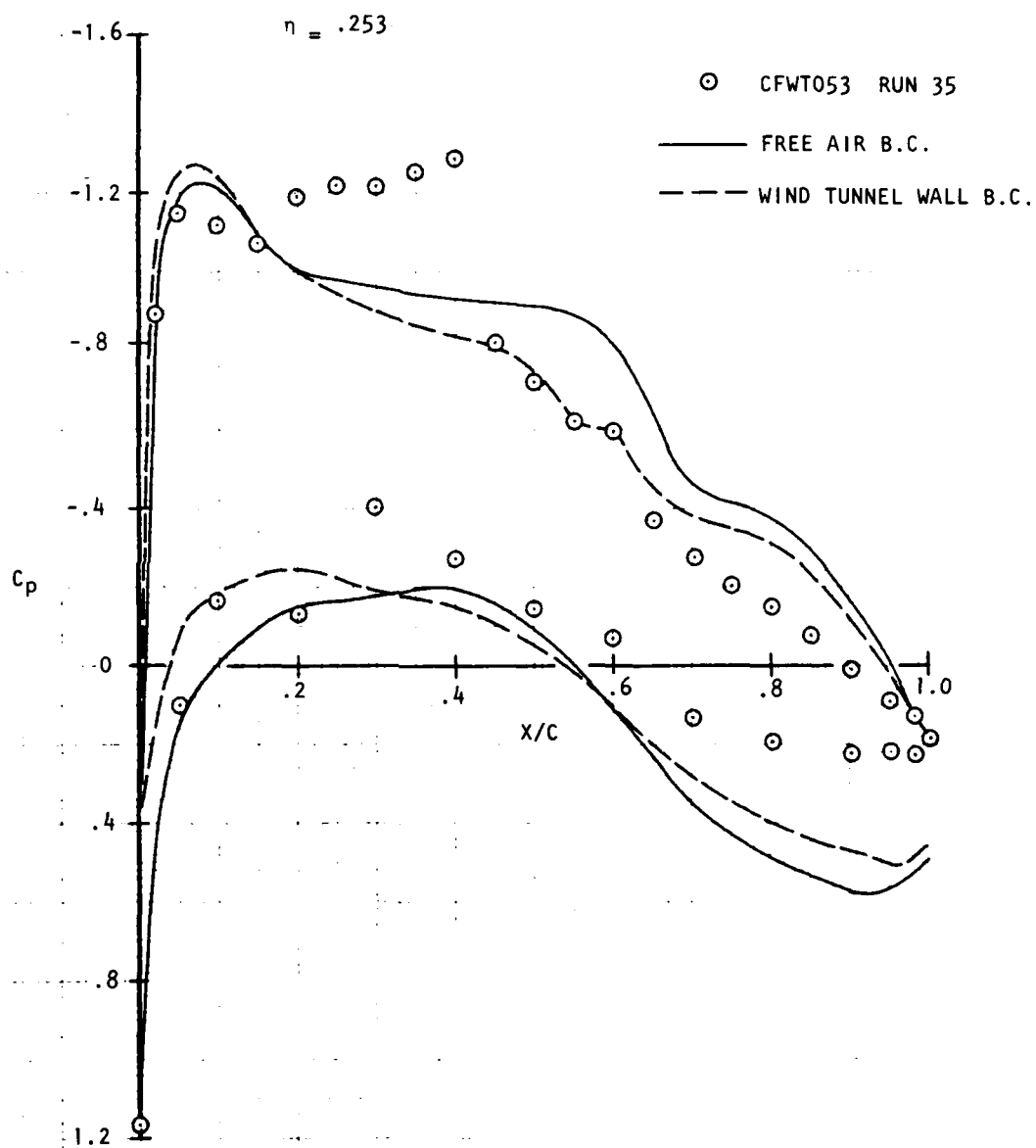


Figure 47. (Continued) (2)

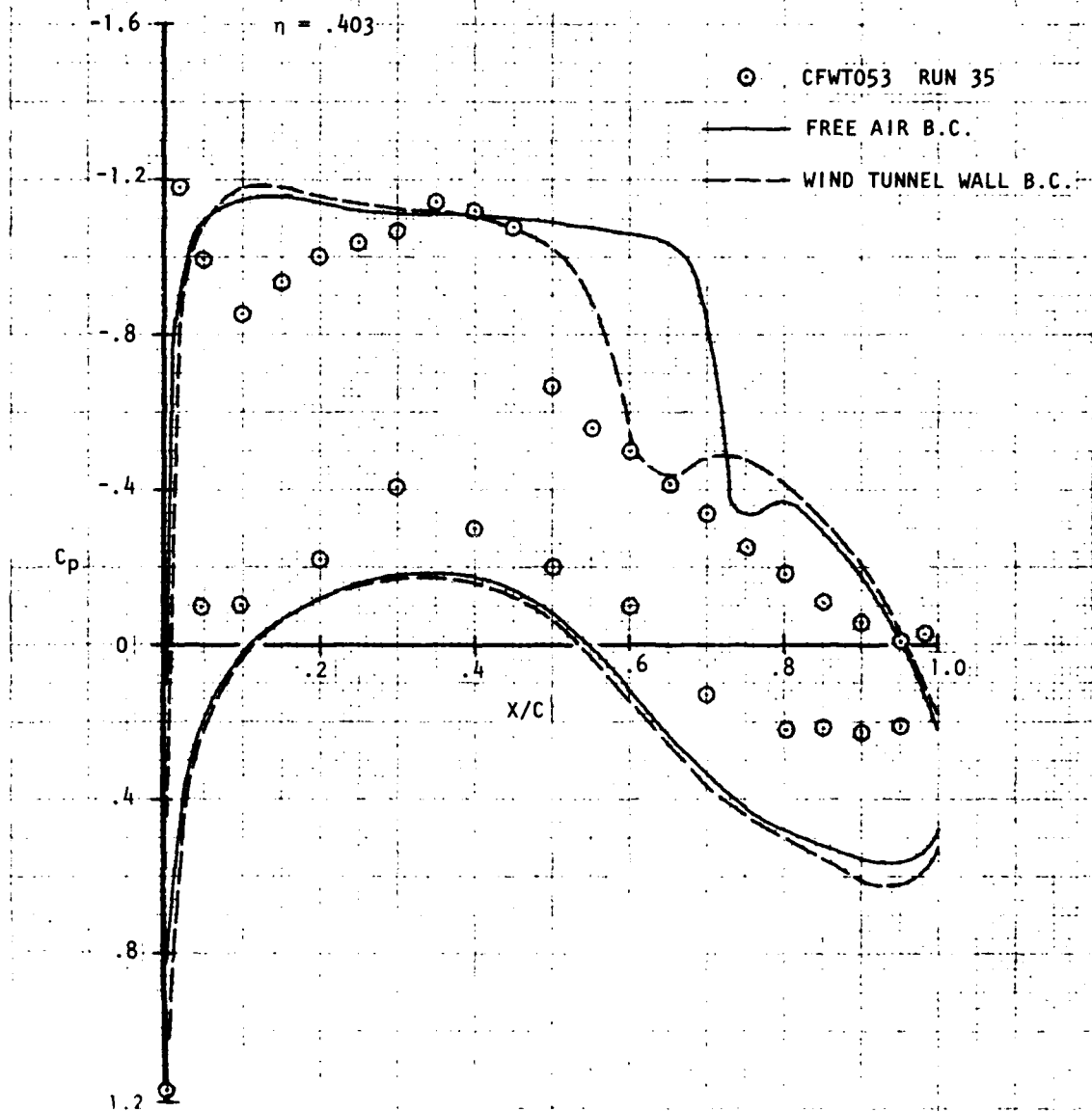


Figure 47. (Continued) (3)

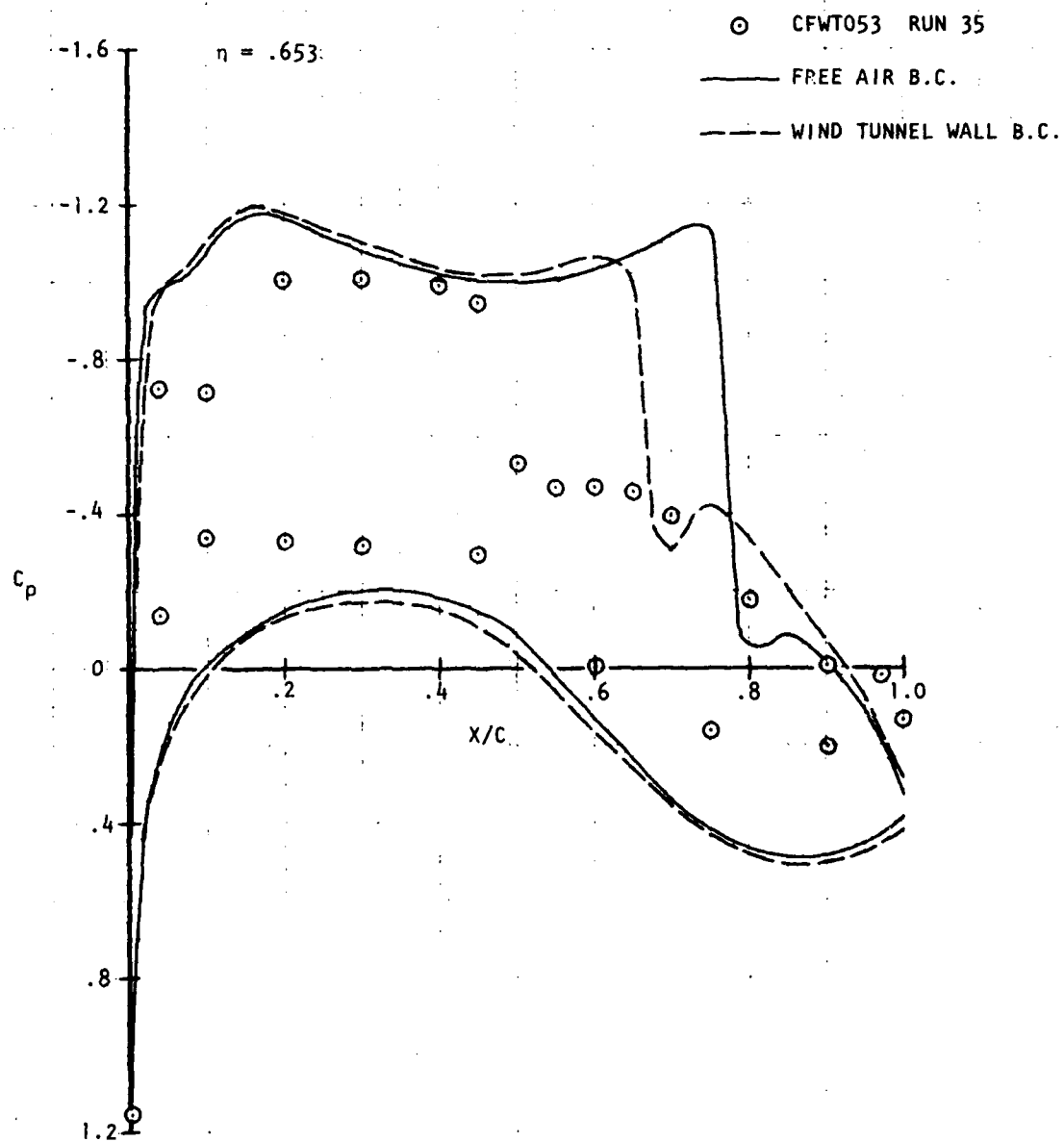


Figure 47. (Continued) (4)

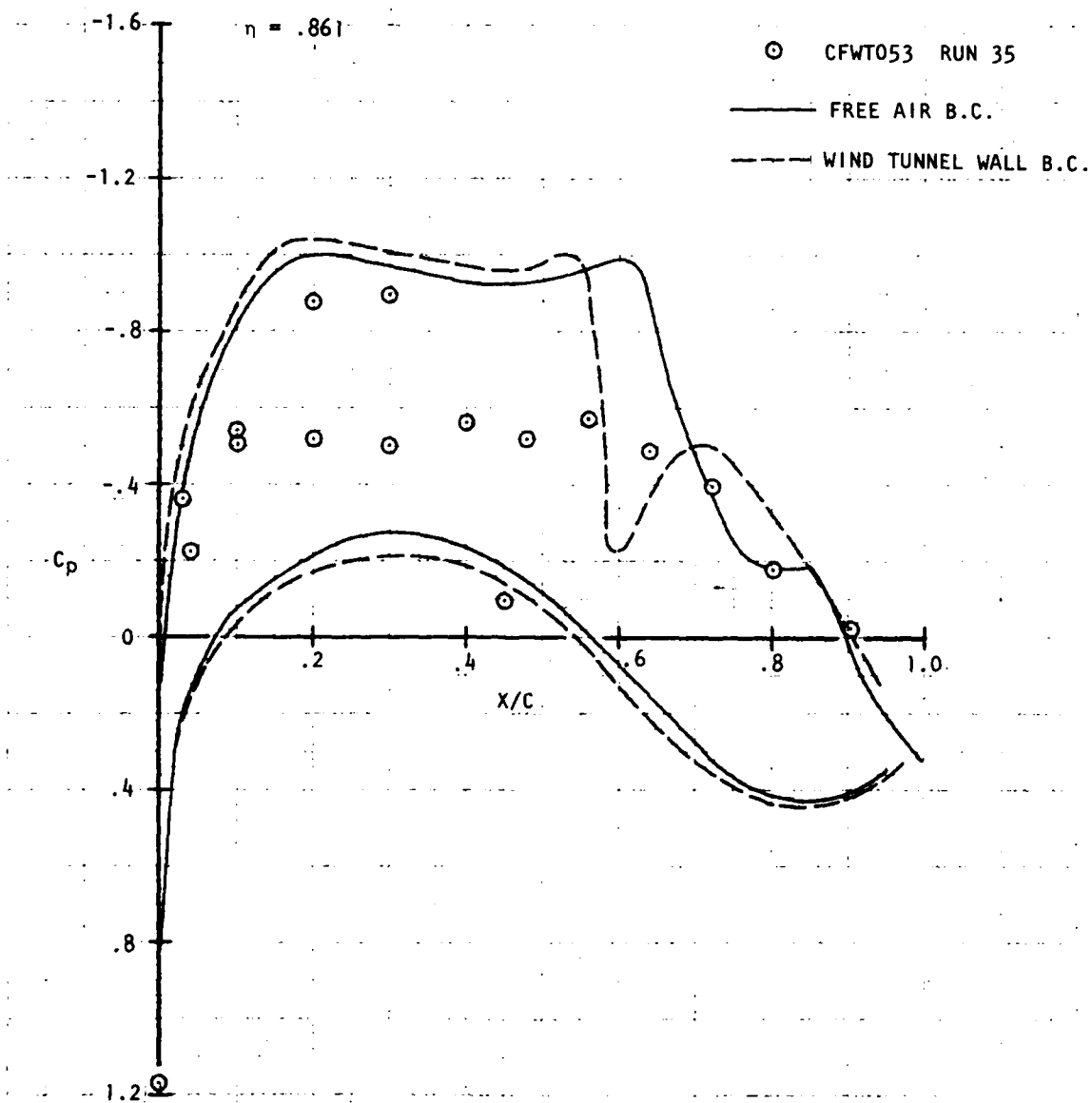


Figure 47. (Continued) (5)

$M = .8$

$R_N \sim 5E+6$

	BALANCE	PRESSURES
WING ALONE	—●—	—○—
WING + FUSELAGE	-▲-	-△-

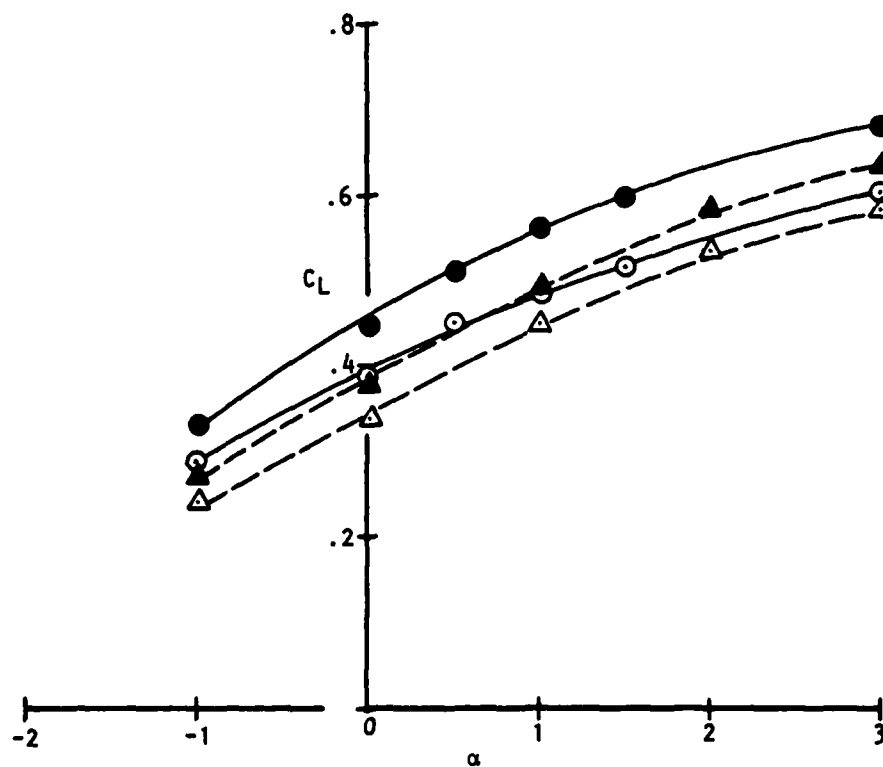


Figure 48. Pressure Integration vs. Force Balance Comparisons

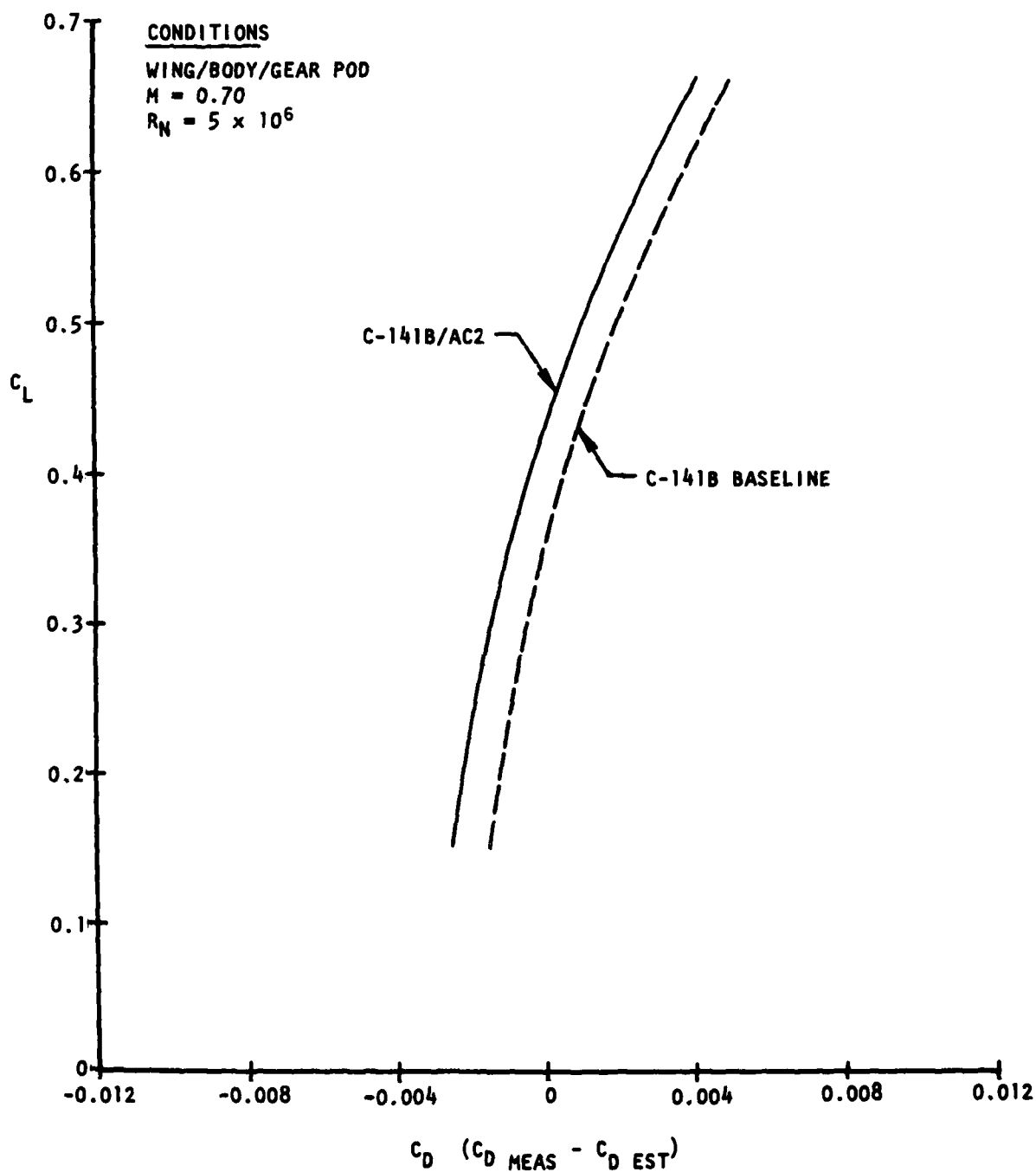


Figure 49. Comparison of Measured Model Drag With Estimates

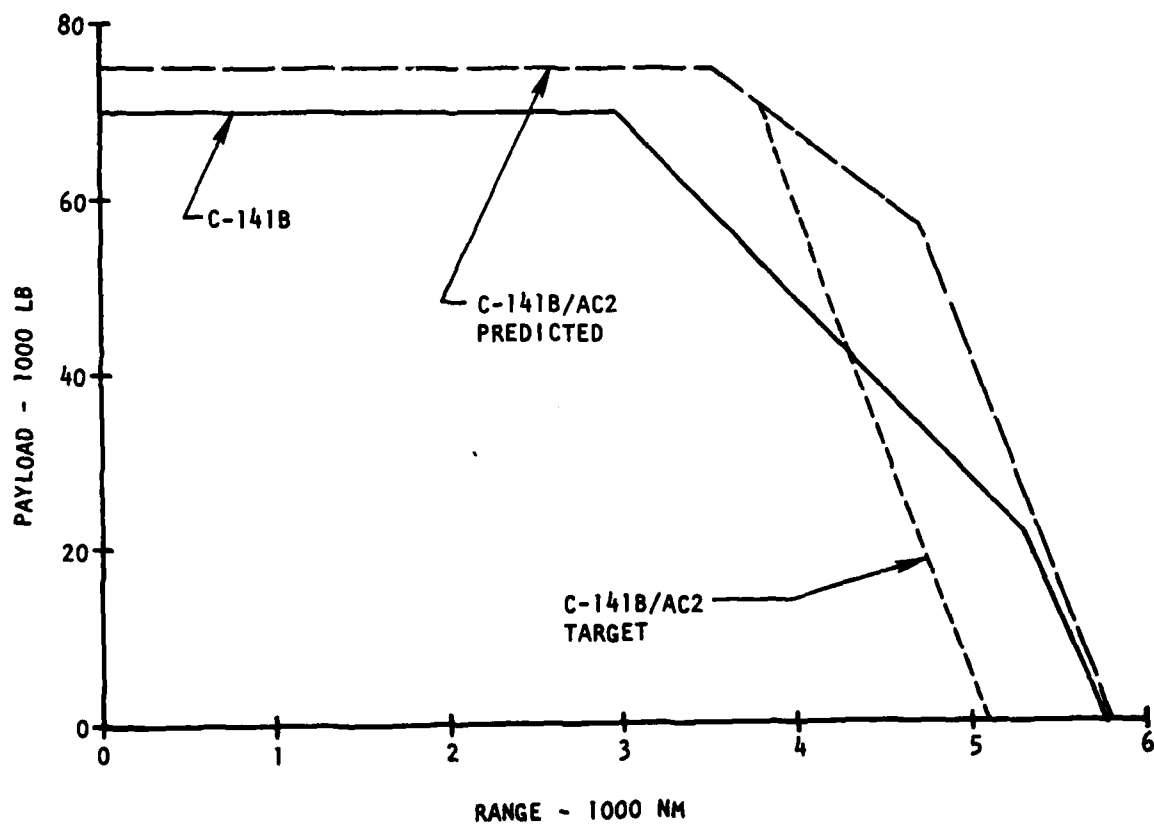


Figure 50. Payload - Range Performance

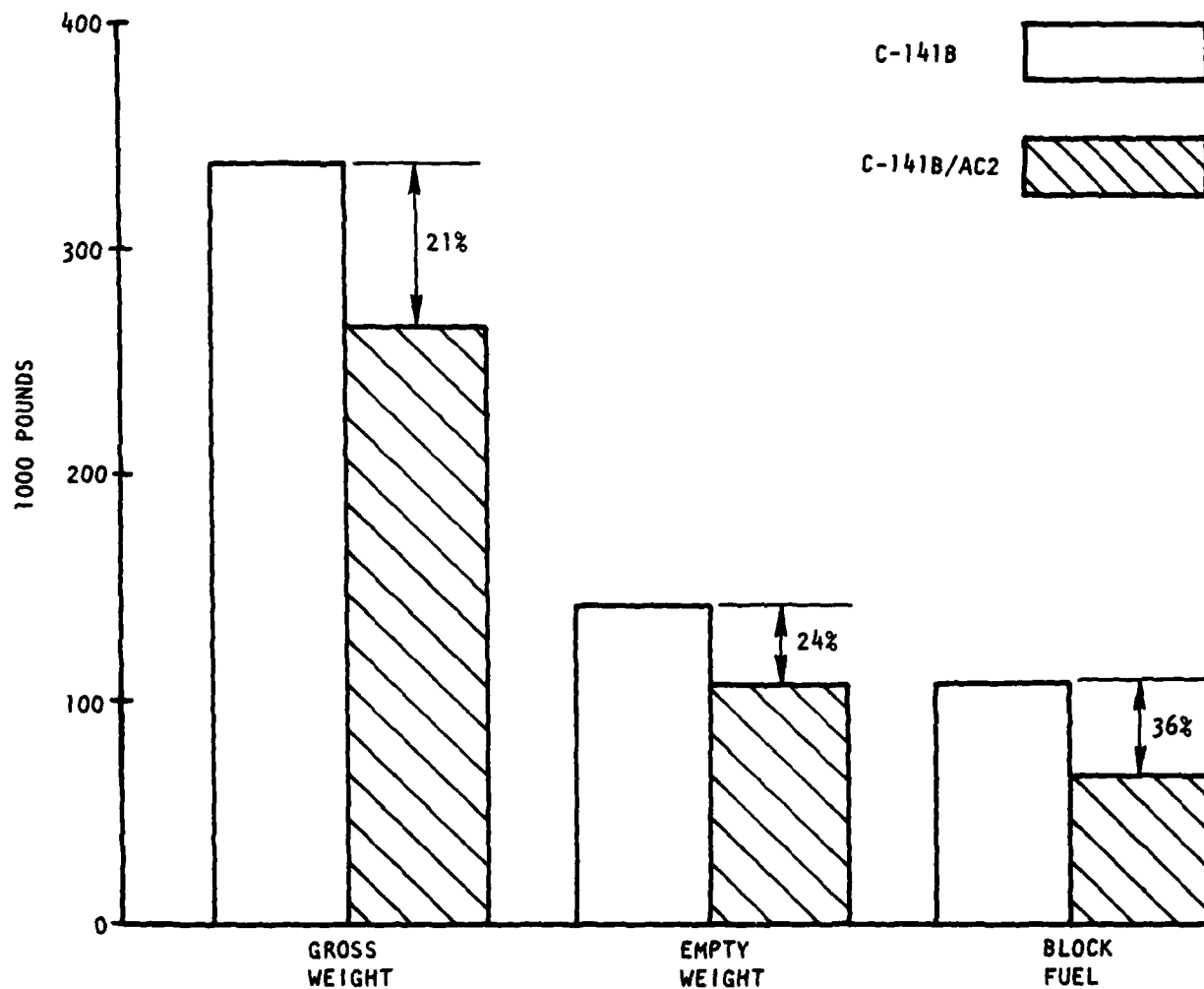


Figure 51. Summary of Aircraft Parameters

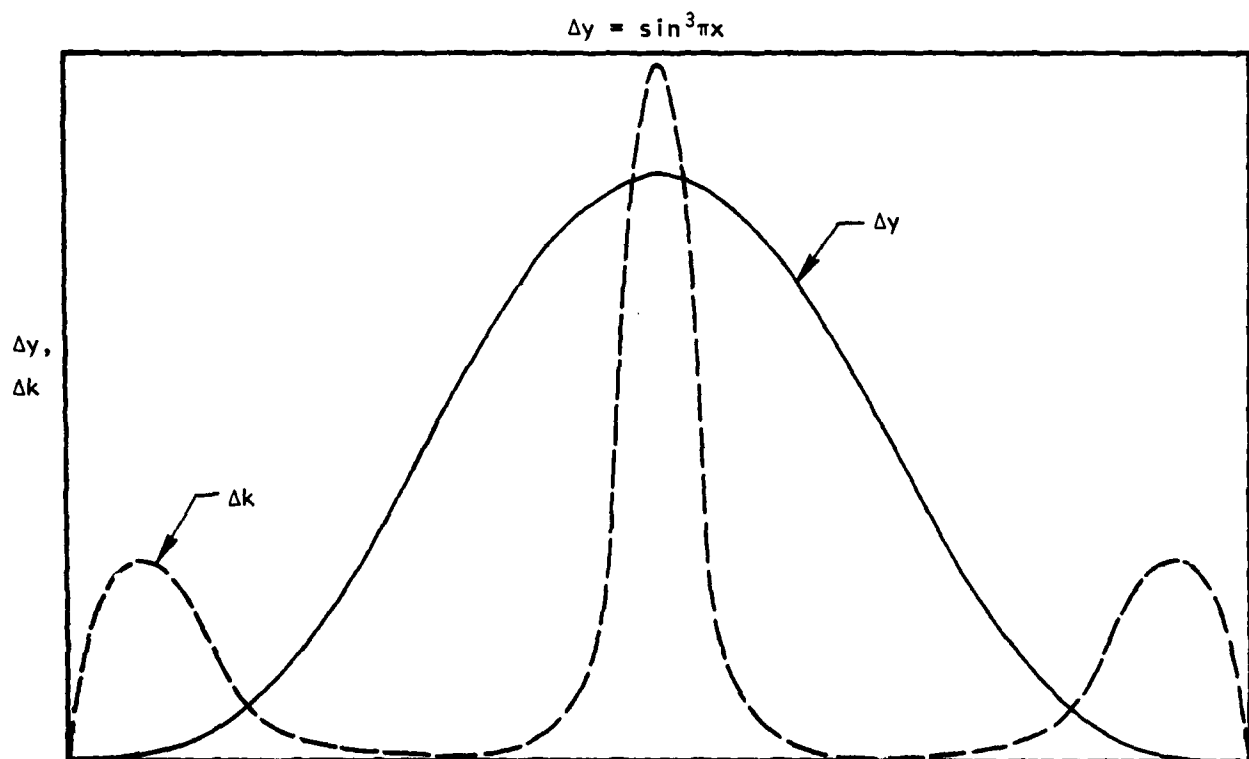


Figure 52. Airfoil Ordinate And Curvature Change.

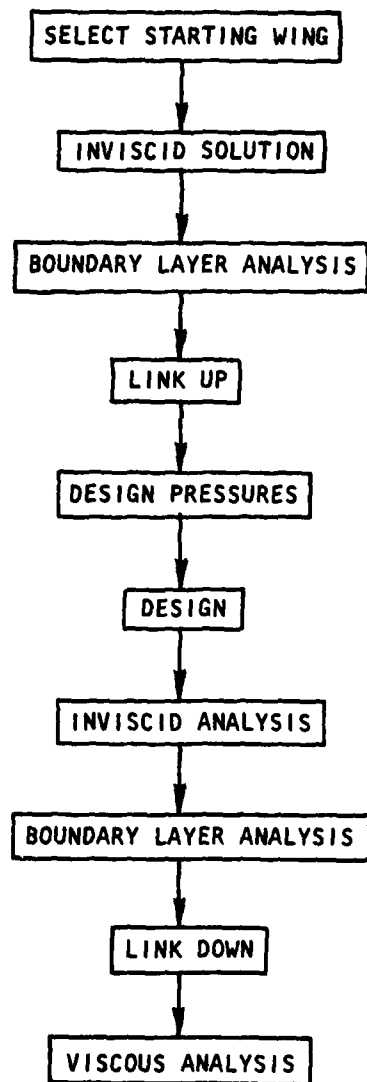


Figure 53. Design Procedure

**DAT
FILM**